**NASA**
**Reference**
**Publication**
**1235**

May 1990

# Exhaust Nozzles for Propulsion Systems With Emphasis on Supersonic Cruise Aircraft

Leonard E. Stitt

**NASA**

# Exhaust Nozzles for Propulsion Systems With Emphasis on Supersonic Cruise Aircraft

Leonard E. Stitt
*Sverdrup Technology, Inc.*
*Lewis Research Center Group*
*Cleveland, Ohio*

# Preface

According to the theory of aerodynamics, and as may be readily demonstrated through laboratory tests and wind tunnel experiments, the bumble bee is unable to fly. This is because the size, weight, and shape of its body in relation to the total wingspread make flying impossible. But the bumble bee, being ignorant of these profound scientific truths, goes ahead and flies anyway and also manages to make a little honey every day.

—Anonymous

This compendium is dedicated to all of the exhaust system research engineers from Government and industry whose work is summarized herein and whose names appear in the reference lists and the bibliography—and, in particular, to my associates in the former Exhaust Systems Section at NASA Lewis Research Center who designed and tested supersonic nozzles during the years 1963 to 1985. Their dedication and expertise made a valuable contribution to the knowledge of nozzles for use on supersonic cruise and supersonic dash aircraft. They, along with the author, firmly believed that, with careful attention to the propulsion aerodynamics involved, "bumble bees" really could fly. It was my good fortune to have worked closely with that elite group during that exciting time.

The author is greatly indebted to NASA for sponsoring this work and for providing the needed critical reviews. In particular, I would like to thank Mr. William C. Strack, Assistant Chief of the Aeropropulsion Analysis Office at NASA Lewis, for originally conceiving the lecture series that this publication is based on and, together with Mr. J. Michael Barton, Director of the Aeromechanics Department of Sverdrup Technology, Inc., and Mr. Paul Barnhart, Head of the Aerospace Analysis Section, of Sverdrup Technology, Inc., for supporting its completion and encouraging the writing of this document.

The technical review was directed effectively by Dr. Kristine A. Dugas of Sverdrup Technology, Inc., and carried out by Mr. Jeffrey J. Berton and Mr. John D. Wolter of NASA Lewis. These reviewers made many constructive suggestions and improved the technical content. The general editorial work was done by Ms. Carol A. Vidoli, whose careful review resulted in numerous improvements in the form of presentation. This compendium could not have been completed without the constructive collaboration of those just mentioned and many others behind the scenes in the Technical Information Services Division at NASA Lewis whose contributions in the typing, typesetting, graphics, photography, and printing did not come to my direct attention.

Leonard E. Stitt

# Contents

# Chapter 1

# Introduction

One of the most persuasive arguments for a commercial supersonic cruise aircraft is its improved productivity, relative to a subsonic cruise aircraft, measured in seat-miles over time. Ever since the first commercial jet airliners, major improvements in productivity have resulted almost entirely from increases in size. However, increasing speed is another way to improve productivity. An aircraft flying at a cruise speed of Mach 2.0 can carry twice as many passengers per day on long-range flights as a subsonic aircraft of equal size. This higher speed also provides significant time savings for the passengers.

Commercial aircraft designers first turned their attention to supersonic cruise aircraft in the late 1950's. Great Britain and France undertook independent feasibility studies in about 1956. In 1959, NASA began to give serious consideration to a supersonic transport based on a civilian derivative of the XB–70 bomber. Concerns about development and production costs as well as world market requirements led the British and French to agree to a joint effort in November 1962 to build the Concorde aircraft. The Concorde was originally designed for a payload of 112 to 126 passengers (later reduced to 100) with a range of 3500 to 4000 nautical miles. Because aluminum was selected for the airframe structure, the Concorde's speed was limited to Mach 2.2. Construction of the first prototype began in 1965, leading to its first flight in March 1969 and commercial service in January 1976. The production line was closed in September 1979 after 16 Concordes had been built—2 for testing and 14 for sale. The Concorde, which recently celebrated its 20th year of flight, has proven that a commercial supersonic aircraft can be operated safely from existing airports. Its major drawbacks remain its small passenger capacity, its high fuel consumption, and its powerplants, which were designed before noise regulations were imposed.

In response to the European plans the United States Supersonic Transport (SST) Program was begun in June 1963 by President John F. Kennedy. The initial design concept called for a 400 000-lb titanium airplane capable of flying at Mach 2.7 with a range of at least 4000 nautical miles and a capacity of 125 to 160 passengers. Design proposals were received in January 1964 from three aircraft manufacturers (Lockheed, Boeing, and North American Aviation) and three engine companies (Pratt & Whitney, Curtiss-Wright, and General Electric). In May 1964 contracts were awarded to Boeing and Lockheed for further studies of the airplane design and to General Electric and Pratt & Whitney for additional work on the engine. A year and a half later, contracts were awarded to Boeing to build the airframe and to General Electric to produce the engine. Design problems with the airframe and engine, coupled with fears about environmental and economic effects, led to the cancellation of the SST program in May 1971, after 8 years of research and development. At that time both Government and industry recognized that significant technical advancements would be required to make a second-generation supersonic cruise aircraft both economically viable and environmentally acceptable. Generic research on supersonic cruise aircraft continued at a low level under the guidance of the Federal Aviation Administration after the SST program was cancelled.

The program was transferred to NASA in 1972 and was renamed the Supersonic Cruise Aircraft Research (SCAR) Program. The intent of this effort was to identify and investigate areas requiring new or improved technology that would lead to substantial improvements in performance. This was a two-pronged effort involving NASA Langley Research Center as the lead center working closely with three airframe contractors (Boeing, Lockheed, and McDonnell Douglas) and NASA Lewis working with two engine companies (General Electric and Pratt & Whitney).

A major portion of the SCAR program was devoted to propulsion technology. These investigations produced concepts for a variable-cycle engine able to vary its airflow at different power settings. The engine would operate at near optimum fuel efficiency while cruising at either supersonic (turbojet) or subsonic (turbofan) speeds. Because the engine's internal configuration allowed the exit nozzle to move and thus alter the exhaust velocity, it also had the potential for reducing noise at takeoff.

By 1975 the number of candidate engines was reduced to four—Pratt & Whitney's conventional, nonaugmented, low-bypass engine with a mixed-flow nozzle and their variable-stream-control (duct-burning turbofan) engine and General Electric's double- and single-bypass engines. The more

unconventional General Electric double-bypass engine and Pratt & Whitney variable-stream-control engine represented relatively quieter engines, even unsuppressed, but required unique and technically challenging components, such as a duct burner, inverted-velocity-profile nozzles, and variable-area bypass injectors. These two engines were chosen for continued research into low-noise exhaust systems.

As these developments were proceeding, the name of the SCAR program was shortened in 1979 to the Supersonic Cruise Research (SCR) Program. Research continued on advanced propulsion systems until the variable-cycle-engine work was terminated in 1981. Model nozzle testing, which was begun prior to that time, continued until the last test report was published in 1985.

This report summarizes the contributions of the NASA Lewis Research Center and its contractors to supersonic exhaust nozzle research over two decades from 1963 to 1985. The exhaust nozzle is one of the most critical components of the propulsion system: the aircraft payload weight is highly sensitive to the thrust efficiency of the nozzle. For example, it is estimated that for the Concorde at its cruise speed of Mach 2.2 a 1-percent decrease in nozzle performance creates an 8-percent loss in payload. Thus, it is evident that the design and performance of the exhaust nozzle are critical to the success or failure of a supersonic cruise aircraft.

Two major research and technology efforts sponsored the nozzle research work at NASA Lewis between 1963 and 1985—the United States Supersonic Transport Program and the follow-on Supersonic Cruise Research Program. They account for two generations of nozzle technology: the first from 1963 to 1971, and the second from 1971 to 1985.

Nozzles designed during the 1960's for the SST program are considered first-generation supersonic cruise exhaust systems. Two ejector nozzles were designed for the Government by General Electric for the GE–4 afterburning turbojet engine selected to power the original Boeing SST, and a plug nozzle was designed at NASA Lewis. All three nozzles were tested at Lewis in a static test stand for internal performance and in the 8- by 6-Foot Supersonic Wind Tunnel for external flow effects. They were also flight tested on the F–106 testbed aircraft for installation effects.

During the 1970's, as part of the SCR program, both Pratt & Whitney and General Electric designed and tested second-generation nozzles for their variable-cycle engines, also developed under the SCR program. These nozzles included the Pratt & Whitney coannular ejector and the General Electric coannular plug, both of which featured inverted velocity profiles for reduced jet noise at takeoff and landing. The Pratt & Whitney nozzle was tested at Lewis. The General Electric

nozzle was tested under a Lewis contract at the Fluidyne Transonic Wind Tunnel in Minneapolis, Minnesota.

Most of the data generated under NASA's SST and SCR programs were recorded in NASA technical memorandums, contractor reports, and conference papers. However, most of the propulsion engineers who participated in this extensive research effort have moved on to other activities. The corporate memory related to this vast body of research was in danger of being lost to the current generation of propulsion aerodynamicists. NASA Lewis management persuaded the author, who was the head of the Exhaust Systems Section from 1962 to 1972 and a senior engineer in the Variable-Cycle-Engine Project Office from 1975 to 1981, to present a course on supersonic exhaust nozzles to researchers at Lewis. As these lectures concluded, a permanent record of the notes and figures used was to be documented in a formal NASA report. This Reference Publication is a summary of that material.

The publication is organized as follows. First, the equations used to calculate nozzle thrust are introduced. Then, the general types of nozzles are presented, followed by a discussion of those types proposed for supersonic aircraft. Next, first-generation nozzles designed specifically for the Boeing SST and second-generation nozzles designed under the SCR program are separately reviewed and then compared. A chapter on throttle-dependent afterbody drag is included, since drag has a major effect on the off-design performance of supersonic nozzles. Boattail drag data are supplemented by research work concluded at the NASA Langley Research Center in the late 1950's.

A chapter on the performance of supersonic dash nozzles, based on research at both Lewis and Langley, follows. This research was conducted during the same time period as the SST and SCR programs, and the nozzles have similar problems in their design.

Finally, the nozzle test facilities used at NASA Lewis during this nozzle research effort are identified and discussed. These facilities included static test stands, a transonic wind tunnel, and a flying testbed aircraft. Both subscale models and full-scale nozzle hardware were used to obtain the isolated and installed nozzle performance presented herein.

A concluding section points to the future—a third generation of nozzles designed for a new era of high-speed civil transports to produce even greater advances in performance, to meet new noise rules, and to ensure the continuity of over two decades of NASA research into high-speed commercial aircraft.

The symbols used in the report are defined in appendix A. A bibliography of the research reports used by the author in writing this compendium is provided as appendix B.

# Chapter 2

# Nozzle Performance Equations

The function of an exhaust nozzle is rather simple. It is a device that converts the potential energy (pressure and temperature) of the engine exhaust gases into kinetic energy (velocity) to produce a useful thrust. Although exhaust nozzles have existed for centuries, it was not until 1883 that DeLaval developed the first practical steam turbine, using a convergent-divergent nozzle to direct the steam into the turbine wheel. Today, exhaust systems have become rather sophisticated and enjoy a wide range of applications, from use in engine components (compressors, turbines, and injectors) to use as thrust producers for air-breathing and rocket propulsion systems. Although this report emphasizes the application of nozzles to air-breathing propulsion systems, the thrust equations are equally applicable to all types of propulsion. For example, turbojet and turbofan nozzles are required to operate over a fairly limited range of pressure and area ratios; ramjet nozzles operate at slightly higher pressure and area ratios; and nozzles for rocket engines, which perform from sea level to vacuum conditions in space, cover the whole spectrum from moderate to infinite pressure ratios.

## 2.1 Nozzle Efficiency

There are several indicators of the efficiency of an exhaust nozzle. Which one to use depends primarily on its application; that is, whether it is to be used in an engine component or as a thrust producer for a propulsion system. The most efficient method of converting high pressure and high temperature into kinetic energy is to expand the flow isentropically over a given pressure ratio to realize the greatest change in enthalpy. However, most expansion processes in nozzles occur with some friction and an increase in entropy so that the actual change in enthalpy is always less than the ideal change in enthalpy. The nozzle adiabatic efficiency is defined to relate the actual change in enthalpy to the ideal:

$$\text{Adiabatic efficiency} = \frac{\text{Actual enthalpy change}}{\text{Ideal enthalpy change}}$$

An isentropic expansion process will produce the ideal exit velocity. However, the actual velocity is always less owing to nonisentropic expansion processes and divergence losses. A nozzle velocity coefficient can therefore be defined as

$$\text{Velocity coefficient, } C_V = \frac{\text{Actual velocity}}{\text{Ideal velocity}}$$

Thus, both the velocity coefficient and the adiabatic efficiency of the nozzle are indicators of the amount of losses in the nozzle.

Propulsion engineers are primarily interested in the exhaust nozzle as a thrust-producing device. It is therefore appropriate to use an efficiency term that reflects the ability of the nozzle to produce the maximum thrust. A nozzle efficiency based on thrust is defined as

$$\text{Nozzle thrust efficiency, } (C_F)_\eta = \frac{\text{Actual thrust}}{\text{Ideal thrust}}$$

Normally, the ideal thrust is based on the assumption of the one-dimensional flow of an ideal gas. The ideal flow rate is also based on one-dimensional isentropic flow. However, because the actual flow rate is always less than the ideal flow rate, the two are related through a discharge coefficient:

$$\text{Discharge coefficient, } C_d = \frac{\text{Actual flow rate}}{\text{Ideal flow rate}}$$

In most nozzle test programs both the thrust and flow rate for the nozzle system are accurately measured with load cells and venturis, respectively. It becomes more meaningful then to base the ideal thrust on a measured flow rate so that the nozzle efficiency can be defined as

$$\text{Nozzle thrust efficiency, } (C_F)_\eta = \frac{\text{Measured thrust}}{C_d \times \text{Ideal thrust}}$$

3

## 2.2 Nozzle Thrust

Experimental research on exhaust nozzles at the Lewis Research Center is focused on producing thrust for propulsion systems. The function of a nozzle is to produce the maximum thrust with the minimum weight and mechanical complexity. Many nozzle types and concepts can be considered, and each design can significantly influence the nozzle's efficiency. Since nozzle thrust has been selected as the measure of nozzle efficiency, it is appropriate to consider the thrust equations and some of the inherent thrust losses before considering specific types of nozzles.

### 2.2.1 Flow Stations

In a discussion of exhaust nozzles for air-breathing propulsion systems, it is appropriate to identify the flow stations in typical turbojet or turbofan engines. These stations, which will be used throughout this report, are indicated in figure 2–1. In general, they are accepted and used throughout Government agencies and in industry. Of interest to nozzle researchers are stations 7, 8, and 9, which refer to the nozzle inlet, throat, and exit, respectively.

### 2.2.2 Brayton Cycle

The temperature-entropy diagram for a typical turbojet engine cycle is shown in figure 2–2, where the various engine component functions and typical turbojet engine stations are identified. The temperature-entropy diagram was constructed to show the nozzle function for either an afterburning or a nonafterburning engine. In either case, dry or reheat, the function of the nozzle is identical; that is, the nozzle is required to expand the flow between two specified levels of pressure and temperature, from the nozzle inlet total pressure (high) to the free-stream static pressure (low). If the propulsion system does have the capability for afterburning, the nozzle throat area $A_8$ must be variable to match the degree of temperature increase. The throat area of the variable nozzle must permit temperature variations in the exhaust gas while maintaining a constant turbine inlet temperature. Because afterburning has been used for many years on military aircraft, the variable-area nozzle throat is not a new feature.

The nozzle receives the hot exhaust gases at the inlet (station 7, fig. 2–3) and must expand them efficiently to the exit (station 9) in order to obtain the maximum thrust to propel the vehicle. At station 7 the nozzle pressures for a typical supersonic turbojet engine may vary by an order of magnitude, from 5 to 50 psia. For an afterburning engine the nozzle inlet temperature may be as high as 3340 °F. The nozzle inlet flow velocity is subsonic.

### 2.2.3 Net and Gross Thrust

The net thrust of an air-breathing propulsion system is defined to be the difference between the gross thrust at the nozzle exit plane and the free-stream ram drag:

$$\text{Net thrust} = \text{Gross thrust} - \text{Ram drag}$$

or

$$F_{\text{net}} = [\dot{m}_9 V_9 + (p_9 - p_0)A_9] - (\dot{m}_9 V_0)$$

This equation reveals that the ram drag $\dot{m}_9 V_0$ is independent of the nozzle design and is dependent only on free-stream conditions; that is, for a given flow rate from the engine $\dot{m}_9$, the ram drag is identical for any nozzle configuration that is assumed. For this reason the nozzle gross thrust can be a useful parameter in selecting a nozzle for a particular application or in comparing one nozzle concept to another. The gross thrust is therefore a good measure of the efficiency of a nozzle and
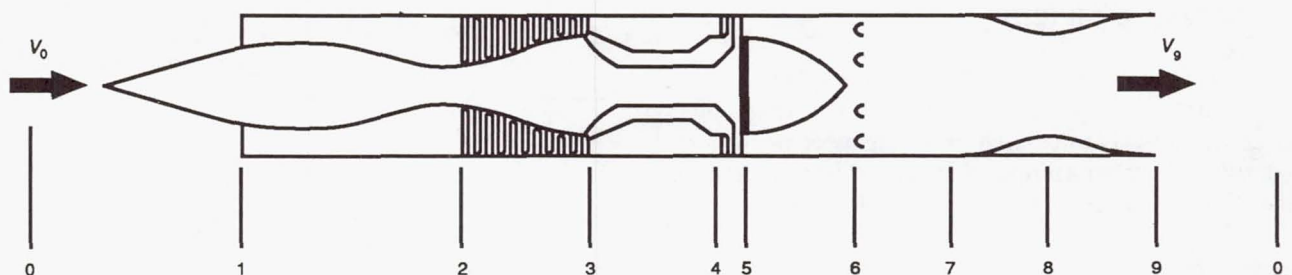


| Station | Description | Station | Description |
|---------|-------------|---------|-------------|
| 0 | Free stream [a] | 5 | Turbine exit |
| 1 | Inlet lip [a] | 6 | Tailpipe inlet |
| 2 | Compressor inlet [a] | 7 | Nozzle inlet [a] |
| 3 | Compressor exit [a] | 8 | Nozzle throat [a] |
| 4 | Turbine inlet | 9 | Nozzle exit [a] |

[a] Also applies to fan systems.

Figure 2–1.—Flow stations for a typical propulsion system.
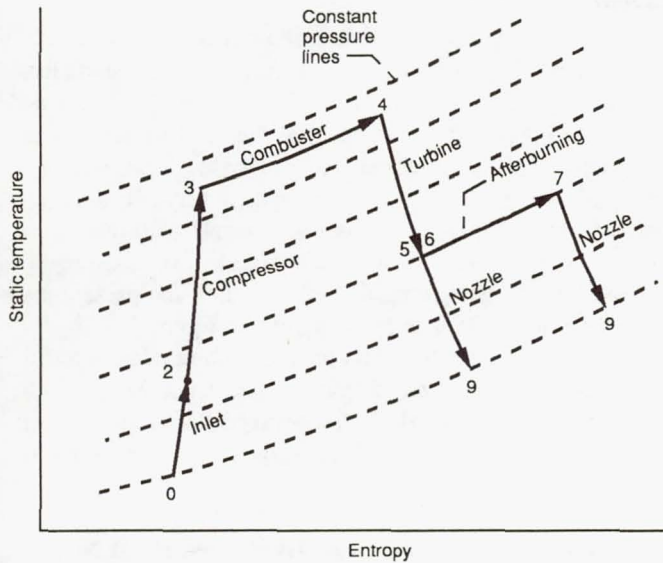
Figure 2-2.—Turbojet engine cycle (Brayton).
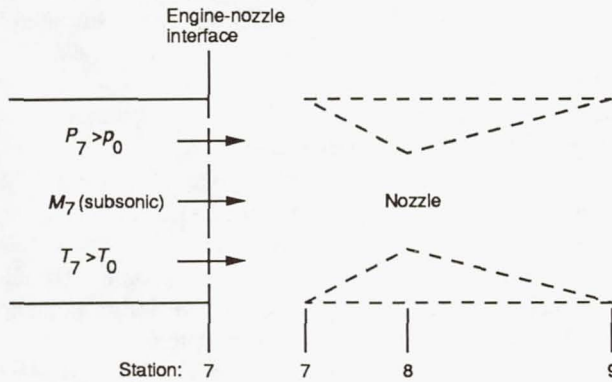


Figure 2-3.—Nozzle function—expand high-pressure exhaust gases to obtain maximum thrust.

is obtained from the flow conditions at the nozzle exit plane (station 9):

$$F_g = \dot{m}_9 V_9 + (p_9 - p_0)A_9$$

### 2.2.4 Ideal Thrust

The ideal thrust of the nozzle occurs when the nozzle exit pressure $p_9$ is equal to the free-stream static pressure $p_0$, or

$$F_i = \dot{m}_9 V_9$$

The ideal thrust can be rewritten as follows:

$$F_i = \gamma p_0 M_9^2 A_9$$

This thrust can be put into coefficient form by referencing it to the total pressure and area at the nozzle throat (station 8):

$$\frac{F_i}{P_8 A_8} = \gamma \left(\frac{p_0}{P_8}\right)\left(\frac{A_9}{A_8}\right)M_9^2$$

where

$P_8/p_0$  nozzle pressure ratio (assuming $P_8 = P_7$)

$A_9/A_8$  nozzle area ratio

$M_9$  nozzle exit Mach number

These nozzle parameters are all interdependent; that is, for a given nozzle area ratio there is a unique and corresponding pressure ratio and exit Mach number. For a given ratio of specific heats $\gamma$ the variation of pressure ratio and area ratio can be found as a function of Mach number in various tabulations; that is, in appendix C of reference 2-1 for a $\gamma$ of 1.4 and in reference 2-2 for a range of $\gamma$'s from 1.100 to 1.667. The second reference also contains a listing of the ideal thrust coefficients.

It is apparent from the preceding equation that the ideal thrust coefficient is a unique function of the nozzle pressure ratio if the ratio of specific heats is constant. This variation is shown in figure 2-4 for a $\gamma$ of 1.4. This curve also implies that the nozzle area ratio varies continuously with changes in the nozzle pressure ratio in order for the flow to remain perfectly expanded. Three typical cases are indicated in figure 2-4 for nozzle pressure ratios of 1.9, 10.6, and 26.3; the corresponding area ratios are 1.0, 2.0, and 3.43.

A schematic of the nozzle geometry required to satisfy these three cases is shown in figure 2-5. As mentioned previously, the nozzle inlet flow is subsonic at station 7. This Mach number can be increased by converging the flow area at station 8, but only until the nozzle becomes choked (i.e., when $M_8$ becomes sonic). The first case represents the nozzle pressure ratio (1.9) that is sufficient to choke the nozzle. If a nozzle were required for this pressure ratio, a convergent nozzle with an area ratio of 1.0 would provide the ideal thrust. For nozzle pressure ratios greater than the critical value of 1.9 (e.g., for pressure ratios of 10.6 or 26.3), the nozzle exit Mach number can be
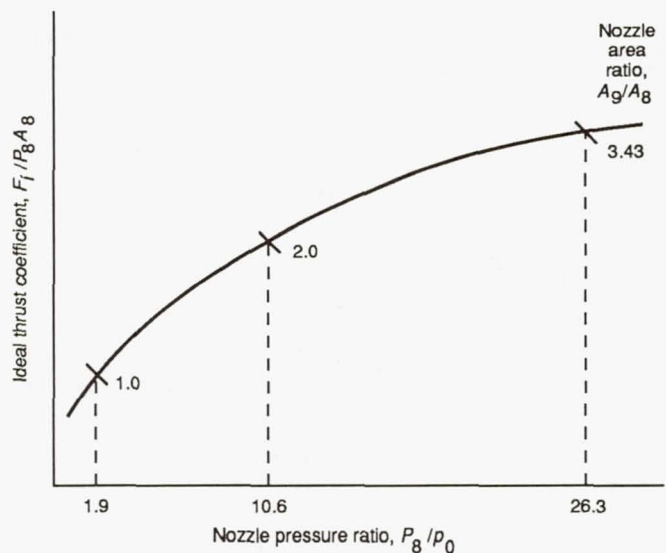


Figure 2-4.—Ideal thrust coefficient. Ratio of specific heats, $\gamma$, 1.4.

5

Figure 2-5.—Ideal nozzle—variable area.

supersonic if a divergent section is added downstream of the nozzle throat. The resulting convergent-divergent nozzles would have area ratios of 2.0 and 3.43, respectively.

## 2.2.5 Gross Thrust With Fixed Area Ratio

The preceding discussion has indicated that the ideal thrust of a nozzle would be realized if the nozzle area ratio were allowed to vary with changes in the nozzle pressure ratio (i.e., with a variable-area-ratio or "rubber" nozzle). If the nozzle area ratio is fixed, the thrust can be calculated as follows:
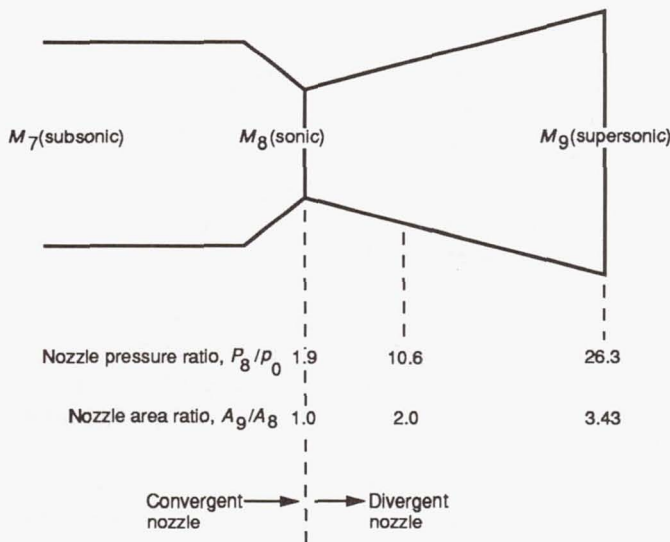
$$\text{Gross thrust} = \dot{m}_9 V_9 + (p_9 - p_0)A_9$$

A gross thrust coefficient is defined, with reference to the nozzle throat area and pressure, as

$$\frac{F_g}{P_8 A_8} = \left[ \gamma \left( \frac{p_9}{P_8} \right) \left( \frac{A_9}{A_8} \right) M_9^2 + \left( \frac{p_9}{P_8} \right) \left( \frac{A_9}{A_8} \right) \right] - \left( \frac{p_0}{P_8} \right) \left( \frac{A_9}{A_8} \right)$$

If the nozzle area ratio $A_9/A_8$ is constant, all of the terms inside the brackets are constant and independent of the nozzle pressure ratio $P_8/p_0$. The gross thrust coefficient $F_g/P_8 A_8$ reaches its maximum value, equal to the summation of the terms in the brackets, when the nozzle pressure ratio is infinite so that the term outside the brackets becomes zero. The summation of the terms in the brackets is therefore usually referred to as the "vacuum thrust coefficient" and is a constant value for any specified nozzle area ratio and $\gamma$. For a rocket engine application this is the thrust coefficient that would be attained in space.

## 2.2.6 Thrust Efficiency

The calculated thrust coefficient of a fixed-area-ratio nozzle (shown in fig. 2-6) is compared with the ideal thrust coefficient over a range of nozzle pressure ratios. As shown, the thrust of the fixed-area-ratio nozzle attains the ideal thrust only at its design pressure ratio and falls below the ideal value on either side of the design point. A convenient way of comparing the performance of a fixed-area-ratio nozzle with that of an ideal nozzle is to divide the thrust coefficient values from figure 2-6 over the range of nozzle pressure ratios and present the result as a nozzle efficiency, as shown in figure 2-7. Again it is evident that a fixed-area-ratio nozzle attains its peak thrust efficiency at its design pressure ratio. The major thrust losses in a fixed-area-ratio nozzle then depend primarily on whether the nozzle is operating at a pressure ratio above or below its design point.

## 2.2.7 Overexpansion Losses in Fixed-Area-Ratio Nozzle

A nozzle is said to be overexpanded if it is operating at a pressure ratio below its design point, as shown in figure 2-7. The pressure distribution inside the divergent shroud of the nozzle (fig. 2-8) illustrates the overexpanded case. The nozzle flow expands to free-stream pressure $p_0$ at some point between the nozzle throat and exit stations. For optimum thrust the nozzle shroud should be terminated at this point. However, the nozzle flow continues to expand beyond this point and the pressures are less than ambient pressure. All of the divergent shroud with pressures less than ambient constitutes a drag on the system, as shown by the crosshatching on the sketch. The dropoff in thrust efficiency below the design point in figure 2-7 is directly related to this drag term.

Normally, a nozzle will overexpand and flow without separation until the ratio of the exit to the ambient static
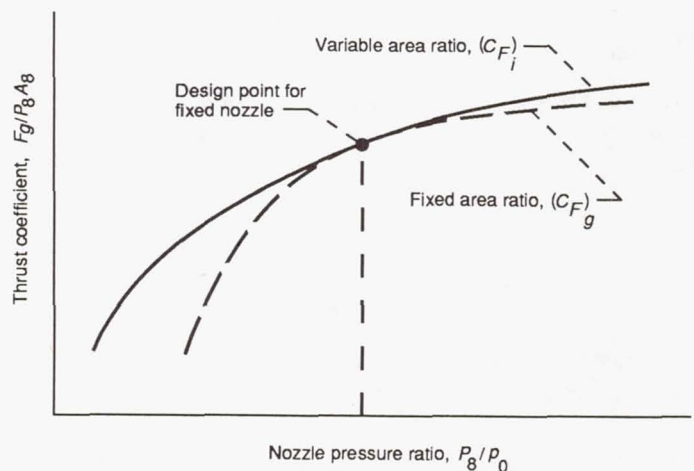


Figure 2-6.—Comparison of fixed and variable nozzles.
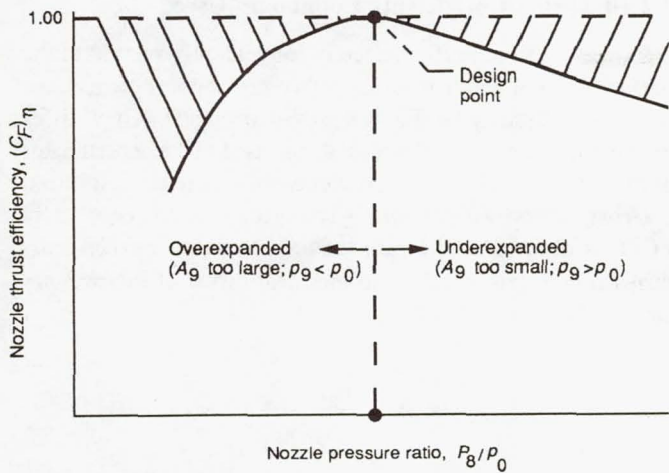
Figure 2-7.—Nozzle efficiency—fixed area ratio.



Figure 2-8.—Overexpanded nozzle ($A_9$ too large).

to damage or break the shroud wall. Because the overexpanded nozzle that separates is by far the most difficult to predict or analyze, it is the most serious case from the standpoint of nozzle stability.

### 2.2.8 Underexpansion Losses in Fixed-Area-Ratio Nozzle

A nozzle is said to be underexpanded if it is operating at a nozzle pressure ratio above its design point. The underexpanded case is illustrated in figures 2-7 and 2-9. Here the nozzle area ratio is too low and the flow expands to a nozzle exit pressure that is greater than ambient pressure. In the case illustrated in figure 2-9 an extension to the divergent portion of the nozzle would be required to attain the ideal thrust. The portion of the potential thrust that is lost by the shorter nozzle accounts for the decrease in nozzle thrust efficiency shown in figure 2-7. The underexpanded case is the simplest to analyze analytically, since flow separation cannot occur in underexpanded nozzles.

### 2.2.9 Other Losses in Nozzles

In addition to the losses in thrust due to overexpansion and underexpansion, other losses are associated with friction, nonaxial divergence angles, and leakage in variable-geometry configurations. As mentioned earlier, both the adiabatic efficiency of the nozzle and the velocity coefficient are indicators of the losses in the nonideal flow process. The Reynolds number in the nozzle flow is usually high enough to assume turbulent boundary layer flow. There are empirical correlations and semiempirical solutions to the boundary layer

pressure falls below some critical value. When this occurs, the exhaust gases will separate from the nozzle wall and form a shock wave that increases the nozzle flow pressure to ambient conditions. Nozzle flow separation is beneficial from the standpoint of thrust. In fact, the ideal thrust could be realized if the nozzle flow could be made to separate at the point in the divergent shroud where the nozzle static pressure equals the ambient pressure (fig. 2-8). However, when the nozzle flow separates, it will usually attach itself to one side of the nozzle shroud. In most cases the interaction of the shock and the boundary layer is unsteady, and the flow will shift or rotate around the shroud wall. Sometimes this instability is sufficient
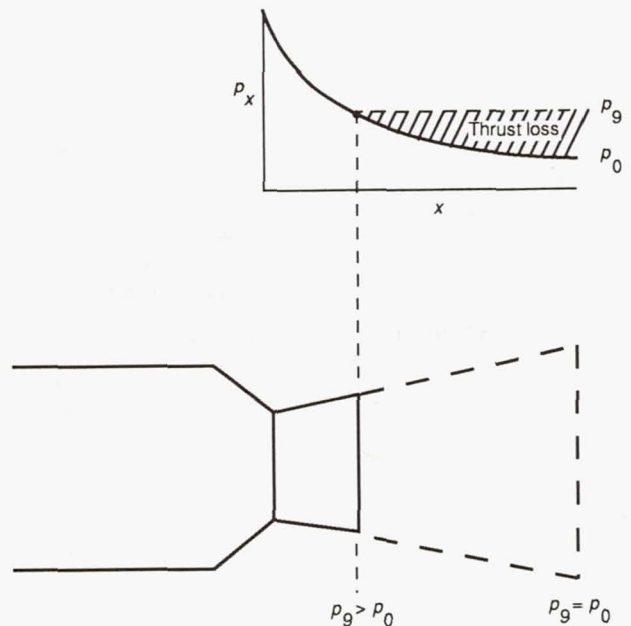


Figure 2-9.—Underexpanded nozzle ($A_9$ too small).

equations for turbulent flow in the presence of high heat transfer rates and large negative pressure gradients (e.g., p. 314 of ref. 2-3, which also identifies other approximate solutions that can be used to estimate the losses due to friction).

The thrust efficiency of a nozzle is also affected by the nonuniform distribution of both the magnitude and direction of the velocity vector at the exit plane. Thrust is based on the axial component of momentum; the normal component does not produce thrust. The loss due to wall divergence can be estimated through the use of a divergence factor:

$$\text{Divergence factor, } \lambda = \frac{1 + \cos \alpha}{2}$$

where $\alpha$ is the nozzle divergence half-angle. The variation of divergence factor with $\alpha$ is shown in figure 2-10.

Nozzle shape can also contribute to additional losses in thrust. Isentropic shapes are desirable but tend to be long. Nonisentropic shapes can induce weak compression waves in the supersonic flow in divergent shrouds that result in small losses in total pressure and thrust.

Variable-area nozzles must also be sealed properly to minimize gas leakage and additional thrust losses.



$$F_g = \lambda \dot{m}_g V_9 + (p_9 - p_0) A_9$$
$$\lambda = \frac{1}{2}(1 + \cos \alpha)$$
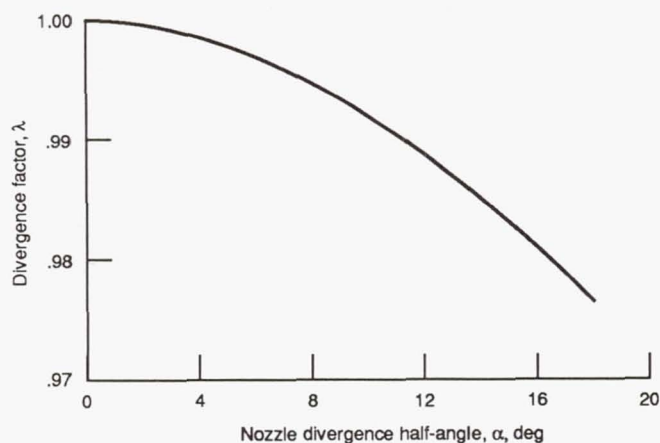
Figure 2-10.—Divergence loss from conical exit.

## 2.2.10 Thrust Coefficients Commonly Used

Exhaust system performance is conveniently related to the performance of an ideal system. Two thrust coefficients have been used to describe the system performance. They differ only in the definition of the ideal thrust used in the denominator of the equation. The two coefficients are explained as follows:

*Gross thrust coefficient.*—The gross thrust coefficient $(C_F)_g$ is defined as the ratio of the measured nozzle gross thrust minus external drag to the ideal thrust of the primary stream. In equation form

$$(C_F)_g = \frac{F_g - D_{ext}}{\dot{m}_p (V_p)_i}$$

If a secondary flowstream exists in a nozzle, this thrust coefficient can have a value greater than 1.00, since the ideal thrust of the secondary stream is not included in the denominator of the equation.

*Nozzle efficiency.*—The nozzle efficiency $(C_F)_\eta$ relates the overall efficiency of the exhaust system by including the ideal thrust contribution of the secondary flow, as follows:

$$(C_F)_\eta = \frac{F_g - D_{ext}}{\dot{m}_p (V_p)_i + \dot{m}_s (V_s)_i}$$

As defined, this nozzle efficiency cannot have a value greater than 1.00 and is truly an indication of how well the nozzle system expands all of its internal flowstreams.

## 2.3 References

2-1. Hesse, W.J.; and Mumford, N.V.S., Jr.: Jet Propulsion for Aerospace Applications, Second ed., Pitman Publishing Corp., New York, 1964.
2-2. Tables of Compressible Flow Functions, Pratt & Whitney Aircraft Co., 1963.
2-3. Handbook of Supersonic Aerodynamics—Section 17, Ducts, Nozzles, and Diffusers, NAVWEPS Report 1488, Vol. 6, Jan. 1964.

# Chapter 3
# Types of Nozzles and Their Internal Performance

Several types of nozzles can produce thrust for propulsion systems. They cover the spectrum from the simple, fixed-area convergent and fixed-area convergent-divergent (C–D) nozzles shown in figure 3–1 to the more complex ejector nozzles with independent control of throat and exit areas. The simple convergent nozzle has been used for many years on commercial subsonic transports; the more complex cooling-air ejector nozzles have been used for supersonic military aircraft with afterburning engines. For a supersonic cruise aircraft such as the supersonic transport, the nozzle area ratio should be continuously varied over all flight conditions to provide the optimum thrust efficiency.

Several nozzle types are discussed in this chapter, along with the thrust equations and experimental data bases that are available for use in determining their internal performance characteristics. Computer programs are currently available throughout the industry and Government for calculating the performance of most nozzle concepts. These programs are identified and sample performance curves are presented.

## 3.1 Simple Convergent Nozzles

The simplest exhaust nozzle is the fixed-area convergent nozzle, as shown in figure 3–1(a). It is currently used on subsonic cruise aircraft (commercial or military) where the nozzle pressure ratio is low enough that little or no divergence is required. It has also been used as a reference or referee nozzle in nozzle test programs to facilitate load cell and flow rate calibrations. This is possible, since the thrust and flow characteristics of convergent nozzles have become well documented over the years. Correction coefficients have been accurately measured for a large range of convergence angles to account for friction, angularity losses, and discharge coefficients.
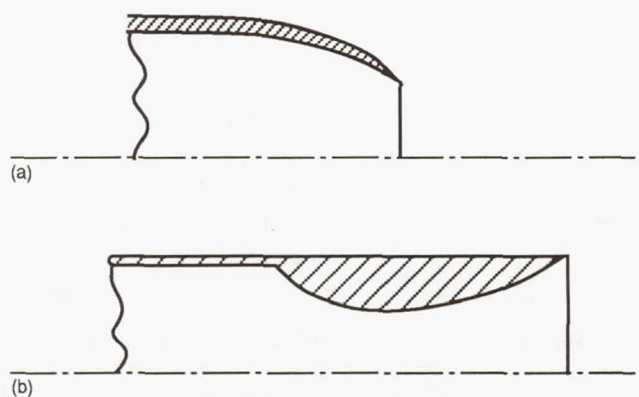


(a) Simple convergent nozzle.
(b) Simple convergent-divergent nozzle.

Figure 3–1.—Simple nozzle types.

### 3.1.1 Thrust Equations

The gross thrust of a convergent nozzle is calculated from the geometric and flow conditions at its exit (station 8):

$$F_g = \dot{m}_8 V_8 + (p_8 - p_0)A_8$$

This equation can be rewritten to include the correction coefficients for the losses due to friction $C_V$ and flow angularity $C_\theta$:

$$F_g = (C_V C_\theta)\gamma p_8 M_8^2 (A_8)_e + (p_8 - p_0)A_8$$

where $(A_8)_e$ is the effective exit area. The thrust can be put into a coefficient form by dividing by $(A_8)_e$ and the nozzle total pressure $P_8$:

$$\frac{F_g}{P_8(A_8)_e} = (C_V C_\theta)\gamma\left(\frac{p_8}{P_8}\right)M_8^2 + \frac{1}{(C_d)_8}\left(\frac{p_8}{P_8} - \frac{p_0}{P_8}\right)$$

9

where

$$(C_d)_8 = \text{Discharge coefficient} = \frac{(A_8)_e}{A_8}$$

## 3.1.2 Thrust Efficiency

The thrust efficiency is defined as

$$(C_F)_\eta = \frac{\text{Actual gross thrust coefficient}}{\text{Ideal gross thrust coefficient}}$$

or

$$(C_F)_\eta = \frac{(C_V C_\theta)_\gamma \left(\dfrac{p_8}{P_8}\right) M_8^2 + \dfrac{1}{(C_d)_8} \left(\dfrac{p_8}{P_8} - \dfrac{p_0}{P_8}\right)}{\left[\dfrac{F_i}{P_8 (A_8)_e}\right]}$$

where

$$\frac{F_i}{P_8 (A_8)_e} = \left\{ \frac{2\gamma^2}{\gamma-1} \left(\frac{2}{\gamma+1}\right)^{\frac{\gamma+1}{\gamma-1}} \left[1 - \left(\frac{p_0}{P_8}\right)^{\frac{\gamma-1}{\gamma}}\right] \right\}^{\frac{1}{2}}$$

## 3.1.3 Empirically Derived Correction Coefficients

Several correction factors must be applied to the thrust equations to remove the assumptions of one-dimensional and isentropic flow. Three basic corrections were accounted for:
(1) A convergence factor $C_\theta$ to account for the angularity of the exhaust velocity vector at the exit plane
(2) A velocity coefficient $C_V$ to account for the loss due to friction in the boundary layer
(3) A discharge coefficient $C_d$ to relate the effective flow area to the geometric area or the actual flow rate to the ideal flow rate
These correction factors have been accurately measured over the years in experimental test programs. The empirically derived correction coefficients are presented in figures 3–2 to 3–4 for a range of convergence half-angles $\theta$ from 0° to 40°, for conic nozzles.

## 3.1.4 Performance Characteristics

By using the thrust equations and empirically derived correction factors, a computer program was written to calculate the internal performance of a family of conical nozzles. Two applications of this program are shown in figures 3–5 and 3–6. The first example (fig. 3–5) presents the performance characteristics of three conical nozzles over a range of nozzle pressure ratios. Any one of these three configurations could
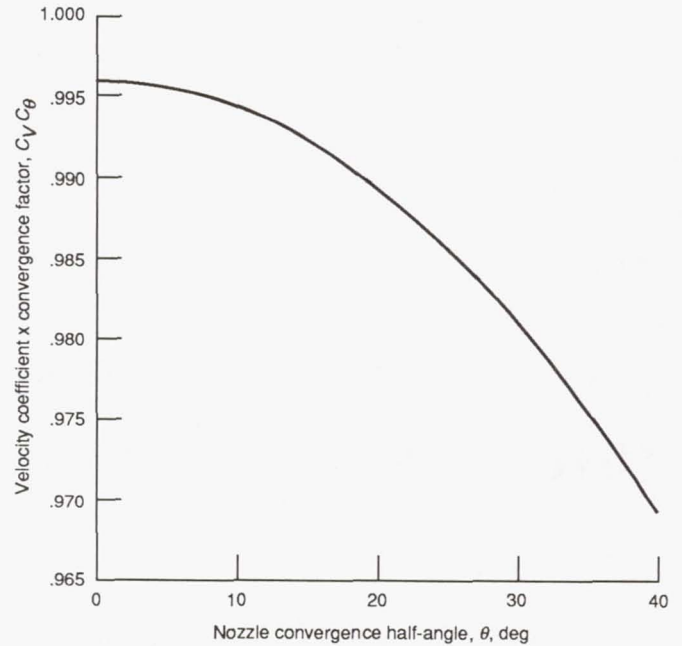


Figure 3–2.—Convergent nozzle correction coefficients versus convergence half-angle.
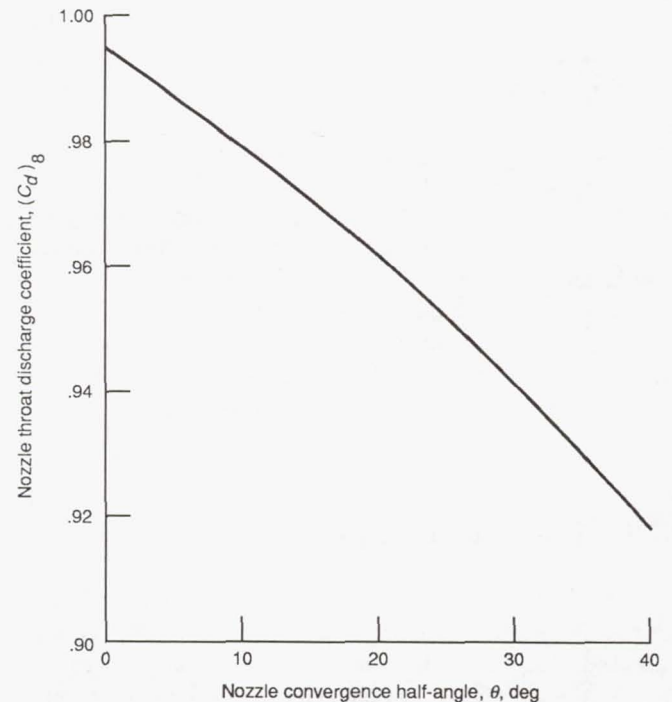


Figure 3–3.—Choked convergent nozzle flow coefficients.

be considered as a reference nozzle for calibrating the thrust and flow rate measurements during an experimental nozzle test program. All three nozzles have been and continue to be used for this purpose throughout Government and industry.

The second example (fig. 3–6) shows the effect of conical half-angle on nozzle thrust at selected values of nozzle pressure ratio. Plots like this one can be used to select an optimum
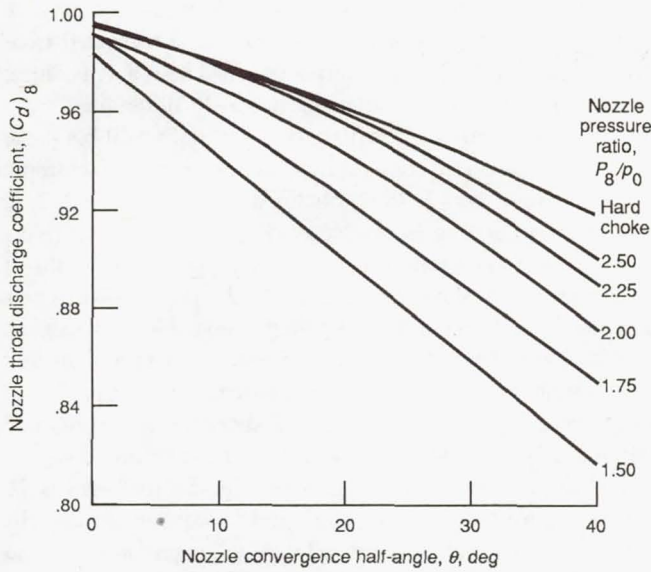
Figure 3-4.—Unchoked convergent nozzle flow coefficients.
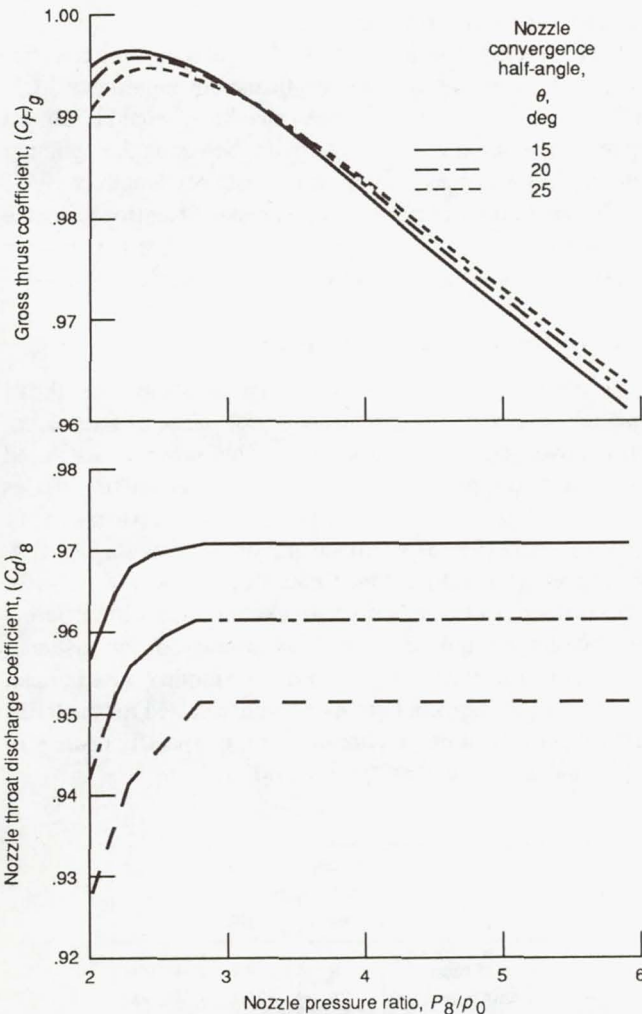


Figure 3-5.—Convergent nozzle performance.
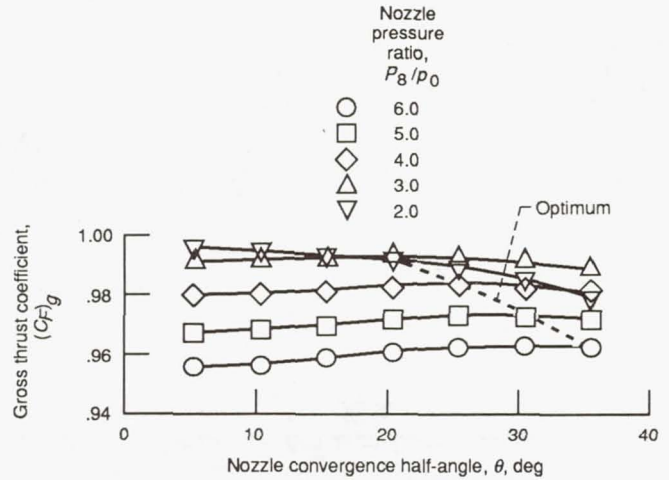


Figure 3-6.—Effect of convergence angle on nozzle thrust.

convergence angle for any predetermined nozzle pressure ratio; for example, a 5° half-angle cone is near the optimum for a pressure ratio of 2.0, but a 35° half-angle cone would be near the optimum for a pressure ratio of 6.0. An optimum convergent nozzle for a pressure ratio range from 2.0 to 6.0 would have a half-angle of about 25°.

## 3.2 Simple Convergent-Divergent Nozzles

For nozzle pressure ratios much above 2.0 a convergent-divergent nozzle is required to expand the exhaust flow to free-stream static pressure. The required area ratio increases with increasing nozzle pressure ratio as a function of flight Mach number and altitude. Ideally, the internal expansion should be varied continuously as a function of nozzle pressure ratio to provide optimum thrust. A simple fixed-area-ratio C–D nozzle (fig. 3–1(b)) has historically been used for rocket engines. The thrust equations for a simple C–D nozzle are presented in this section, followed by an example of this nozzle as applied to the Atlas-Centaur launch vehicle.

### 3.2.1 Thrust Equations

The gross thrust of a convergent-divergent nozzle is calculated from the geometric and flow conditions at its exit (station 9):

$$F_g = \dot{m}_9 V_9 + (p_9 - p_0) A_9$$

This equation can be rewritten to include the correction factors for the losses due to friction $C_V$ and flow angularity $C_\theta$:

$$F_g = (C_V C_\theta) \gamma p_9 M_9^2 (A_9)_e + (p_9 - p_0) A_9$$

The thrust can be put into coefficient form by dividing $F_g$ by the effective nozzle throat area $(A_8)_e$ and the nozzle total pressure $P_8$:

11

$$\frac{F_g}{P_8(A_8)_e} = (C_V C_\theta)\gamma \left(\frac{p_9}{P_8}\right) \left[\frac{(A_9)_e}{(A_8)_e}\right] M_9^2$$

$$+ \frac{1}{(C_d)_8} \left(\frac{A_9}{A_8}\right) \left(\frac{p_9}{P_8} - \frac{p_0}{P_8}\right)$$

where

$$C_\theta = \frac{1+\cos\,\alpha}{2}$$

and $\alpha$ is nozzle divergence half-angle. If the nozzle area ratio is fixed, the preceding equation can be rearranged, as follows:

$$\frac{F_g}{P_8(A_8)_e} = \left\{ (C_V C_\theta)\gamma \left(\frac{p_9}{P_8}\right) \left[\frac{(A_9)_e}{(A_8)_e}\right] M_9^2 \right.$$

$$\left. + \frac{1}{(C_d)_8} \left(\frac{A_9}{A_8}\right) \frac{p_9}{P_8} \right\} - \frac{1}{(C_d)_8} \left(\frac{A_9}{A_8}\right)\left(\frac{p_0}{P_8}\right)$$

Note that the terms contained within the braces are constant for a given fixed-area-ratio nozzle and are independent of nozzle pressure ratio $P_8/p_0$. The value of $F_g/P_8(A_8)_e$ is equal to the terms in the braces when the nozzle pressure ratio is infinite and is therefore referred to as the "vacuum thrust coefficient."

### 3.2.2 Thrust Efficiency

The thrust efficiency is defined as

$$(C_F)_\eta = \frac{\text{Actual gross thrust coefficient}}{\text{Ideal gross thrust coefficient}}$$

or

$$(C_F)_\eta = \frac{(C_V C_\theta)\gamma\left(\frac{p_9}{P_8}\right)\left[\frac{(A_9)_e}{(A_8)_e}\right]M_9^2 + \frac{1}{(C_d)_8}\left(\frac{A_9}{A_8}\right)\left(\frac{p_9}{P_8}-\frac{p_0}{P_8}\right)}{\left[\frac{F_i}{P_8(A_8)_e}\right]}$$

where

$$\frac{F_i}{P_8(A_8)_e} = \left\{ \frac{2\gamma^2}{\gamma-1}\left(\frac{2}{\gamma+1}\right)^{\frac{\gamma+1}{\gamma-1}}\left[1-\left(\frac{p_0}{P_8}\right)^{\frac{\gamma-1}{\gamma}}\right]\right\}^{\frac{1}{2}}$$

### 3.2.3 Divergent Shroud Shapes

The nozzle designer has some leeway in selecting the contour, length, and exit angle of the divergent section of a fixed-area-ratio C–D nozzle, as shown in figure 3–7. All of the nozzle configurations shown were designed for an area ratio of 25. They include a long isentropic, a truncated isentropic, a short isentropic, a short overturned bell, and a conical nozzle. The long isentropic shape (fig. 3–7(a)), obtained from reference 3–1, provides the highest thrust coefficient but is the longest and heaviest configuration. The truncated isentropic nozzle contour (fig. 3–7(b)), obtained from reference 3–2, is shorter than the long isentropic nozzle, but the nozzle divergence angle has been increased, reducing the axial thrust efficiency. The short isentropic nozzle (fig. 3–7(c)) was designed to be 20 percent shorter than an equivalent 15° conical nozzle. The design of this nozzle contour, a parabola tangent to the circular arc at the throat, was based on results presented in reference 3–3. This configuration is shorter than the truncated isentropic nozzle and has almost the same exit angle.

The short overturned bell nozzle (fig. 3–7(d)) also is 20 percent shorter than an equivalent 15° conical nozzle. Its contour was formed by a curved section tangent to the throat arc and exit angle. This configuration is the same length as the short isentropic nozzle but has a much lower exit angle. Data from its tests indicated that the overturning of the flow resulted in internal disturbances within the expanding jet that reduced the thrust efficiency.

The last configuration is a 15° half-angle conical nozzle (fig. 3–7(e)). It has an intermediate length and the highest exit angle of the series. The thrust loss due to angularity would be almost 2 percentage points at the design point. Selecting the optimum contour thus becomes a compromise between length (weight) and internal thrust performance. The short isentropic nozzle (fig. 3–7(c)) is probably the best choice of the five shown when thrust and weight are important design criteria.

### 3.2.4 Performance Characteristics

A computer program was written that uses the thrust equations to calculate the internal performance of fixed-area-ratio convergent-divergent nozzles. This program was used to calculate the performance of simple C–D rocket nozzles applied to a typical launch vehicle as follows: An Atlas-Centaur launch vehicle (fig. 3–8), consisting of an Atlas stage-and-a-half concept (fig. 3–9) and the Centaur upper stage (fig. 3–10), was assumed for this example. Rocket nozzles with different area ratios are required for the booster section, the sustainer section, and the upper stage. In order to simplify the example, the following nozzle configurations were selected for the thrust calculations, assuming a constant ratio of specific heats $\gamma$ of 1.286 and a chamber pressure of 600 psi:

| | Nozzle area ratio | Design pressure ratio | Design altitude, ft |
|---|---|---|---|
| Booster section | 8 | 75 | 18 000 |
| Sustainer section | 25 | 360 | 47 000 |
| Upper stage | 50 | 925 | 68 000 |
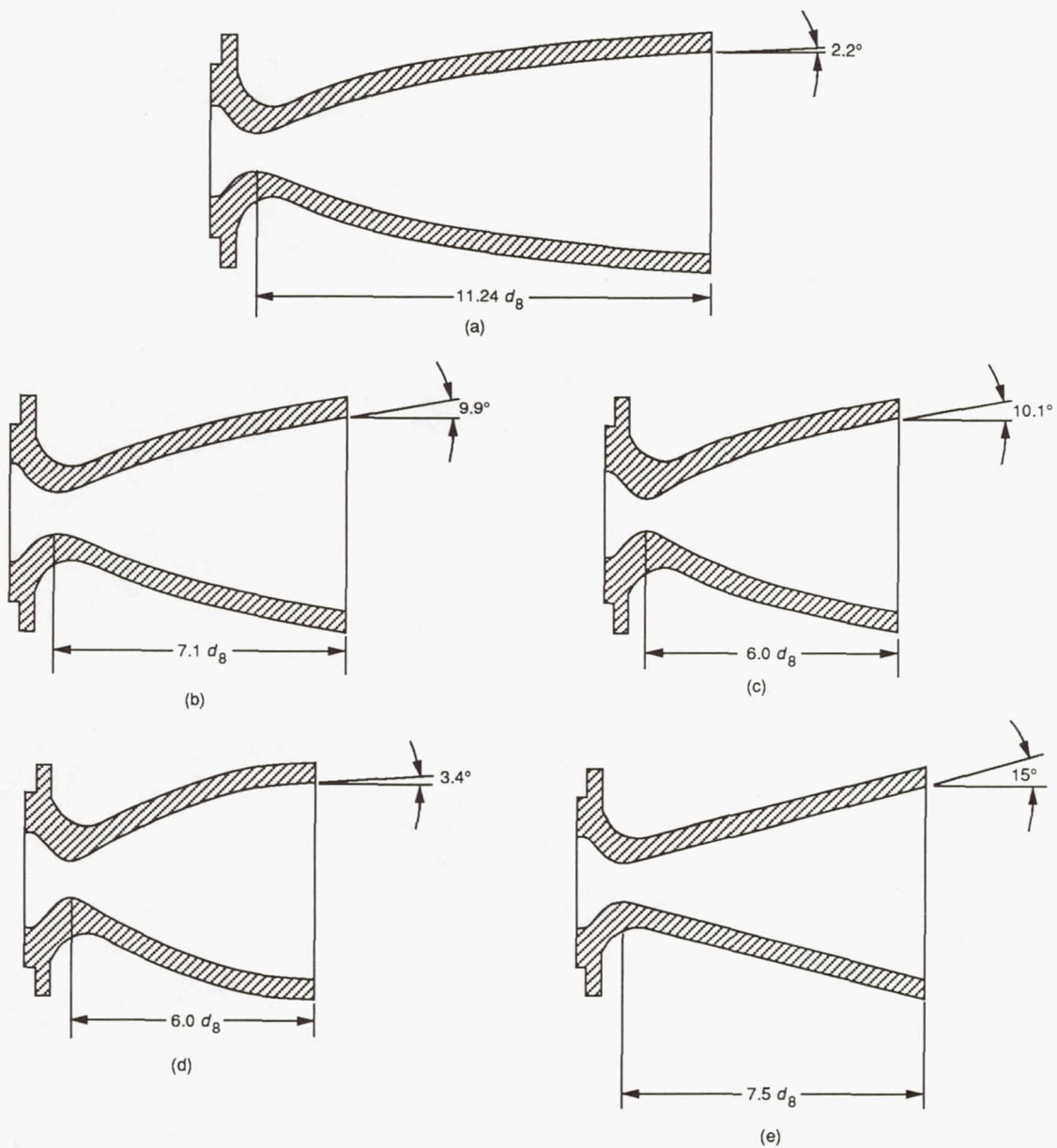
(a) Long isentropic nozzle.
(b) Truncated isentropic nozzle.
(c) Short isentropic nozzle.
(d) Short overturned bell nozzle.
(e) Conical nozzle.

Figure 3–7.—Nozzle divergent shroud shapes.
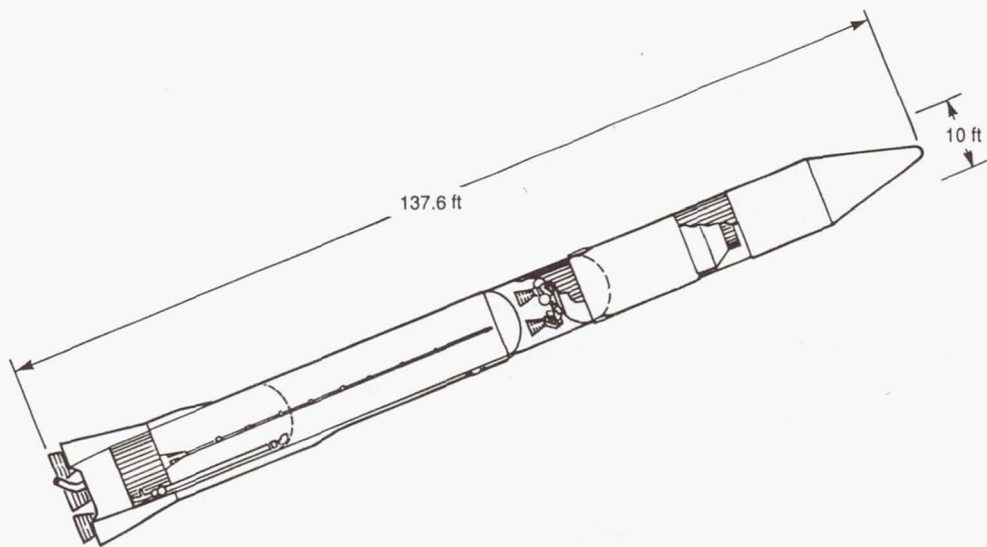
Figure 3-8.—Atlas G–Centaur launch vehicle.

137.6 ft

10 ft



Sustainer section
(contains propellant
tanks for both booster
and sustainer engines)

Booster section
(a half-stage owing to
absence of propellant
tanks in booster
section)
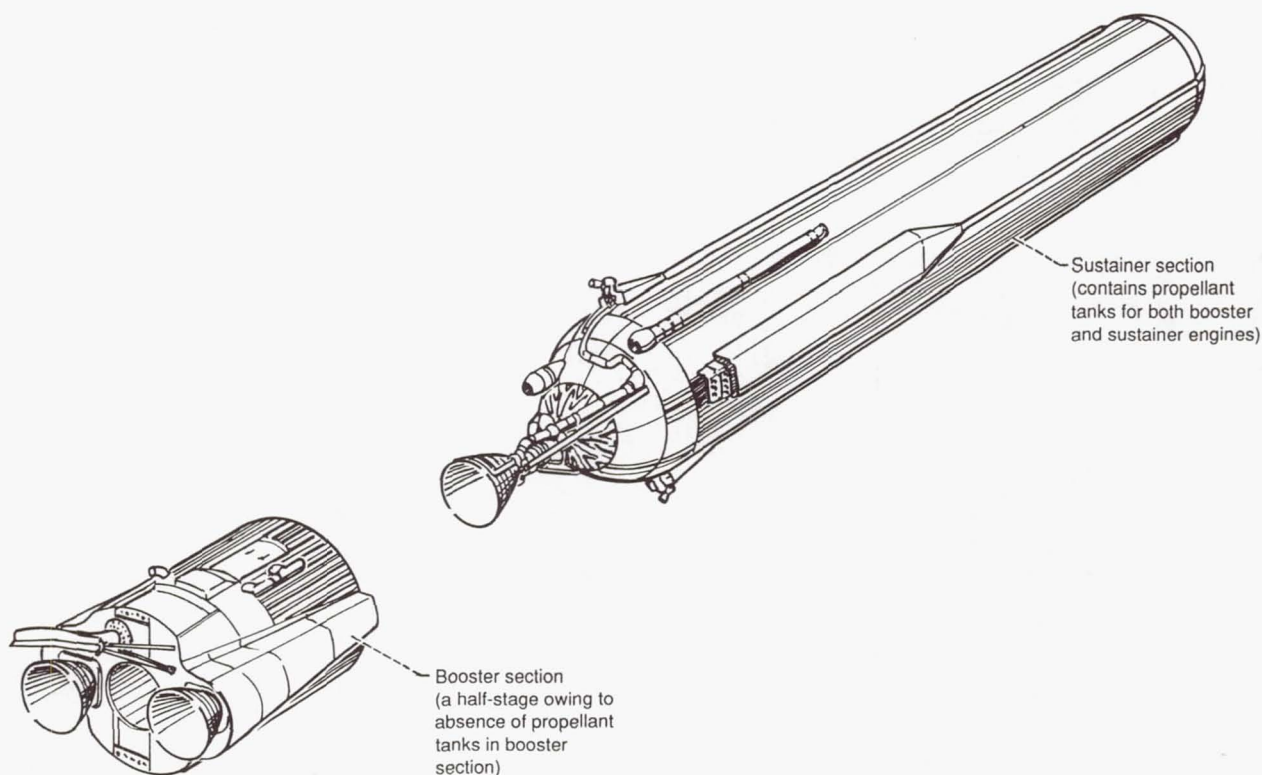
Figure 3-9.—Atlas stage-and-a-half concept.

By using the computer program, the nozzle thrust efficiency was calculated for the three different nozzle configurations over a range of nozzle pressure ratios and vehicle altitudes. For the calculations it was assumed that $C_V C_\theta = 0.99$; $(A_9)_e/(A_8)_e = A_9/A_8$; and $(C_d)_8 = 1.00$. The calculated thrust efficiency for the three nozzle configurations is shown in figure 3-11 over a range of nozzle pressure ratios and in figure 3-12 over a range of vehicle altitudes. These figures reveal that the booster engine nozzles are on design at an altitude of 18 000 ft with booster engine cutoff generally occurring at about 50 000 to 75 000 ft; the sustainer engine nozzle is on design at an altitude of 47 000 ft with sustainer engine cutoff occurring at about 100 000 ft. In addition, the upper-stage nozzles are on design at 68 000 ft. The area ratio selected for the design altitude of the upper-stage nozzles can be limited by the maximum diameter of the upper stage, since the nozzle skirts must be contained within this diameter, as shown in figure 3-10.
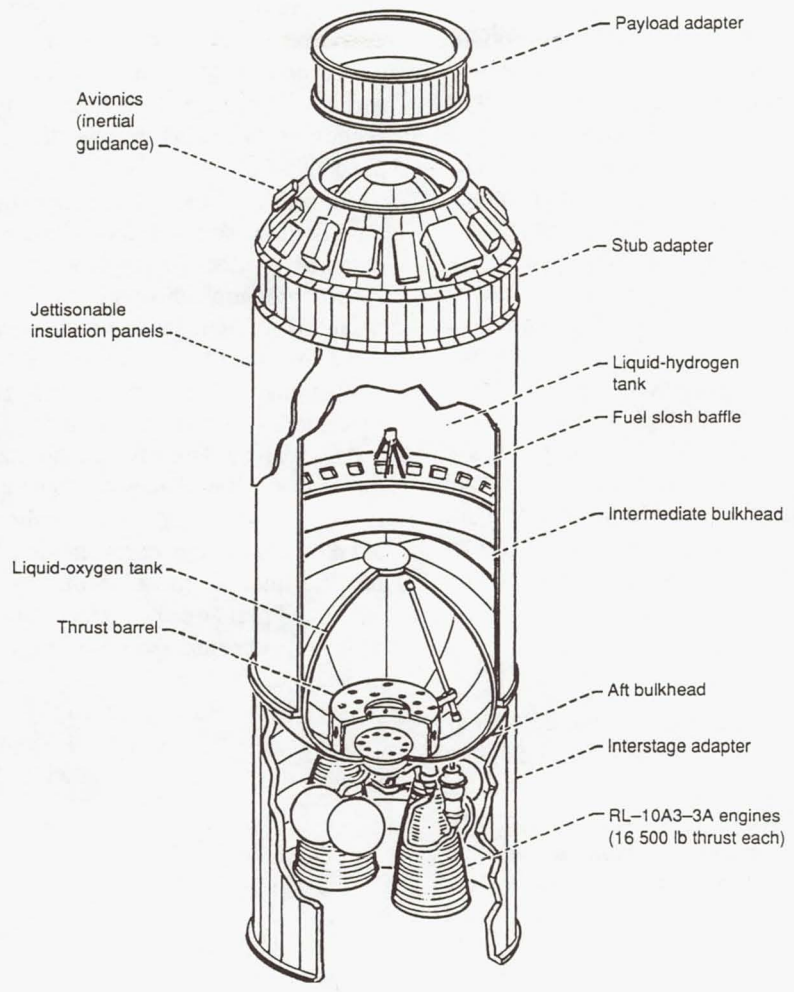
Figure 3–10.—Centaur upper stage.
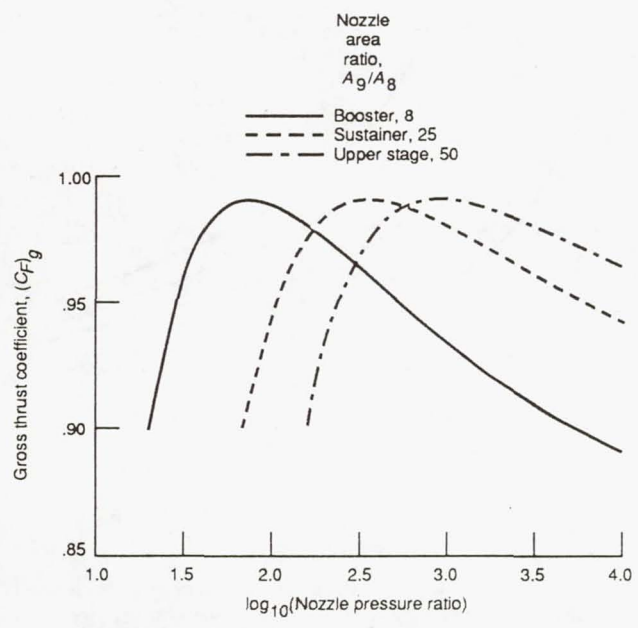


Figure 3–11.—Nozzle thrust versus nozzle pressure ratio.
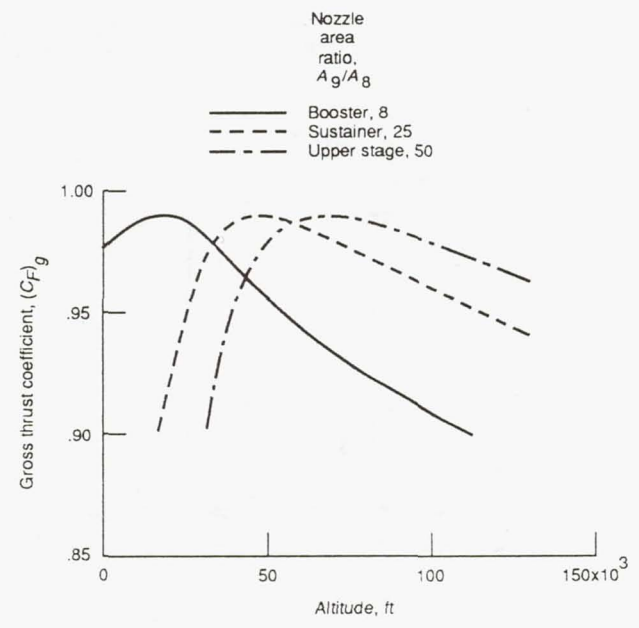


Figure 3–12.—Nozzle thrust versus altitude.

15

## 3.3 Ejector Nozzles

Ejector nozzles are currently being used to provide tailpipe and nozzle cooling for high-speed jet aircraft because they meet the cooling requirements with little loss (or possibly with some gain) in thrust characteristics. The usual advantages of ejectors over other pumping devices, such as lightness and simplicity of construction and maintenance, are also important factors. Various design considerations distinguish the ejector suitable for aircraft cooling from the type commonly employed heretofore. A cooling ejector must pump a small amount of cooling air (typically about 5 percent of the primary air) through a small pressure rise. Depending on the type of cooling-air intake employed and the ducting losses experienced, a pressure drop may be available for an appreciable range of flight speeds.

One of the most important geometrical requirements for ejector nozzle installation on aircraft is that the shroud or mixing section be as short as possible to save weight. In addition, current aircraft design practice usually includes a convergent primary nozzle rather than the convergent-divergent type commonly used with industrial ejectors.

### 3.3.1 Cylindrical Ejectors

A schematic of a typical cylindrical ejector nozzle with its important geometric parameters is shown in figure 3–13. The critical parameters are the diameter ratio $d_s/d_p$ and the spacing ratio $L/d_p$. The factors affecting the pumping characteristics of cylindrical ejectors suitable for aircraft cooling were investigated both theoretically and experimentally and were reported in reference 3–4. The investigation covered a range of $d_s/d_p$ from 1.1 to 1.6, shroud lengths $L$ from 0.20 to 2.28 nozzle diameters, corrected secondary to primary weight flow ratios $\omega\sqrt{\tau}$ from 0 to 0.12, and nozzle pressure ratios from 1.43 to 16.70. For high nozzle pressure ratios the primary jet expanded to a supersonic velocity as it left the nozzle. With no secondary flow the expansion continued until the jet struck the shroud wall and a stable supersonic flow in which the primary stream completely filled the shroud was established. With secondary flow both streams accelerated until the secondary Mach number equaled unity (i.e., until the shroud "choked"). In both cases the flow up to the shroud section at which the expansion ceased was relatively independent of mixing effects.

The results of a simplified theoretical analysis based on each type of flow were in good agreement with experimentally obtained results. The theoretical variation of the minimum ejector pressure ratio with $d_s/d_p$ for several values of $\omega\sqrt{\tau}$ from this reference is shown in figure 3–14. The theoretical values obtained by employing the equations for conservation of mass and momentum have also been shown to be in good agreement with the corresponding experimental values.

An excellent data base on the thrust and pumping characteristics of cylindrical ejectors can be found in reference 3–5. A series of cylindrical ejector shrouds were tested with an afterburning turbojet engine mounted in a nacelle in an altitude facility. Internal thrust, secondary flow pumping characteristics, and pressure and temperature profiles along the ejector walls were obtained. Secondary flow temperature rise and total pressure drop characteristics through the nacelle secondary passage were also determined. The engine power setting was varied from part power to maximum afterburning, yielding exhaust gas temperatures to 3140 °F. In addition, $\omega\sqrt{\tau}$ was

Figure 3–13.—Typical cylindrical ejector nozzle. Diameter ratio, $d_s/d_p$; spacing ratio, $L/d_p$.
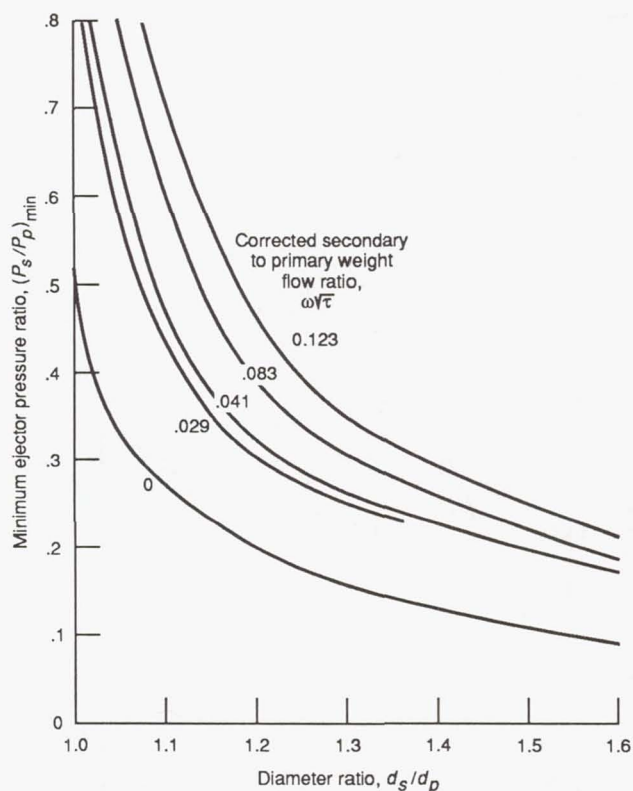
Figure 3–14.—Theoretical variation of minimum ejector pressure ratio with diameter ratio for several values of corrected secondary to primary weight flow ratio $\omega\sqrt{\tau}$.

varied from about 0.02 to 0.08 over a range of nozzle pressure ratios from 2.0 to 9.0. For the ejectors tested the ratio of ejector exit to primary nozzle diameter $d_9/d_8$ ranged from 1.1 to 1.6, and the ratio of ejector length to primary nozzle diameter $L/d_8$ ranged from 0.9 to 2.1.

The thrust and pumping characteristics of 2 of the 17 cylindrical ejector configurations are shown in figure 3–15 as an example of the type of data to be found in reference 3–5. These data are shown as a function of nozzle pressure ratio at interpolated secondary cooling flows of 0.02, 0.04, 0.06, and 0.08. The performance characteristics are shown for a low ejector diameter ratio in figure 3–15(a) and for a high ratio in figure 3-15(b). Similar performance characteristics were recorded for all of the configurations tested. These data, obtained with full-scale hardware and at engine operating conditions, represent an ideal data base for cylindrical ejectors.

The data from reference 3–5 have been cross-plotted in figure 3–16 to show the effect of ejector diameter ratio on the thrust characteristics of cylindrical ejectors. The data are shown over a range of nozzle pressure ratios at $\omega\sqrt{\tau}$ of 0.02 and 0.04. For the range of pressure ratios selected it is obvious that the thrust peaked at an ejector diameter ratio of about 1.17.

Figure 3–17 compares the thrust efficiency of two ejectors that differ only in shroud length. The data are shown for a $d_9/d_8$ of 1.42 and $L/d_8$ of 1.03 and 2.06 (i.e., double the shroud length). Note that the thrust efficiency of both ejectors was comparable at nozzle pressure ratios near the design value of 9.7. However, there was a marked difference at low pressure ratios, with the short ejector having considerably higher thrust efficiency because the primary jet separated more readily from the shroud with the short ejector when the ejector was overexpanded.

The minimum nozzle pressure ratio at which the primary jet separated from the cylindrical shroud is shown in figure 3–18 for the long (length to diameter ratio of about 2.0) and short (length to diameter ratio of about 1.0) ejectors. Again it is obvious that for a given ejector diameter ratio the jet separated from the short shroud at a higher nozzle pressure ratio than it did from the long shroud.

### 3.3.2 Divergent Ejectors

A schematic of a typical divergent ejector nozzle with its important geometric dimensions and flow rates is shown in figure 3–19. The two critical shroud inlet parameters are the



(a) $d_9/d_8 = 1.21$.
(b) $d_9/d_8 = 1.65$.
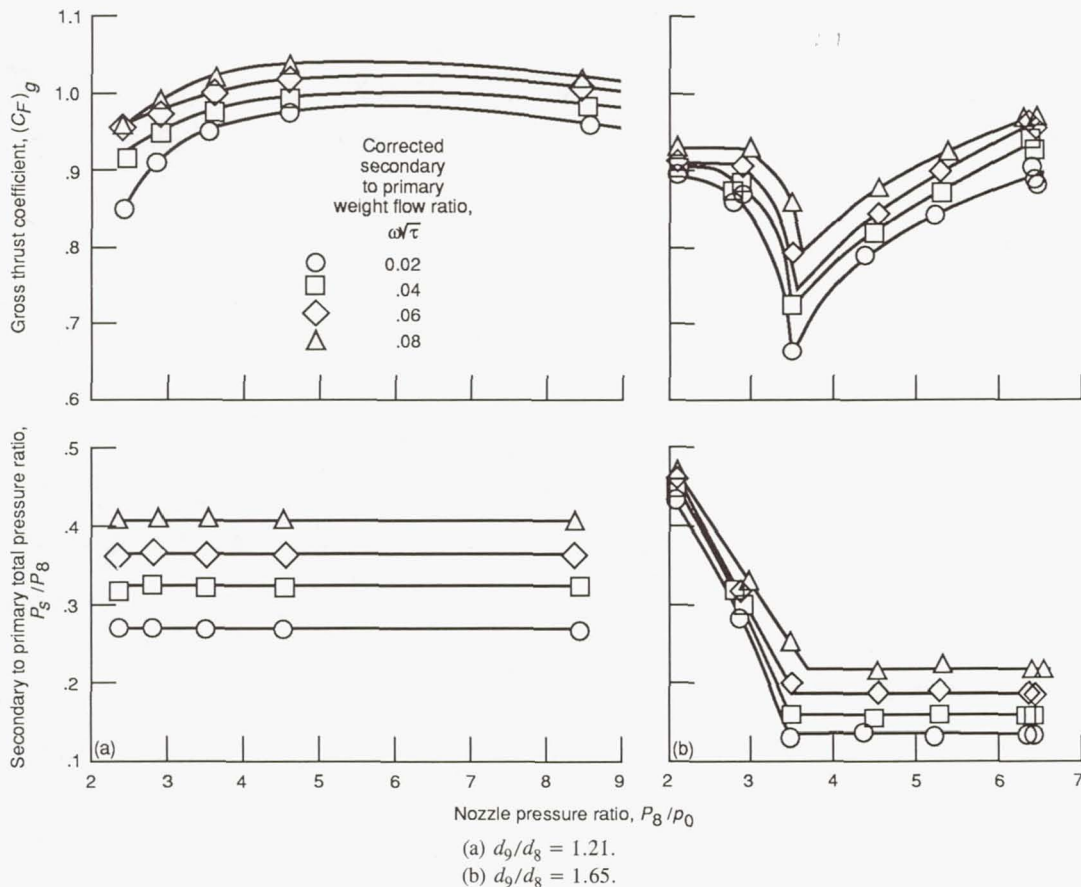
Figure 3–15.—Cylindrical ejector nozzle performance characteristics for two ejector nozzle diameter ratios $d_9/d_8$.

Figure 3-16 region:

Nozzle
pressure
ratio,
$P_8/p_0$

○ 6.0
□ 5.0
◇ 4.0
△ 3.0

Gross thrust coefficient, $(C_F)_g$

1.1
1.0
.9
.8
.7

(a)

(b)

1.1  1.2  1.3  1.4  1.5  1.6  1.7  1.1  1.2  1.3  1.4  1.5  1.6  1.7

Ejector diameter ratio, $d_9/d_8$

(a) $\omega\sqrt{\tau} = 0.02$.
(b) $\omega\sqrt{\tau} = 0.04$.
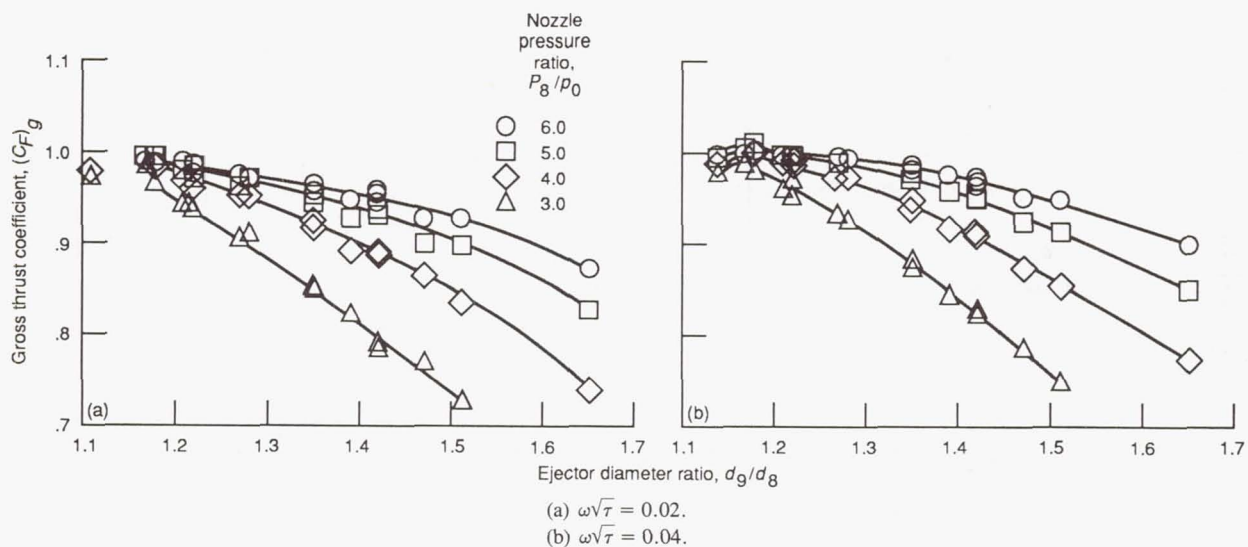
Figure 3-16.—Effect of diameter ratio on cylindrical ejector nozzle thrust for two corrected secondary to primary weight flow ratios $\omega\sqrt{\tau}$.

Figure 3-17 region:

Nozzle efficiency, $F_g / \left[ (F_p)_i + (F_s)_i \right]$

1.0
.9
.8
.7

1.0
.9
.8

(a)
(b)
(c)
(d)

Ejector | Ratio of ejector length to primary nozzle diameter, $L/d_8$
○ Long | 2.06
□ Short | 1.03

0  2  4  6  8  0  2  4  6  8

Nozzle pressure ratio, $P_8/p_0$

(a) $\omega\sqrt{\tau} = 0.02$.
(b) $\omega\sqrt{\tau} = 0.04$.
(c) $\omega\sqrt{\tau} = 0.06$.
(d) $\omega\sqrt{\tau} = 0.08$.
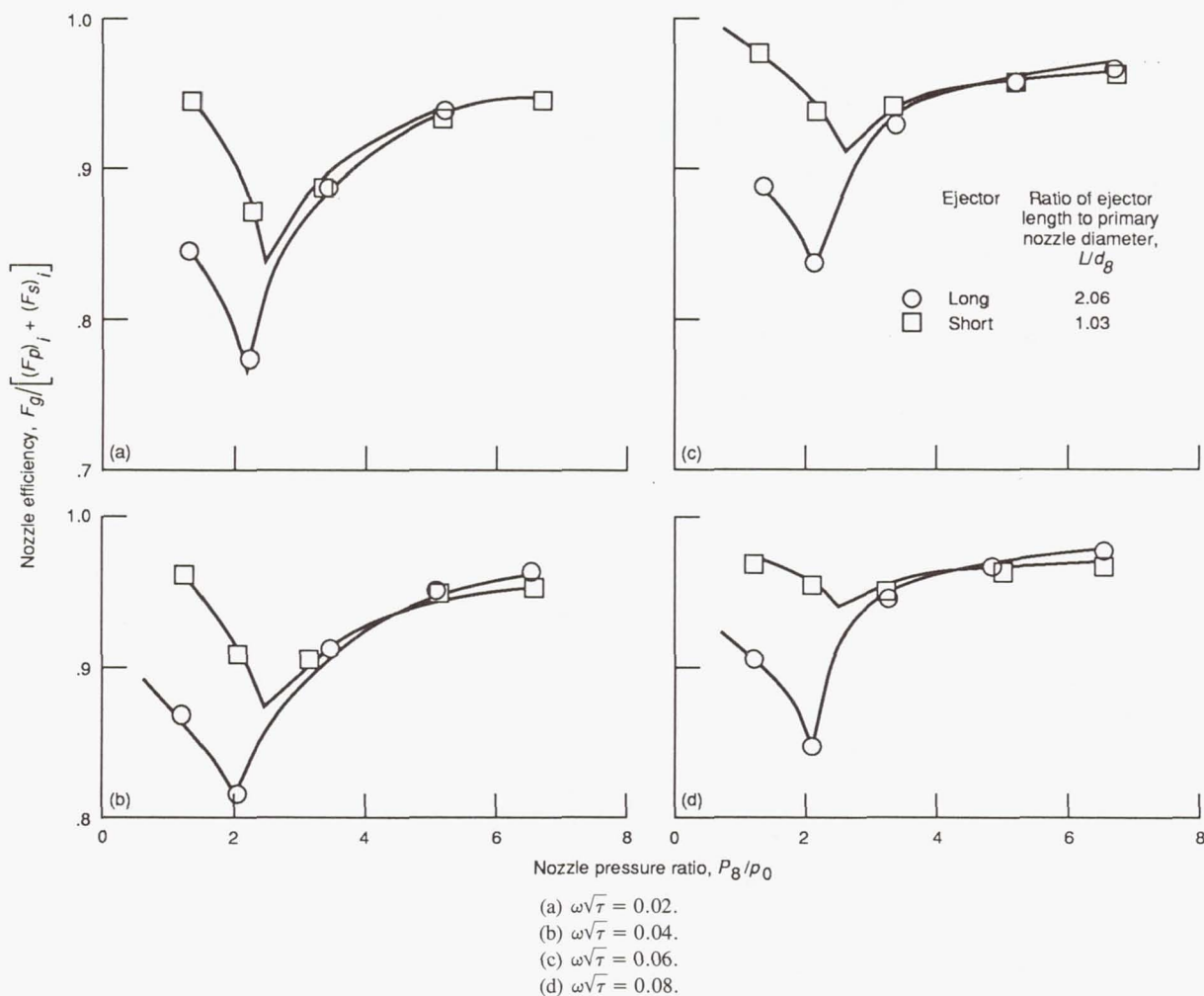
Figure 3-17.—Comparison of thrust characteristics of long and short ejector nozzles for four corrected secondary to primary weight flow ratios $\omega\sqrt{\tau}$. Ejector nozzle diameter ratio, $d_9/d_8$, 1.42; design nozzle pressure ratio, $P_8/p_0$, 9.7.

18
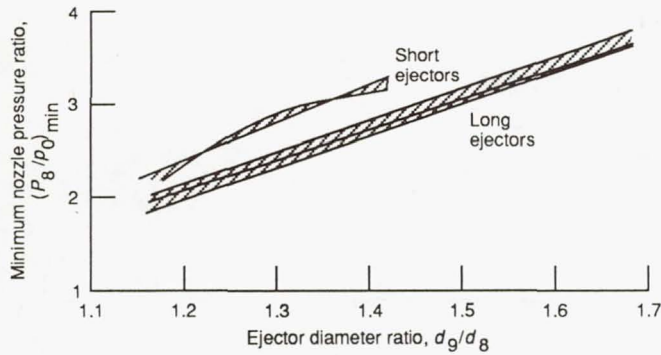
Figure 3-18.—Ejector separation pressure ratio.
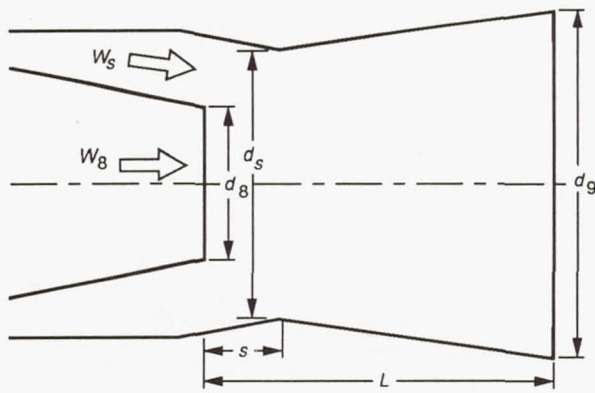


Figure 3-19.—Typical divergent ejector nozzle.

diameter ratio $d_s/d_8$ and the spacing ratio $s/d_8$. The corresponding shroud exit parameters are the diameter ratio $d_9/d_8$ and the spacing ratio $L/d_8$. An excellent data base for divergent ejectors was generated by Convair, a division of the General Dynamics Corporation, in Fort Worth, Texas, in 1958. It was obtained with cold-flow models and included measured thrust and pumping characteristics over a wide range of nozzle pressure ratios. Altogether, 43 configurations were tested covering a range of $d_9/d_8$ from 1.11 to 1.65. Variations were also included for shroud inlet diameter ratios and spacing ratios as well as for the shroud exit spacing ratio. Ejector gross thrust and pumping characteristics for three of the Convair ejector configurations are shown in figure 3-20. The three ejectors selected as examples of the data base include low, intermediate, and high values of $d_9/d_8$ (1.11, 1.35, and 1.65, respectively). As can be seen in these examples, the data cover a wide range of nozzle pressure ratios and $\omega\sqrt{\tau}$. Although this data base is unpublished, it has been used in developing a computer program to calculate the performance of ejector nozzles, as described next.

### 3.3.3 Computer Program for Ejector Nozzle Performance

The General Electric Company has developed a computer software package for calculating ejector nozzle gross thrust and pumping characteristics (ref. 3-6). The work was performed by the General Electric Company for the Foreign Technology Division, Wright Patterson Air Force Base, under Air Force Contract F33600-82-C-0540. The software pack-



| Ejector | Shroud exit diameter ratio, $d_9/d_8$ | Shroud exit spacing ratio, $L/d_8$ | Shroud inlet diameter ratio, $d_s/d_8$ | Shroud inlet spacing ratio, $s/d_8$ |
|---------|------|------|------|------|
| a | 1.11 | 1.04 | 1.11 | 0 |
| b | 1.35 | .86 | 1.26 | 0 |
| c | 1.65 | 1.28 | 1.36 | .24 |

(a) Ejector a.

Figure 3-20.—Divergent ejector nozzle performance characteristics.

Gross thrust coefficient, $(C_F)_g$

Secondary to primary total pressure ratio, $P_s/P_8$

(b)

Gross thrust coefficient, $(C_F)_g$

Secondary to primary total pressure ratio, $P_s/P_8$

(c)

Nozzle pressure ratio, $P_8/p_0$

| Ejector | Shroud exit diameter ratio, $d_9/d_8$ | Shroud exit spacing ratio, $L/d_8$ | Shroud inlet diameter ratio, $d_s/d_8$ | Shroud inlet spacing ratio, $s/d_8$ |
|---------|------|------|------|------|
| a | 1.11 | 1.04 | 1.11 | 0 |
| b | 1.35 | .86 | 1.26 | 0 |
| c | 1.65 | 1.28 | 1.36 | .24 |

Corrected secondary to primary weight flow ratio, $\omega\sqrt{\tau}$

0
.02
.04
.06
.08
.10
.12
.14

(b) Ejector b.
(c) Ejector c.

Figure 3-20.—Concluded.
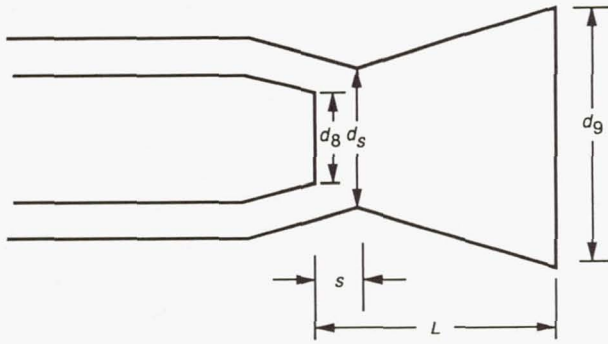
| Ejector | Four geometric parameters that define ejector | | | |
|---|---|---|---|---|
| | $d_9/d_8$ | $d_s/d_8$ | $s/d_8$ | $L/d_8$ |
| Conical[a] | ✓ | ✓ | ✓ | |
| Cylindrical[a] | ✓ | ✓ | ✓ | ✓ |
| Divergent | ✓ | ✓ | ✓ | ✓ |

[a]For conical and cylindrical ejectors $d_s/d_8 = d_9/d_8$.

Figure 3-21.—Sketch of typical ejector nozzle.



Figure 3-22.—Ejector thrust and pumping characteristics. Ejector diameter ratio, $d_9/d_8$, 1.39.

age is based on prediction equations derived by using multiple regression analysis techniques to fit existing ejector nozzle data. The prediction equations are capable of accurately reproducing ejector performance characteristics over a wide range of geometric variables, primary nozzle pressure ratios, and $\omega\sqrt{\tau}$. The program includes performance predictions for conic, divergent, and cylindrical ejector shrouds, as shown in figure 3-21. An extensive literature search was conducted to establish the existing data base. The selected data were entered into a computer data bank, which contained data fully specifying nearly 7000 separate test points for 154 different ejector configurations. In each case the prediction accuracy appears to reflect the accuracy or scatter in the available data, all of which were taken in the 1950's and early 1960's.

### 3.3.4 Inlet-Ejector Matching Characteristics

One of the unique functions of an ejector nozzle is pumping its own secondary flow to provide tailpipe and nozzle cooling. Nozzle thrust and pumping characteristics are usually measured in an experimental test program and are presented as a function of nozzle pressure ratio, as shown in figure 3-22. This configuration was one of the cylindrical ejectors tested at Lewis and reported in reference 3-5. The nozzle performance is shown for a range of $\omega\sqrt{\tau}$ from 0.02 to 0.08. The inlet-ejector matching procedure can be demonstrated by selecting a flight Mach number and a corresponding nozzle pressure ratio. In the example shown in figure 3-23 a Mach number of 2.0 and a pressure ratio of 9 were chosen. The ejector thrust and pumping characteristics were cross-plotted from the preceding figure and presented as a function of $\omega\sqrt{\tau}$.
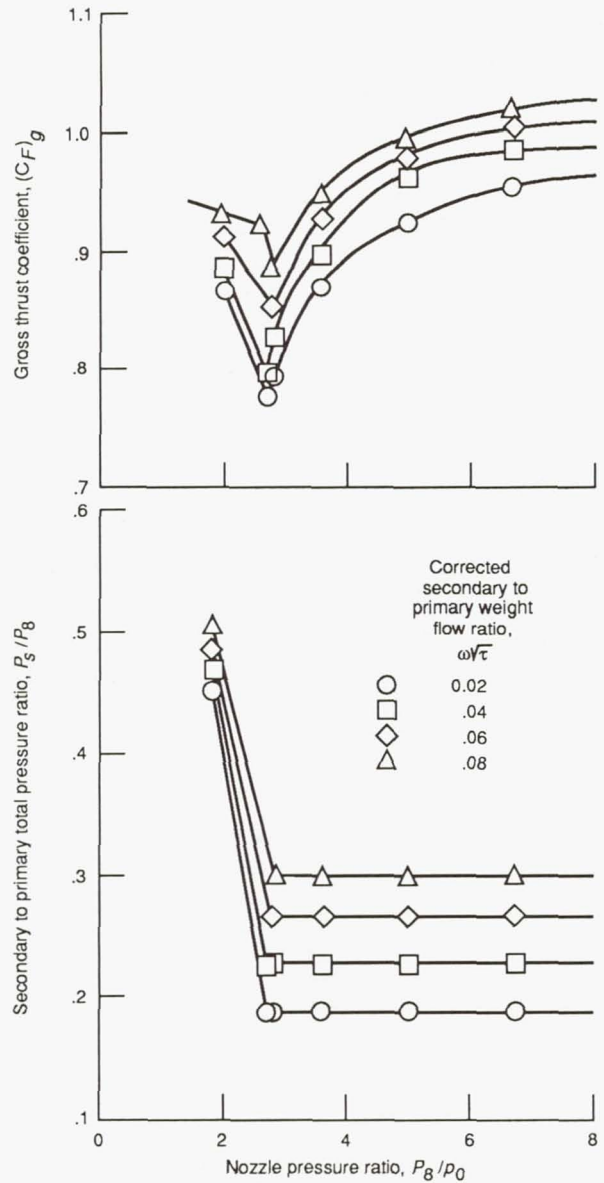
The next step in the matching process is to add the inlet performance curve to figure 3-23. The source of the inlet flow (e.g., bypass flow, boundary layer bleed, or auxiliary inlet flow) is usually specified by the airframe company. The pressure recovery characteristics of the secondary flow depend on the source location and the losses incurred in ducting the cooling flow to the ejector nozzle inlet station. Auxiliary inlets (either flush or scoop) may be located close to or far from the nozzle. An example of the total pressure recovery levels that can be obtained with auxiliary inlets is shown in figure 3-24. The bottom curve represents a low limit where the pressure recovery of the secondary flow is equal to the free-stream static pressure.
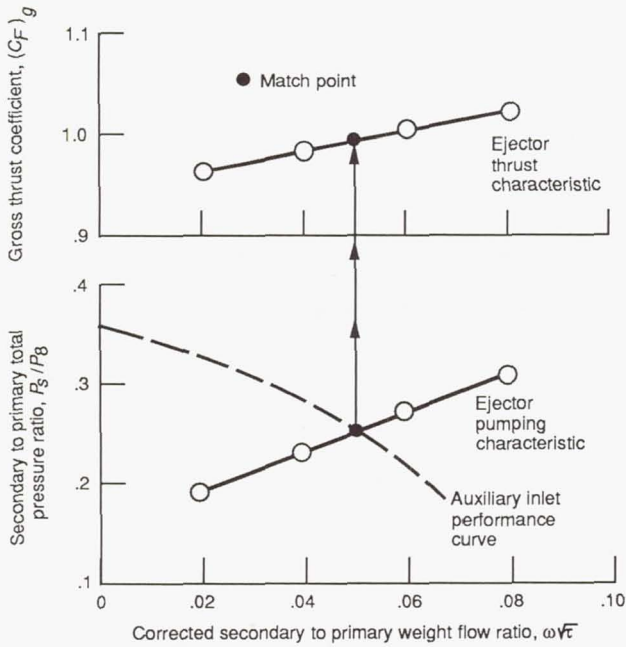
Figure 3-23.—Inlet-ejector matching. Mach number, 2.0; nozzle pressure ratio, 9.0.



Figure 3-24.—Auxiliary-inlet total pressure recovery characteristics.

A recovery level was assumed to complete the matching example and is shown in figure 3-23. The intersection of the inlet performance curve and the ejector pumping characteristic specifies the match point (solid symbol). For the example shown, the cylindrical ejector nozzle would pump an $\omega\sqrt{\tau}$ of 0.05 and provide a gross thrust coefficient of 0.995.

# 3.4 References

3-1. Rao, G.V.R.: Contoured Rocket Nozzles. Ninth International Astronautical Congress, F. Hecht, ed., Vol. 2, Springer-Verlag, 1958, pp. 752-763.

3-2. Sivo, J.N.; Meyer, C.L.; and Peters, D.J.: Experimental Evaluation of Rocket Exhaust Diffusers for Altitude Simulation. NASA TN D-298, 1960.

3-3. Rao, G.V.R.: Approximation of Optimum Thrust Nozzle Contour. ARS J., vol. 30, no. 6, June 1960, p. 561.

3-4. Kochendorfer, F.D.; and Rousso, M.D.: Performance Characteristics of Aircraft Cooling Ejectors Having Short Cylindrical Shrouds. NACA RM E51E01, May 1951.

3-5. Samanich, N.E.; and Huntley, S.C.: Thrust and Pumping Characteristics of Cylindrical Ejectors Using Afterburning Turbojet Gas Generator. NASA TM X-52565, 1969.

3-6. Brooke, D.; and Anderson, B.: Specialized Software Package for Ejector Nozzle Performance. Vols. 1 and 2, General Electric Company, Aircraft Engine Business Group, Cincinnati, OH, 1983.

# Chapter 4
# Supersonic Cruise Exhaust Nozzles

A major problem in designing an exhaust system for a supersonic airplane is that its geometrical shape should change as flight conditions vary. The sonic area and the expansion ratio must be variable for afterburning and for changes in nozzle pressure ratio. It might also be required to reverse and vector thrust and to suppress jet noise or infrared radiation. Because the mechanisms that are needed to vary the geometrical shape can be complicated and heavy, designing exhaust systems involves tradeoffs between weight and performance.

Maintaining high nozzle efficiency at supersonic speeds has not been the most important factor in procuring military aircraft such as the B–70 and the SR–71. However, the whole concept of an economical supersonic transport, such as the British-French Concorde and the Soviet TU–144, depends on obtaining the maximum propulsion and aerodynamic efficiency from all aircraft components. At the supersonic cruise point the ratio of lift to drag is low and the specific fuel consumption is high relative to subsonic jetliners. The aircraft payload weight thus becomes highly sensitive to nozzle efficiency. For example, for the Concorde at its cruise speed of Mach 2.2 a 1-percent decrease in nozzle performance is estimated to be equivalent to an 8-percent loss in payload. It is therefore evident that the design of the exhaust nozzle cannot be compromised at the supersonic cruise point.

Commercial transports, however, must also be efficient at the other flight speeds. An efficient nozzle can help reduce the jet noise at takeoff. The aircraft must also be efficient at subsonic speeds for subsonic cruise, hold, or diversion to alternative airports. Because most aircraft have high drag at transonic speeds, an efficient nozzle will provide the maximum excess thrust for efficient acceleration through the transonic regime with minimal reheat.

## 4.1 Evolution of Nozzle Variability

This discussion of the evolution of nozzle variability focuses on air-breathing propulsion systems. In general, rocket nozzles do not include provisions for varying the area ratio, since they are staged to minimize weight and optimum area ratios can be selected for each stage and altitude. The selected fixed geometry is usually a compromise that obtains reasonable performance over the entire proposed flight trajectory.

### 4.1.1 Subsonic Aircraft

Today's commercial subsonic transports do not generally require area variation in the exhaust nozzle system. These nozzles operate at low nozzle pressure ratios, from 2.0 to 3.0, so that a simple convergent or a very low-area-ratio convergent-divergent nozzle produces adequate thrust. The losses due to underexpansion at the cruise speed are usually less than 1 percent. Because these commercial airliners do not feature afterburners, throat area modulation is not required. In contrast, military aircraft have used afterburners for many years; the variable-area nozzle throat is not uncommon on these vehicles. At subsonic speeds the variation in nozzle primary area is all that is needed for good thrust performance when afterburning is required.

### 4.1.2 Supersonic Aircraft

The simple, fixed-area, convergent and very low-area-ratio C–D nozzles are normally inadequate for supersonic flight speeds, especially at Mach 2.0 to 3.0 and above. Nozzle pressure ratios increase rapidly above Mach 1.0, as seen in figure 4–1. For example, at Mach 2.0, a simple convergent nozzle operating at a nozzle pressure ratio of 14 would have about a 12-percent loss in thrust from underexpansion. As a result supersonic military aircraft are now equipped with convergent-divergent nozzles. Initially these nozzles had fixed secondary shrouds; more recently they have completely variable nozzle hardware. However, high expansion efficiency at supersonic speeds has not been an important consideration for military aircraft, especially those with only supersonic dash capability, such as the B–58, F–4, F–111, B–1, and F–14. These supersonic dash aircraft fly long distances subsonically but are also able to go supersonic for relatively short periods of time.

As an example, the nozzle used for the Mach 2.0 B–58 bomber featured a completely variable convergent primary
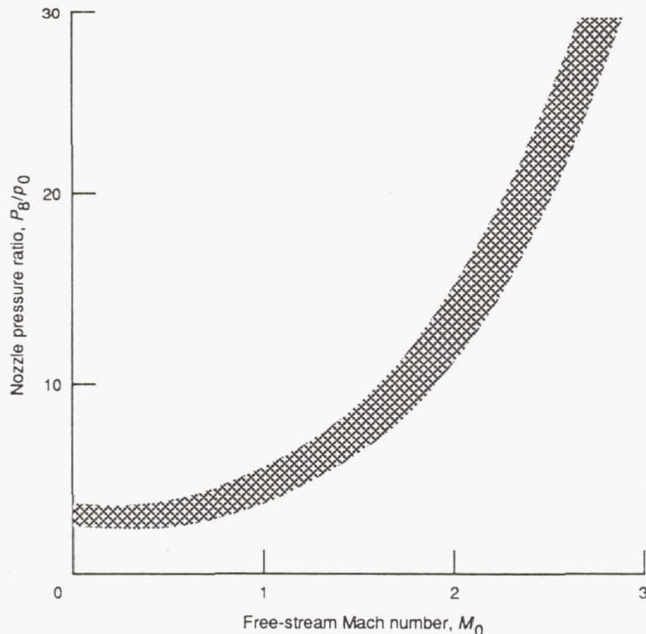
Figure 4–1.—Typical nozzle pressure ratio schedule for supersonic cruise aircraft (dependent on engine cycle, e.g., turbofan or turbojet).

expand and only fill a part of the divergent shroud. Auxiliary air from the free stream or inlet bypass is used to fill the excess area and thus prevent overexpansion of the primary flow. The auxiliary inlets can either be actuated or aerodynamically positioned (free floating). Another type of nozzle, the plug nozzle, automatically adjusts the free streamline with nozzle pressure ratio aerodynamically.

### 4.1.4 Variability Required for Supersonic Cruise Aircraft Nozzles

The exhaust nozzle for a supersonic cruise aircraft must be efficient over Mach numbers from takeoff to supersonic cruise. The corresponding nozzle pressure range can vary from a low of 2.0 to 4.0 at takeoff to as high as 30.0, depending on the cruise speed and altitude selected, as shown in figure 4–1. A simple convergent nozzle would be desirable at takeoff and subsonic speeds (fig. 4–2) but inefficient at transonic and supersonic speeds. On the other hand, a fixed convergent-divergent nozzle that is efficient at supersonic cruise suffers from large overexpansion losses at transonic speeds. As is evident from figure 4–2, the nozzle area ratio must be varied continuously to maintain high performance at all flight conditions.

As mentioned previously, nozzle performance cannot be compromised at supersonic cruise conditions, since the payload weight is highly sensitive to nozzle efficiency. Because the largest area ratio is required at supersonic cruise, the nozzle may have the configuration shown in figure 4–3(d). At supersonic cruise conditions the nozzle is fully expanded. The divergent shroud can be shaped to minimize internal shock and divergence losses. The nozzle exit diameter is usually the largest dimension of the nacelle, so that the external shroud may be cylindrical. Under these conditions the effect of the

nozzle and a two-position divergent shroud. The shroud had a small exit area for nonafterburning subsonic cruise and a larger exit area for supersonic dash when the afterburner was on and the nozzle was operating at a high pressure ratio.

Military aircraft with supersonic cruise capability have required more sophisticated nozzle systems than those with supersonic dash capability. Independent control is normally required of the throat area to match the afterburning requirements, and a separate control of the exit area provides the proper expansion ratio at each flight speed and altitude. The Mach 3.0 B–70, for example, used a C–D ejector nozzle that featured independent control and actuation of both the convergent and divergent portions.

### 4.1.3 Methods of Varying Nozzle Geometry

The nozzle area can be varied either mechanically or aerodynamically. Historically, the convergent portion (primary nozzle) has been positioned mechanically. Iris primary nozzles feature a number of flaps and seals, with the latter usually riding on the flap surfaces. Iris secondary shrouds have also been used, again made up of alternate flaps and seals; these shrouds were initially positioned mechanically (e.g., B–58 and B–70). Later attempts were made (e.g., on the F–111 and SR–71) to free float the outer shroud in order to decrease weight and eliminate the complexity of an added actuation system.

The so-called ejector nozzles are able to change the nozzle exit area while maintaining a fixed shroud. At low pressure ratios, where the exit area is too large, the primary gases
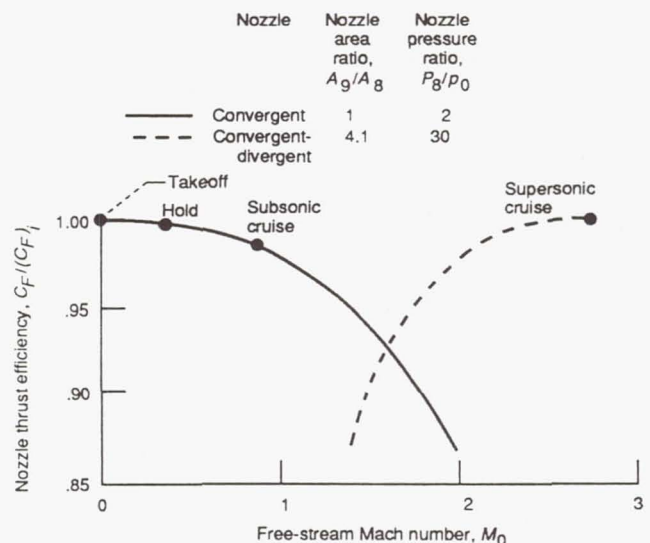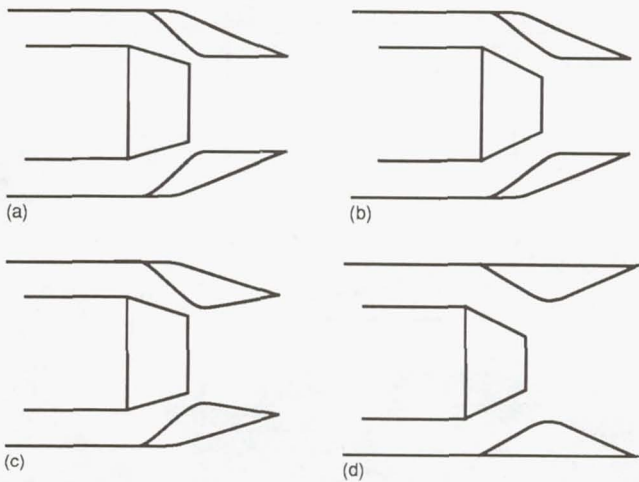


Figure 4–2.—Variation of nozzle efficiency for fixed-geometry nozzles.

(a) Takeoff (nozzle pressure ratio, ~3; exhaust gas temperature, ~3140 °F). Important considerations: pumping, cooling, noise.

(b) Subsonic cruise or loiter (nozzle pressure ratio, ~4; exhaust gas temperature, ~1340 °F). Important consideration: boattail drag.

(c) Transonic acceleration (nozzle pressure ratio, ~7; exhaust gas temperature, ~3140 °F). Important considerations: boattail drag and cooling.

(d) Supersonic cruise or dash (nozzle pressure ratio, ~28; exhaust gas temperature, ~1740 °F). Important consideration: high internal performance.

Figure 4-3.—Nozzle operating modes.

external stream is negligible, and nozzle efficiencies can be as high as 98 to 99 percent of the ideal.

At off-design speeds the required nozzle area ratios are lower, particularly at takeoff and subsonic conditions (figs. 4-3(a) and (b)). This results in a reduction of the nozzle exit area and a boattailed nacelle with its corresponding external drag. At the subsonic cruise condition, when the engine is throttled to a low power setting, the boattail drag can be as large as 15 to 20 percent of the net thrust of the engine. By studying the tradeoffs between internal thrust and external drag, it is possible to arrive at the optimum geometry to provide the maximum thrust minus external drag.

Note that in figure 4-3 the nozzle throat area varies to accommodate various levels of exhaust gas temperature and total pressure. The nozzle operates under maximum afterburning conditions at takeoff and transonic acceleration, where cooling and pumping characteristics become important. Nozzle jet noise also becomes an important consideration near airports and over surrounding communities during takeoff and landing.

Reference 4-1 presents an excellent discussion on the exhaust nozzle design philosophy for several exhaust nozzle systems that can be installed on commercial supersonic aircraft propulsion systems. Three basic exhaust systems emerged as promising candidates for this application:

(1) Convergent-divergent nozzle
(2) Two-stage ejector nozzle
(3) Annular plug two-stage ejector nozzle

Integration of the reverser and secondary air system require-

ments into the exhaust nozzle is also covered. Performance data from scale model tests are presented, along with a discussion of the advantages and disadvantages of each system.

## 4.2 Nozzle Concepts of Interest

The basic nozzle types being considered for supersonic cruise aircraft include ejector nozzles and the low-angle annular plug nozzle, as shown in figure 4-4. Engine contractors developed the ejector nozzles and the Government in-house effort concentrated on the low-angle plug nozzle. A brief description of each of these nozzle types follows.

### 4.2.1 Variable-Flap Ejector Nozzle

The variable-flap ejector nozzle (fig. 4-4(a)) uses secondary flow to cushion the expanding primary stream. The primary flow pumps the secondary air, which is used primarily for internal cooling of the afterburner liner, the primary nozzle, and the secondary shroud. The shroud lengths are usually less than that required for the primary and secondary flows to be completely mixed. Because ejector flow is quite complicated, many early nozzles were empirically designed.

For afterburner operation in a turbojet engine the primary area is varied about 40 percent, and some kind of iris mechanism is required. The nozzle exit area is also variable and can either be actuated or aerodynamically positioned. The divergent shroud is made up of several overlapping flaps and seals so that it can be opened at supersonic speeds and closed at subsonic speeds. Because only a small amount of secondary flow is used in a turbojet, this nozzle requires the largest variation in exit area and correspondingly the highest boattail angles at off-design speeds. A typical subsonic boattail angle would be 15°. The variable-flap ejector nozzle has been used on the B-58 and B-70 bombers.

### 4.2.2 Auxiliary-Inlet Ejector Nozzle

At the supersonic cruise point the auxiliary-inlet ejector nozzle is similar to the variable-flap ejector nozzle, and secondary flow is still used to cool the hot parts. At low speeds the divergent shroud also has multiple flaps and seals, but in order to simplify the flap mechanism and to reduce boattail area, it does not close down as far as the variable-flap ejector nozzle. Auxiliary inlets are opened in the secondary flow passage at these low speeds to bring in additional air to help fill the exit area. The dashed lines in the sketch of figure 4-4(b) indicate the position of the doors when the inlets are opened. The minimum diameter inside the shroud is larger than it is on the variable-flap ejector nozzle so that the auxiliary inlet air can get through. Note that the auxiliary inlet doors can be actuated or free floating. Free-floating doors may be susceptible to stability problems and installation effects.

25
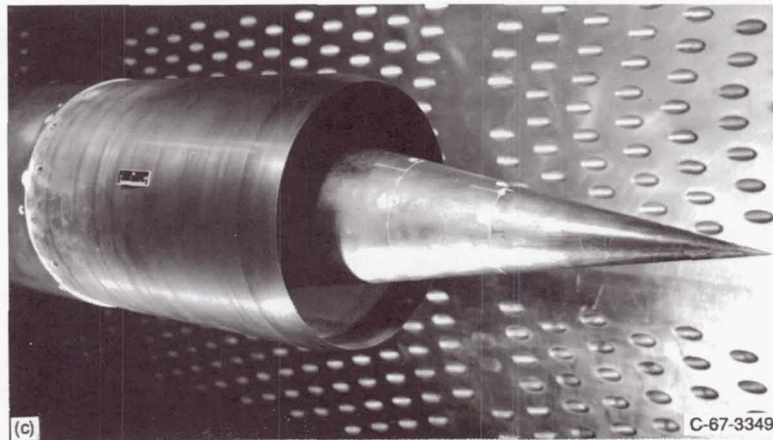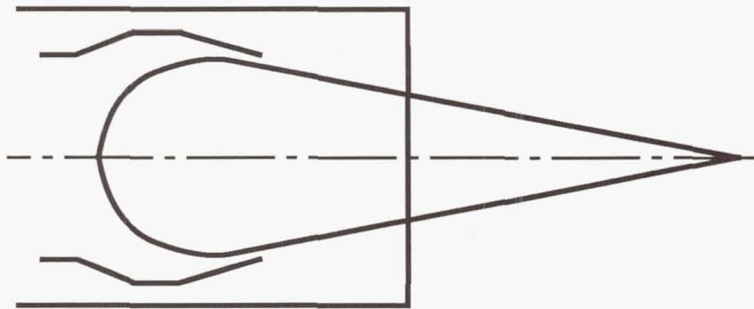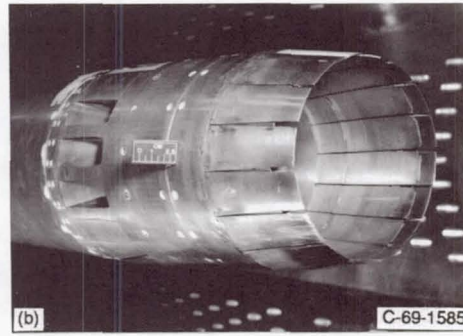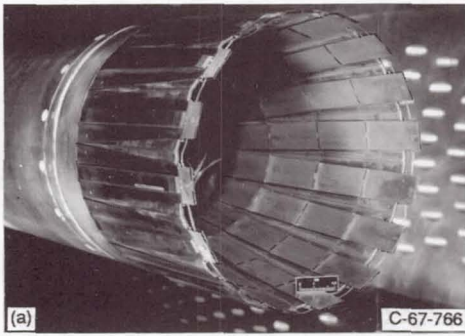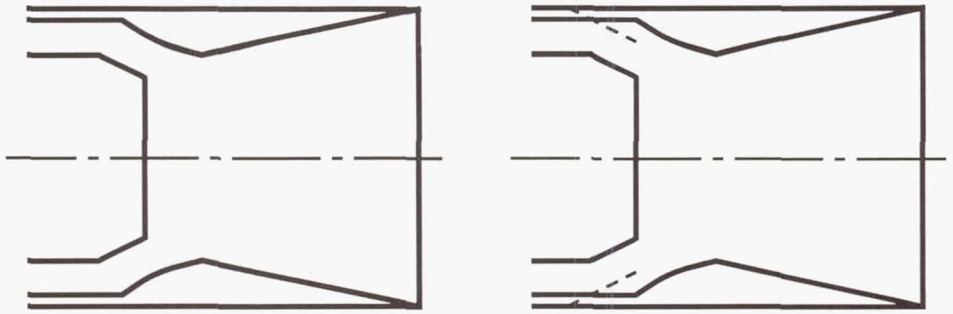
(a) Variable-flap ejector.
(b) Auxiliary-inlet ejector.
(c) Plug.

Figure 4–4.—Exhaust nozzle concepts for supersonic cruise aircraft.

Auxiliary-inlet ejector nozzles have been used on the F–111 and SR–71 aircraft and are being considered for low-noise nozzles.

### 4.2.3 Plug Nozzle

The conical plug nozzle shown in figure 4–4(c) is a more recent idea than the divergent ejectors and has not yet been used on a supersonic production engine. The outer boundary of the divergent shroud is replaced by a free streamline that can adjust automatically with changes in nozzle pressure ratio and thus maintains a high thrust efficiency over a wide range of expansion. The ability of the plug nozzle to be "altitude compensating" and to eliminate overexpansion losses has been demonstrated experimentally.

If it is to be used in an afterburning engine, the plug nozzle must include some way to vary the primary area. Various schemes to vary the throat area include the standard iris flap, translation of a fixed flap or plug, and the variable-area centerbody. At high speeds internal expansion occurs in the annular flow passage between the plug and the outer shroud. The internal expansion ratio can be varied by translating the outer shroud. At low speeds the shroud is completely retracted so that the flow is not overexpanded and the primary flap is exposed to the external flow. Because low-angle plugs (half-angles of 10°) tend to be long, it may be desirable to truncate some portion of the plug.

One of the main problems of a plug nozzle applied to an afterburning engine is the method of cooling the plug and its support struts, or sting. Several cooling concepts have been proposed, as shown in figure 4–5, and include convection, film, and transpiration cooling. A completely convection-cooled plug (fig. 4–5(a)) may also discharge its cooling flow in the base of a truncated plug to reduce the plug base drag. From an overall performance consideration it may be better to convectively cool part of the plug and to film cool the rest (fig. 4–5(b)). It is desirable to obtain the maximum thrust from the cooling flow. A transpiration-cooled plug is also of interest (fig. 4–5(c)), where the plug would be fabricated from a porous material and the cooling air blown through.

If the cooling problem can be solved, the plug nozzle has some distinct advantages. First, it would not leak as much as a nozzle with flaps and seals, since the length of seal between the movable surfaces could be decreased by an order of magnitude. In addition, the actuation mechanisms appear to be simpler and might be more durable. Finally, some jet noise tests also indicate that annular flow is inherently a little quieter than an equivalent circular jet.

## 4.3 Supersonic Cruise Performance

The first step in calculating the performance of an exhaust system for a supersonic cruise aircraft is to get some idea how sensitive a mission is to its design. Some results of an analysis



(a) Convection.
(b) Film.
(c) Transpiration.
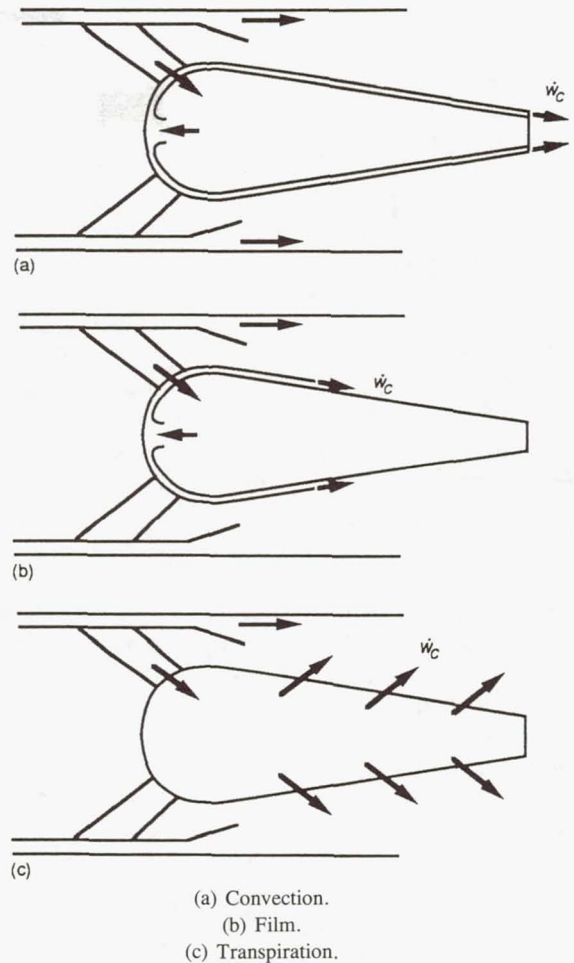
Figure 4–5.—Plug nozzle cooling concepts.

for a supersonic cruise aircraft are shown in figure 4–6. The aircraft is assumed to have a takeoff gross weight of 750 000 lb and a payload equal to 6.5 percent of the takeoff weight (49 000 lb). In figure 4–6(a) the changes in range for a 1-percent change in nozzle gross thrust coefficient at cruise and loiter are compared with the changes in range for a 1-percent change in nozzle weight. The cruise speed is Mach 2.7 and the range is 3930 nautical miles. Getting enough range out of a supersonic cruise aircraft has always been a fundamental problem, and it is even more critical for commercial operations. For this mission the cruise nozzle efficiency affects range by 3.5 percent and is quite important. In fact, a 1-percent gain here is at least three times as effective as a 1-percent gain in performance of any other component of the propulsion system. In figure 4–6(b) it is assumed that this same airplane flies an all-subsonic mission at a cruise speed of Mach 0.9 for 3280 nautical miles. A 1-percent change in subsonic cruise thrust coefficient affects range by about 2 percent, and the sensitivity to loiter thrust is the same as it was before. It can be worth a great deal of nozzle weight to keep performance high at all flight speeds.

(a) Supersonic cruise mission (Mach 2.7). Range, 3930 n mi.
(b) Subsonic cruise mission (Mach 0.9). Range, 3280 n mi.

Figure 4–6.—Mission sensitivity to exhaust nozzles. Supersonic cruise aircraft; takeoff gross weight, 750 000 lb; payload, 49 000 lb.

## 4.3.1 Ejector Flow Model

Because the performance of a high-speed nozzle is important, small geometric differences can affect the optimization of its design. Many configurations must be tested, but their experimental performance is hard to measure with sufficient accuracy to predict range. Some methods of analysis have been improved and are becoming quite helpful in determining supersonic cruise performance.

The ejector flow model is based on the inviscid and viscid interaction between a high-energy stream (primary flow) and a low-energy stream (secondary flow) as shown in figure 4–7. These two streams begin to interact at the primary nozzle lip. For the ejector operating in the supersonic regime the secondary flow is effectively "sealed off" from ambient conditions. When this occurs, the ejector mass flow characteristics become independent of the ambient static pressure. It is this ejector operating condition that is considered in the theoretical analysis. The flow regimes occurring within the ejector system can be categorized on the basis of the predominant flow mechanisms.



(a) Low secondary flow (impingement).
(b) High secondary flow (choked).

Figure 4–7.—Divergent ejector flowfield.

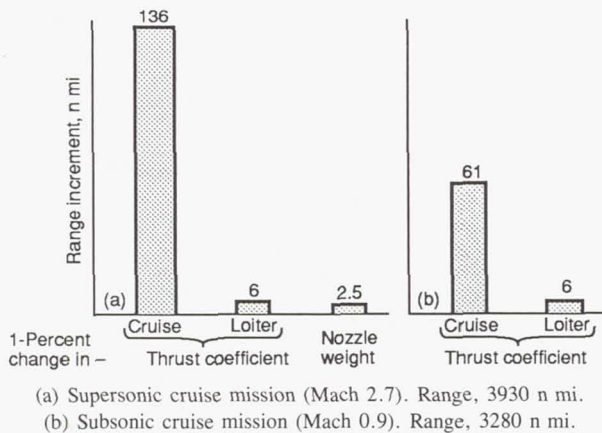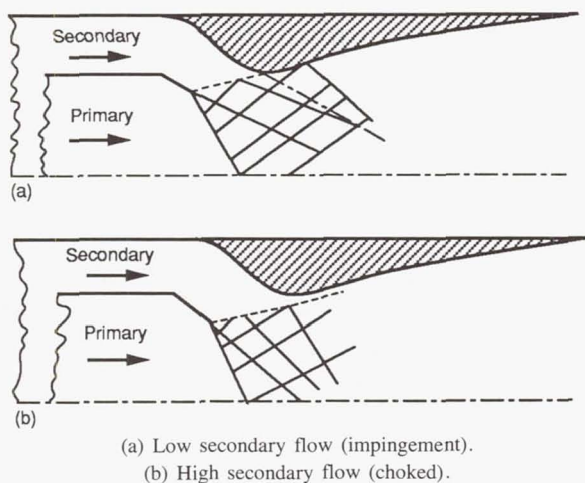When the secondary flow to the ejector is low, the primary flow plumes out and impinges on the shroud wall, as shown in figure 4–7(a). This causes an oblique shock to form and effectively seals off the secondary flow from ambient conditions. The secondary flow is "dragged" through the oblique shock by mixing with the higher velocity primary jet flow. If the secondary flow is increased, the secondary pressure increases and pushes the primary jet away from the shroud wall. Because the oblique shock can no longer be sustained at the shroud wall, the secondary flow accelerates and chokes within the shroud, as shown in figure 4–7(b).

The aerodynamic phenomena that determine equilibrium conditions at low secondary ejector flows are the same as those that determine the base pressure behind a rearward-facing step. The zero secondary flow, which is the mass flow entrained by the mixing process, must be equal to the mass flow reversed by the pressure rise through the recompression zone (oblique shock). This condition is satisfied when the total pressure on the dividing streamline in the mixing zone equals the recompression static pressure rise. Within this base flow concept, the fluid that leaks past the recompression zone has a total pressure greater than the pressure rise through the recompression zone. Equilibrium conditions are thus established in the low ejector flow regime when the amount of secondary flow supplied to the ejector is equal to the fluid that leaks past the recompression zone associated with the oblique shock.

For high ejector flows the interaction between the two streams is such that the secondary flow accelerates to a sonic condition somewhere downstream of the primary nozzle lip. The viscous interaction between the two streams occurs along the interface, dashed lines in figure 4–7. Mixing transfers energy (shear work) from the primary jet flow to the secondary stream and modifies the pumping characteristics due to the displacement thickness of the mixing zone.

## 4.3.2 Comparison of Theory and Experiment

In figure 4–8 the two effects of mixing are evaluated for an ejector with a large secondary shoulder diameter relative to its primary nozzle exit diameter. An inviscid analytical solution (solid curve) is obtained if mixing between the two streams is neglected. The primary flowfield is determined by the method of characteristics; the secondary flow is assumed to be one-dimensional, adiabatic, and reversible. Two conditions were applied along the interface boundary: (1) the local static pressure must be equal for both streams at their boundary and (2) continuity between the streams must be preserved. The effects of mixing along the interface boundary have been evaluated by locally superimposing the mixing region on the established inviscid flowfield solution (solid curve) at the critical secondary flow area. The assumption is that mixing takes place as though the interface were a constant-pressure boundary. The results of such a mixing correction are represented by the long-dashed line in figure 4–8.
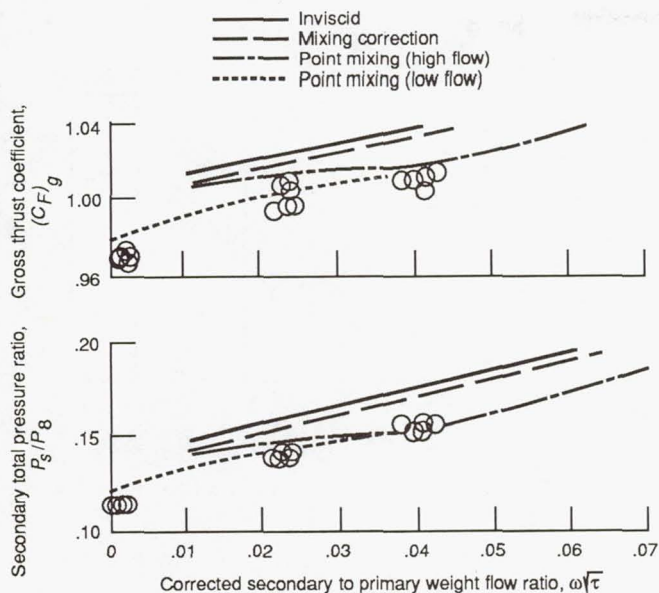
Figure 4–8.—Comparison of experimental and theoretical ejector characteristics.



Figure 4–9.—Shroud contour sensitivity of auxiliary-inlet ejector nozzle. Corrected secondary to primary weight flow ratio, $\omega\sqrt{\tau}$, 0.02.

Inherent in this type of mixing correction is the assumption that the displacement effects from mixing have a negligible effect on pumping characteristics. When this kind of correction is used, the effects of mixing result in an increase in the corrected secondary to primary weight flow ratio $\omega\sqrt{\tau}$ over that given by the inviscid solution. Continuity is thus preserved by increasing the initial $\omega\sqrt{\tau}$ by the amount that was entrained as a result of mixing and by assuming the two flowfields are not appreciably changed by mixing.

In order to account for the changing shape of the primary jet boundary due to mixing, the mixing correction must be applied at each point along the interface boundary. The results of this type of mixing solution are shown in figure 4–8 for both low and high $\omega\sqrt{\tau}$. Continuity was applied along the interface boundary by requiring that the sum of the inviscid weight flow ratio plus the mixing component be the same as the $\omega\sqrt{\tau}$ supplied to the ejector. This requirement resulted in a much larger mixing effect than was originally calculated. In general, these solutions agreed quite well with the data, as indicated by the circular symbols in figure 4–8.

### 4.3.3 Shroud Contour Sensitivity

The foregoing analysis is particularly useful in trying to find the best shape for the divergent shroud. For the auxiliary-inlet ejector the minimum diameter at the shoulder must be relatively large to accommodate the auxiliary air at off-design speeds. The position of this shoulder downstream of the primary nozzle exit must then be chosen to ensure high nozzle performance.

Figure 4–9 shows calculations that help in making this choice. The nozzle gross thrust coefficient is shown as a function of the spacing ratio, which is defined as the distance between the shoulder and the primary nozzle exit divided by the primary nozzle exit diameter. With a relatively sharp contour at the shoulder an abrupt loss in thrust occurs if the spacing is too small, as shown by the lower curve. If the shoulder is more rounded, the ejector is less sensitive to spacing, and higher performance results, as indicated by the upper curve. In most designs the position of this shoulder is fixed, but the flaps must be moved to vary the divergent shroud exit area.
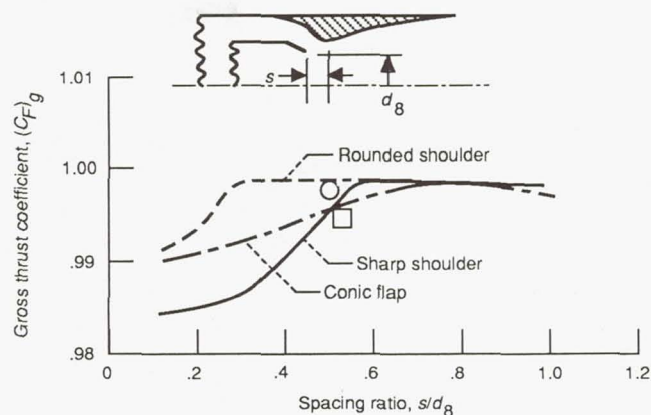
The shape of these flaps is another design variable. For the sharp-shoulder performance curve it was assumed that the flaps had an isentropic contour. If the flaps were changed to a conic shape, the middle curve resulted, and it may be a better choice. The data points shown in the figure verify the theoretical results. The circle is for a rounded shoulder configuration; the square is for a conic flap configuration with a sharp shoulder.

These curves are shown for the auxiliary-inlet ejector nozzle. A similar study made for a variable-flap ejector nozzle showed an even greater sensitivity to shroud geometry than is shown here.

### 4.3.4 Weight Flow Sensitivity

All of the preceding curves are for a corrected secondary to primary weight flow ratio $\omega\sqrt{\tau}$ of 0.02. These results may be sensitive to this flow ratio. In figure 4–10 $\omega\sqrt{\tau}$ is varied. Theoretical results are shown for the geometry with a sharp shoulder and contoured flaps. Here the $\omega\sqrt{\tau} = 0.02$ curve is repeated from the previous figure; however, for this particular figure, the ram drag of the secondary flow has been subtracted from the gross thrust. Curves for $\omega\sqrt{\tau}$ of 0.04 and 0.08 percent are also shown. Although higher performance is reached at an $\omega\sqrt{\tau}$ of 0.04, a study of the overall design of the propulsion system is needed to decide whether these higher flows should be used or can be even achieved. The experimental data points again show good correlation with the theory.
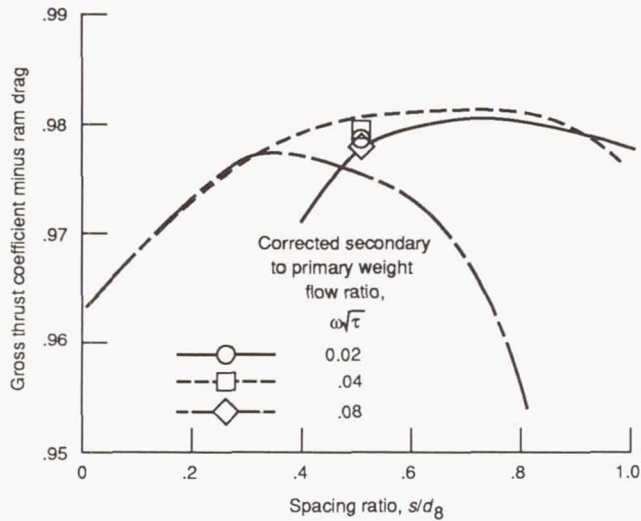
Figure 4–10.—Weight flow sensitivity of auxiliary-inlet ejector nozzle with sharp shoulder and contoured flap.



Figure 4–11.—Nozzle performance at supersonic cruise. Corrected secondary to primary weight flow ratio, $\omega\sqrt{\tau}$, 0.02

### 4.3.5 Nozzle Performance at Supersonic Cruise

Supersonic cruise nozzle performance is summarized in figure 4–11. The gross thrust coefficient for three different nozzle concepts is shown at an $\omega\sqrt{\tau}$ of 0.02. The top of the bar is the theoretical maximum performance that could be obtained with an optimized design. The performances of the variable-flap and the auxiliary-inlet ejectors were taken from curves similar to those in figure 4–9. Preliminary calculations for a plug nozzle indicate that its performance could be as high as that shown for the variable-flap ejector. The auxiliary-inlet ejector's performance is lower because it requires a larger secondary shroud diameter. Note that the best experimental results are indicated by the dashed lines and are quite close to the predictions.

The factors that influence the analysis and design of ejector nozzles are discussed in reference 4–2, where a theoretical analysis of the viscous interaction between the primary and secondary streams of ejector nozzles is developed. The analysis accounts for real sonic-line effects and the streamwise variation in stream and boundary layer mixing within the ejector. The aspects of the analysis are explained and illustrated by applying the theory to a variety of ejector configurations, including cylindrical shroud, contoured divergent shroud, and plug nozzle. Extensive comparisons are made between theory and data to show the importance of various analytical assumptions as well as such design variables as diameter ratio, spacing ratio, total temperature ratio, and primary nozzle geometry.

## 4.4 References

4–1. Dusa, D.J.: Commercial Supersonic Transport Exhaust Nozzle Design Philosophy. Paper presented at the ASME 14th Annual International Gas Turbine Conference and Products Show, Cleveland, OH, Mar. 9–13, 1969.

4–2. Anderson, B.H.: Factors Which Influence the Analysis and Design of Ejector Nozzles. NASA TM X–67976, 1972.
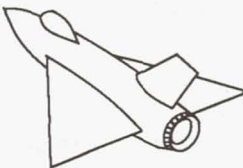
# Chapter 5
# Supersonic Transport Nozzles (1963–1971)—The First Generation

The United States Supersonic Transport (SST) Program was begun in June 1963 by President John F. Kennedy. The initial design concept called for a 400 000-lb titanium aircraft capable of flying at Mach 2.7 or faster with a range of at least 4000 nautical miles and a payload of 125 to 160 passengers. Design proposals were received by the Government in January 1964 from three U.S. aircraft manufacturers (Lockheed, Boeing, and North American Aviation) and three engine companies (Pratt & Whitney, Curtiss-Wright, and General Electric). In May 1964, contracts were awarded to Boeing and Lockheed for further airframe design studies and to General Electric and Pratt & Whitney for additional work on the engine. In December 1966, contracts were awarded to Boeing to build the airframe and to General Electric to produce the engine. Design problems with the airframe and the engine, coupled with fears about environmental and economic effects, led to the cancellation of the program in May 1971.

The first-generation exhaust nozzles to be discussed in this chapter were specifically designed and tested for the Boeing SST concept, which was to feature the General Electric GE-4 afterburning turbojet engine, was to cruise at Mach 2.7, and was expected to carry 150 passengers. Th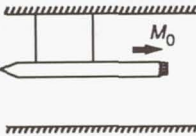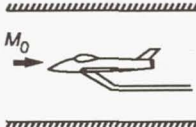ree nozzle concepts were evaluated for this program: (1) a variable-flap ejector designed by General Electric, (2) an auxiliary-inlet ejector also designed by General Electric, and (3) a low-angle plug nozzle designed by the NASA Lewis Research Center. All three nozzle concepts were evaluated in a coordinated wind tunnel and flight test program at NASA Lewis that used the best features of each test technique (table 5–I).

In this chapter the isolated performance of each nozzle, obtained in a static stand and a wind tunnel, is discussed first and then the effect of installing the nozzle in an underwing flow field to simulate an SST installation. Some work on nozzle cooling for these same nozzle concepts is also presented.

TABLE 5–I. METHODS FOR EXPERIMENTAL DETERMINATION OF EXHAUST SYSTEM PERFORMANCE

| Configuration | Type of test | Objectives |
|---|---|---|
| | Static stand (outdoor and indoor) | Internal performance and noise |
| $M_0$ | Wind tunnel (isolated configuration) | External flow effects |
| $M_0$ | Wind tunnel (installed configuration) | Installation effects |
| | Flight test (installed configuration) | Installation effects and flyover noise |

## 5.1 Variable-Flap Ejector Nozzle

General Electric designed the variable-flap ejector nozzle in the mid-1960's as its first attempt to support the Boeing supersonic transport. In order to operate over a wide range of flight conditions and power settings, the variable-flap ejector had to be designed for extensive geometric variations of the primary nozzle and the ejector shroud. Originally, variable-

flap ejector nozzles were fitted with mechanical actuators to accomplish the geometric variations. At the time this nozzle was designed, however, aerodynamically positioned shrouds and boattails were coming into vogue. General Electric included these free-floating features in their variable-flap ejector nozzle in an attempt to minimize the number of actuation systems required.

An 8.5-in.-diameter model of the variable-flap ejector nozzle for wind tunnel testing was designed and fabricated by General Electric, then tested at NASA Lewis in 1967 at simulated flight conditions from takeoff to supersonic cruise. The tests were conducted both in the NASA Lewis 8- by 6-Foot Supersonic Wind Tunnel from Mach 0 to 2.0 and in a NASA Lewis static test stand over a range of nozzle pressure ratios up to and including supersonic cruise. Nozzle thrust efficiency, pumping characteristics, boattail floating position, and boattail pressure drag were measured. Results of the model test program are presented in reference 5-1 and summarized in this section.

### 5.1.1 Configuration Details

The 8.5-in.-diameter wind tunnel model of the variable-flap ejector nozzle is shown in figure 5-1. The shroud is shown in the open position (supersonic cruise) in figure 5-1(a) and in a partially closed position (off design) in figure 5-1(b). The secondary shroud and the external boattail were both made of flaps and seals. Secondary cooling air passed around the leading edge of the inner flaps as well as through the slots in the inner flaps. Pins at the shroud trailing edge were used as exit-area inner stops, and a cable at the shroud trailing edge was used as the exit-area outer stop. An end view of the star-shaped primary nozzle, used to promote mixing between the primary and secondary streams, is shown in figure 5-1(c).

Figure 5-2 is a sketch of the shroud-boattail linkage and the primary nozzle. The solid lines show configuration A (used for subsonic cruise, dry acceleration, and supersonic cruise), and the dashed lines show configuration B (used for reheat acceleration and idle descent). The two configurations were achieved by making manual changes in shroud and primary nozzle geometry. For configuration A a small-area primary nozzle was installed, and the links at the leading edge of each flap were pinned at point $a$. For configuration B a large-area primary nozzle was installed, and the links at the leading edge of each flap were pinned at point $a'$. The shroud and the boattail moved as a four-bar linkage composed of links $a$–$b$ (or $a'$–$b$), $b$–$c$, $c$–$d$, and $d$–$a$ (or $d$–$a'$). In full scale the primary nozzle and shroud-boattail linkage could be interconnected so that the shroud-boattail linkage would change
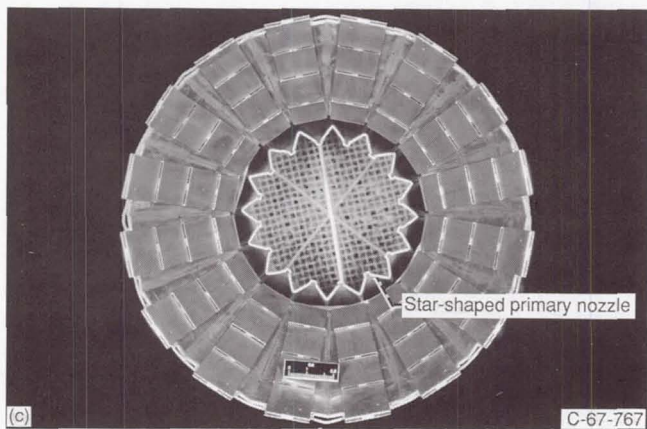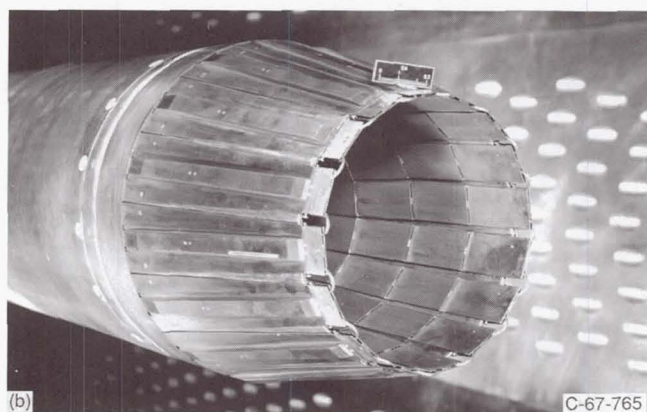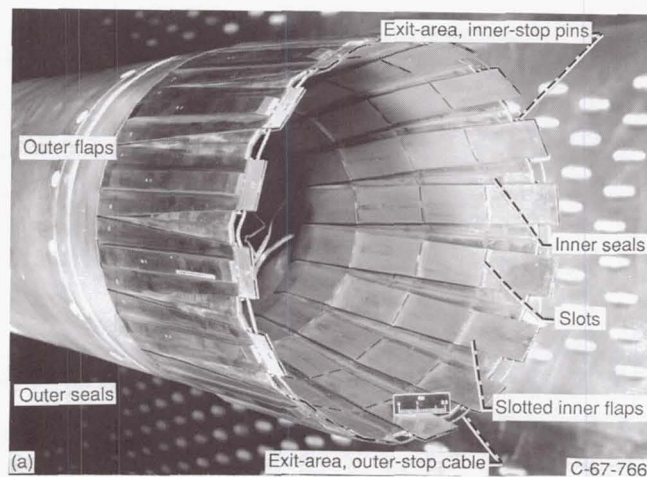


(a) Shroud open.
(b) Shroud partially closed.
(c) Open shroud and star-shaped primary nozzle.

Figure 5-1.—Model of variable-flap ejector nozzle in wind tunnel.
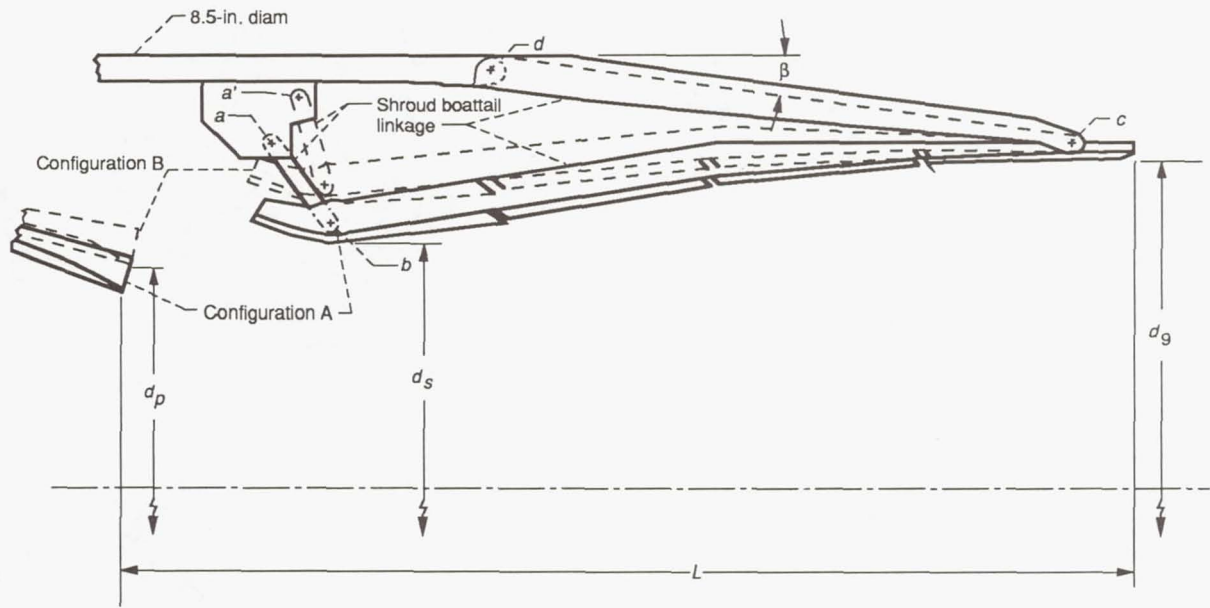
Figure 5-2.—Variable-flap ejector geometry and linkage.

with the area of the primary nozzle. The ejector length ratio $L/d_p$ was approximately 2.0 and the ejector diameter ratio $d_s/d_p$ was about 1.2. In order to avoid possible flow instability from low area ratios (as discussed in ref. 5–2), the minimum nozzle area ratio was restricted to 1.35 for both configurations. The maximum boattail angles were 15.5° for configuration A and 13.0° for configuration B.

### 5.1.2 Nozzle Performance Characteristics

The nozzle pressure ratio schedule shown in figure 5–3 was used as a guide for setting pressure ratios over the range of free-stream Mach numbers for each power setting. Supersonic cruise efficiency was obtained in a static test stand at a pressure ratio of 26 and a corrected secondary to primary weight flow ratio of 0.02. The static efficiency was reduced by 0.003 to account for an estimated friction drag on the boattail.

Figure 5–4 shows the resulting thrust efficiency of the variable-flap ejector nozzle over a range of free-stream Mach numbers at several simulated power settings. The corrected secondary to primary weight flow ratios chosen were typical of the values that could be used for the supersonic transport. Note that the performance was good over most of the flight regime. The peak nozzle thrust efficiency (0.975) occurred at supersonic cruise; the lowest efficiency (0.856) occurred at subsonic cruise (Mach 0.9).
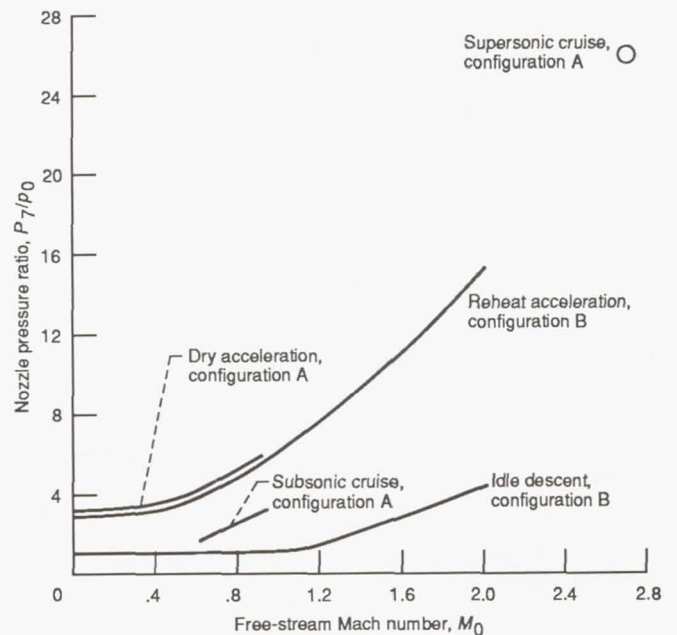


Figure 5–3.—Schedule of variable-flap ejector nozzle pressure ratio with free-stream Mach number for five simulated power settings.
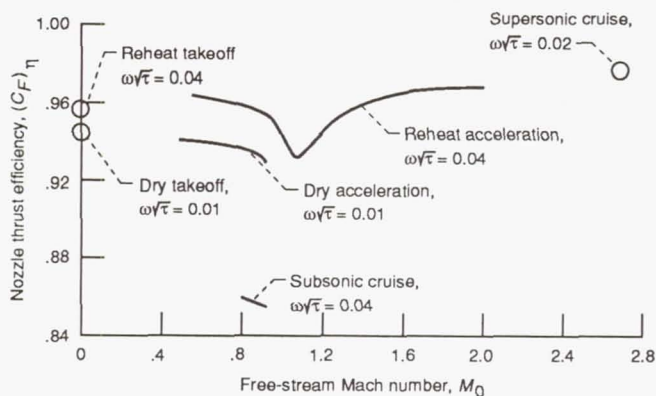
Figure 5-4.—Efficiency of variable-flap ejector at various corrected secondary to primary weight flow ratios $\omega\sqrt{\tau}$.



Figure 5-5.—Boattail pressure drag loss for variable-flap ejector at various corrected secondary to primary weight flow ratios $\omega\sqrt{\tau}$.
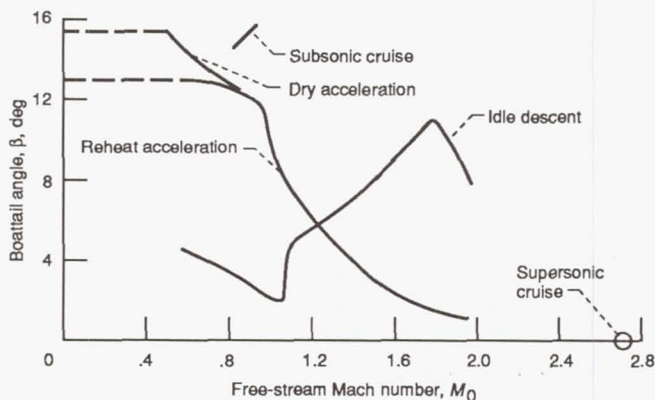


Figure 5-6.—Variation of boattail angle with Mach number for five simulated power settings of variable-flap ejector nozzle.

### 5.1.3 Boattail Drag

At subsonic cruise, where the lowest performance occurred, the thrust level was low and the boattail angles were high. The portion of the external flow effect due to boattail pressure drag is shown in figure 5-5, which is a plot of the boattail pressure drag loss against free-stream Mach number $M_0$ for three simulated power settings. Observe that at subsonic cruise the boattail pressure drag loss attained a maximum value of 6 percent of the ideal gross thrust.

The high boattail drag resulted from the high boattail angles. Figure 5-6 shows the observed boattail angles for five simulated power settings. The highest boattail angles occurred at subsonic cruise and at takeoff. A minimum boattail angle of about 1° was observed in the wind tunnel at Mach 1.97. A boattail angle of 0° was observed in the static stand at simulated supersonic cruise operation (i.e., at a pressure ratio of 26).

### 5.1.4 Ejector Pumping Characteristics

The secondary total pressure recoveries required for secondary to primary weight flow ratios $\omega\sqrt{\tau}$ at various flight conditions and power settings are shown in figure 5-7. At subsonic cruise power settings (fig. 5-7(a)) the secondary total pressure recovery required for an $\omega\sqrt{\tau}$ of 0.04 was only 0.63. At takeoff power setting (fig. 5-7(b) and (c)), however, the secondary total pressure recovery became more critical. At the reheat acceleration power setting (fig. 5-7(c)) a secondary total pressure recovery of 0.985 was required for an $\omega\sqrt{\tau}$ of

0.04. These data indicate that auxiliary inlets close to the ejector may be required to provide sufficient secondary total pressure.

### 5.1.5 Concluding Remarks

Nozzle thrust efficiency varied from a high of 0.975 at supersonic cruise to a low of 0.856 at subsonic cruise. At subsonic cruise the boattail drag amounted to about 6 percent of the ideal thrust. Pumping characteristics at takeoff with a reheat power setting were marginal and suggested that an auxiliary inlet for secondary air may be required. The aerodynamically positioned shroud was stable at all Mach numbers and simulated power settings. The shroud position was dictated by internal pressures at all simulated power settings (except idle and cruise at $M_0 = 0.8$) and was independent of free-stream and secondary flow effects.
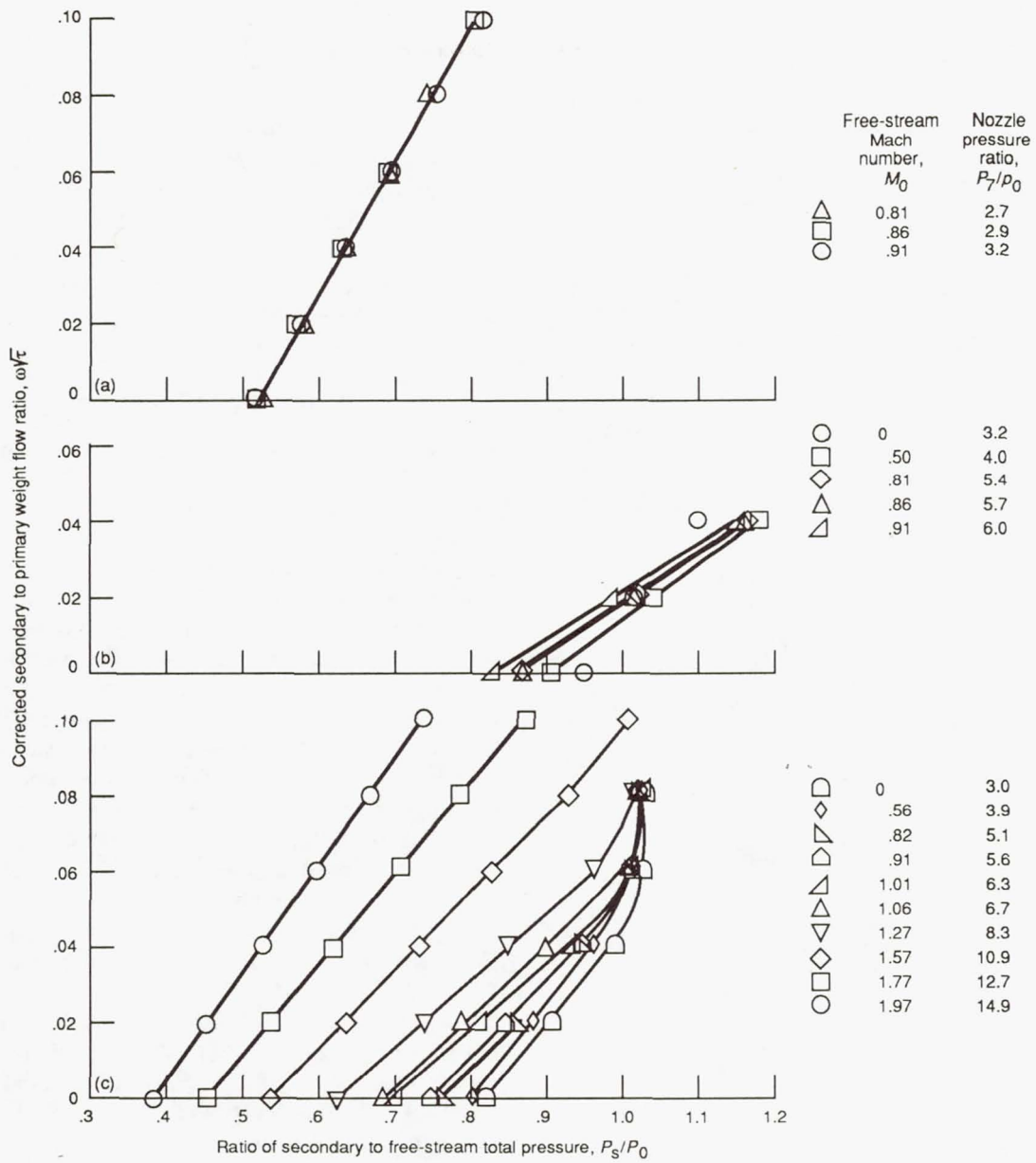
(a) Subsonic cruise, configuration A.
(b) Dry acceleration, configuration A.
(c) Reheat acceleration, configuration B.

Figure 5.7—Ratio of secondary total pressure to free-stream total pressure required for corrected secondary to primary weight flow ratios at various free-stream Mach numbers—variable-flap ejector nozzle.

35

## 5.2 Auxiliary-Inlet Ejector Nozzle

General Electric designed the auxiliary-inlet ejector nozzle for the Boeing supersonic transport in the late 1960's as a follow-on concept to the variable-flap ejector nozzle. At supersonic cruise this nozzle was similar to the variable-flap ejector. However, at takeoff and subsonic flight conditions auxiliary inlets opened to admit tertiary air and thus minimize primary flow overexpansion. This tertiary air filled part of the secondary shroud, reducing the amount of exit-area variation required, with an associated reduction in boattail area. Since the variable-flap ejector nozzle performed poorly at subsonic cruise because of high boattail drag, it was hoped that the auxiliary-inlet concept, with its reduced boattail area, would provide better installed performance at subsonic cruise.

The internal performance for an auxiliary-inlet ejector nozzle with fixed geometry was obtained in a NASA Lewis static test stand in 1968 (ref. 5–3). Because the simulated supersonic cruise performance was high and equivalent to that obtained with the variable-flap ejector, the performance of this nozzle concept was measured at other critical flight conditions. General Electric designed and fabricated an 8.5-in.-diameter model of the auxiliary-inlet ejector nozzle and then tested it in the NASA Lewis 8- by 6-Foot Supersonic Wind Tunnel in 1969 at Mach numbers from 0 to 2.0. This new nozzle configuration featured both aerodynamically positioned auxiliary-inlet doors and secondary shroud flaps. Two primary nozzles were tested: (1) a small-area nozzle to simulate subsonic and supersonic cruise as well as dry acceleration and (2) a large-area nozzle to simulate both reheat acceleration and idle descent. Nozzle thrust efficiency, pumping characteristics, and the floating position of the doors and flaps were measured. Results of the model tests are presented in reference 5–4 and are summarized in this section.

### 5.2.1 Configuration Details

The wind tunnel model is shown in figure 5–8 with secondary flaps in the open and closed positions. Each primary nozzle had 16 tabs (shown in figs. 5–8 and 5–9) that were used during reverse thrust operation. In practice, the primary nozzle translated downstream to seal against the secondary nozzle; then the primary's flaps and tabs closed to block the primary flow, thereby directing it upstream and out through the tertiary inlet doors. During forward thrust operation the tabs were in a position to provide some guidance to the flow expansion. An air guide was provided in the secondary-flow annulus to direct some of the cooling flow over the primary nozzle flaps.

The ejector shroud had 16 single-hinge, free-floating tertiary inlet doors on the 3° 23′ fixed boattail portion of the model, as well as 16 floating trailing-edge flaps (fig. 5–9). The three doors at the 2, 6, and 10 o'clock locations were fixed in the closed position to simulate an installed condition within a wing structure, and the remaining 13 unsynchronized doors were free to float to admit tertiary air. The secondary shroud was made up of flaps and seals that were free to float so that the exit area could aerodynamically adjust to the nozzle pressure ratio. This ejector nozzle had a maximum boattail angle of 12° 58′, in contrast to 15° 30′ for the variable-flap ejector nozzle, and a projected boattail area one-third less than the VFE.

Between the tertiary doors were hollow support beams that ducted a portion of the secondary flow into the secondary flap cavity. This secondary flow simulated shroud film cooling flow and exited through two internal annular slots on the flaps. It was anticipated that at low pressure ratios this flow would pressurize the cavity and help close the flaps.

### 5.2.2 Nozzle Performance Characteristics

Nozzle performance was obtained over a range of nozzle pressure ratios and free-stream Mach numbers. The schedule shown in figure 5–10 was used as a guide for setting pressure ratio over the range of Mach numbers from 0 to 2.0 for each power setting. The auxiliary-inlet ejector nozzle was tested with two different primary nozzles to simulate afterburning and nonafterburning operation. The performance characteristics are summarized in figure 5–11. The corrected secondary to primary weight flow ratio $\omega\sqrt{\tau}$ of 0.04 was selected as a basis for comparison at all flight Mach numbers except supersonic cruise, where an $\omega\sqrt{\tau}$ of 0.02 was selected.

Figure 5–11(a) shows that at takeoff conditions a high thrust efficiency of 0.98 was obtained with the afterburning configuration. Figures 5–11(b) and (c) show that the flaps were fully closed at this condition and the doors were fully open. As indicated in figure 5–11(d), secondary-flow pumping was marginal, since a secondary-flow recovery of 1.00 was needed for an $\omega\sqrt{\tau}$ of 0.04; a recovery of 0.965 would be required for a reduced $\omega\sqrt{\tau}$ of 0.02.

The performance at subsonic cruise was sensitive to nozzle pressure ratio (fig. 5–11(a)). At a typical subsonic cruise pressure ratio of 3.27 the nozzle efficiency at Mach 0.9 was about 0.87. The flaps tended to float open at the lower pressure ratios (fig. 5–11(b)), thereby increasing the overexpansion losses. The tertiary doors were only slightly more than half open (fig. 5–11(c)). Because the secondary total pressure was slightly less than the ambient static pressure, internal drag forces existed. The pumping characteristics, however, were adequate (fig. 5–11(d)).

The supersonic cruise configuration was tested at the maximum wind tunnel speed (Mach 2.0) to obtain an approximation of supersonic cruise performance. Because the difference in external flow effects between Mach 2.0 and 2.7 is relatively minor, the data are shown in figure 5–11 at Mach 2.7. A nozzle thrust efficiency of 0.971 was measured (fig. 5–11(a)). Figures 5–11(b) and (c) show thrust efficiency when the inlet doors were closed and the secondary flaps were wide open. A secondary total pressure recovery of about 0.35 was required to pump an $\omega\sqrt{\tau}$ of 0.02 (fig. 5–11(d)).
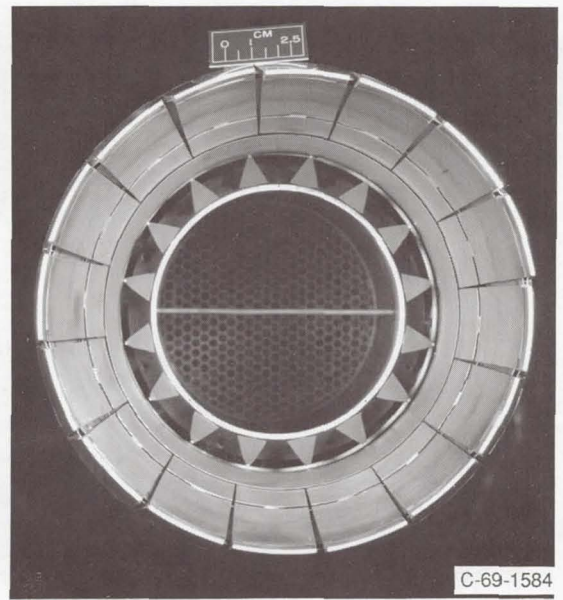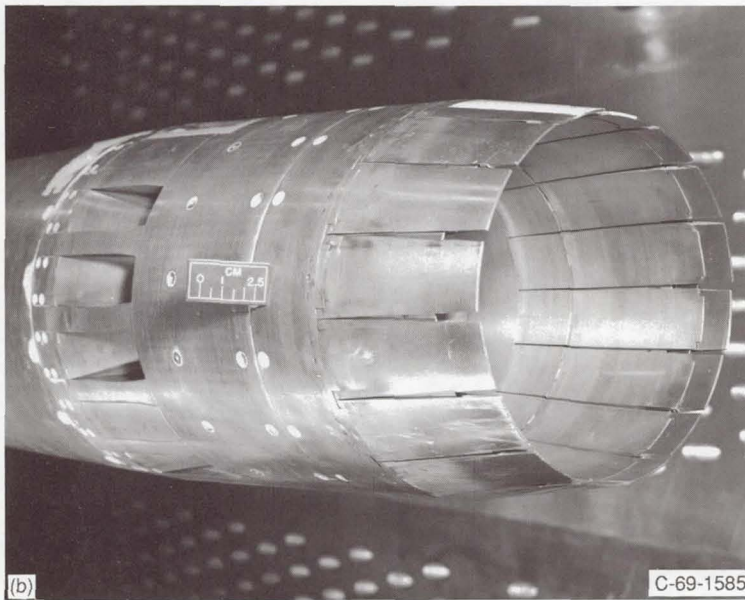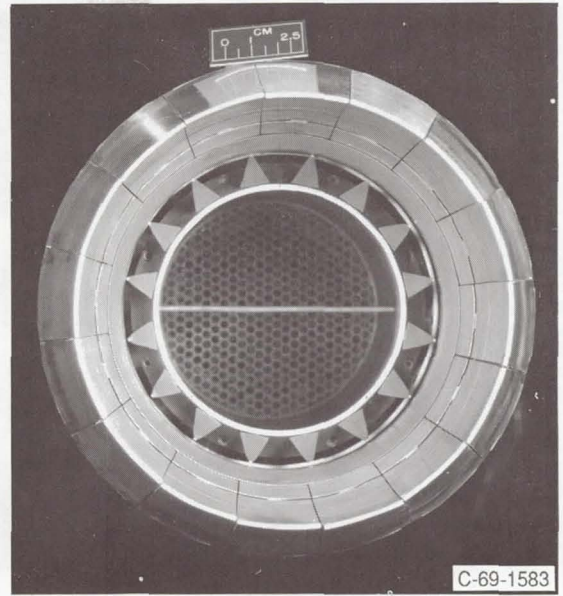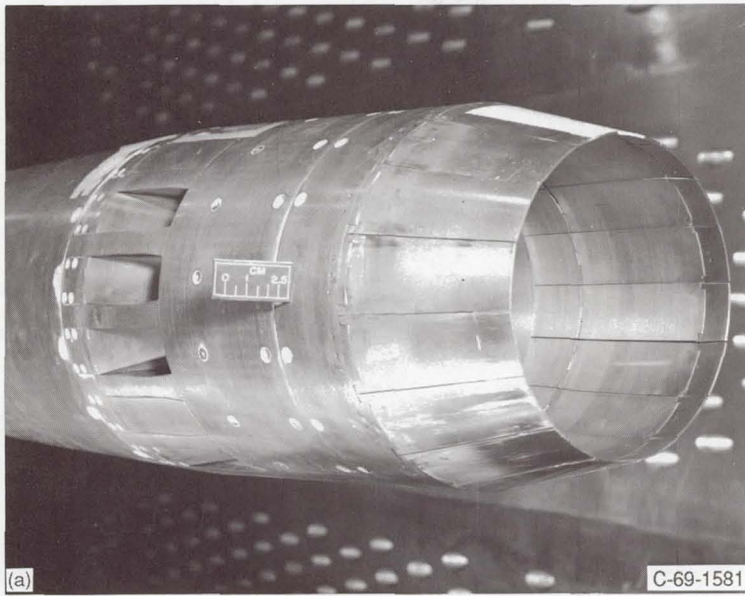
(a) Flaps closed.
(b) Flaps open.

Figure 5–8.—Model of auxiliary-inlet ejector nozzle in wind tunnel.

### 5.2.3 Concluding Remarks

The auxiliary-inlet ejector nozzle had better takeoff and subsonic cruise performance than the variable-flap ejector nozzle tested earlier. However, the improvement in efficiency at subsonic cruise was modest (about 1.5 percentage points) and was still inadequate for a supersonic cruise aircraft. Although boattail drag was reduced at subsonic cruise, the added drag of the auxiliary-inlet system almost negated that improvement. The variable-flap ejector and the auxiliary-inlet ejector had comparable supersonic cruise performance.
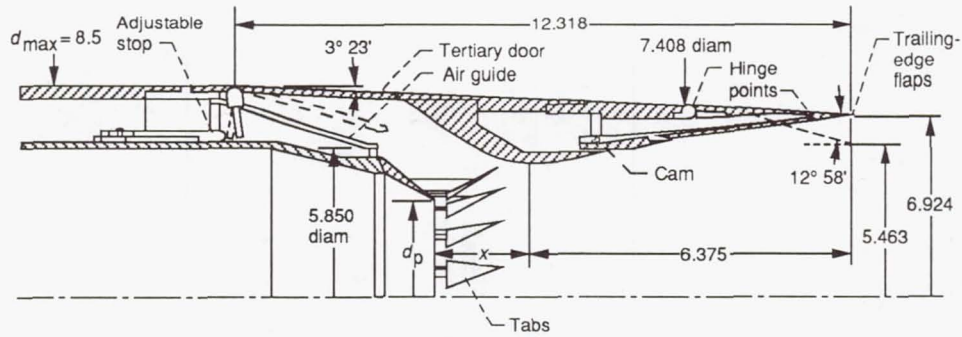
| Configuration | Primary nozzle diameter, $d_p$, in. | Axial distance, $x$, in. | Discharge coefficient, $C_d$ |
|---|---|---|---|
| Nonafterburning | 3.660 | 1.9365 | 0.944 |
| Afterburning | 4.341 | 1.8125 | .972 |

Figure 5–9.—Basic dimensions of auxiliary-inlet ejector nozzle. (Linear dimensions are in inches.)
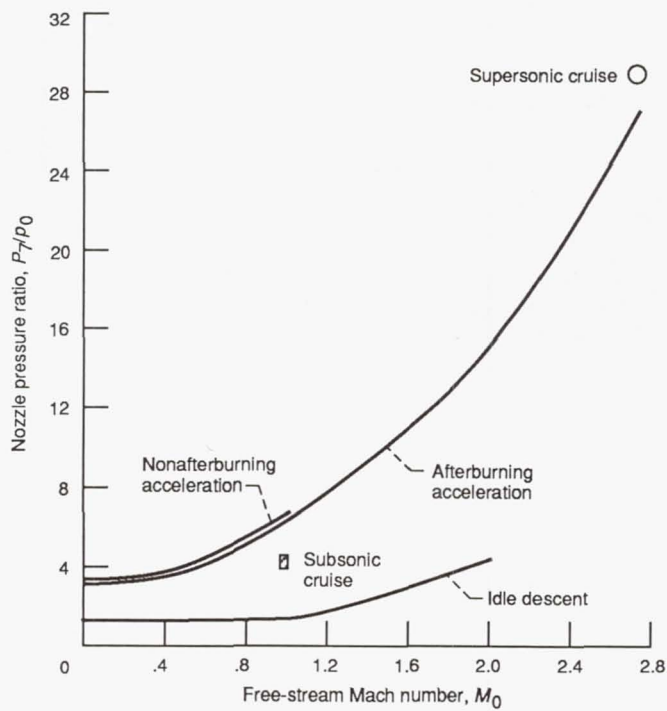


Figure 5–10.—Schedule of auxiliary-inlet ejector nozzle pressure ratio with free-stream Mach number for simulated power settings.

Primary
configuration

○  Afterburning
□  Nonafterburning
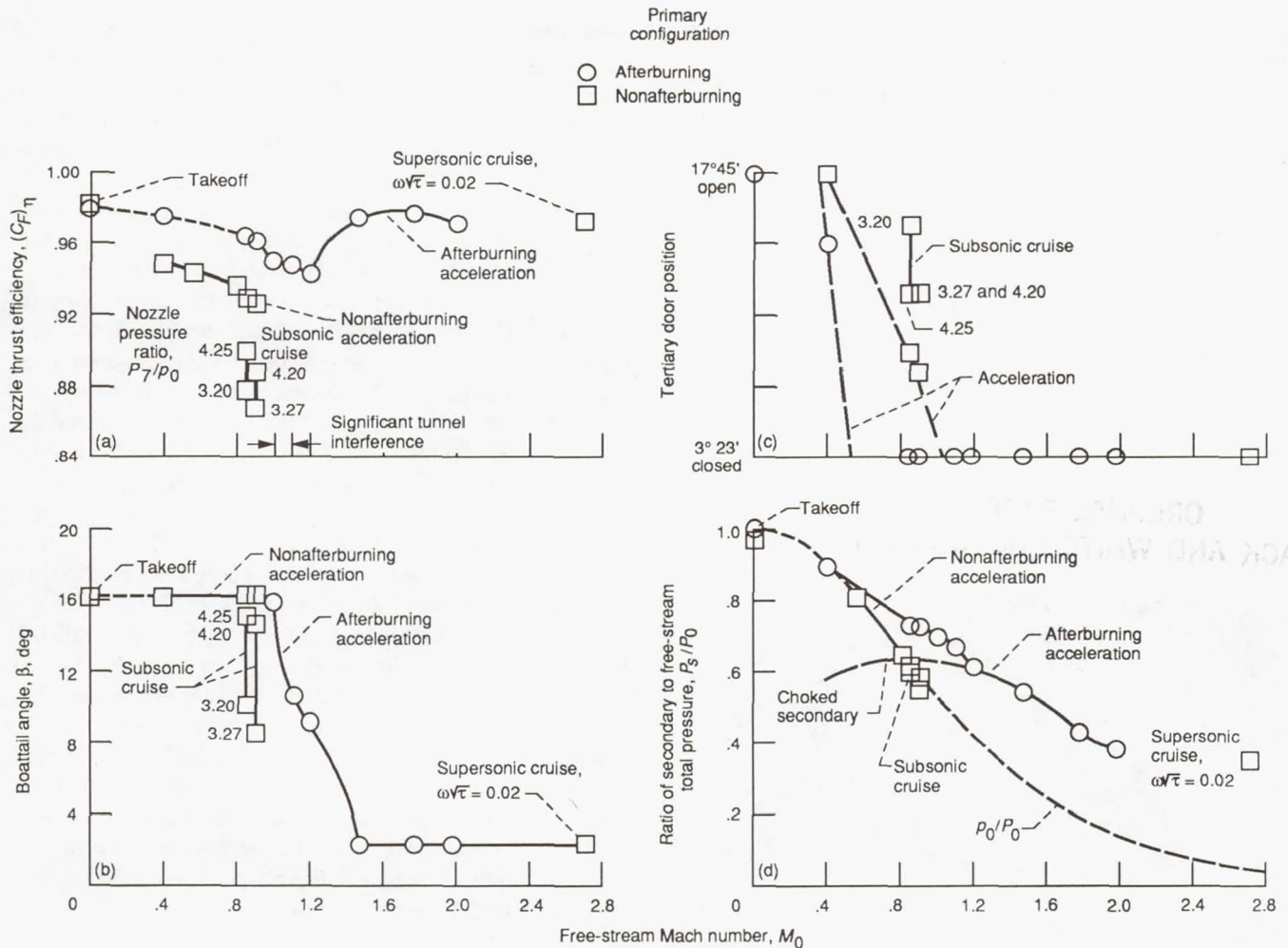
(a) Nozzle efficiency.
(b) Boattail angle.
(c) Tertiary door position.
(d) Secondary total pressure recovery requirements.

Figure 5–11.—Performance of auxiliary-inlet ejector nozzle over flight Mach number range at corrected secondary to primary weight flow ratio $\omega\sqrt{\tau}$ of 0.04.

## 5.3 Low-Angle Plug Nozzle

Of the three basic nozzle types considered for the Boeing supersonic transport during the mid-1960's, General Electric concentrated on the variable-flap and auxiliary-inlet ejector nozzles already discussed. The in-house research effort at NASA Lewis focused on the low-angle plug nozzle as an alternative concept. Experimental tests conducted at the National Gas Turbine Establishment (NGTE) in Great Britain between 1960 and 1965 (ref. 5–5) had shown that a plug nozzle with a parallel outer shroud was an attractive candidate for an SST aircraft. After cone half-angles from 7.5° to 15° were studied, it was concluded that 10° was the optimum angle from an aerodynamic point of view.

Consequently, NASA Lewis designed and fabricated an 8.5-in.-diameter model of a low-angle (10°) plug nozzle and then in 1967 tested it in the Center's static test stand and 8-by 6-Foot Supersonic Wind Tunnel. The nozzle had a 10° half-angle cone and was suitable for an afterburning turbojet engine designed to cruise at Mach 2.7. In order to provide for changes in engine-operating conditions such as an afterburner, the nozzle had a fixed centerbody and simulated iris primary flaps to modulate the throat area. A translating external cylindrical shroud provided proper internal expansion to the design pressure ratio of 26.3 at supersonic cruise. Internal performance was obtained in the static stand, and external flow effects were obtained in the wind tunnel at Mach numbers to 2.0. Plug truncation was also studied. Results of the model test program are presented in reference 5–6 and are summarized herein.

39

## 5.3.1 Configuration Details

The low-angle plug nozzle installed in the wind tunnel is shown in figure 5–12. Basic nozzle dimensions are shown in figure 5–13(a). The nozzle configurations consisted of a 10° half-angle cone with fixed shrouds of varying length to simulate translation. A circular-arc boattail was designed at the trailing edge of the outer shroud to minimize base drag at subsonic cruise. The projected area of the boattail was only about 10 percent of the maximum nacelle area. Figure 5–13(b) shows the shroud extensions that were tested. The plug was fabricated with several aft sections (fig. 5–13(c)) so that the effect of plug truncation on nozzle performance could be studied. The simulated iris primary flaps, consisting of two fixed-geometry primary nozzles with a 17° 30′ boattail (afterburner off) and a 7° 36′ boattail (afterburner on), provided a 40-percent change in throat area (fig. 5–14).
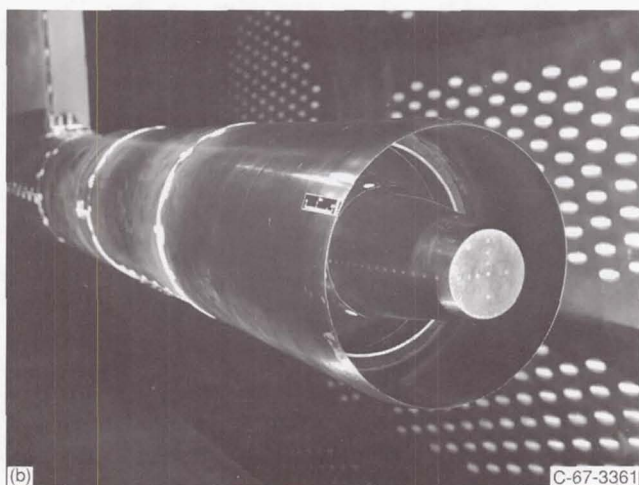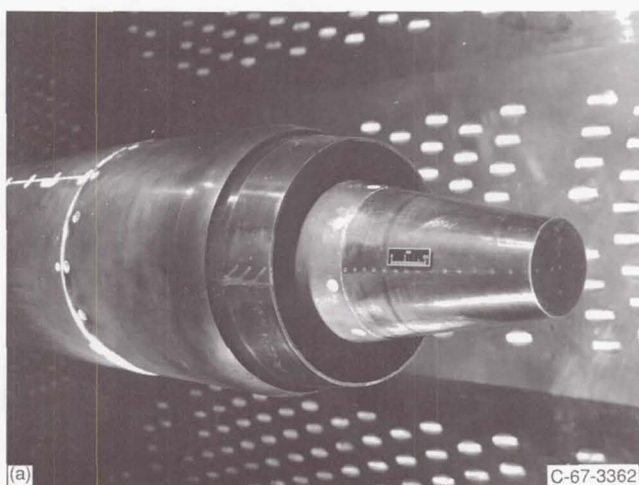
(a) Shroud retracted.
(b) Shroud extended.

Figure 5–12.—Model of low-angle plug nozzle in wind tunnel.

## 5.3.2 Nozzle Performance Characteristics

The full-length plug nozzle was tested with shrouds of varying length to simulate translation and with two primary nozzles to simulate iris throat flaps for afterburner on and off operation. Each configuration was tested over a range of nozzle pressure ratios and Mach numbers corresponding to the typical schedule for a supersonic turbojet engine (fig. 5–15).

The full-length plug nozzle performance at various Mach numbers from takeoff to supersonic cruise is summarized in figure 5–16. Each point indicates the performance obtained at the optimum shroud position tested, based on the assumed schedule. The secondary to primary weight flow ratios indicated were based on anticipated cooling requirements. Static test data were used to determine both supersonic cruise and takeoff performance, where the external flow effects are negligible. The shroud was fully retracted for all subsonic operations except when the afterburner was on at Mach 0.9, where an intermediate shroud position gave slightly higher performance. For optimum performance at Mach 1.2 and higher, the shroud was extended to the position corresponding to 80-percent internal expansion ($x/d = 0.618$).

The overall performance of this low-angle plug nozzle was excellent. The nozzle thrust efficiency remained above 0.965 for all flight conditions shown except subsonic cruise. The maximum external flow effects occurred at subsonic cruise, where the performance was sensitive to both pressure ratio and Mach number. Because the nozzle operated at a low pressure ratio, the external drag became a large fraction of the relatively low ideal thrust. Increasing the pressure ratio from 3.25 to 4.0 increased the nozzle thrust efficiency at subsonic cruise from 0.918 to 0.942.

## 5.3.3 Truncated Plugs

The performance of a truncated plug for supersonic and subsonic cruise is summarized in figure 5–17. At supersonic cruise with the shroud extended, the effects of truncation were slight, about a 0.5-percentage-point loss with 50-percent truncation. At subsonic cruise with the shroud retracted, the effect of truncating the plug was considerably greater, almost a 2-percentage-point loss in efficiency with the 50-percent plug.

The effect of introducing bleed flow in the base of these truncated plugs was not studied. However, previous tests (ref. 5–7) had shown that small amounts of bleed flow could reduce the loss due to truncation. With 1.5-percent bleed, about half the loss could be regained.

## 5.3.4 Ejector Pumping Characteristics

The pumping characteristics of the low-angle plug nozzle were such that secondary flow could be provided to cool the primary nozzle and the shroud at all flight conditions except takeoff. In general, optimum nozzle efficiency was obtained with an $\omega\sqrt{\tau}$ of 0.04 to 0.06.
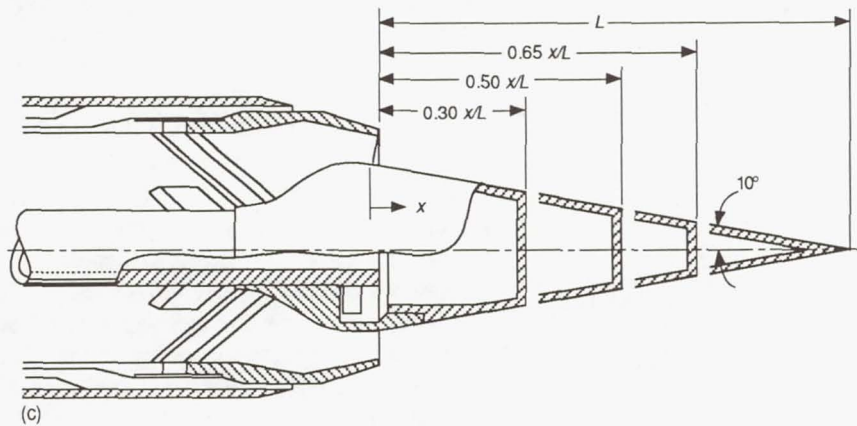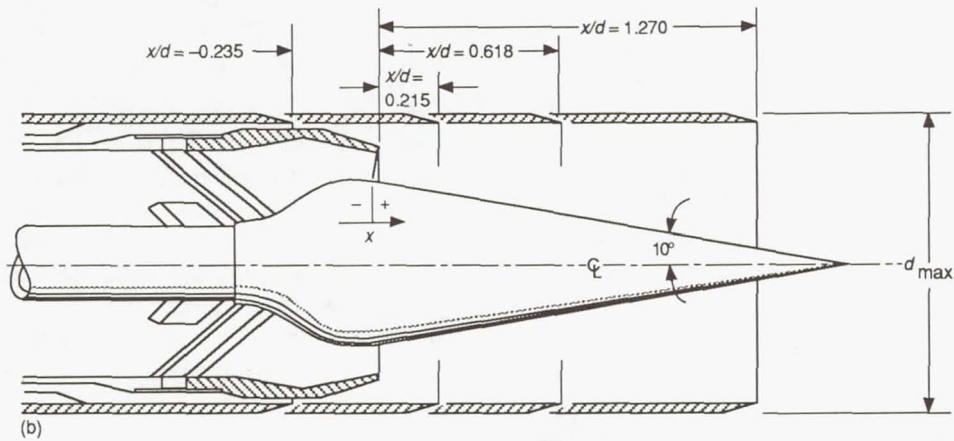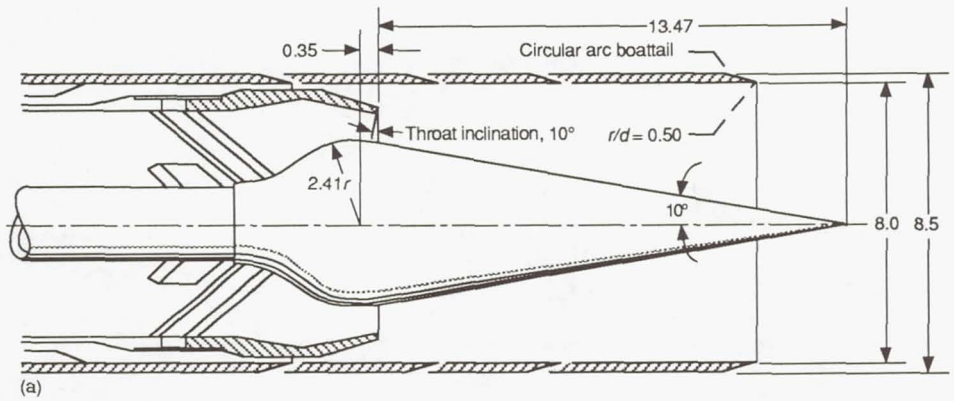
(a) Model dimensions.
(b) Shroud locations.
(c) Nozzle truncations.

Figure 5–13.—Basic dimensions and geometric variables for low-angle plug nozzle. (Linear dimensions are in inches.)
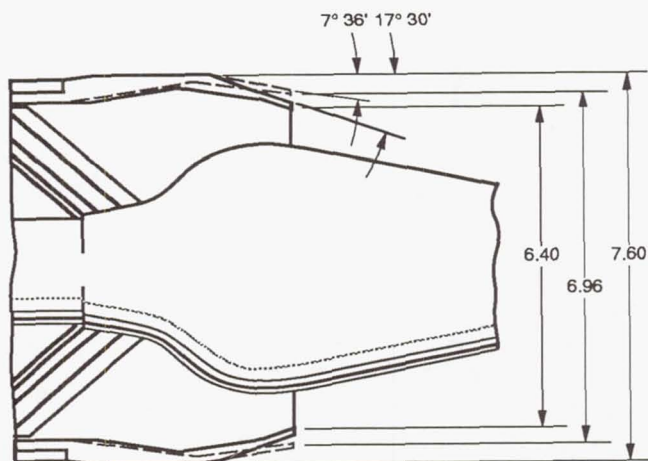
Figure 5-14.—Iris primary nozzle. (Linear dimensions are in inches.)
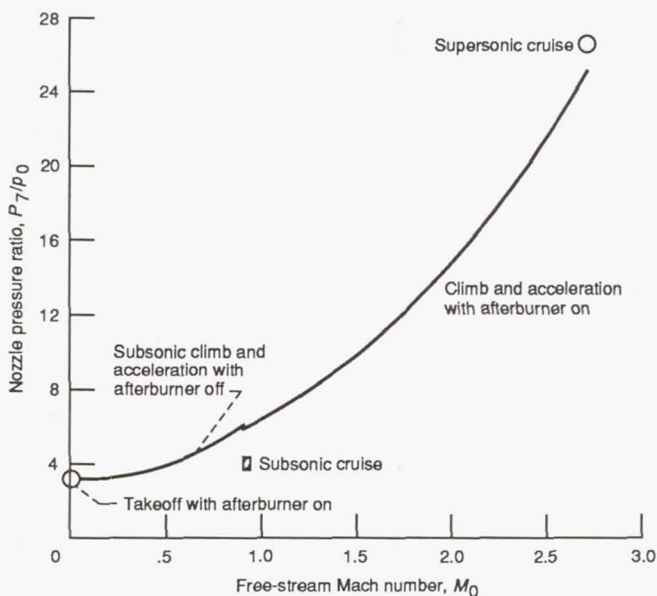


Figure 5-15.—Pressure ratio schedule for typical turbojet engine.
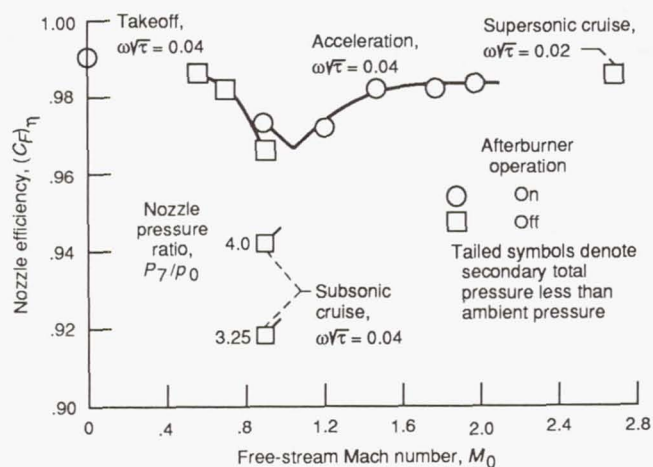


Figure 5-16.—Efficiency of full-length plug nozzle over flight Mach number range.
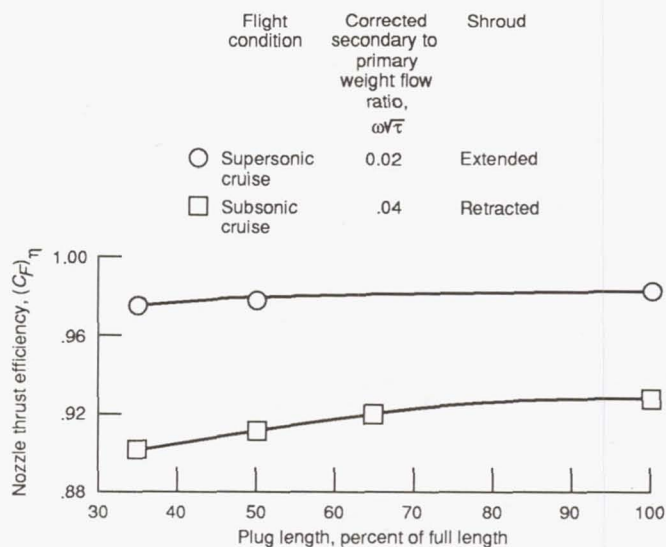


Figure 5-17.—Effect of plug truncation on efficiency of low-angle plug nozzle.

### 5.3.5 Concluding Remarks

The low-angle plug nozzle provided the best isolated nozzle performance of the three first-generation nozzles designed for the Boeing supersonic transport in the mid-to-late 1960's. This was most evident at the subsonic cruise condition, where the plug nozzle had a thrust efficiency of 0.918 at Mach 0.9, compared with 0.856 for the variable-flap ejector and 0.870 for the auxiliary-inlet ejector. Plug nozzle efficiency at all other flight conditions was greater than 0.965 and reached a high of 0.985 at supersonic cruise (Mach 2.7).

## 5.4 Installation Effects

The off-design performance of a nozzle is difficult to analyze because of the interactions between the internal and external flows. Therefore, engineers have to rely more heavily on experimental data. The isolated nozzle model shown in figure 5-18(a) was used to obtain the isolated performance of the supersonic transport nozzles, as discussed in the preceding sections of this chapter. However, the transonic performance of a nozzle is difficult to obtain because the tunnel walls interfere with the flow. Yet the most important airframe installation effects occur at transonic speeds. The external flow is distorted by the airframe and varies depending on the engine location. The transonic testing problem is therefore made even more difficult, since a large section of the airframe must be tested along with the exhaust nozzle. As a result the nozzle model is considerably smaller than preferred when working within the size limits of present wind tunnels. One approach to solving this problem is to have a coordinated flight and wind tunnel model program that uses the best features of each test technique.
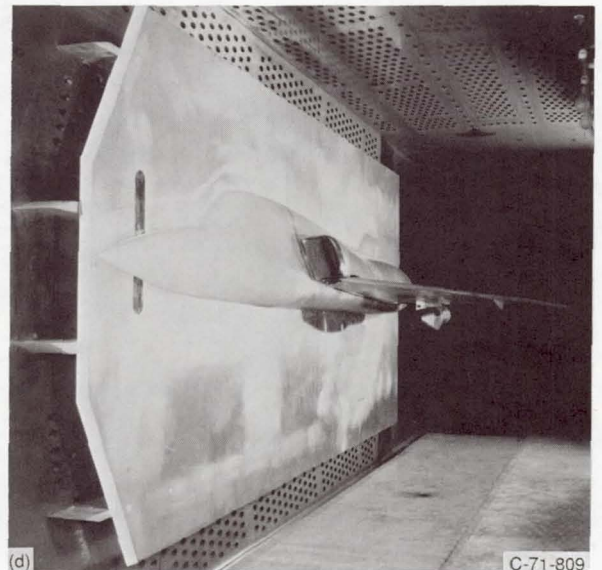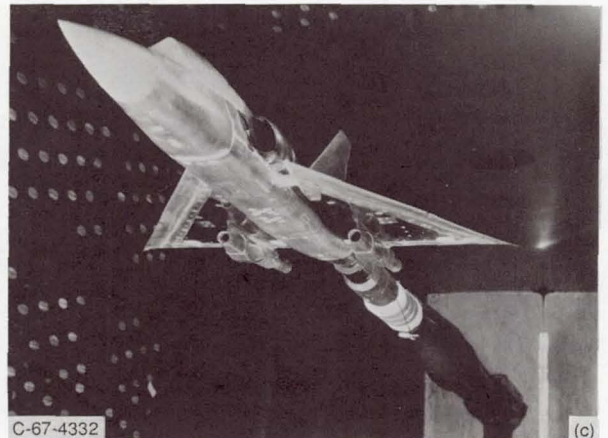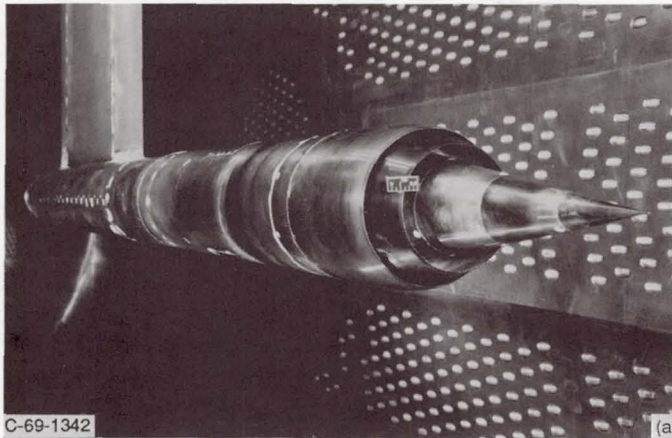
(a) Isolated nozzle.
(b) F–106 flight.
(c) Full-span F–106 model.
(d) Half-span F–106 model.

Figure 5–18.—Variety of test installations.

Such an effort was conducted at NASA Lewis in the late 1960's and early 1970's to support supersonic transport nozzle research. A modified F–106 (fig. 5–18(b)) was selected as the flight test aircraft. A new engine nacelle was added under each wing so that the nozzle extended downstream of the wing's trailing edge, the same kind of engine installation as proposed for the Boeing supersonic transport. This installation was used because the wing can shield the inlet from angle-of-attack effects and can provide favorable interference effects on its aft undersurfaces. An afterburning General Electric J–85 turbojet engine was used in each of two pods. These pods, 25 in. in diameter, were designed to accept any of the nozzles that gave good results in isolated tests. A research nozzle was installed on one nacelle and a referee nozzle was installed on the other. For each nozzle design the airplane was also flown at low altitudes for flyby noise measurements.

In addition to the flight tests, a wind tunnel model program was also conducted in an effort to study more nacelle shapes and locations. For example, models of the F–106 were designed at 1/20 scale and 22-percent half-span (figs. 5–18(c) and (d)). The full-span model was small enough to avoid the transonic wall interference problems, but the nacelle diameter was only 1.25 in. and the wing structure was so thin that no pressurized air could be routed to the nacelle to simulate jet effects. In contrast, the nacelle size on the half-span F–106 model was 5.5 in., allowing for the installation of a small turbojet engine simulator in the nacelle to simulate jet effects.

Flights were made with the F–106 at Mach 0.4 for noise
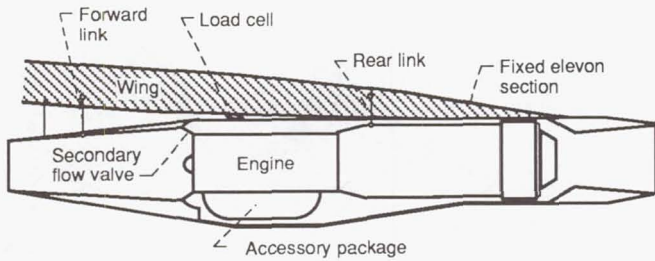
Figure 5-19.—Nacelle-wing installation.

flyby measurements and at Mach 0.6 to 1.3 for exhaust nozzle evaluation. Note that Mach 0.9 is used in the following discussion of subsonic cruise.

The nacelles were installed tangent to the wing lower surface at the trailing edge of the wing, attached by two links (fig. 5-19). Axial forces were measured by a load cell. A simple normal shock inlet was adequate for the Mach number range used. A movable rotating valve was located at the engine face to control secondary airflow to the nozzle.

With an exhaust nozzle located in the combined flowfields of the wing and nacelle, flow conditions differed from those around the isolated nozzle of figure 5-18(a). In the discussion that follows, these flowfield differences are first noted, and then the effect of installing the various nozzle types in an underwing flowfield is described.

### 5.4.1 Installed Flowfields

The variation of static pressure coefficient under the wing at a spanwise location near the nacelle is presented in figure 5-20. Data are shown at a free-stream Mach number of 0.9, both with and without the nacelle. Without the nacelle the static pressure coefficient dropped along the wing chord and then rose to zero at the wing's trailing edge. When the nacelle was added, the combined flowfield raised the pressure in the vicinity of the inlet. The flow then overexpanded around the juncture of the inlet and the nacelle; the pressure coefficient
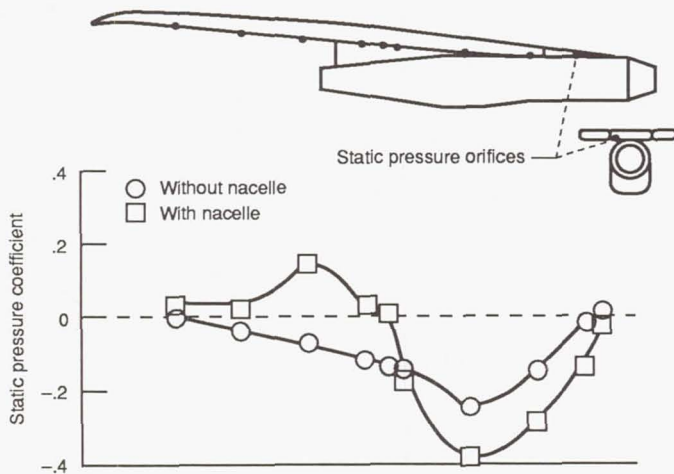
dropped to a lower value than with the clean wing and then rose back to zero. In addition, high pressure near the inlet increased inlet drag. Some of this drag may be cancelled, however, by pressure forces acting on the wing surfaces. Nozzle boattail drag may also be reduced if the pressure coefficient downstream of the wing's trailing edge reaches a value greater than zero; some nozzles may be more effective than others in cancelling drag. Finally, the position of a compression shock in the pressure rise near the wing trailing edge varied with free-stream Mach number.

The movement of this compression shock with $M_0$ is shown in figure 5-21. At Mach 0.8 there was a small amount of overexpansion and a gradual rise in pressure coefficient back to zero near the wing's trailing edge and above zero on the nozzle boattail. At Mach 0.9 more overexpansion was followed by a sharp rise in pressure; the compression shock was located in this steeply rising pressure region. At Mach 0.95 the shock had moved rearward near the wing's trailing edge, and at Mach 1.0 it had moved off the end of the nozzle. Note that the pressure remained low along the entire length of the nacelle and the nozzle. Low pressure on the nozzle boattail for this condition results in high nozzle drag.

The external static pressure coefficient was uniform at near zero along the isolated model in the wind tunnel for all subsonic conditions. No circumferential variation in pressure occurred around the isolated model. This was also the case in flight about one nozzle diameter ahead of the boattail juncture and at the rear of the boattail. Just downstream of the wing's trailing edge, however, the external pressure was higher around the top of the nozzle than at the bottom.

There were differences in external boundary layer measured upstream of the nozzle. The boundary layer was generally thinner (based on boundary layer thickness divided by nacelle diameter) in flight than on the isolated model, except in the corners between the nacelle and the wing and over the top of the wing. In flight, regions of low energy existed within the



Figure 5-20.—Installation effect on wing pressures. Free-stream Mach number, $M_0$, 0.9.
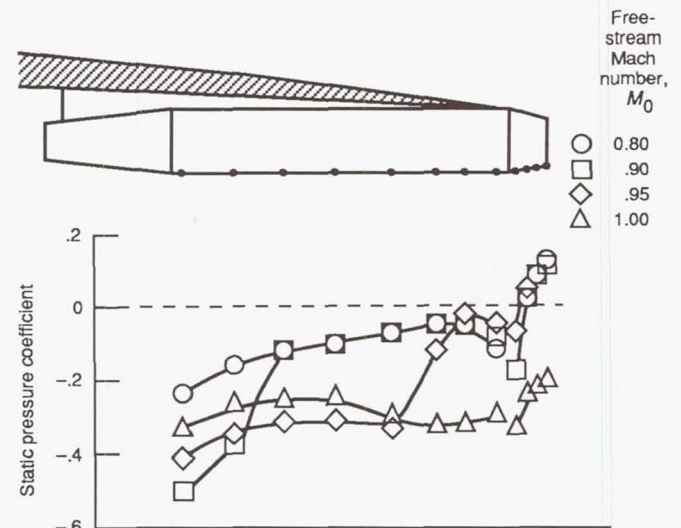


Figure 5-21.—Installation effect on nacelle pressures.

boundary layer all around the nacelle as a result of the more complex flowfield and the presence of shocks.

All three exhaust nozzles discussed in this chapter were tested in this flowfield on the F-106. The isolated nozzle performance was obtained prior to the flight tests. A discussion of the installation effects on each of the three nozzle concepts follows.

### 5.4.2 Variable-Flap Ejector Nozzle

Figure 5-22 shows a variable-flap ejector nozzle mounted at the trailing edge of the F-106 wing. Flight performance for this nozzle type is reported in reference 5-8. A section of the elevon was cut out and rigidly attached to the wing. In order to simplify its fabrication, the nozzle boattail was made solid rather than made of individual flaps and seals, and the area ratio was fixed at the proper value for subsonic cruise.

The installation effect on nozzle boattail drag is shown in figure 5-23 for a sharp-junctured variable-flap ejector. Installation greatly reduced boattail drag at the higher subsonic speeds (e.g., at subsonic cruise). The installed drag was about zero from Mach 0.8 to 0.9, where the compression shock was ahead of the nozzle. At Mach 0.95, where the shock was near the nozzle, there was a thrust on the boattail. The boattail drag rose sharply when the compression shock moved off the end of the nozzle at higher speeds.

For the isolated nozzle, rounding the boattail juncture was effective in reducing boattail drag. The effect in flight of doing this is shown in figure 5-24. Data are shown for a sharp corner ($r/d = 0$) and for a rounded corner ($r/d = 2.5$). Little decrease in drag below the already low subsonic values was obtained; but some reduction in boattail drag occurred above Mach 1.0.

### 5.4.3 Auxiliary-Inlet Ejector Nozzle

The auxiliary-inlet ejector nozzle is shown installed on the F-106 in figure 5-25; results of the flight test are reported in reference 5-9. This nozzle had 16 auxiliary inlet doors that
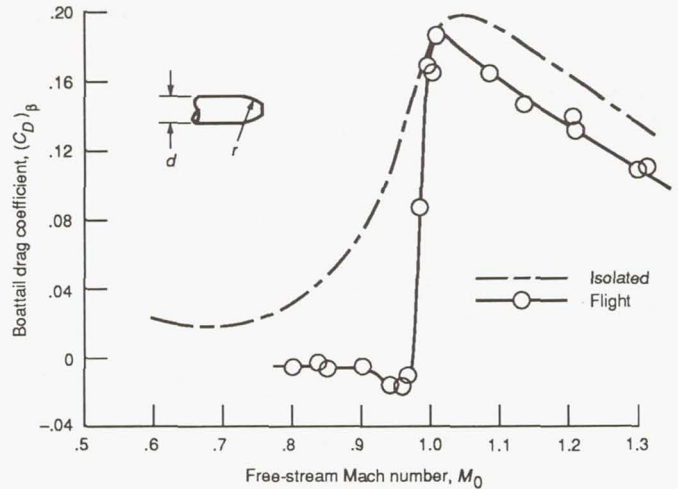


Figure 5-23.—Installation effect on boattail drag of variable-flap ejector nozzle. Ratio of radius to diameter, $r/d$, 0.
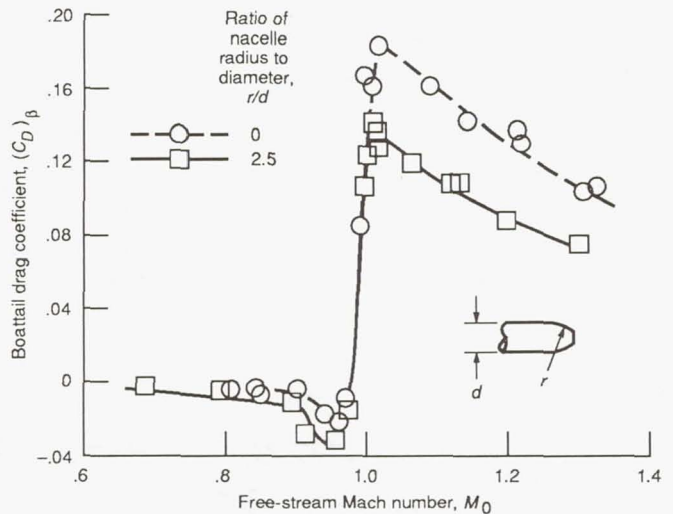


Figure 5-24.—Effect of rounded juncture on boattail drag for variable-flap ejector nozzle. Flight conditions.



Figure 5-22.—Variable-flap ejector nozzle installation. Ratio of radius to diameter, $r/d$, 2.5.



Figure 5-25.—Auxiliary-inlet ejector nozzle installation and elevon trough.

could either be fixed in place or free floating. The top three doors opened into the trough built into the wing. The nozzle boattail was again fixed at the subsonic cruise area ratio.

The Mach 0.9 performance of the auxiliary-inlet ejector nozzle, both isolated and in flight, is shown in figure 5-26. Nozzle gross thrust coefficient and boattail drag ratioed to ideal thrust are presented as a function of inlet door position. The isolated performance (dashed curve in fig. 5-26(a)) continued to rise as the doors were opened. The flight performance was somewhat better; it rose as the doors were opened but leveled off to equal the isolated performance for full-open doors. The boattail drag (fig. 5-26(b)) was lower in flight. This lower drag accounted for the higher performance with the doors partly open or closed; however, the benefit of the lower drag was lost when the doors were wide open.

As indicated in figure 5-26, the performance of the floating
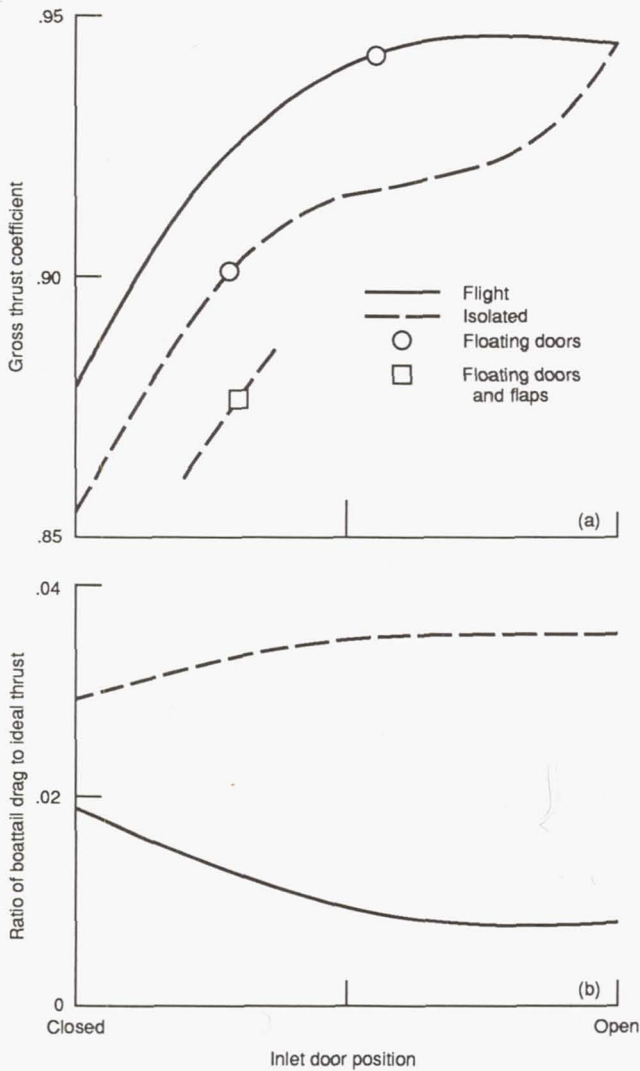
doors in flight was nearly optimum. The doors floated to an average position somewhat past mid-open. For the isolated configuration floating door performance was considerably lower. When the trailing secondary shroud flaps were also allowed to float, performance was even lower. In flight the trailing flaps probably would have floated to a lower area ratio position than they did in the isolated tests, since boattail pressures were higher in flight because of a compression shock. This position would have reduced internal over-expansion losses and resulted in better performance.

Positions of the floating inlet doors in flight (Mach 0.9) are shown in figure 5-27. The door trailing edges are viewed from the rear. The higher external pressure around the top of the nozzle held the doors open in that region; the lower external pressure on the bottom and inboard side closed the doors in those regions. When all of the doors were fixed open, little air entered the doors on the bottom. The performance shown in the previous figure for this condition was about the same as that for the floating doors.

### 5.4.4 Plug Nozzle

The plug nozzle, shown installed on the aircraft in figure 5-28, was uncooled and was operated with the primary throat in the fixed position shown, with the engine in the nonafterburning mode. The plug was not truncated.

The installed performance of this nozzle is compared with isolated data in figure 5-29, where the effect of the movement of the compression shock can be seen. The shock is ahead of the nozzle below Mach 0.9, but at Mach 0.95 it is near the primary exit, where the highest nozzle performance was obtained. The performance dropped sharply near Mach 1.0, where the compression shock moved off the end of the nozzle and low pressures were felt on the plug surface. (Flight performance data for this nozzle are presented in ref. 5-9.)



(a) Gross thrust coefficient.
(b) Boattail drag.

Figure 5-26.—Installation effect on auxiliary-inlet ejector nozzle performance. Free-stream Mach number, $M_0$, 0.9.
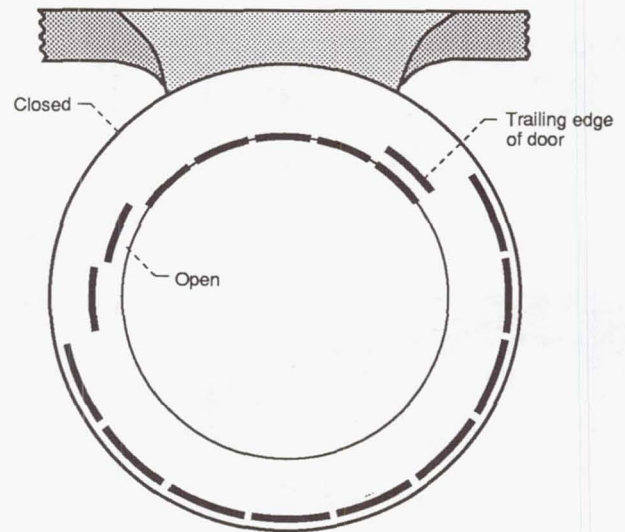


Figure 5-27.—Position of floating doors on auxiliary-inlet ejector nozzle. Free-stream Mach number, $M_0$, 0.9.

Figure 5–28.—Low-angle plug nozzle installation.
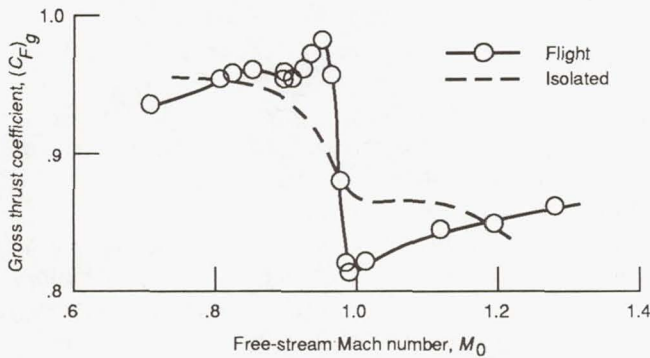


Figure 5–29.—Installation effect on low-angle plug nozzle performance.

### 5.4.5 Installation Effect on Nozzle Thrust Efficiency

The installation effect on nozzle thrust efficiency is shown in figure 5–30 for the three nozzle concepts studied for the Boeing supersonic transport from 1963 until 1971. Isolated cold flow model data from the NASA Lewis 8- by 6-Foot Supersonic Wind Tunnel are compared with the F–106 flight test data for the variable-flap ejector, auxiliary-inlet ejector, and low-angle plug nozzles. All data were obtained at an $\omega\sqrt{\tau}$ of 0.04 and at similar nozzle pressure ratios.

For the variable-flap ejector nozzle with a 15° boattail angle the installed boattail drag trend (fig. 5–23) resulted in improved installed nozzle efficiency (relative to the isolated data) across the entire speed range, as shown in figure 5–30(a). At Mach 0.9, the 3-percentage-point improvement in installed nozzle thrust efficiency was equivalent to an approximate 6-percentage-point reduction in total aircraft drag for a supersonic transport aircraft operating off design at part power. The isolated nozzle data between Mach 1.0 and 1.2 are somewhat unreliable because the wind tunnel wall interfered with terminal shock movement over the boattail.

For the auxiliary-inlet ejector nozzle with a 15° boattail angle (fig. 5–30(b)), the isolated and installed nozzle results
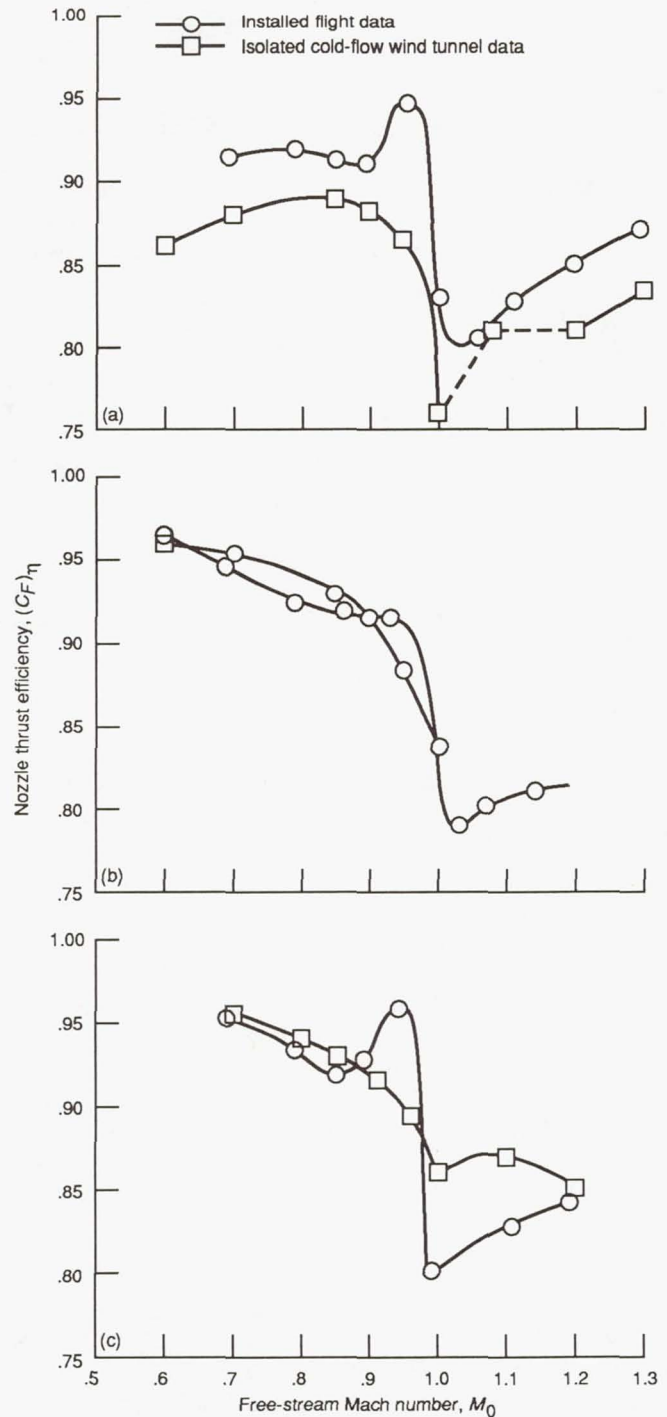


(a) Variable-flap ejector nozzle.
(b) Auxiliary-inlet ejector nozzle.
(c) Low-angle plug nozzle.

Figure 5–30.—Installation effect on nozzle efficiency.

were nearly identical at all Mach numbers tested. Between Mach 0.63 and 0.89 the installed efficiency was slightly lower than the isolated results, but this trend was reversed between Mach 0.89 and 0.99. Even though the installation effect reduced the boattail drag of this nozzle, just as it did for the

47

variable-flap ejector nozzle, this benefit was offset by added drag in the auxiliary-inlet system. These inlets did not perform as well as they did in the isolated tests because the installation effects created thick and unsymmetrical boundary layers ahead of the inlets that were not duplicated when the nozzles were tested as isolated components.

For the conical-plug nozzle with a 17° primary flap angle and retracted shroud (fig. 5–30(c)), a large favorable installation effect occurred between Mach 0.88 and 0.97. Above Mach 0.97 the installed nozzle thrust efficiency was significantly lower than the isolated efficiency, but below Mach 0.88 it was only slightly lower.

### 5.4.6 Concluding Remarks

The effect of the airframe installation on nozzle performance depended strongly on the nozzle design. Favorable and unfavorable effects were observed, and in some cases these effects were self-compensating, so that the overall effect was minor. The variable-flap ejector nozzle, however, seemed to benefit most from the airframe installation, since its performance was improved at virtually all Mach numbers. In all cases the installed performance at subsonic cruise (Mach 0.9) was as good as or better than the isolated performance.

Reference 5–10 is an excellent paper that reviews the integration of engine nacelles on commercial transport aircraft with special emphasis on the aerodynamic forces that produce lift and drag. Both subsonic and supersonic cases are considered.

## 5.5 Nozzle Cooling

So far in this chapter aerodynamic performance has been stressed. Nozzle cooling is another problem, particularly with the plug nozzle. Experimental heat transfer studies were made at NASA Lewis in the late 1960's and early 1970's on both ejector and plug nozzles to support the supersonic research effort. These experimental results are discussed briefly in this section.

### 5.5.1 Film Cooling

Figure 5–31 shows some typical results from an ejector cooling study. A cylindrical ejector was tested on a J–85 afterburning turbojet engine in an NASA Lewis altitude facility. Ejector cooling was accomplished by film cooling and radiation. Film cooling is a means of insulating the ejector wall from the hot primary jet with a layer of the cooler secondary air. Ejector wall temperatures are shown as a function of distance from the primary nozzle exit for maximum afterburning (3100 °F) and a high $\omega\sqrt{\tau}$. The predicted temperatures were obtained from a heat balance calculation for the wall (ref. 5–11). The insulating effect of the secondary stream was calculated by using a modified Hatch-Papell film-cooling correlation. This correlation was empirically developed for a flat plate, subsonic flow, and no pressure gradient. It was modified
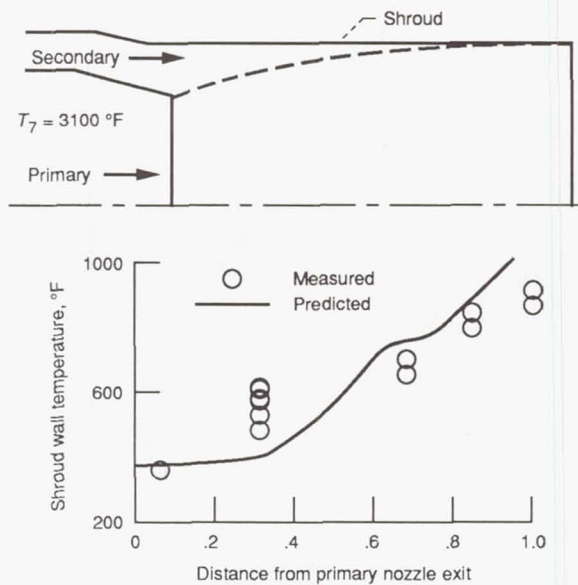


Figure 5–31.—Ejector shroud cooling.

for annular flow with varying pressures. The predicted temperatures agreed reasonably well with the measured values.

The various calculated heating and cooling mechanisms are compared in figure 5–32: the parameters that heat the wall in figure 5–32(a), and the cooling terms as a function of distance from the primary exit in figure 5–32(b). Note that radiation from the hot gas to the wall was approximately uniform over the entire ejector. The secondary airstream film cooled the wall for about two-thirds of the ejector length. At this point the secondary airstream became hotter than the wall and added heat to it. Radiation from the wall to the surroundings was the only cooling mechanism over the last one-third of the nozzle. Because similar results were obtained for other pressure ratios and secondary flow ratios, the prediction



(a) Heat in.
(b) Heat out.
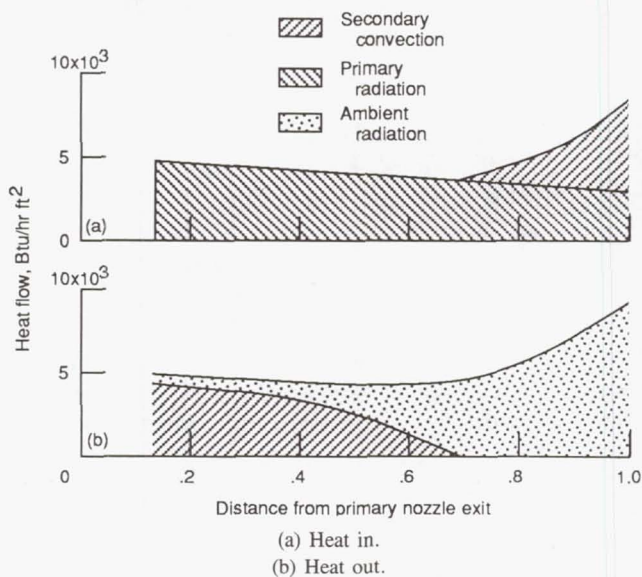
Figure 5–32.—Heat distribution in nozzle. Primary flow temperature, 3100 °F.
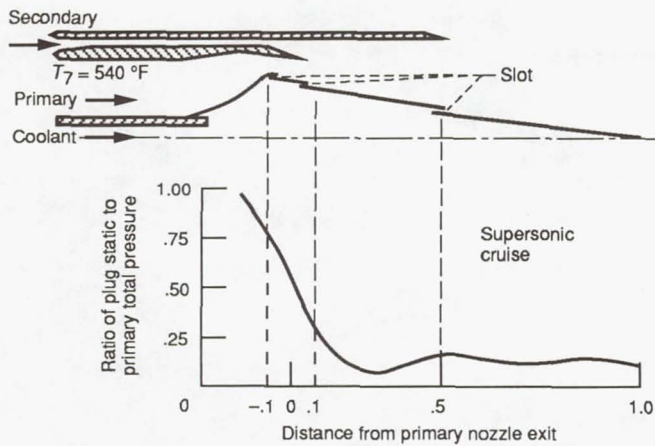
Figure 5–33.—Plug static pressure distribution in film-cooled plug nozzle.

techniques developed in reference 5–11 can be used with confidence to design ejector nozzles.

Figure 5–33 shows some typical results from a plug film-cooling study in which three separate 8.5-in.-diameter plug models were tested in an altitude facility. The model first had a film-cooling slot at the 50-percent point (i.e., halfway between the primary throat and the end of the plug); the second had a slot at the 10-percent point; the third plug had a slot upstream of the nozzle throat at the minus 10-percent point. Tests were made to primary flow temperatures of 540 °F, and the cooling air entered the plug through a sting mount. A typical plug static pressure distribution is shown for a high nozzle pressure ratio. Typically, the pressure distributions downstream of the 50-percent slot location were about constant; pressure gradients following the other two slot locations were at first favorable and then adverse.

Figure 5–34 compares measured cooling efficiencies with the Hatch-Papell film-cooling correlation. Cooling efficiency is simply a ratio of the primary recovery temperature minus the wall temperature to the primary recovery temperature minus the coolant inlet static temperature. When the wall temperature is equal to the coolant temperature, this ratio is 1.0; as the wall temperature increases, the ratio decreases. The Hatch-
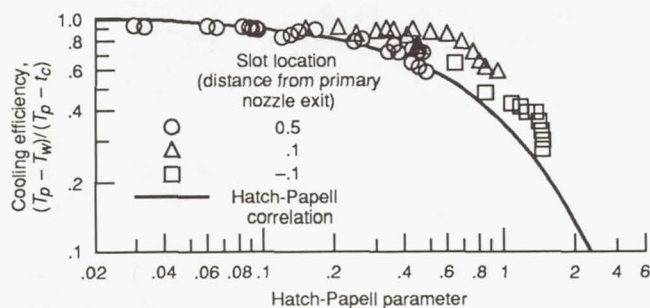
Papell parameter contains about 10 terms, including the distance from the slot exit and the coolant flow rate (ref. 5–11).

The curve in figure 5–34 represents the Hatch-Papell film-cooling correlation. The circular symbols, representing the 50-percent slot location, correlate well for all pressure ratios, coolant flow rates, and appropriate secondary shroud positions; the triangular symbols, representing the 10-percent slot location, generally fall above the correlation line. The "knee" in the data corresponds to the point where the pressure gradient turned from favorable to adverse. The favorable pressure gradient retarded the mixing of the primary and coolant streams, keeping the wall temperatures low. The adverse pressure gradient accelerated the mixing, sharply increasing the wall temperature. Similar results were obtained for the minus 10-percent slot location. All of the data of interest fall on or above the correlation line. Therefore, the measured wall temperatures were lower than would be predicted by the film-cooling correlation. As a result, using the correlation should result in a conservative prediction of plug wall temperatures.

### 5.5.2 Convective Cooling

Heat transfer tests were also made on a convectively cooled plug nozzle system, as reported in reference 5–12. The plug was strut supported for easy attachment to the J–85 after-burning turbojet engine (fig. 5–35). Cooling air was obtained from the compressor discharge ports of the engine. Cooling channels (shown in section A–A in fig. 5–35) were formed along the surfaces of the plug and struts by attaching nickel fins to the high-strength outer wall. Nickel was used because of its high thermal conductivity and the resulting high effective heat transfer from the outer wall to the coolant. A conical extension was attached to the 60-percent point on the plug and was film cooled with the cooling air discharging from the plug cooling channels. The plug nozzle is shown in figure 5–36 during a high-temperature test in the altitude facility. The





Figure 5–34.—Plug surface film-cooling correlation.
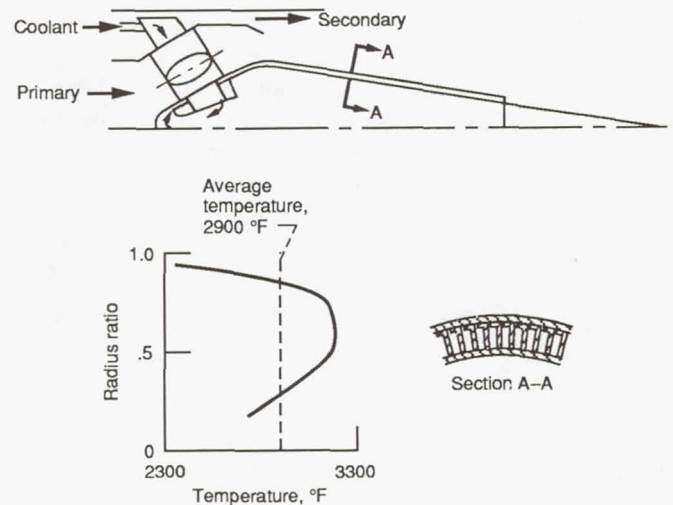
Figure 5–35.—Convectively cooled plug nozzle.

49
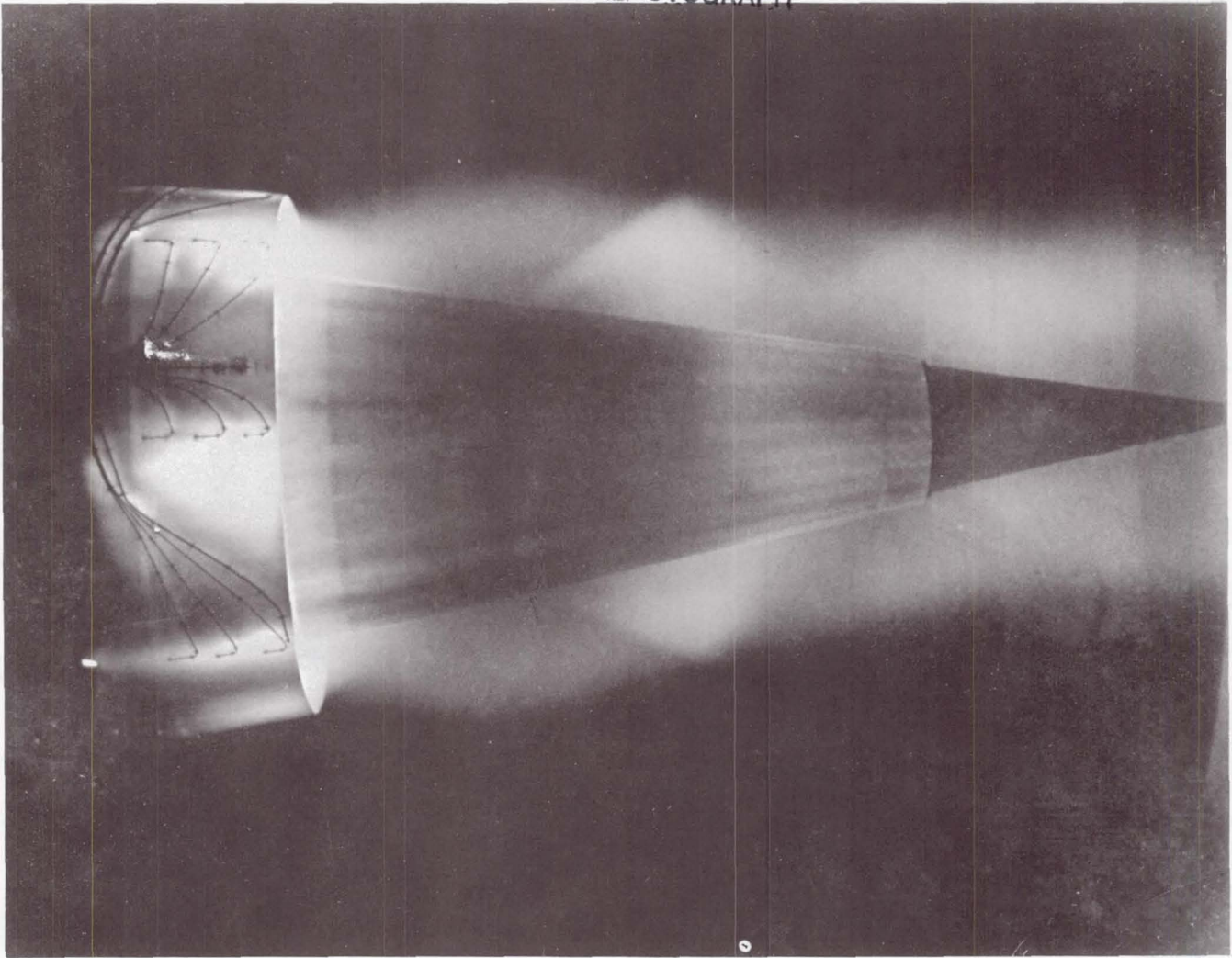
Figure 5–36.—Convectively cooled plug nozzle at afterburning temperature of 2900 °F.

primary gas temperature was 2900 °F and the nozzle pressure ratio was about 3.0. The plug and the struts were cooled with 3.5 percent of the primary airflow.

Although the plug was designed for wall temperatures of 1740 °F with this cooling flow rate, the maximum temperature measured on the plug was only 1500 °F. Note that the highest temperature measured on the plug tip extension was only 1300 °F and that the highest temperature on the primary nozzle flap was about 1700 °F. The plug wall temperatures were lower than expected because of the gas temperature profile that existed in the engine. A typical profile is shown in figure 5–35. A radius ratio of zero is on the centerline and a radius ratio of 1.0 is on the primary wall. This profile resulted from the particular afterburner fuel nozzle design for this engine. Temperatures at the plug surface were found to be as much as 500 deg F below the maximum gas temperature. This profile, which eases the plug cooling problem, could be designed into any advanced plug nozzle system.

### 5.5.3 Concluding Remarks

The purpose of the experimental tests described was to develop the prediction methods necessary to evaluate advanced nozzle systems. The experimental heat transfer tests are summarized as follows:

(1) For ejector nozzles the Hatch-Papell film-cooling correlation yielded a reasonable prediction of wall temperature when combined with radiation terms.

(2) For the film-cooled plug nozzle the Hatch-Papell correlation resulted in a conservative prediction of plug wall temperatures.

(3) An air-cooled plug could be cooled in an afterburning turbojet engine with a reasonable amount of compressor bleed air.

# 5.6 Aircraft Mission Studies

Once the reliability of the cooling prediction methods had been established, the next logical step was to use them in conjunction with the measured aerodynamic performance characteristics to determine the effect of nozzle type on the range of a supersonic transport aircraft.

## 5.6.1 Full-Size Plug Nozzle Design

Two theoretical studies were conducted to extrapolate the small-scale plug nozzle data to a full-size supersonic transport engine that could then be used in aircraft mission studies. In the first study, engine fuel was used to regeneratively cool the plug. In the second, compressor bleed air was used as the coolant. In both studies a sting-supported plug was selected rather than struts, which would have been immersed in the hottest region of the hot gas.

Because the fuel-cooled nozzle appeared to be feasible, from a heat transfer standpoint, for cooling both the plug and the sting support, no engine cycle air would be required to cool the plug. Plug wall temperatures could be kept below 1000 °F when using fuel cooling.

The theoretical study using compressor bleed air cooling indicated that for maximum afterburning 2.5 percent of the engine cycle air would be required to cool the plug below 1740 °F. The afterburner was presumed to be on during supersonic cruise, resulting in primary temperatures of about 1900 °F. The plug would not have a long life at this temperature unless it were cooled. The calculations show that 0.5 percent of the engine cycle air would be needed to ensure reasonable plug temperatures during supersonic cruise.

## 5.6.2 Effect of Nozzle Type on Aircraft Range

The effect of nozzle type on the range of a supersonic transport aircraft, if the cooling requirements are included along with the aerodynamic performance characteristics, is shown in figure 5-37. The airplane and the two missions illustrated are the same as those illustrated in the preceding chapter (fig. 4-6). The auxiliary-inlet ejector nozzle was used as a baseline configuration; it provided a range of 3930 nautical miles for a typical Mach 2.7 mission. Both analytical calculations and experimental data (fig. 4-11) have shown that the variable-flap ejector has about a 0.5-percentage-point higher gross thrust during supersonic cruise and therefore provides an additional 68 nautical miles of range.

The plug nozzle was competitive with the variable-flap ejector if the plug surface was cooled with the engine fuel at no loss in cycle efficiency. In contrast, a plug cooled with compressor discharge air showed little gain in range over the baseline nozzle. The range of the air-cooled plug could be improved, however, if an interstage bleed could be used as the source for the cooling flow. Although the range comparison shown did not account for any of these factors, the plug nozzle has other features that make it an attractive nozzle concept. It may be easier to seal, has less mechanical complexity, and may be inherently quieter.

Finally, the plug nozzle provided the most range for an all-subsonic mission at Mach 0.9, as shown in figure 5-37(b), whereas the two ejector nozzles had essentially the same installed performance at Mach 0.9. The plug nozzle concept had the highest installed performance at subsonic cruise, based on in-flight thrust measurements using the F-106 aircraft (fig. 5-30).
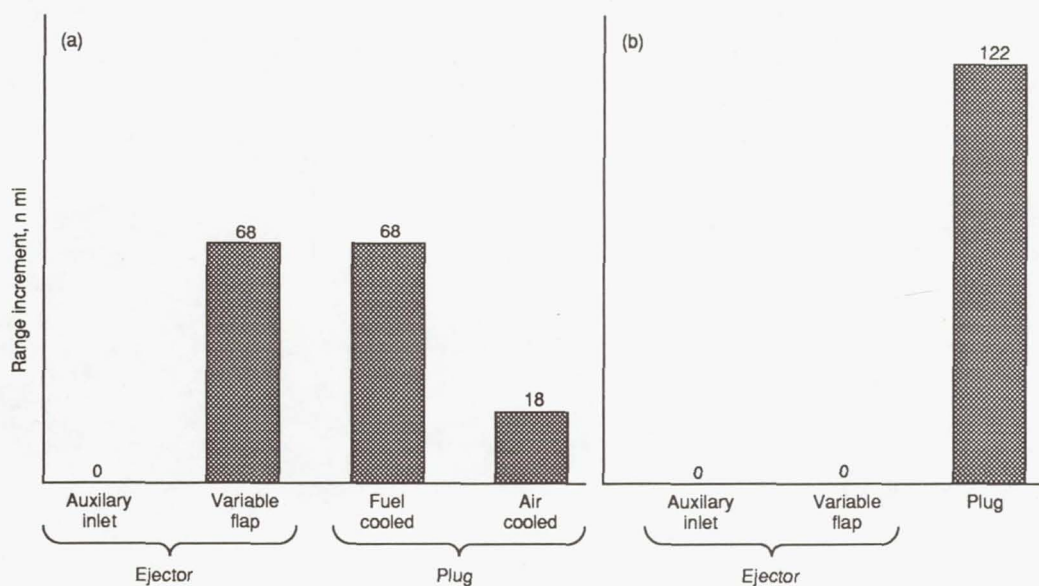


(a) Supersonic cruise mission; range, 3930 n mi.
(b) Subsonic cruise mission; range, 3280 n mi.

Figure 5-37.—Effect of nozzle type on range. Supersonic cruise aircraft; takeoff gross weight, 750 000 lb; payload, 49 000 lb.

# 5.7 References

5-1. Steffen, F.W.; and Jones, J.R.: Performance of a Wind Tunnel Model of an Aerodynamically Positioned Variable Flap Ejector at Mach Numbers From 0 to 2.0. NASA TM X-1639, 1968.

5-2. Alford, J.S.; and Taylor, R.P.: Aerodynamic Stability Considerations of High-Pressure Ratio, Variable-Geometry Jet Nozzles. J. Aircraft, vol. 2, no. 4, Jul.-Aug. 1965, pp. 308-311.

5-3. Shrewsbury, G.D.; and Jones, J.R.: Static Performance of an Auxiliary Inlet Ejector Nozzle for Supersonic Cruise Aircraft. NASA TM X-1653, 1968.

5-4. Bresnahan, D.L.: Performance of an Aerodynamically Positioned Auxiliary Inlet Ejector Nozzle at Mach Numbers From 0 to 2.0. NASA TM X-2023, 1970.

5-5. Herbert, M.V.: Centre-Body Nozzles for Supersonic Transport Aircraft. J. Roy. Aeronaut. Soc., vol. 71, no. 1, Jan. 1967, pp. 14-22.

5-6. Bresnahan, D.L.: Experimental Investigation of a 10° Conical Turbojet Plug Nozzle With Iris Primary and Translating Shroud at Mach Numbers From 0 to 2.0. NASA TM X-1709, 1968.

5-7. Bresnahan, D.L.; and Johns, A.L.: Cold Flow Investigation of a Low Angle Turbojet Plug Nozzle With Fixed Throat and Translating Shroud at Mach Numbers From 0 to 2.0. NASA TM X-1619, 1968.

5-8. Mikkelson, D.C.; and Head, V.L.: Flight Investigation of Airframe Installation Effects on a Variable Flap Ejector Nozzle of an Underwing Engine Nacelle at Mach Numbers From 0.5 to 1.3. NASA TM X-2010, 1970.

5-9. Samanich, N.E.; and Burley, R.R.: Flight Performance of Auxiliary Inlet Ejector and Plug Nozzle at Transonic Speeds. Paper 70-701, AIAA, June 1970. (Also NASA TM-52784, 1970.)

5-10. Swan, W.C.: A Discussion of Selected Aerodynamic Problems on Integration of Propulsion Systems With the Airframe on Transport Aircraft. Aerodynamics of Power Plant Installation, Part 1, Agardograph-103-Pt-1, AGARD, Neuilly-Sur-Seine, France, 1965, pp. 23-68.

5-11. Chenoweth, F.C.; and Lieberman, A.: Prediction of Heat Transfer Characteristics for Ejector Exhaust Nozzles. Analytical Methods in Aircraft Aerodynamics. NASA SP-228, 1969, pp. 623-638.

5-12. Clark, J.S.; Graber, E.J.; and Straight, D.M.: Experimental Heat Transfer and Flow Results From an Air-Cooled Plug Nozzle System. NASA TM X-52897, 1970.

# Chapter 6

# Supersonic Cruise Research Nozzles (1971–1985)—The Second Generation

The United States Supersonic Transport (SST) Program was terminated in May 1971 after 8 years of research and development. At that time both the Government and the industry recognized that significant technical advancements would be required to make a second-generation supersonic cruise aircraft economically viable and environmentally acceptable. Generic research on supersonic cruise aircraft continued at a low level after the cancellation of the SST program in 1971, under the guidance of the Federal Aviation Administration. The program was transferred to NASA in 1972 and named the Supersonic Cruise Aircraft Research (SCAR) Program. The intent of this effort was to identify and investigate areas requiring new or improved technologies that would lead to substantially improved aircraft and engine performance. The two-pronged effort involved the NASA Langley Research Center as the lead center working closely with three airframe contractors (Boeing, Lockheed, and McDonnell Douglas) and the NASA Lewis Research Center working with two engine companies (General Electric and Pratt & Whitney).

A major portion of the SCAR program was devoted to propulsion technology. These investigations produced concepts for a variable-cycle engine able to vary the airflow at different power settings. The engine may be able to operate at nearly optimum fuel efficiency while cruising at either supersonic (turbojet) or subsonic (turbofan) speeds. The variable-cycle engine also features a coannular exhaust nozzle system. At takeoff the coannular nozzle operates with an inverted velocity profile; that is, the lower velocity jet is surrounded by the higher velocity jet, with a velocity ratio of about 1.6 to 1.7. This inverted velocity profile significantly reduces takeoff jet noise.

By 1975 the number of candidate engines was reduced to four. Two were designed at Pratt & Whitney: a conventional, nonaugmented, low-bypass-ratio engine with a mixed-flow nozzle, and a variable-stream-control (ductburning turbofan) engine; and two were designed at General Electric, a double- and a single-bypass engine. The more unconventional General Electric double-bypass and Pratt & Whitney variable-stream-control engines represented relatively quieter engines, even unsuppressed, but required unique and technically challenging components, such as a duct burner, inverted-velocity-profile nozzles, and variable-bypass injectors. These unconventional engines were chosen as the two engines for continued research into low-noise exhaust systems. Research on second-generation nozzles continued until variable-cycle engine testing was terminated in 1981. However, model nozzle testing, which had begun prior to that time, continued until the last test report was published in early 1985. In 1979 the name of the SCAR program was shortened to the Supersonic Cruise Research (SCR) Program.

This chapter discusses the second-generation nozzle concepts designed and tested by the two engine companies for use on their variable-cycle engines. These nozzles featured inverted velocity profiles to reduce jet noise at takeoff and landing. The in-house and contracted efforts of NASA Lewis in engine selection, testbed experiments, and noise reduction research over the decade from 1972 to 1981 are described in reference 6–1.

## 6.1 Pratt & Whitney Coannular Ejector Nozzle

As part of the SCR program Pratt & Whitney identified the variable-stream-control engine as an attractive concept in terms of system performance and potential for low noise. These studies indicated that a high-performance coannular ejector nozzle with an inverted velocity profile is a critical component of its propulsion system. Acoustic tests of this nozzle concept have demonstrated the ability to reduce jet noise at both static and simulated takeoff flight conditions, as reported in references 6–2 and 6–3. A follow-on program, reported in reference 6–4, extended the demonstration of coannular exhaust system performance to key supersonic and subsonic flight conditions.

Two configurations of a variable-geometry coannular ejector nozzle were identified as promising for the variable-stream-

control engine exhaust system. These configurations were selected for their potential for low jet noise at takeoff and good supersonic cruise thrust efficiency. The baseline configuration was a variable-area, short-flap fan nozzle with a contoured flow splitter. The alternative configuration was a variable-area, iris-flap fan nozzle with a conical flow splitter. The iris flap was chosen for its potentially better subsonic performance. Common to both configurations was a translating plug in the primary stream and an actuated-inlet ejector shroud with a clamshell reverser. Three configurations, approximately one-tenth scale, of each design were tested in the NASA Lewis 8- by 6-Foot Supersonic Wind Tunnel. The models simulated takeoff, subsonic cruise, and supersonic cruise configurations of full-scale exhaust systems. The results of these tests are contained in reference 6-4 and are summarized herein.

### 6.1.1 Exhaust Nozzle System Design

Figure 6-1 shows the basic arrangement of the major engine components of the Pratt & Whitney variable-stream-control engine. It also illustrates the inverted jet velocity profile at takeoff. The engine was a twin-spool configuration similar to a conventional turbofan but with the added feature of a burner in the fan duct. The engine derived its name from its ability to independently control the primary and bypass streams. The coannular nozzle provided variable throat areas for the core and fan duct flow and also included an ejector thrust-reverser system. At takeoff the primary stream was throttled to an intermediate power setting while the duct burner was operated at its maximum design temperature. The independent control of the two streams provided the unique inverted velocity profile needed to take advantage of the coannular nozzle noise benefit. The bypass jet velocity was about 60 to 70 percent higher than the primary jet velocity. This inverted velocity profile significantly reduced takeoff jet noise.

Refinements of the ejector nozzle design for the variable-stream-control engine formed the basis for the test configurations. The first configuration (fig. 6-2) featured an isentropic contoured splitter so that the merging fan and primary flows would exit nearly parallel. Fan nozzle area was varied by using a short flap that rotated in a radial plane. The design reflected the minimum overall length required for optimum thrust minus drag at the critical supersonic cruise condition. A translating centerbody plug controlled the primary nozzle area. Two internal clamshells were positioned to provide the initial portion of the ejector shroud's expansion surface. At low-speed conditions the nozzle converted to an actuated auxiliary-inlet ejector. Actuated inlet flaps were opened to admit external airflow into the shroud, and the internal clamshells were aligned with the inlet flow. Floating tail flaps were aerodynamically positioned to provide the proper exit flow area. The clamshells were also used for thrust reversal by rotating them back to the nozzle centerline. The reversed flow was then expelled through the open inlet doors.

The iris nozzle configuration (fig. 6-3) had the potential for improving subsonic performance relative to the short-flap configuration because there was less tendency for inlet flow separation off the longer, smoother flap. The isentropic splitter was replaced with a conical splitter to quantify the loss of a modest splitter flow impingement angle.

One-tenth scale model configurations of both the iris and short-flap nozzle designs were fabricated for testing. The models were designed to simulate the exhaust systems operating in the takeoff, subsonic cruise, and supersonic cruise modes. Scale models of these nozzle configurations were tested in the NASA Lewis 8- by 6-Foot Supersonic Wind Tunnel (fig. 6-4) in the fall of 1978.

### 6.1.2 Supersonic Cruise Performance

The iris and short-flap nozzle efficiencies at supersonic cruise engine operating conditions are compared in figure 6-5. Secondary flow for the supersonic cruise models was provided by bleeding flow from the fan duct stream to an annulus around the fan nozzle, where it then flowed into the ejector shroud. The bleed flow passed through a series of holes in the fan duct
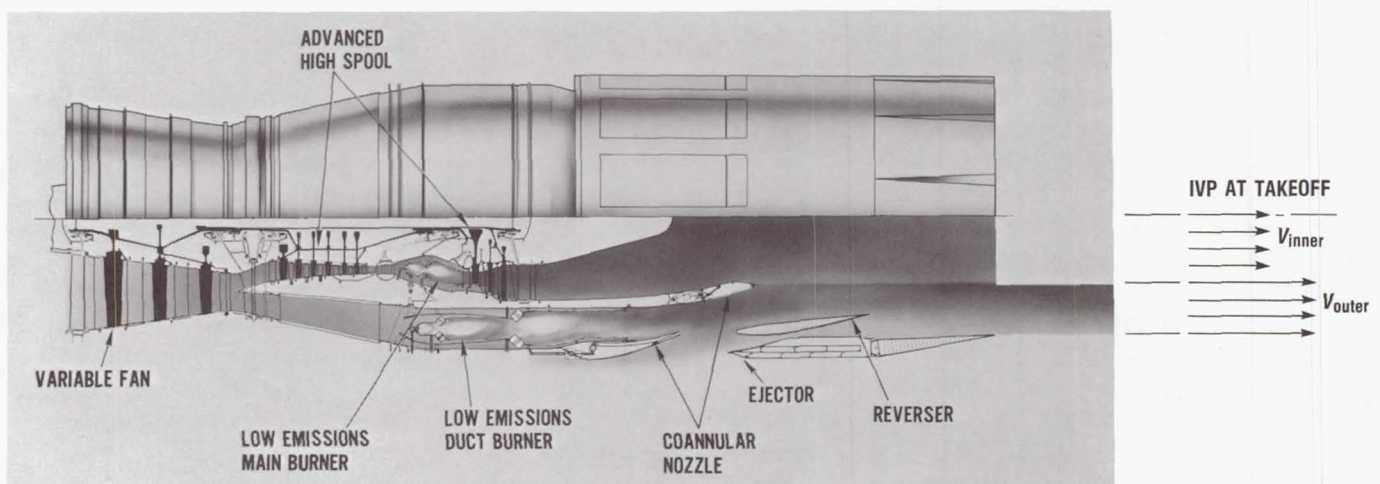


Figure 6-1.—Pratt & Whitney variable-stream-control engine.

Transonic climb

Subsonic cruise

Takeoff and
subsonic
climb

Supersonic
cruise

Reverse

Isentropic
splitter

Takeoff and
subsonic
cruise

Subsonic cruise

Takeoff

Short-flap fan nozzle
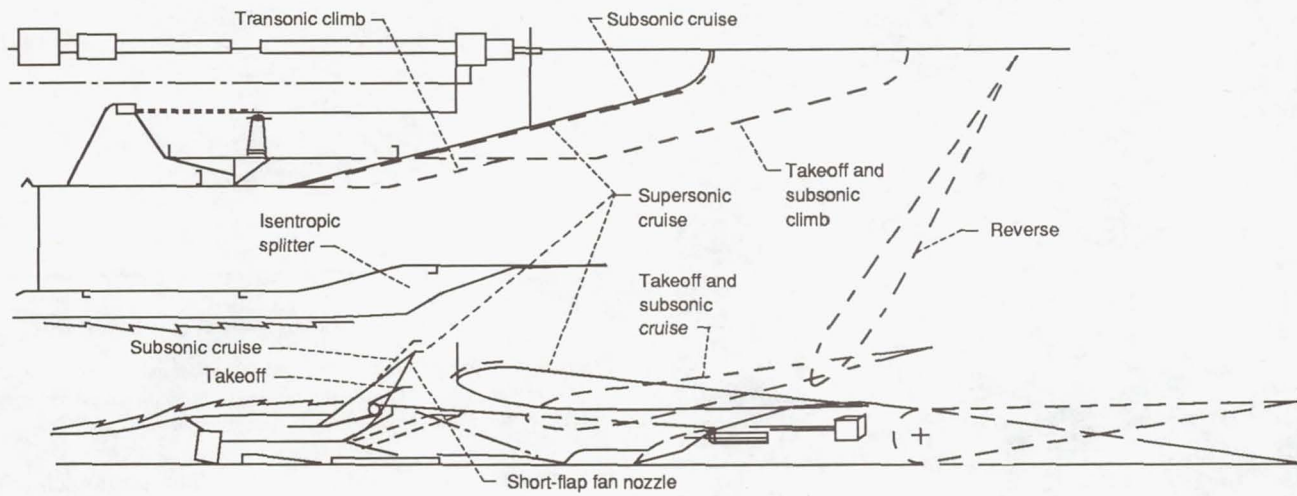
Figure 6–2.—Short-flap nozzle.

All other hardware except
in this area is the same as
shown in figure 6–2

Conical splitter

Supersonic cruise

Subsonic cruise

Takeoff

Iris flap
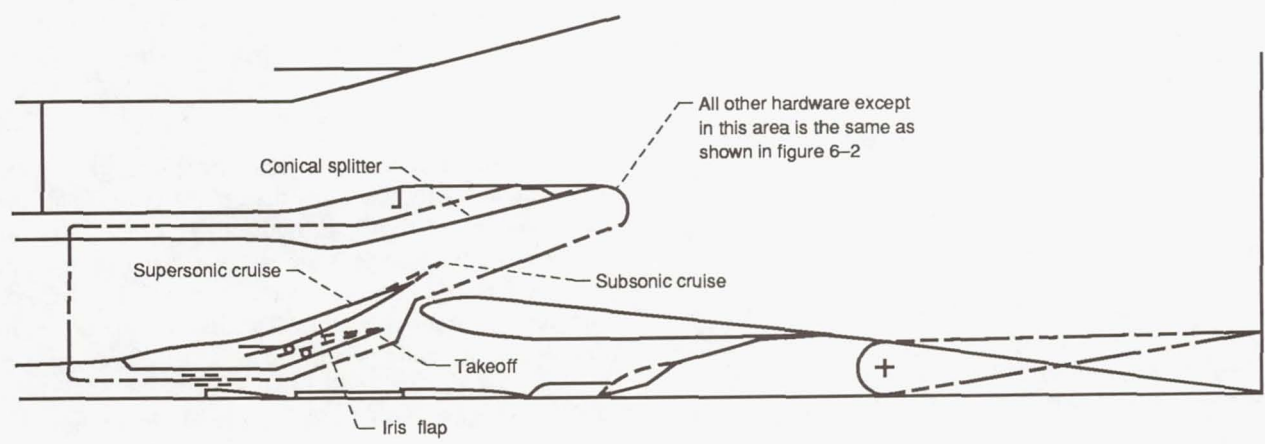
Figure 6–3.—Iris nozzle.

55
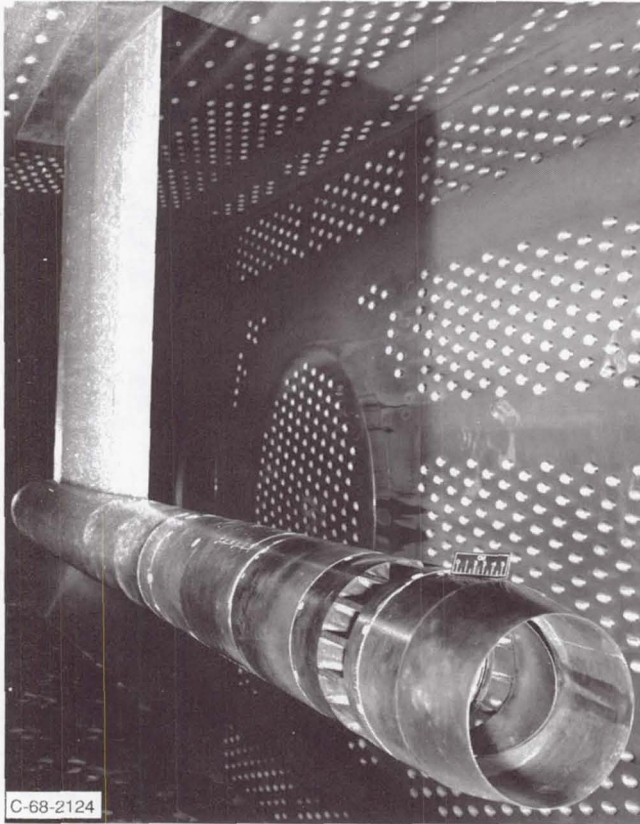
Figure 6–4.—Variable-stream-control engine nozzle model in NASA Lewis 8- by 6-Foot Supersonic Wind Tunnel.
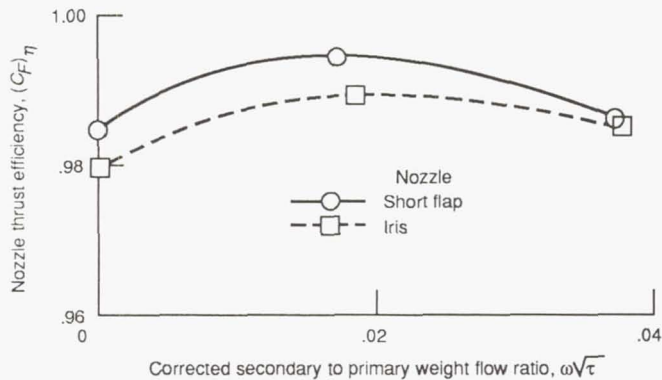


Figure 6–5.—Efficiency of short-flap and iris nozzles at supersonic cruise. Free-stream Mach number, $M_0$, 2.0; fan nozzle pressure ratio, $P_f/p_0$, 27.5; fan to primary pressure split, $P_f/P_p$, 2.32.

outer wall. The corrected secondary to primary weight flow ratio $\omega\sqrt{\tau}$ was set by varying the number of open holes. The nozzle thrust efficiency used herein does not penalize the nozzle for external skin friction drag.

The comparison in figure 6–5 shows that at $\omega\sqrt{\tau}$ from 0 to 0.04 the overall performance of the short-flap nozzle was superior to that of the iris configuration. Data trends indicated that an $\omega\sqrt{\tau}$ of only 0.02 is required to obtain maximum nozzle
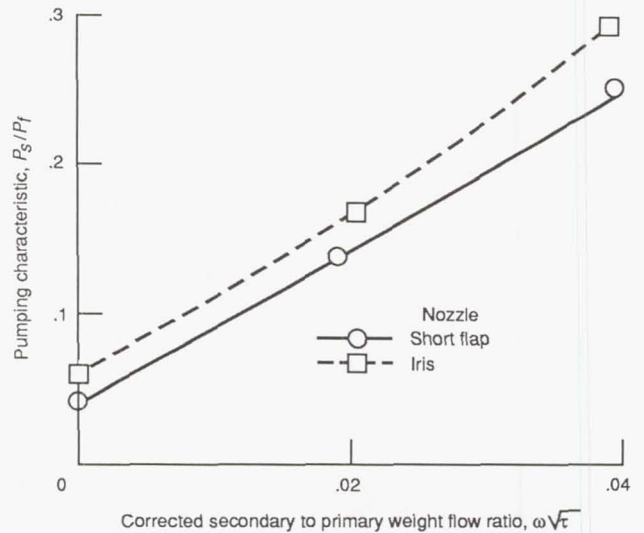


Figure 6–6.—Pumping characteristics of short-flap and iris nozzles at supersonic cruise. Free-stream Mach number, $M_0$, 2.0; fan nozzle pressure ratio, $P_f/p_0$, 27.5; fan to primary pressure split, $P_f/P_p$, 2.32.

performance. At this ratio the short-flap nozzle achieved a maximum thrust efficiency of 0.995 and the iris configuration, 0.990.

A comparison of pumping characteristics for the iris and short-flap configurations tested over a range of $\omega\sqrt{\tau}$ (fig. 6–6) shows that this parameter is dependent on the nozzle geometry. Since both configurations were tested with the same ejector, the difference in nozzle pumping characteristics was attributed to the variance of the fan nozzle design (i.e., isentropic versus conical flow splitter). Previous experience indicated that the pumping characteristics were influenced by the nozzle shape as well as by the spacing between the fan nozzle and the minimum diameter of the ejector shroud. The short-flap configuration exhibited better pumping characteristics.

### 6.1.3 Subsonic Performance

Both configurations were tested over a range of subsonic Mach numbers to determine the effects of external flow on performance, as shown in figure 6–7. The data show that performance deficiencies were related to external flow effects, since both nozzles demonstrated significantly higher performance levels at static conditions. The iris configuration provided the highest subsonic performance, as expected.

### 6.1.4 Comparison of Performance With Advanced Supersonic Transport Study Goals

Measured nozzle performance was compared with goals assumed in the advanced supersonic transport propulsion studies. Data are shown in figure 6–8 for both the iris and short-flap configurations at simulated engine operating conditions and flight Mach numbers. The comparison shows that at supersonic cruise conditions the performance of both configurations at zero secondary flow achieved the study goals.
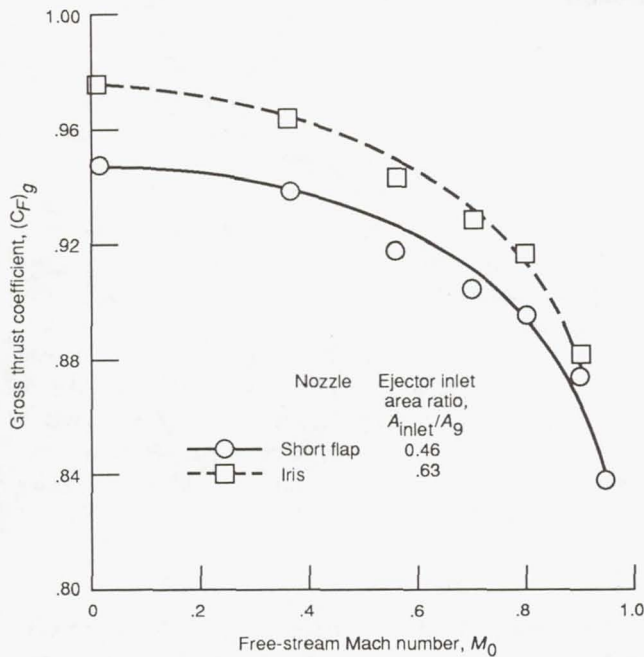
Figure 6–7.—Effect of free-stream Mach number on nozzle performance. Fan nozzle pressure ratio, $P_f/p_0$, 5.26; fan to primary pressure split, $P_f/P_p$, 1.97; clamshell angle, $17°$.
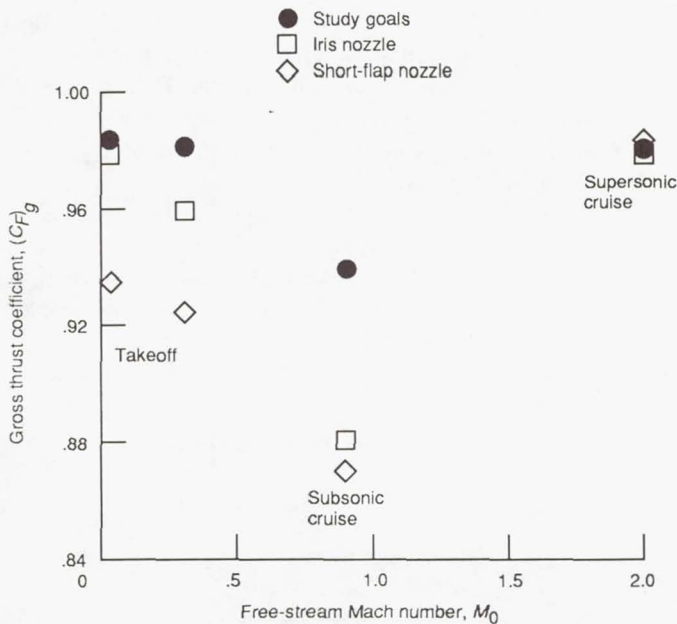


Figure 6–8.—Measured nozzle performance compared with propulsion study goals. Corrected secondary to primary weight flow ratio, $\omega\sqrt{\tau}$, 0.

The iris and short-flap configurations demonstrated gross thrust coefficients of 0.980 and 0.984, respectively. The performance of both configurations was deficient at subsonic cruise conditions relative to the study goal—6 percentage points for the iris and 7.5 percentage points for the short-flap configuration. At takeoff conditions the performance of the iris configuration approached the study goals within

0.5 percentage point statically, but was 2 percentage points lower at climbout. The short-flap configuration, however, was deficient by 4 and 6 percent at takeoff and climbout, respectively.

### 6.1.5 Concluding Remarks

The low-speed performance of Pratt & Whitney's coannular ejector nozzle was disappointing, especially at subsonic cruise conditions, where the measured performance levels were from 6 to 7.5 percentage points lower than the study goals. Diagnostic tests of the subsonic cruise configurations showed that the lower performance levels were the result of an aerodynamic flow separation over the ejector's inlet doors. It was obvious that additional work was required to improve the off-design performance of this ejector nozzle concept.

This concern resulted in a redesign of the nozzle and a follow-on wind tunnel test of an improved configuration. The aerodynamic redesign requirements were intended to improve performance at the critical off-design operating points. This was accomplished by reducing the ejector inlet turning angles, minimizing internal overexpansions and static pressure mismatches, and minimizing core/bypass flow impingement angle.

The refined ejector nozzle configuration was subsequently designed, fabricated, and tested in the NASA Lewis 8- by 6-Foot Supersonic Wind Tunnel. Performance of the refined actuated-inlet ejector nozzle is presented in reference 6–5 and compared with that of the iris and short-flap configurations at takeoff, subsonic, and supersonic cruise conditions in figure 6–9.
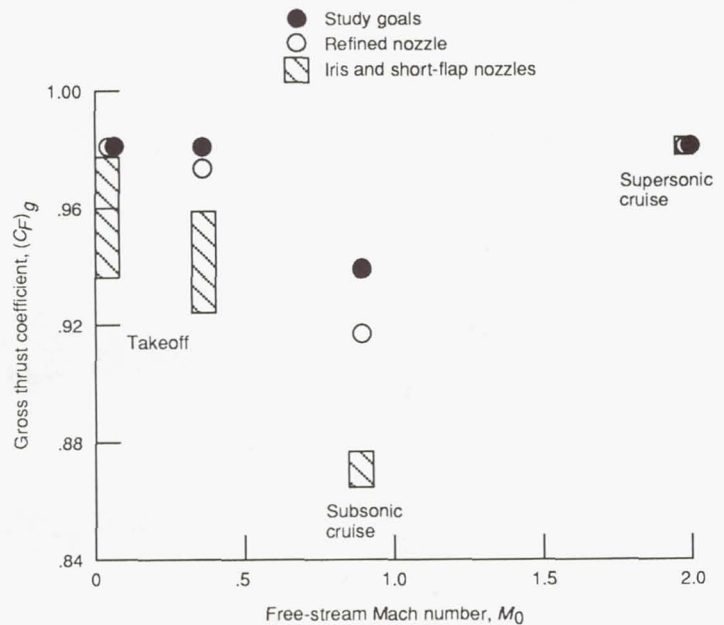


Figure 6–9.—Nozzle performance of refined actuated-inlet ejector nozzle compared with previous ejector test results and propulsion study goals.

Relative to the iris nozzle, which had the better takeoff and subsonic cruise performance, the refined design showed a takeoff performance improvement of 0.3 percentage point statically and 1.6 percentage points at flyover conditions. At subsonic cruise the refined design showed a significant 4.2-percentage-point improvement in performance. At supersonic cruise the refined configuration achieved the same high level of nozzle performance previously demonstrated. Comparing the test results with the performance goals established in the propulsion study showed that the takeoff goal was met at static conditions and nearly achieved, within 0.9 percentage point, at Mach 0.36 flyover conditions. Subsonic cruise performance was within 2.3 percentage points of the goal. The critical supersonic cruise performance goal was attained.

## 6.2 General Electric Coannular Plug Nozzle

Jet noise reduction and control has been one of the dominant forces in supersonic cruise research. Hence, the exhaust system, the primary component through which the jet noise abatement schemes are carried out, has received considerable attention at General Electric. Their product design engines for the NASA SCR program include coannular nozzle concepts because of their potential for noise reduction. These exhaust nozzle system concepts feature inverted-flow coannular designs for their double-bypass, variable-cycle engine, as shown in figure 6–10. The double-bypass engine concept is a turbofan engine in which the fan has been split into two blocks, each with its own bypass duct for better control of the flow over a broad spectrum of operating conditions. The enlarged front-block fan is designed to accommodate all of the airflow required for takeoff with reduced specific thrust (jet velocity) for low jet noise in the double-bypass operating mode. The lower-capacity rear-block fan is sized for the nominal single-bypass, high-specific-thrust, operating mode needed for transonic and supersonic acceleration and supersonic cruise.

In the low-noise takeoff mode, bypass flow is brought through crossover struts to the inside of the plug nozzle, as shown in the view above the centerline in figure 6–10. The aft portion of the plug centerbody is translated fore and aft to vary the exit area and thus control the flow of the cold fan stream. The hot turbine discharge gases flow around the nozzle support (crossover) struts and over the plug crown to surround the cold fan discharge stream and thus provide an inverted velocity profile for reduced jet noise.

In the more conventional single-bypass operating mode, shown below the centerline in figure 6–10, all of the fan bypass flow is mixed with the turbine discharge gases, and the cold flow discharge from the inner plug is shut off by translating the aft portion of the plug centerbody. Mixing is desired at flight conditions where jet noise reduction is of no concern, to provide a uniform exhaust velocity profile for greater propulsive efficiency.

### 6.2.1 Exhaust System Design

Three nozzle systems were designed: a baseline coannular nozzle, a 20-chute suppressor nozzle, and an ejector shroud nozzle (figs. 6–11 to 6–13). The basic exhaust system was a high-radius-ratio plug nozzle with a fixed primary nozzle cowl and a translating center plug nozzle. A translating outer shroud adjusted the exit area ratio for high performance throughout the pressure ratio range. The outer shroud's inner surface was contoured to closely match the primary throat area requirements at the more important operating points. The translating center plug nozzle exhausted the excess bypass airflow that could not flow through the primary nozzle throat.

During noise suppression takeoff, bypass flow was ducted from the outer-passage fan duct through the crossover ducts into the plug centerbody and then to the center plug nozzle. This arrangement, along with the high-radius-ratio primary nozzle, provided the characteristic inverted-jet-velocity-profile coannular suppression. Additional suppression was attained by deploying 20 chutes in the outer stream during suppressed operation, as shown in figure 6–12. Still higher suppression was attained by shrouding the nozzle discharge with ejected
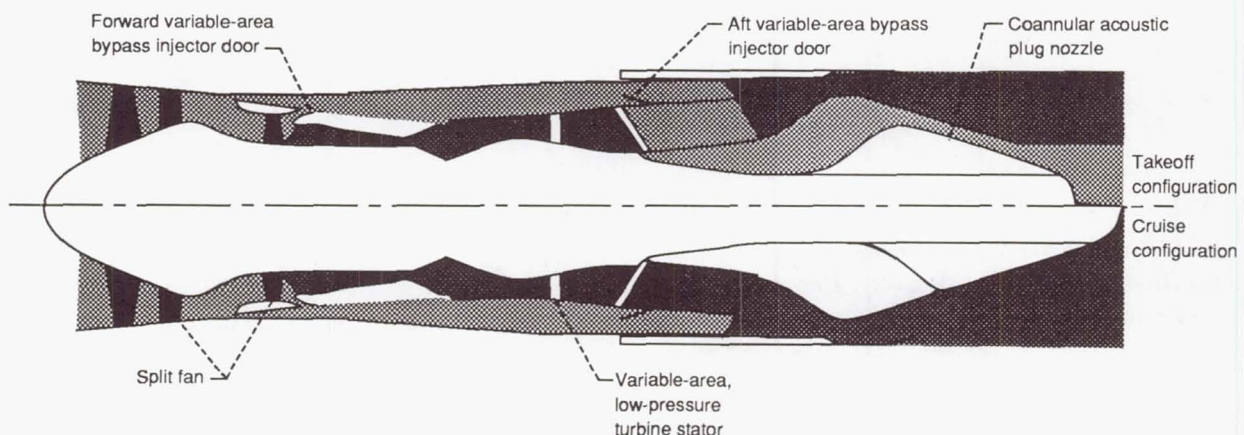


Figure 6-10.—General Electric double-bypass engine.

Thrust-reverser
cascades

Translating
shroud system

Variable-area
bypass injector
door

Augmentor
flame holders

Translating plug
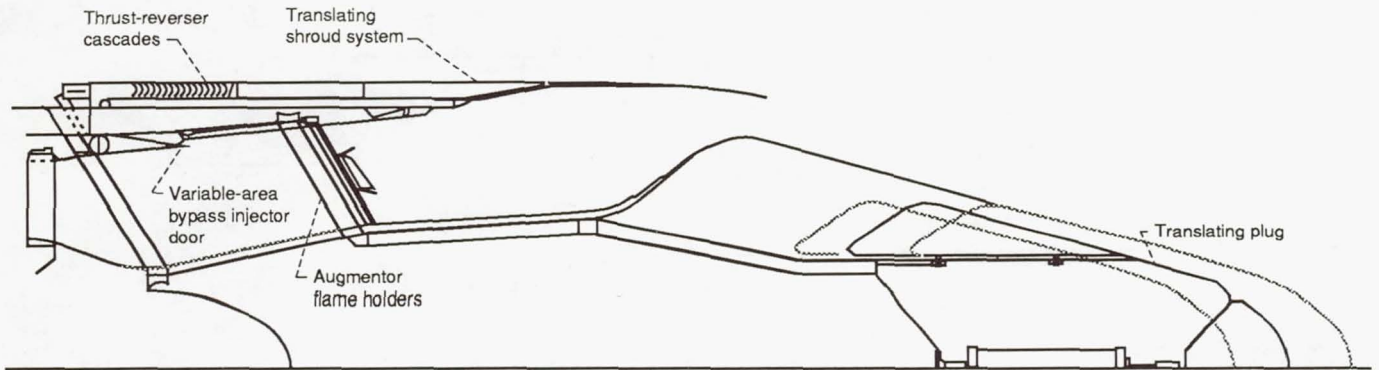
Figure 6–11.—Baseline coannular nozzle.

Thrust-reverser
cascades

Translating
shroud system

Deployed
chutes

Variable-area
bypass injector
door

Augmentor
flame holders
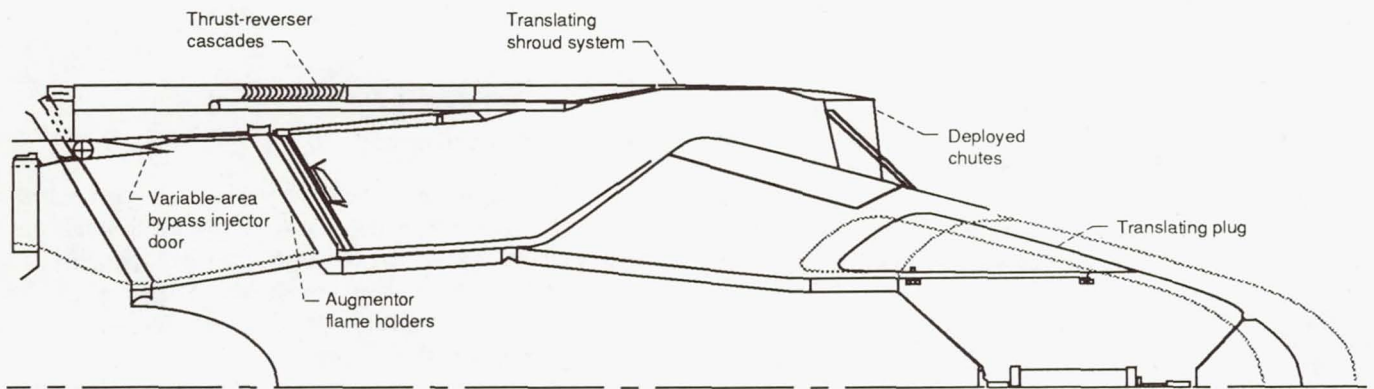
Translating plug

Figure 6–12.—20-Chute suppressor nozzle.

Thrust-reverser cascades ─

Translating shroud system ─

Ejector translating beams ─

Ejector flap and seal systems ─

Suppressor chutes ─

Variable-area bypass injector door ─

Translating plug ─

Augmentor flame holders ─

(a)

Closed ejector inlet ─

Stowed chutes ─

Closed inner nozzle ─

(b)

(a) Takeoff mode.
(b) Supersonic cruise mode.
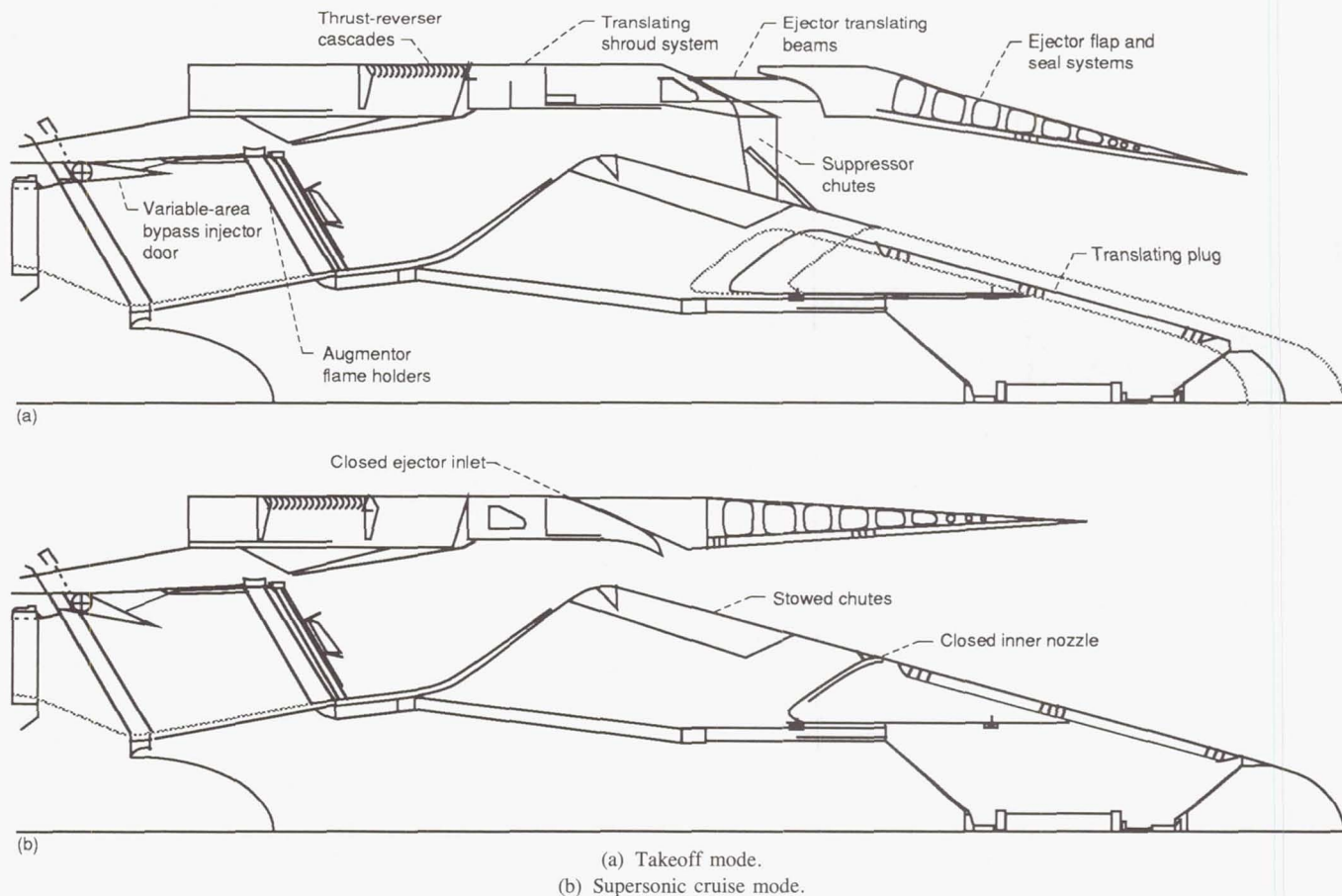
Figure 6–13.—Ejector shroud nozzle.

ambient air and a mechanical shroud lined with sound-absorbing material (fig. 6–13(a)). The ejector shroud was attached to the aft end of the translating shroud. For unsuppressed operation most of the bypass air was mixed with the core stream, the suppressor chutes were stowed in the nozzle plug outer surface, and the ejector inlet was closed for high internal performance, as shown in figure 6–13(b). The ejector shroud was made of variable-area flaps and seals so that the required expansion ratio for good performance could be met throughout the wide pressure ratio operating range.

The exhaust system included a cascade thrust reverser. The thrust-reverser cascades were attached to the forward end of the translating outer shroud. When the shroud was fully extended, the cascades were exposed on the outside and the inside, and a shroud-mounted door assembly was expanded to contact the fixed plug crown and thus block the flow through the primary nozzle. A low-temperature-rise augmenter was used in the exhaust system to provide augmented thrust during acceleration.

## 6.2.2 Nozzle Performance

Models of the three nozzle concepts were designed, fabricated, and tested in a static test stand and a transonic wind tunnel at the Fluidyne Medicine Lake Aerodynamics Laboratory. The three nozzle configurations are shown in figure 6–14. The results of this experimental test program are discussed in detail in reference 6–6 and are summarized in table 6–I.

For this program full-scale coefficient analyses were performed for all three nozzle systems. Model test coefficients were transformed to rid them of model-dependent losses and finally transformed to full-scale coefficients to put back full-scale-dependent loss effects as evidenced by higher temperatures, higher Reynolds numbers, etc. The full-scale losses were calculated by using full-scale dimensions and engine aerothermodynamic variables for the actual flightpath.

All nozzle concepts tested showed good thrust-minus-drag characteristics within practical limits for conventional nozzles with the exception of the ejector subsonic cruise configuration

TABLE 6-I.—COMPARISON OF
MEASURED PERFORMANCE

| Operating mode | Nozzle | Nozzle thrust efficiency, $(C_F)_\eta$ |
|---|---|---|
| Supersonic[a] | Coannular | 0.985 |
| | 20 Chute | .981 |
| | Ejector | .978 |
| Transonic[a] | 20 Chute | 0.944 |
| | Ejector | .921 |
| Subsonic | Coannular | 0.933 |
| | 20 Chute | .902 |
| | Ejector | .810 |
| Takeoff | Coannular | 0.975 |
| | 20 Chute | .929 |
| | Ejector | .923 |

[a]With estimated external drag.
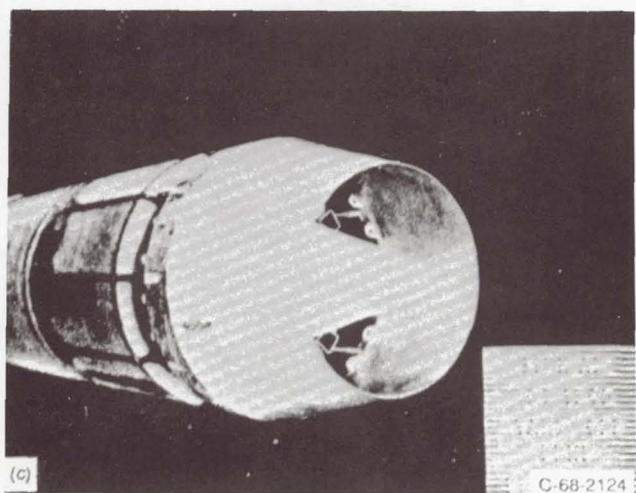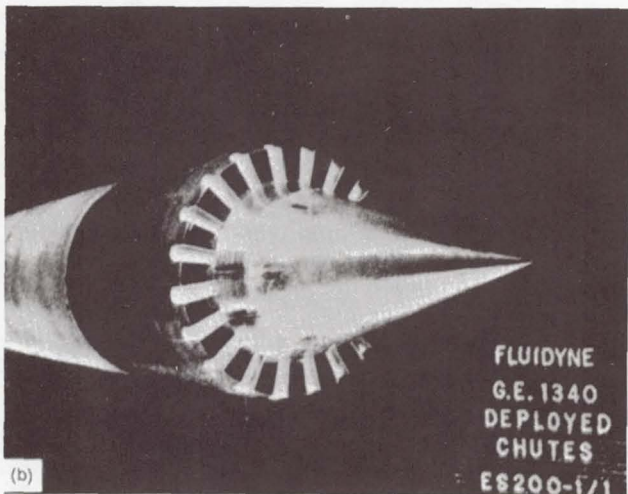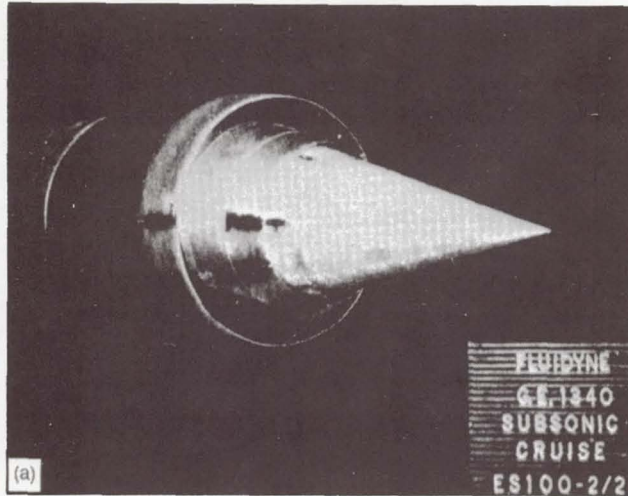
and, to a lesser degree, the 20-chute and ejector takeoff configurations. The aerodynamic performance of the ejector at subsonic cruise was lower because emphasizing takeoff acoustics and supersonic cruise aerodynamics compromised subsonic cruise performance. Examination of performance and loss coefficients showed that for the ejector subsonic cruise configuration, the losses were mainly from internal over-expansion and boattail drag. The 20-chute configuration's takeoff aerodynamics was similarly subordinated to the takeoff acoustics and led to reduced performance for that nozzle.

### 6.2.3 Mission Analysis

The results of the test were evaluated in a mission analysis study to determine engine airflow size and aircraft takeoff gross weight capable of meeting 1969 Federal Aviation Regulation (FAR) 36 stage 3 noise goals for an advanced supersonic transport application. The mission analysis computer program was set up to represent the aerodynamic and weight characteristics of a typical NASA airplane and mission profile. The NASA reference aircraft configuration had a takeoff gross weight of 762 000 lb and carried 292 passengers. The range was 4000 n mi, which included a 600-n mi subsonic cruise segment and supersonic cruise at Mach 2.32 on a hot day. Mission analysis results showing commensurate airflow and takeoff gross weight necessary to satisfy a sideline noise goal of 104.74 dB using measured performance data are summarized in table 6-II. After noise levels at the study conditions were determined, the values were traded off in order to meet the FAR 36 (1969) stage 3 noise rules. Tradeoff rules are described in appendix C of FAR 36 (ref. 6-7).

The mission analysis results show the ejector shroud nozzle to be the best among the three nozzle systems studied for the



(a) Coannular baseline.
(b) 20-Chute suppressor.
(c) Ejector shroud.

Figure 6-14.—Nozzle models.

TABLE 6–II.—SUMMARY OF
TAKEOFF GROSS WEIGHT
(MEASURED PERFORMANCE)

[Airplane and engine were sized to satisfy
sideline noise goal (effective perceived
noise level) of 104.74 dB.]

| Nozzle | Airflow, lb/sec | Takeoff gross weight,[a] lb |
|---|---|---|
| Ejector shroud | 858 | 806 000 |
| 20-Chute suppressor | 1270 | 885 000 |
| Coannular baseline | (b) | (b) |

[a]Difference between ejector shroud and 20-chute
suppressor takeoff gross weight, ~ 79 000 lb.
[b]Not realistically achievable.

mission within the constraints of FAR 36 (1969) stage 3 noise goals. The ejector shroud nozzle system had a 79 000-lb advantage in takeoff gross weight over a similar aircraft with a 20-chute nozzle. The coannular nozzle did not appear to be an attractive concept. The noise goals could not be achieved with a realistically sized airplane or engine.

**6.2.4 Concluding Remarks**

Although the ejector shroud nozzle performed well at supersonic cruise and reasonably well at takeoff, it did not meet subsonic performance levels projected during the conceptual design phase. Conflicting requirements between takeoff and supersonic cruise configurations, which are dominated by acoustics and aerodynamics, respectively, compromised the intermediate subsonic cruise point. More work is needed to improve subsonic cruise performance in order to attain the conceptual design goal.

# 6.3 References

6–1. Fishbach, L.H.; et al.: NASA Research in Supersonic Propulsion—A Decade of Progress. AIAA Paper 82–1048, June 1982. (Also NASA TM–82862.)

6–2. Kozlowski, H.; and Packman, A.B.: Aerodynamic and Acoustic Tests of Duct-Burning Turbofan Exhaust Nozzles. NASA CR–2628, 1976.

6–3. Kozlowski, H.; and Packman, A.B.: Flight Effects on the Aerodynamic and Acoustic Characteristics of Inverted Profile Coannular Nozzles. NASA CR–3018, 1978.

6–4. Nelson, D.P.: Model Aerodynamic Test Results for Two Variable Cycle Engine Coannular Exhaust Systems at Simulated Takeoff and Cruise Conditions. (PWA–5550–37, Pratt & Whitney Aircraft; NASA Contract NAS3–20061) NASA CR–159818, 1980.

6–5. Nelson, D.P.: Model Aerodynamic Test Results for a Refined Actuated Inlet Ejector Nozzle at Simulated Takeoff and Cruise Conditions. (PWA–5768–29, Pratt & Whitney Aircraft; NASA Contract NAS3–22738) NASA CR–168051, 1983.

6–6. Wagenknecht, C.D.; and Bediako, E.D.: Aerodynamic Performance Investigation of Advanced Mechanical Suppressor and Ejector Nozzle Concepts for Jet Noise Reduction. (R83AEB122–3, General Electric Co.; NASA Contract NAS3–23038) NASA CR–174860, 1985.

6–7. Noise Standards: Aircraft Type and Airworthiness Certification. Federal Aviation Regulation 36, U.S. Dept. of Transportation, 1969.

# Chapter 7

# Comparison of First- and Second-Generation Supersonic Cruise Nozzles

The nozzles discussed in chapters 5 and 6 were designed and tested as part of the United States Supersonic Transport (SST) Program (1963 to 1971) and Supersonic Cruise Research (SCR) Program (1971 to 1985). Since the SCR program followed the SST program and each lasted about a decade, the nozzle concepts have been referred to herein as first- and second-generation supersonic cruise configurations. All of the exhaust systems were designed for a commercial supersonic cruise aircraft, as shown in figure 7–1. The propulsion pods are mounted under the wing to shield the inlet from angle-of-attack effects and, with proper nacelle shaping and wing reflexing, to recover some or all of the nacelle pressure drag with increased wing lift. The nozzles extend beyond the wing trailing edge and are aligned for optimum thrust in the flight direction at cruise. In fact, the centerlines of the inlet, the engine, and the nozzle can all be different, resulting in a warped or bent nacelle, as shown in figure 7–1. The aft nozzle location is useful during thrust-reverser operation to distribute the reversed exhaust gases both over and under the wing.

The three first-generation supersonic transport nozzles are shown in figure 7–2; the performance characteristics of each are presented in references 7–1 to 7–3. All of these nozzles were designed for the General Electric SST engine, the GE–4 afterburning turbojet. Although each was a different type of nozzle with unique features, they all were ejectors in that the primary flow was used to pump the secondary cooling air. In
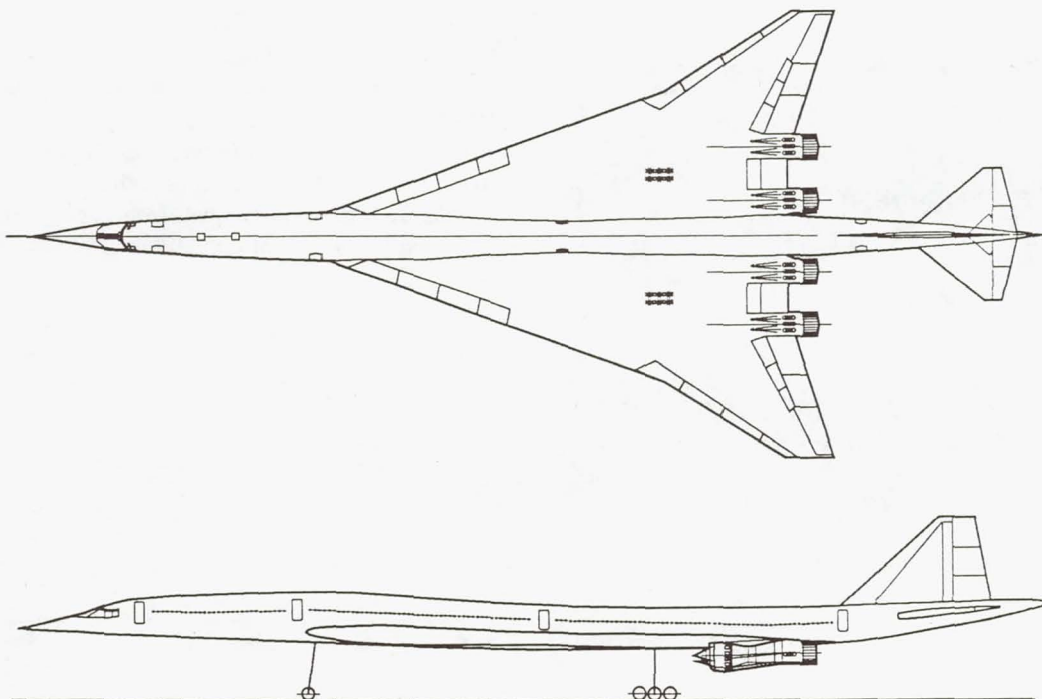


Figure 7–1.—Typical supersonic transport configuration.
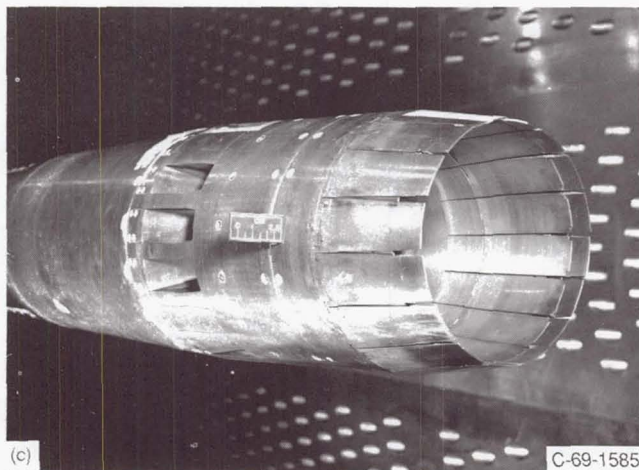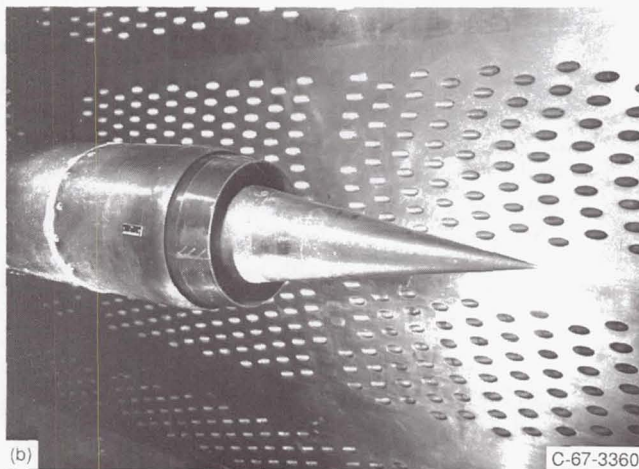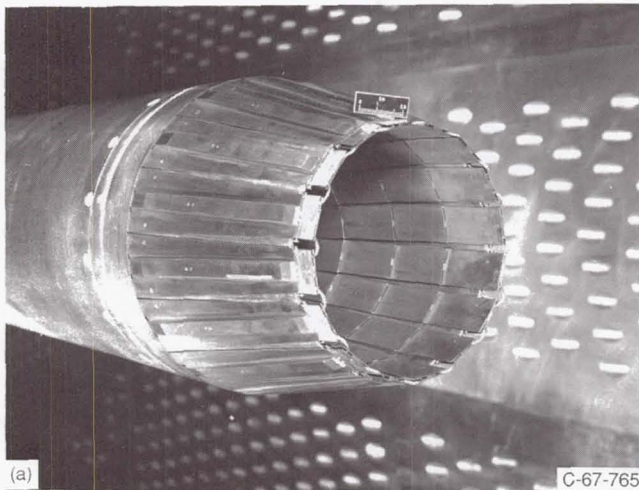
(a) General Electric variable-flap ejector.
(b) NASA Lewis low-angle plug.
(c) General Electric auxiliary-inlet ejector.

Figure 7-2.—First-generation supersonic transport nozzles.

In addition to the primary and secondary flows, the auxiliary-inlet ejector nozzle also provided a tertiary flow at subsonic speeds when the nozzle pressure ratio was low. The various flows considered for these first-generation nozzles, as well as the second-generation nozzles, are presented in table 7–I.

During the SCR program the engine companies developed engines that were able to vary cycle conditions for good propulsive efficiency at both subsonic and supersonic cruise conditions. These variable-cycle engines featured coannular nozzles, as shown in figures 6–1 and 6–10, to take advantage of the inverted velocity profile for low noise at takeoff. Pratt & Whitney provided the inverted velocity profile in their variable-stream-control engine by increasing the outer fan stream velocity with duct burning and reducing the velocity in the inner core stream. General Electric achieved the same effect by ducting the lower velocity fan stream into the middle of the plug through crossover ducts. General Electric also chose a high-radius-ratio plug nozzle configuration for additional noise suppression at takeoff.

Both second-generation nozzles (figs. 6–1 and 6–10) were designed for turbofan engines, which feature both core and fan flows. In addition, both nozzles included a tertiary flow at takeoff, as shown in table 7–I, again to promote jet mixing for reduced noise. The Pratt & Whitney actuated inlets were also open at subsonic speeds to reduce internal overexpansion losses. The performance characteristics of the second-generation exhaust nozzle concepts are presented in references 7–4 to 7–6.

This chapter compares the performance of the first- and second-generation supersonic cruise nozzles at four key operating points for a commercial aircraft. Changes in engine cycle and increased emphasis on low jet noise at takeoff have also influenced the design and performance of the exhaust system. The four key operating points are supersonic cruise, transonic acceleration, subsonic cruise, and takeoff. The supersonic cruise design point was the most important operating condition; however, considerable thought had to be given to the performance at the other off-design points. The nozzle had to be practical from an overall commercial standpoint at all flight conditions.

TABLE 7-1.—NOZZLE FLOWS

| Nozzle concept | Core flow | Fan flow | Secondary flow | Tertiary flow | Engine cycle |
|---|---|---|---|---|---|
| Variable-flap ejector | X | --- | X | --- | Turbojet |
| Low-angle plug | X | --- | X | --- | Turbojet |
| Auxiliary-inlet ejector | X | --- | X | X | Turbojet |
| Coannular ejector | X | X | --- | X | Turbofan |
| Coannular plug | X | X | --- | (a) | Turbofan |

aOnly at takeoff and climbout.

# 7.1 Supersonic Cruise

Because supersonic cruise is the most critical operating condition for a supersonic cruise aircraft, the exhaust nozzle system was designed for optimum nozzle efficiency at this point. A 1-percentage-point change in nozzle gross thrust coefficient can have a major effect on aircraft performance for typical missions. For example, General Electric has estimated that a 1-percentage-point change in nozzle gross thrust coefficient can result in a 10 000-lb change in takeoff gross weight for a typical commercial supersonic cruise aircraft.

External flow effects are generally minimal at supersonic cruise since the aft end of the nacelle is cylindrical and there is no boattail present. External drag is therefore reduced to the skin friction drag on the outer surfaces and to any drag caused by the shape of the alternate flaps and seals that make up the divergent shroud. The internal expansion ratio was designed to match the nozzle pressure ratio at cruise. The internal losses resulted from expansion mismatch, friction, angularity, and leakage. A nozzle thrust efficiency of 0.982 was selected as a practical study goal for the advanced supersonic transport during the scr program in the late 1970's and early 1980's, as shown in figure 7–3.

The thrust efficiency for the first- and second-generation nozzles is also shown in figure 7–3. The nozzle thrust efficiency is defined as the measured thrust minus external drag divided by the ideal thrust of all of the internal exhaust flows. The nozzle configurations are arranged in the figure from left to right in chronological order; the first three are the first-generation configurations and the last two are second generation. All of the nozzles shown in the figure were designed for a cruise Mach number of 2.7.

All of the nozzle configurations had typically high efficiencies at the supersonic cruise condition. There was a difference of only 1.5 percentage points in the efficiency of all five configurations—a remarkable outcome, since the measurement accuracy in the model wind tunnel test programs is generally quoted as ±0.5 percentage point. Two of the nozzles exceeded the study goals, indicating that nozzle efficiencies of over 98 percent are attainable with careful consideration to the design details of the exhaust system.

The low supersonic cruise thrust efficiency of the first-generation General Electric auxiliary-inlet ejector nozzle was attributed to the large secondary internal shroud diameter required to pass auxiliary inlet flow when the inlet doors were open at low-speed conditions. The poor performance of the second-generation General Electric plug nozzle was attributed to the stowed 20-chute suppressor and the long ejector shroud, both required to meet the noise goals at takeoff. A baseline coannular plug nozzle, without the two low-noise features, had a nozzle thrust efficiency of 0.985 at supersonic cruise. This was the same performance level attained with the NASA Lewis Research Center low-angle plug nozzle, as shown in figure 7–3, which also did not have any of the low-noise features.

# 7.2 Transonic Acceleration

Nozzle thrust efficiency is not as critical at transonic acceleration as at supersonic and subsonic cruise. It is, however, important from a time-to-climb consideration and is usually measured in a wind tunnel test program. The General Electric Company estimated that a 1-percentage-point change in transonic acceleration gross thrust coefficient is equivalent to a 2000-lb change in takeoff gross weight for a typical supersonic cruise aircraft. The sensitivity is therefore about one-fifth of that at supersonic cruise. The scr program did not set a study goal for this flight condition, but a nozzle efficiency of 0.95 would probably be realistic.

The measured transonic thrust efficiency of the first- and second-generation nozzles is shown in figure 7–4 for an afterburning acceleration at Mach 1.2. The efficiency of the Pratt & Whitney actuated-inlet ejector was not obtained at this flight condition. The performance of the three first-generation nozzles was good. The low-angle plug nozzle had the best
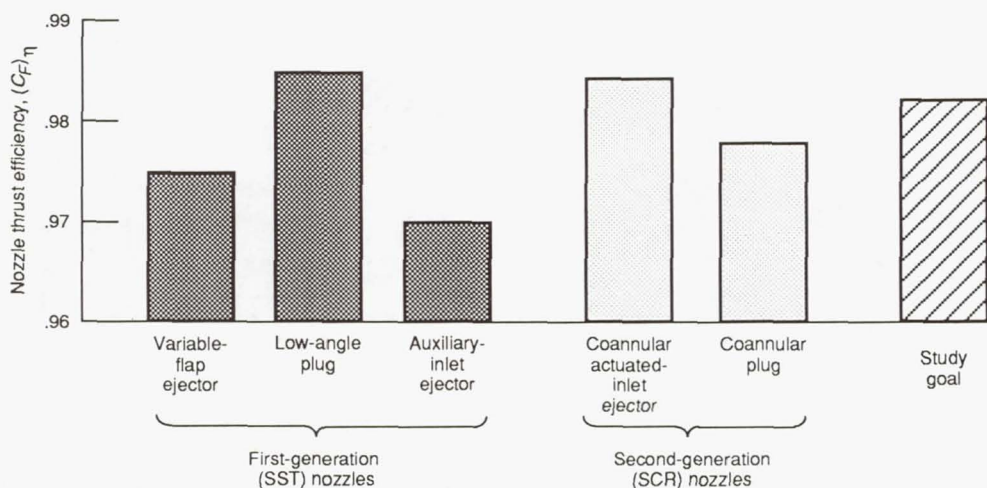


Figure 7–3.—Supersonic cruise (Mach 2.7) thrust efficiency.
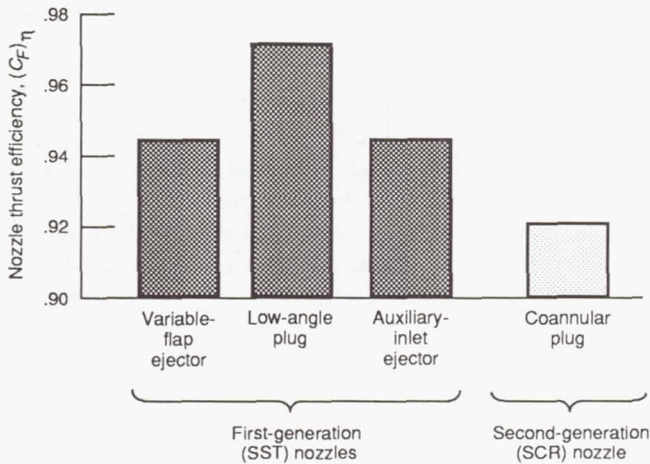
Figure 7–4.—Transonic acceleration (Mach 1.2) thrust efficiency.

performance. This nozzle had a small boattail area, and its internal expansion ratio was optimized with the translating cylindrical outer shroud. The aerodynamically positioned flaps on the variable-flap ejector and the auxiliary-inlet ejector floated to a larger exit area than optimum. A combination of internal overexpansion losses and external boattail drag reduced the nozzle thrust efficiency to 0.945. Boattail angles were measured at 6° for the variable-flap ejector and 9° for the auxiliary-inlet ejector.

The thrust efficiency for the second-generation coannular plug nozzle was slightly low at transonic acceleration. It was determined that the losses were mainly from inefficient internal expansion and high external boattail drag.

# 7.3 Subsonic Cruise

The off-design subsonic cruise performance of a nozzle is difficult to analyze because of the interactions between the internal and external flows. Therefore, aeronautical engineers have to rely more on experimental data. At subsonic cruise

the external flow effects are large because the nozzle is operating at a low pressure ratio and the external drag can become a large fraction of the relatively low ideal thrust. General Electric has estimated that a 1-percentage-point change in subsonic nozzle gross thrust coefficient is equivalent to a 3000-lb change in takeoff gross weight for a typical supersonic cruise aircraft with a range of 4000 n mi and a 600-n mi subsonic cruise segment. This sensitivity is about one-third that at the supersonic cruise condition.

The subsonic cruise thrust efficiency of the first- and second-generation supersonic cruise nozzles is shown in figure 7–5. The study goal was hardest to achieve at this flight condition. None of the configurations tested reached the goal. The main losses were attributed to high external drag and internal overexpansion losses. There was a large spread in measured performance between configurations, from a low of 0.81 to a high of 0.918.

The spread in measured performance for the first-generation nozzles was a little over 6 percentage points. The variable-flap ejector nozzle had rather low performance owing to its high boattail drag and high internal expansion losses at the low cruise pressure ratio. The floating flaps were in on their stops and provided a high boattail angle of 15.5°. The low-angle plug nozzle had the best subsonic cruise performance, since the boattail area was small and the external shroud was retracted to reduce overexpansion losses. The auxiliary-inlet ejector had a reduced boattail drag but picked up additional drag on the open doors of the auxiliary-inlet system. This nozzle also suffered added internal losses from overexpansion due to internal area ratio mismatch.

The large difference in performance for the two second-generation nozzles is also shown in figure 7–5. The low performance of the General Electric coannular plug nozzle was traced to the compromise between takeoff acoustics and supersonic cruise aerodynamics. This compromise resulted in an internal nozzle expansion-contraction feature with less than ideal internal area distribution, and this anomaly became a prime suspect. The design compromise also resulted in a high
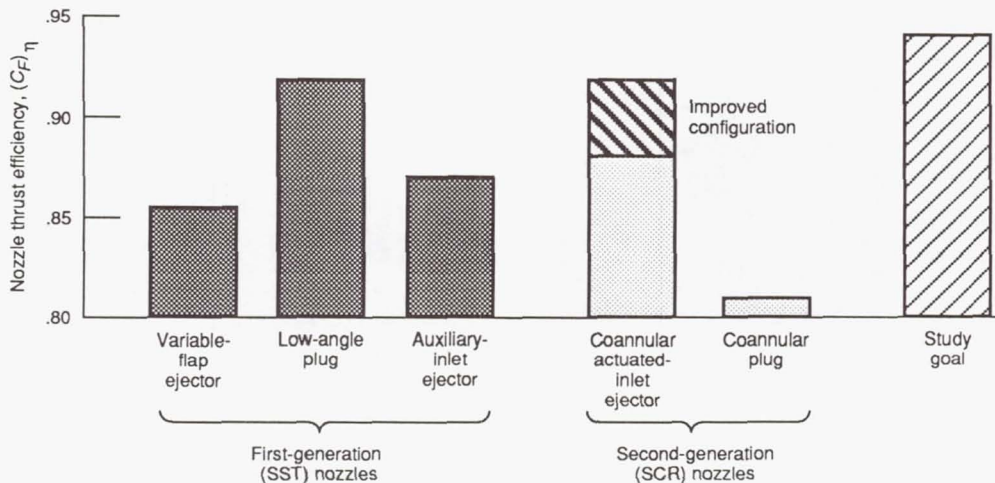


Figure 7–5.—Subsonic cruise (Mach 0.9) thrust efficiency.

boattail angle with about a 13-percentage-point installation loss.

The initial design effort on the second-generation Pratt & Whitney actuated-inlet ejector yielded a subsonic cruise performance of 0.88, as shown in figure 7-5. A large part of the loss was traced to high drag on the auxiliary-inlet system. Diagnostic tests showed that the poor performance levels were the result of an aerodynamic flow separation over the inlet doors. A redesign of the nozzle and a follow-on wind tunnel test of an improved configuration resulted in the higher performance (0.917) shown in the figure. This was accomplished by reducing the ejector inlet turning angles, minimizing internal overexpansions and static pressure mismatches, and minimizing core/bypass flow impingement angle.

## 7.4 Takeoff

Three of the first- and second-generation nozzles were able to meet or nearly meet the study goal thrust efficiency of 0.984 at takeoff, as shown in figure 7-6. These included the low-angle plug, the General Electric auxiliary-inlet ejector, and the improved version of the Pratt & Whitney actuated-inlet ejector.

The first-generation General Electric variable-flap ejector had a takeoff thrust efficiency of 0.955. The minimum area ratio of this nozzle was restricted to 1.35 to avoid possible low-area-ratio flow instability with the aerodynamically positioned flaps. This high area ratio contributed to the excess overexpansion losses of the nozzle at the low takeoff nozzle pressure ratio.

The low performance of the second-generation General Electric coannular plug nozzle is attributed to the features added to the nozzle for jet noise suppression. These features included a 20-chute suppressor and a treated ejector shroud. Without these two noise-reducing devices the measured takeoff performance of a baseline nozzle was 0.975. The loss attributed to low noise was therefore more than 5 percentage points.

General Electric conducted a performance sensitivity study to show the effect of nozzle performance on aircraft takeoff gross weight at several key operating points. The effect was relatively small at takeoff. A 1-percentage-point change in nozzle gross thrust coefficient at takeoff was equivalent to only 750 lb in takeoff gross weight, in contrast to 10 000 lb at supersonic cruise and 3000 lb at subsonic cruise.
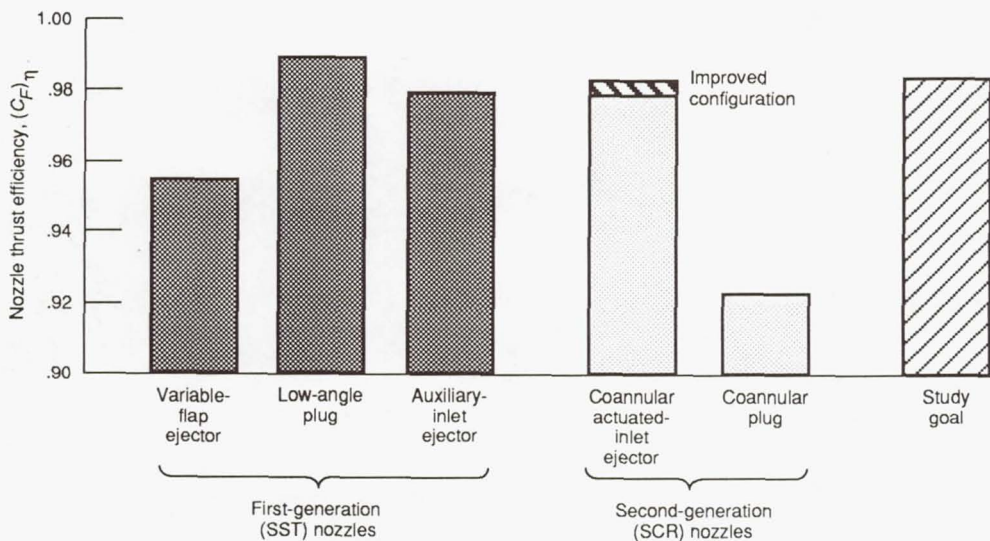


Figure 7-6.—Static (Mach 0) thrust efficiency.

# 7.5 References

7-1. Steffen, F.W.; and Jones, J.R.: Performance of a Wind Tunnel Model of an Aerodynamically Positioned Variable Flap Ejector at Mach Numbers From 0 to 2.0. NASA TM X-1639, 1968.

7-2. Bresnahan, D.L.: Experimental Investigation of a 10° Conical Turbojet Plug Nozzle With Iris Primary and Translating Shroud at Mach Numbers From 0 to 2.0. NASA TM X-1709, 1968.

7-3. Bresnahan, D.L.: Performance of an Aerodynamically Positioned Auxiliary Inlet Ejector Nozzle at Mach Numbers From 0 to 2.0. NASA TM X-2023, 1970.

7-4. Nelson, D.P.: Model Aerodynamic Test Results for Two Variable Cycle Engine Coannular Exhaust Systems at Simulated Takeoff and Cruise Conditions. (PWA-5550-37, Pratt & Whitney Aircraft; NASA Contract NAS3-20061) NASA CR-159818, 1980.

7-5. Nelson, D.P.: Model Aerodynamic Test Results for a Refined Actuated Inlet Ejector Nozzle at Simulated Takeoff and Cruise Conditions. (PWA-5768-29, Pratt & Whitney Aircraft; NASA Contract NAS3-22738) NASA CR-168051, 1983.

7-6. Wagenknecht, C.D.; and Bediako, E.D.: Aerodynamic Performance Investigation of Advanced Mechanical Suppressor and Ejector Nozzle Concepts for Jet Noise Reduction. (R83AEB122-3, General Electric Co.; NASA Contract NAS3-23038) NASA CR-174860, 1985.

# Chapter 8

# Throttle-Dependent Boattail Drag

Supersonic cruise aircraft designed to fly at Mach numbers up to 3.0 operate over a range of nozzle pressure ratios from about 3.0 to 30.0. Efficient propulsion system performance at all flight speeds requires variations in the internal expansion ratio of the nozzle. If the configuration utilizes nacelle-mounted engines and divergent ejector nozzles, it may have a nearly cylindrical afterbody at the design Mach number. Because of the high nozzle pressure ratio at the design Mach number, external flow effects do not significantly influence nozzle performance.

Off-design operation at low nozzle pressure ratios, however, requires a boattailed nacelle afterbody in order to provide a corresponding decrease in nozzle internal expansion ratio. Nozzle drag results from the large, aft-facing areas that project when the nozzle is in this closed, low-power position at subsonic flight conditions. The boattail drag can be a significant part of the overall airplane drag, especially at subsonic cruise, where the engine net thrust is low. It would not be unusual for the boattail drag to account for as much as 15 percent of the overall drag.

Many supersonic aircraft missions require that sizable portions of the flight time be at subsonic Mach numbers. Consequently, the drag characteristics of the nacelle afterbody become significant at subsonic and transonic Mach numbers. As a result, much work has been done to develop low-drag boattail shapes for high subsonic Mach numbers. Some of the factors that influence boattail drag are discussed in this chapter. Then, how the boattail drag is affected by the engine exhaust flow and the local flowfield created by the wing is explained.

## 8.1 Factors That Influence Boattail Drag

The flowfield over a boattail is characterized by a rapid expansion of flow around the corner of the boattail followed by a recompression toward the trailing edge. Some of the aerodynamic factors that influence this flowfield and the resulting drag are shown in figure 8–1. The engine nozzle is normally an exposed portion of a supersonic cruise aircraft. Internal-external flow interactions can be significant, especially at the off-design flight conditions. All of the aerodynamic

factors listed in figure 8–1 can influence boattail drag, as discussed herein. Geometric factors that also influence boattail drag, such as boattail angle and shape and the ratio of exhaust jet area to maximum nacelle area, are also discussed.

The flow patterns and pressure distributions around a typical boattail nozzle are illustrated in figure 8–2 for a high subsonic flight condition. As the flow approaches the boattail shoulder, the pressure is slightly less than the free-stream pressure because of the upstream presence of the wing and the nacelle. As the flow traverses the boattail shoulder, it overexpands. If the radius of the shoulder is small, the overexpansion can be large. Downstream of the shoulder a recompression begins, and, if the flow remains attached, continues along the remaining length of the boattail. At the end of the boattail the flow has generally recompressed to a value greater than the free-stream static pressure. This recompression region presents an adverse pressure gradient to the local boattail boundary layer. If the flow separates, the point of separation is generally downstream of the shoulder, and the resulting loss of recompression (fig. 8–2) increases boattail drag.
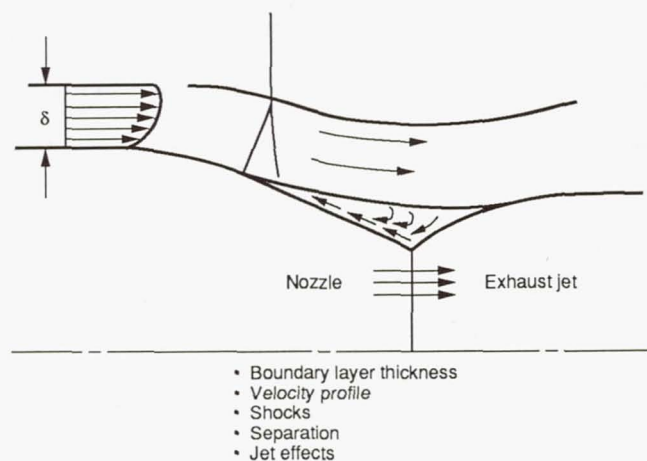


- Boundary layer thickness
- Velocity profile
- Shocks
- Separation
- Jet effects
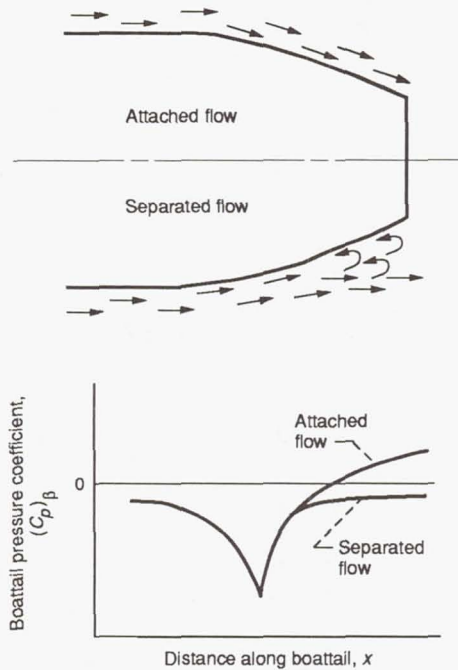
Figure 8–1.—Aerodynamic factors influencing boattail drag.

Figure 8–2.—Typical boattail flows.
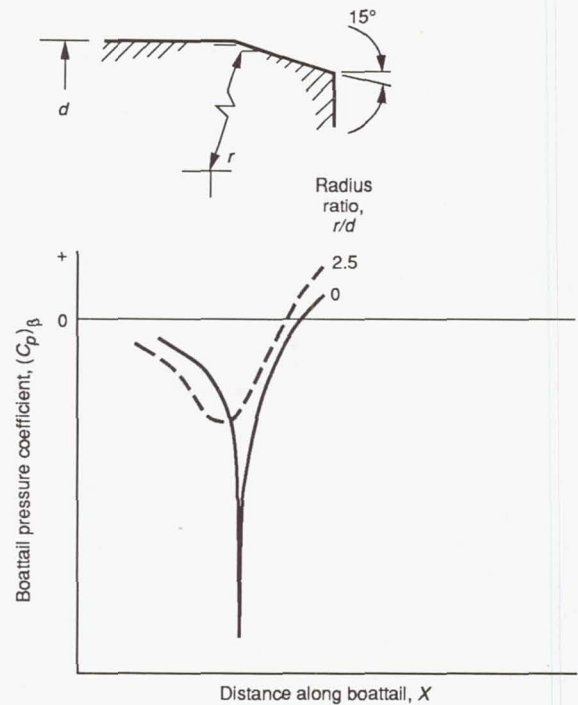


Figure 8–3.—Boattail pressure distribution. Variable-flap ejector; free-stream Mach number, $M_0$, 0.9.



Figure 8–4.—Isolated boattail drag. Variable-flap ejector; free-stream Mach number, $M_0$, 0.9.

The problem of designing an afterbody to fair from a fixed-diameter nacelle to a smaller diameter jet exit, so that minimum drag is obtained for subsonic flight, has received considerable attention over the years. It has been shown that circular-arc afterbodies result in lower drag than conical afterbodies on the basis of the equivalent fineness ratio and the ratio of jet exit diameter to maximum diameter, as discussed in reference 8–1. Although these results do not include the effects of a propulsive jet, the trend of reduced drag with increased corner radius is still valid. Since most supersonic cruise aircraft nozzle geometries are variable, the full circular-arc afterbody, although desirable from a drag standpoint, is mechanically difficult to transform into a smooth cylinder at the design point. Therefore, intermediate transition radii of curvature at subsonic and transonic Mach numbers were examined.

Typical static pressure distributions at a subsonic cruise Mach number of 0.90 for both a sharp- and a rounded-corner 15° boattail are shown in figure 8–3. The flow overexpanded considerably downstream of the sharp corner ($r/d = 0$) and resulted in a high drag. Rounding the corner can reduce the initial overexpansion and the resulting boattail drag, as discussed in reference 8–2.

The isolated drag of a series of 15° boattails is shown in figure 8–4 at a Mach number of 0.9 and as a function of nozzle pressure ratio. The boattail pressure drag was divided by the ideal gross thrust of the primary flow. The highest drag was obtained with a conical boattail ($r/d = 0$) and a thin boundary layer, typical of a nacelle installation. For the example shown, the boundary layer thickness was 7 percent of the nacelle diameter. At a nozzle pressure ratio of 3.2, typical for a turbojet engine at subsonic cruise, the drag of this conical boattail was about 7 percent of the ideal gross thrust of the nozzle. At this flight speed the net engine thrust is about one-half of the gross thrust, so that the boattail drag would be about 14 percent of the airplane drag. A thicker boundary layer, typical of a fuselage installation, reduced the drag of a sharp-cornered boattail to 6 percent of the ideal gross thrust. For this example the boundary layer thickness was 18 percent of the fuselage diameter. A thick boundary layer makes a sharp corner appear rounded by reducing the initial overexpansion and raising the general level of pressures over the boattail. Reference 8–3 presents the effect of boundary layer thickness on the pressure drag of a series of boattails over a range of Mach numbers.
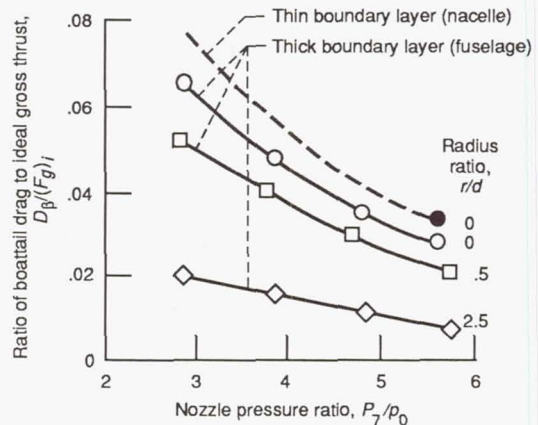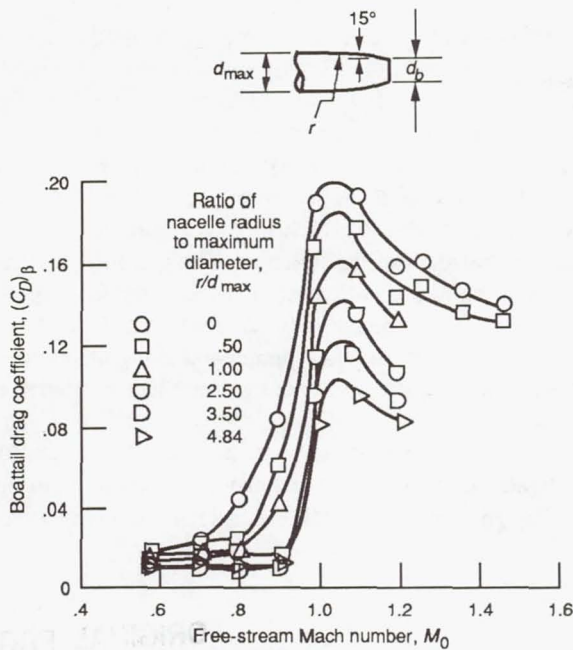
Figure 8-5.—Effect of afterbody shape on rise in transonic drag. Ratio of base diameter to maximum diameter, $d_b/d_{max}$, 0.67.



Figure 8-6.—Effect of exhaust flow on boattail drag. Convergent nozzle; free-stream Mach number, $M_0$, 0.85.; 16° circular-arc boattail.

A small radius at the corner of the boattail with the thicker boundary layer (fig. 8-4) reduced the drag to about 5 percent of the ideal gross thrust at a nozzle pressure ratio of 3.2. This radius ratio ($r/d = 0.5$) appears to be a reasonable value for the type of flap and seal arrangement required for a variable-flap ejector nozzle. A more generous radius can reduce the drag even more. However, it is evident from this figure that the isolated boattail drag for a variable-flap nozzle can be significant at subsonic cruise.

The effect of afterbody shape on the transonic drag rise of a 15° boattail is shown in figure 8-5 for a range of Mach numbers from 0.55 to 1.45. Boattail drag is shown for various 15° boattails on which the boattail juncture with the cylindrical portion of the nacelle had been smoothed with different radii of curvature. The results indicate that increasing the boattail radius of curvature generally delays the onset of a rise in transonic drag and lowers the peak value. The conical configuration ($r/d = 0$) had a drag-rise Mach number near 0.6. Increasing the radius of curvature to $r/d = 1$ delayed the drag-rise Mach number to about 0.8. For $r/d$'s of 2.5 or greater the drag-rise Mach number occurred slightly above Mach 0.9.

## 8.2 Isolated Boattail Drag

Much work has been done to determine jet effects on the boattail drag of isolated nozzles at subsonic and transonic Mach numbers. Two of these published works are summarized in this section, but first a general description of jet effects on boattail drag is provided by using figure 8-6. The data in this figure are intended as a qualitative, rather than a quantitative, description.

Large differences in boattail drag are shown with changes in nozzle pressure ratio. Some are caused by changes in jet plume shape; others result from jet entrainment effects. The jet-off point has the highest boattail drag coefficient. Boattail drag initially decreases when jet flow is initiated, since the plume acts to move the boattail flow streamlines away from the centerline. This movement causes a stronger flow recompression on the boattail surface than occurs in the jet-off condition. The boattail drag continues to decrease until the nozzle jet velocity approaches that of the surrounding flow. Jet entrainment then begins and gains strength with increasing nozzle pressure ratio. This effect is detrimental (increasing drag), since jet entrainment creates an induced speedup of boattail flow and thus reduces boattail pressures. Drag increases until the nozzle is at its design pressure ratio of near 2.0. Further increases in nozzle pressure ratio cause another downward trend in drag. As the pressure ratio increases past the design point, the plume expands and its effect on drag becomes more pronounced by further displacing the boattail flow streamlines. Thus, jet entrainment is detrimental, but the effect of jet plume shape is beneficial. Wind tunnel tests conducted to investigate the effects of jet plume shape and entrainment on boattail pressure drag are reported in reference 8-4. In addition, tests were run with solid plume-shaped sleeves as a means to separate plume-shape effects from jet-entrainment effects.

## 8.2.1 Drag of Conical Afterbodies

An investigation was conducted at the NASA Langley Research Center to determine the drag characteristics of a series of conical boattails with a cold sonic jet issuing from the base, as reported in reference 8–5. The models investigated had boattail angles from 3° to 45° with ratios of the jet diameter to the base diameter $d_j/d_b$ of 0.65 and 0.75; the ratios of the base diameter to the maximum diameter $d_b/d_{max}$ were 0.55, 0.70, and 0.85. The nozzle pressure ratio ranged from the jet-off condition to about 8.

A sketch of a typical model is presented in figure 8–7(a), and 11 of the 22 models tested are depicted in figure 8–7(b). The internal shape of the sonic nozzle was identical for all the models, and consisted of a 10°-included-angle convergent section followed by a short constant-diameter section. The boundary layer was fully turbulent and its thickness was approximately 20 percent of the maximum model diameter.

A typical pressure distribution over a conical afterbody at Mach 0.9 and at a jet pressure ratio of 4 is shown in figure 8–8. A schlieren photograph of the model at these test conditions is shown at the top of the figure. The rapid acceleration of the flow at the cone-cylinder juncture is noted as well as the extent to which this acceleration affected the pressures upstream of the juncture. The pressure coefficient corresponding to the static pressure necessary for sonic flow along the model is indicated by an arrow on the ordinate at $X/d_{max} = -0.4$. As the flow proceeded along the afterbody, it compressed rapidly and exceeded ambient pressures near the base.

The drag components of one of the 22 configurations investigated in this Langley test program are shown in figure 8–9. The 16° conical boattail was selected as being a typical

(a)
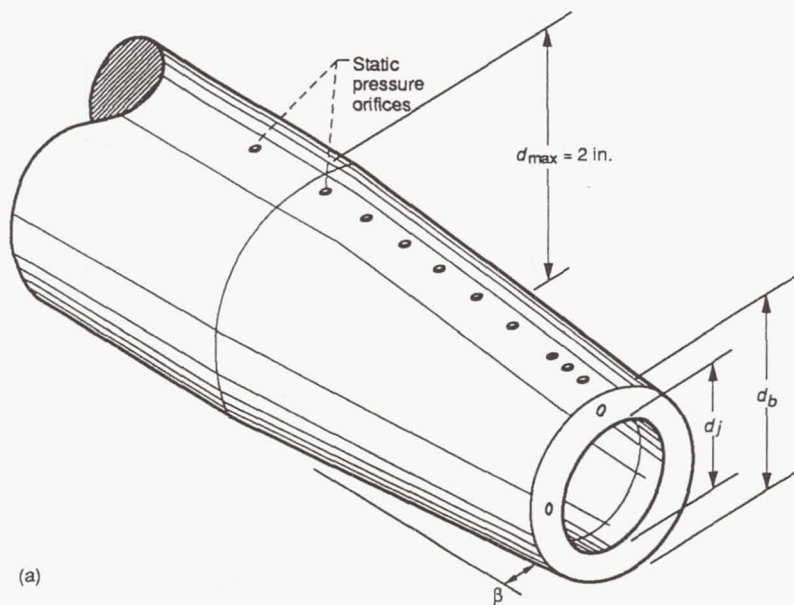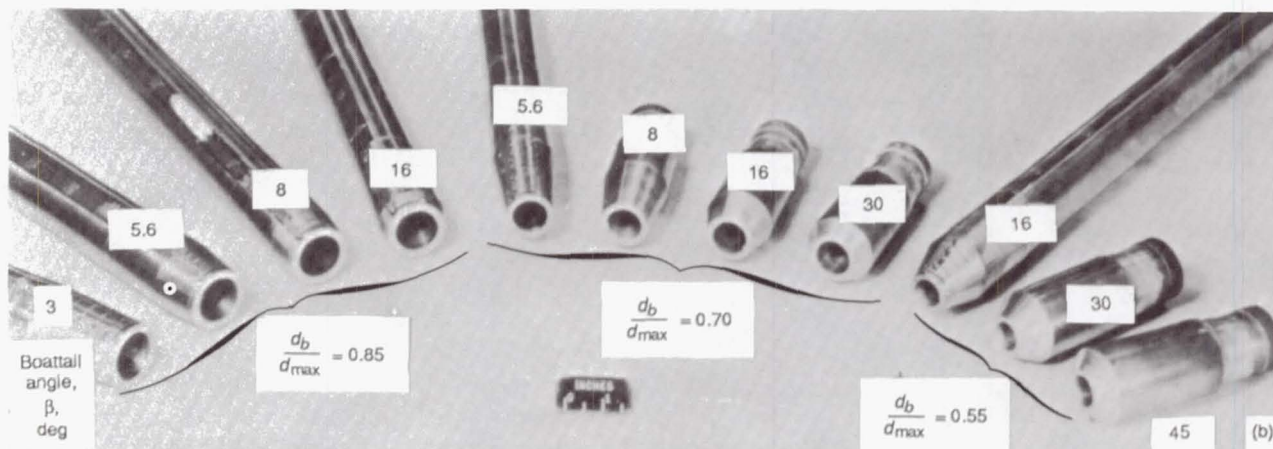
(a) Sketch of typical model.
(b) Afterbody models. Ratio of jet diameter to base diameter, $d_j/d_b$, 0.75.

Figure 8–7.—Afterbody model configurations.
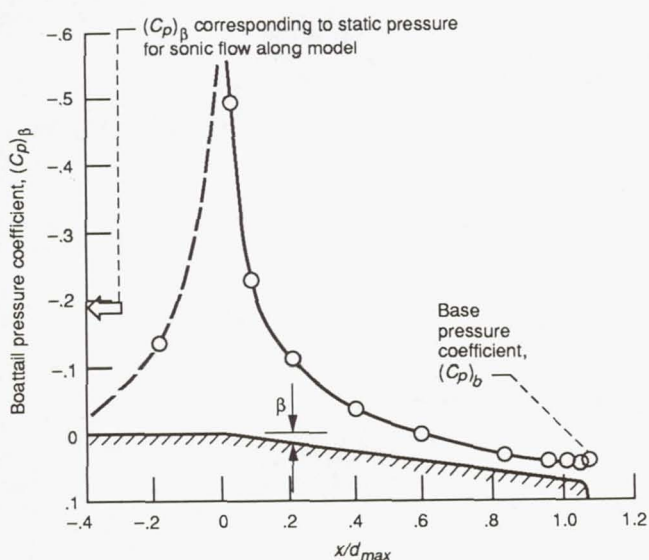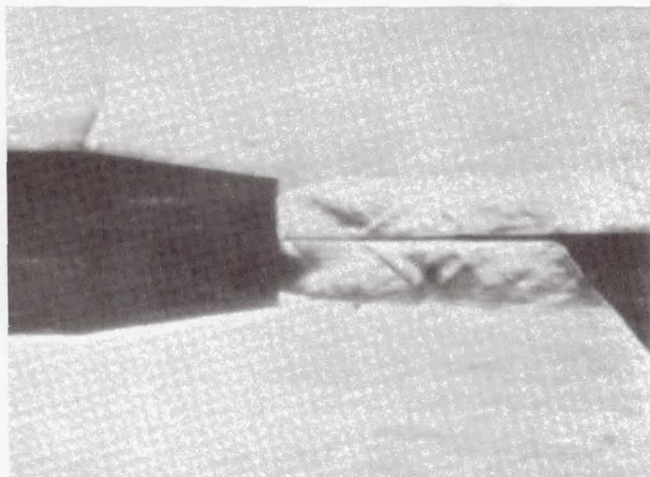
Figure 8-8.—Typical boattail pressure coefficient distribution with jet flow. Free-stream Mach number, $M_0$, 0.9; nozzle pressure ratio, $P_7/p_0$, 4; ratio of base diameter to maximum diameter, $d_b/d_{max}$, 0.70; ratio of jet diameter to base diameter, $d_j/d_b$, 0.75.



Figure 8-9.—Variation of boattail, base, and afterbody drag coefficients with jet total pressure ratio at constant values of Mach number. Boattail angle, $\beta$, 16°; ratio of base diameter to maximum diameter, $d_b/d_{max}$, 0.70; ratio of jet diameter to base diameter, $d_j/d_b$, 0.75.

subsonic cruise configuration for a supersonic cruise aircraft. Boattail $(C_D)_\beta$, base $(C_D)_b$, and afterbody drag coefficients $(C_D)_a$ are presented as a function of nozzle pressure ratio at constant values of Mach number. The afterbody drag is the sum of the boattail and base drags. The ratio of the jet diameter to the base diameter $d_j/d_b$ was 0.75 and the ratio of the base diameter to the maximum diameter $d_b/d_{max}$ was 0.70. For a typical subsonic cruise Mach number of 0.9 the effect of the jet on boattail drag was the same as that shown in figure 8-6. The drag initially decreased at low pressure ratio because of the plume, then increased as jet entrainment dominated, and finally decreased again at nozzle pressure ratios above the design point of 2.0 because of jet plume effects.

### 8.2.2 Drag of Ejector Nozzles

An experimental investigation was conducted at NASA Lewis to determine the effects of a cold jet on the boattail drag of four isolated cylindrical ejector nozzles, as reported in reference 8-6. These nozzles represented the subsonic cruise configuration of nozzles designed for a supersonic cruise aircraft. The Mach number range was 0.6 to 1.47, and the nozzle pressure ratio was varied from approximately 1 (jet off) to 11. The effects of secondary airflow were also studied. The nozzle configurations included three with a 15°-trailing-edge boattail angle and one with a 10° boattail, as shown in figures 8-10(a) to (d). The boattail juncture with the cylindrical
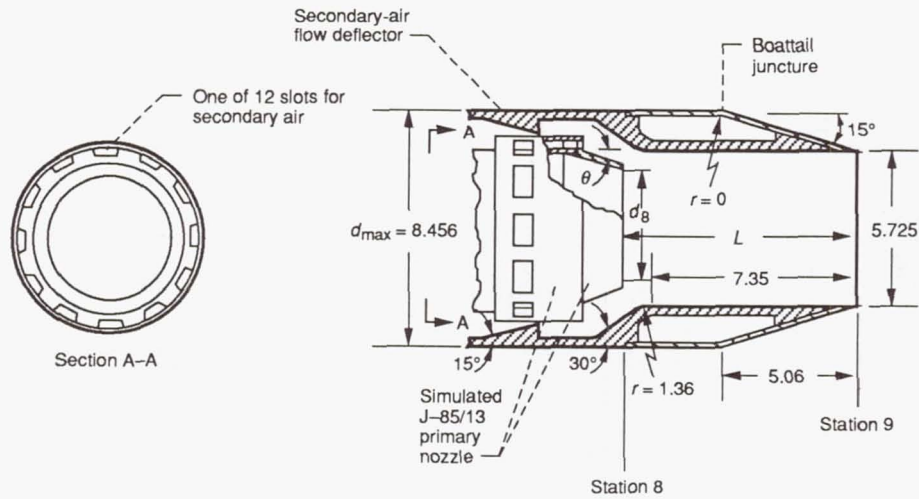
| Primary | Primary flap angle, $\theta$, deg | Nozzle throat diameter, $d_8$, in. | 15° Boattails | 10° Boattails |
|---------|---------|---------|---------|---------|
| | | | Length from primary exit to nozzle exit, $L$, in. | |
| I | 13° 15' | 4.388 | 8.50 | 8.60 |
| II | 5° 18' | 5.192 | 8.92 | 9.02 |

(a)
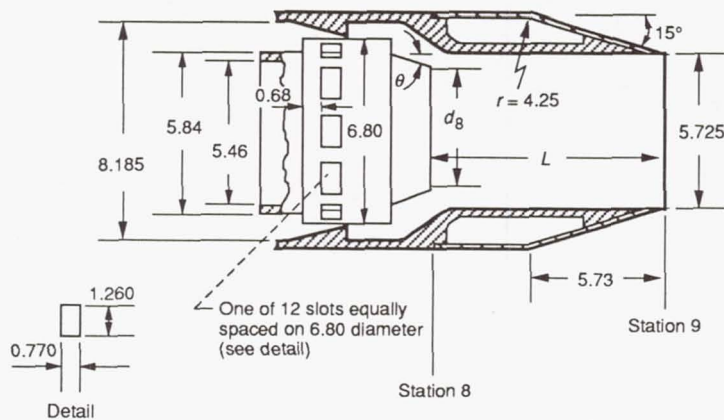
(b)

(a) Boattail angle, 15°; radius ratio, $r/d$, 0.
(b) Boattail angle, 15°; radius ratio, $r/d$, 0.5.

Figure 8–10.—Geometry details of variable-flap ejector nozzle. (All dimensions are in inches.)

portion of the nacelle for the 15° configurations was faired with different radii of curvature. In addition, jet effects were also simulated by a cylinder positioned downstream of the nozzle exit for the 15° configurations (fig. 8–10(e)).

At subsonic speeds the jet significantly reduced the drag of the 15° boattails, as shown in figure 8–11(a), which compares jet-on and jet-off data. This drag reduction was relatively insensitive to nozzle pressure ratio for values much less than the design value. However, boattail drag was further reduced as the nozzle pressure ratio was increased to the design condition and beyond, thereby increasing the tendency for jet pluming to occur downstream of the nozzle exit. Supersonically, the boattail pressure drag was unaffected by the jet until it also approached full expansion. As the jet became underexpanded, the boattail drag was significantly reduced. The trends were basically the same for the 10° boattails except that boattail drag was affected to a lesser degree by the jet (fig. 8–11(b)).
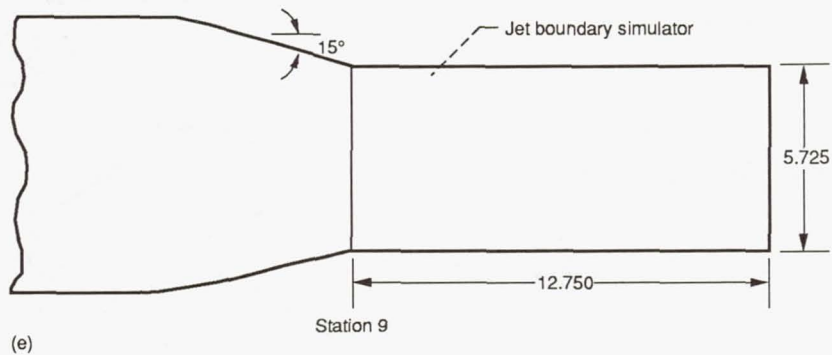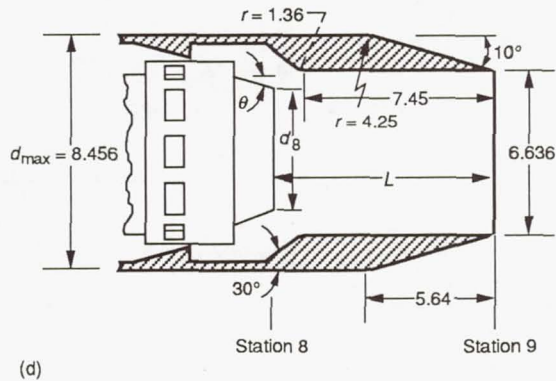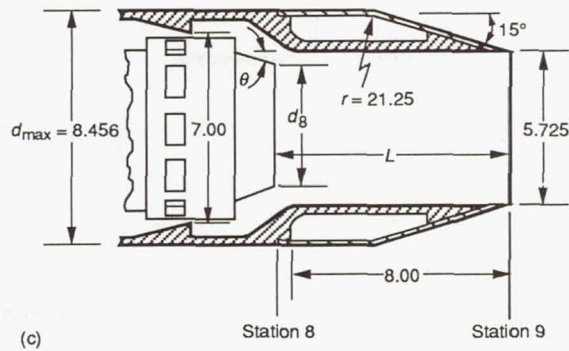
(c) Boattail angle, 15°; radius ratio, $r/d$, 2.5 (see part (a)).
(d) Boattail angle, 10°; radius ratio, $r/d$, 0.5 (see part (a)).
(e) Nozzle with jet boundary simulator (15° boattail configurations only).

Figure 8-10.—Concluded.

In general, the effect of secondary flow was to decrease boattail drag by increasing the jet exit static pressure. Secondary flow was most effective in reducing the boattail drag coefficient at subsonic speeds when the nozzle was operating at or near full expansion or was underexpanded. A cylindrical jet boundary simulator was effective in duplicating a fully expanded jet.

An effort was made to correlate the boattail drag as a function of nozzle exit static pressure ratio, as shown in figure 8-12(a) for a 15° boattail and in figure 8-12(b) for a 10° boattail. The corrected secondary to primary weight flow ratio

$\omega\sqrt{\tau}$ was varied from 0 to 0.15. The results of this correlation attempt indicate that the boattail drag is predominantly a function of exit static pressure ratio when the nozzle is either fully expanded or highly underexpanded and pluming effects are predominant. However, in regions where the nozzle is overexpanded, no simple relation exists between exit pressure ratio and boattail drag because of jet overexpansion and separation effects.

A continuing effort was made to correlate throttle-dependent afterbody drag both with the ratio of exhaust area to maximum nacelle area $A_j/A_{\max}$ and with the ratio of nozzle exit static
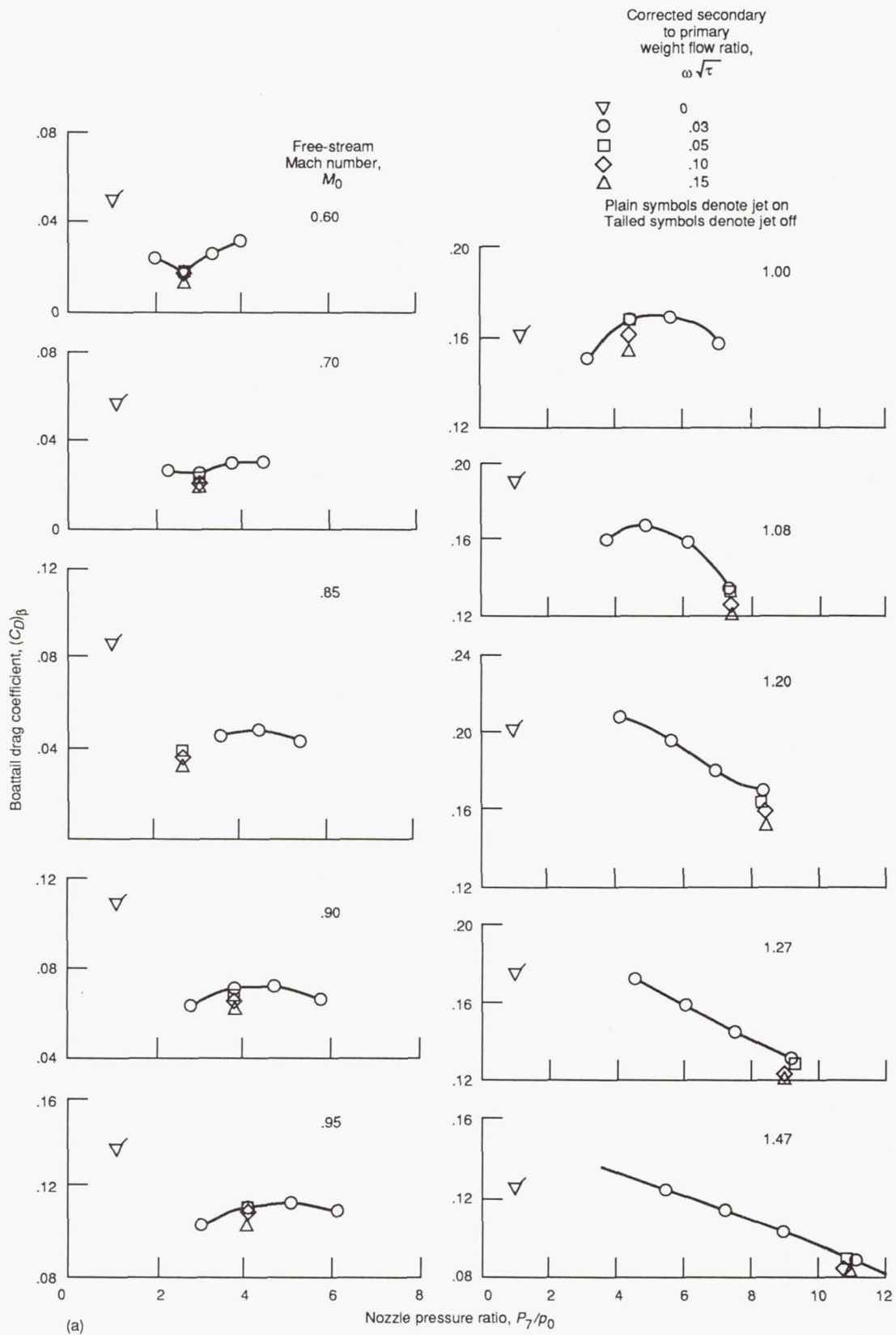
(a) Boattail angle, 15°; radius ratio, $r/d$, 0.5; primary I; ratio of nozzle exit area to throat area, 1.70; design nozzle pressure ratio, 8.0.

Figure 8–11.—Jet effect on boattail pressure drag coefficient.
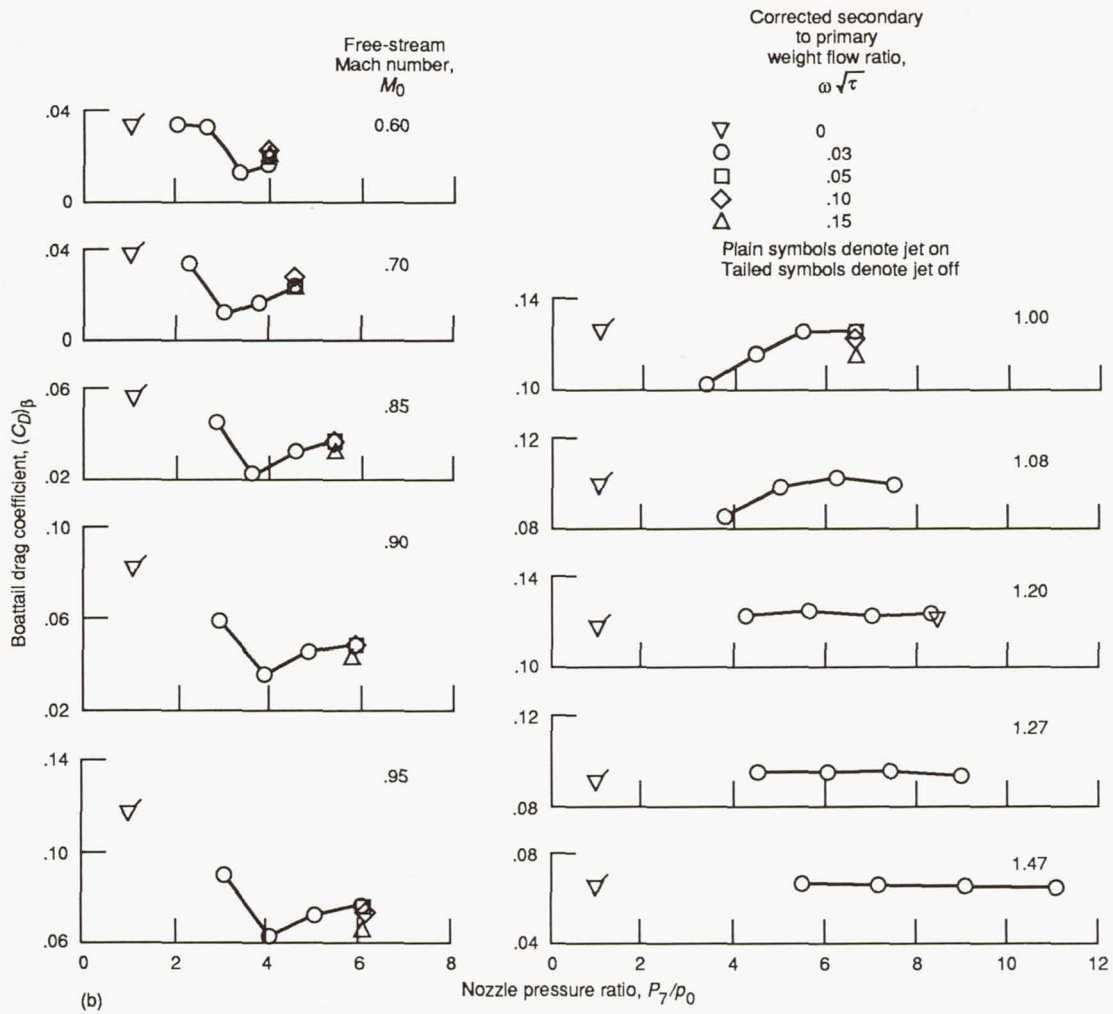
(b) Boattail angle, 10°; radius ratio, $r/d$, 0.5; primary I; ratio of nozzle exit area to throat area, 2.29; design nozzle pressure ratio, 13.5.

Figure 8-11.—Concluded.

77
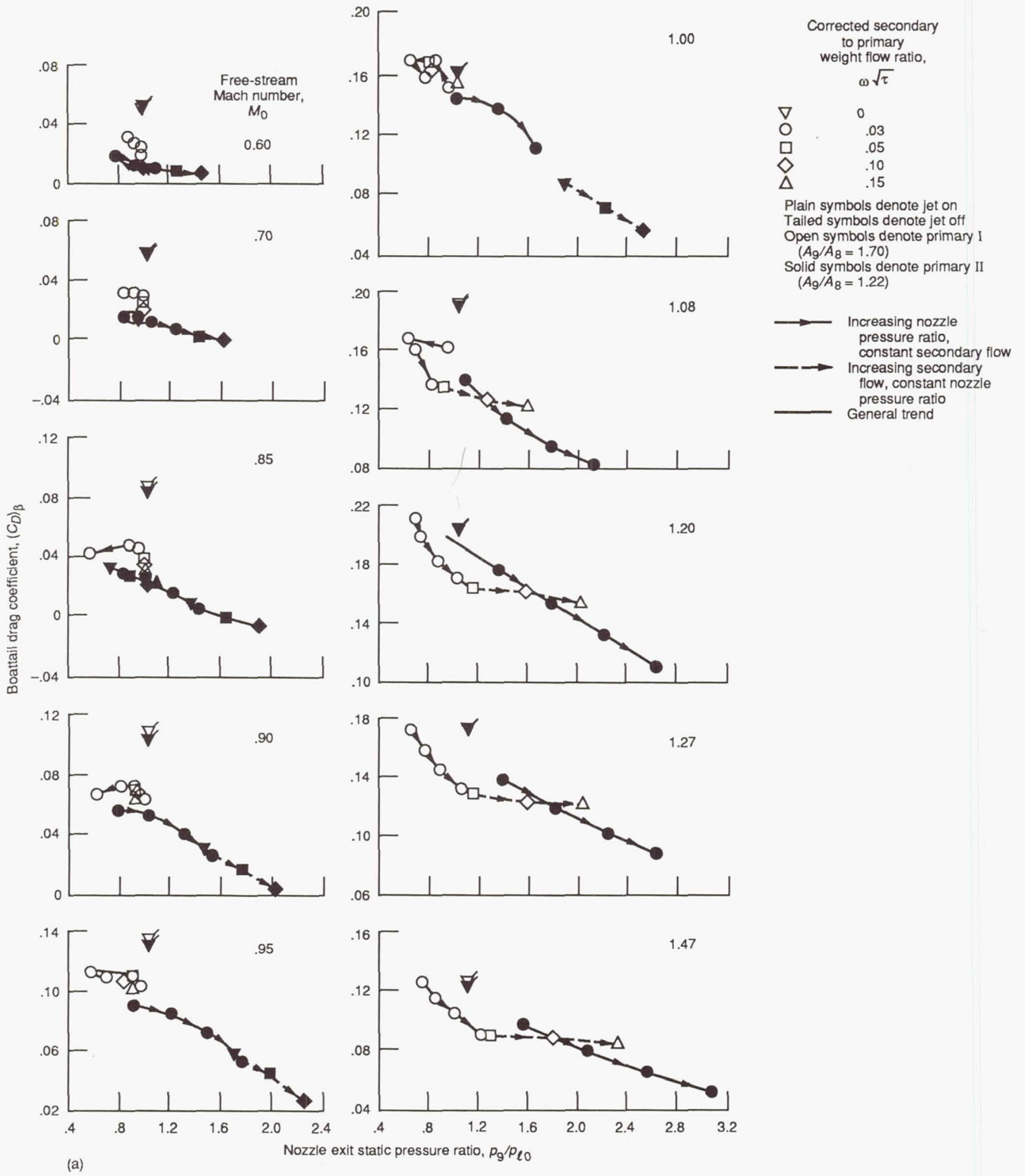
(a) Boattail angle, $\beta$, 15°, radius ratio, $r/d$, 0.5.

Figure 8–12.—Effect of nozzle exit static pressure ratio on boattail drag coefficient.

Corrected secondary
to primary
weight flow ratio,
$\omega\sqrt{\tau}$

| | |
|---|---|
| ▽ | 0 |
| ○ | .03 |
| □ | .05 |
| ◇ | .10 |
| △ | .15 |

Plain symbols denote jet on
Tailed symbols denote jet off
Open symbols denote primary I ($A_9/A_8 = 2.29$)
Solid symbols denote primary II ($A_9/A_8 = 1.64$)

→ Increasing nozzle pressure ratio,
constant secondary flow

Free-stream
Mach number,
$M_0$

Boattail drag coefficient, $(C_D)_\beta$

Nozzle exit static pressure ratio, $p_9/p_{l0}$

(b)
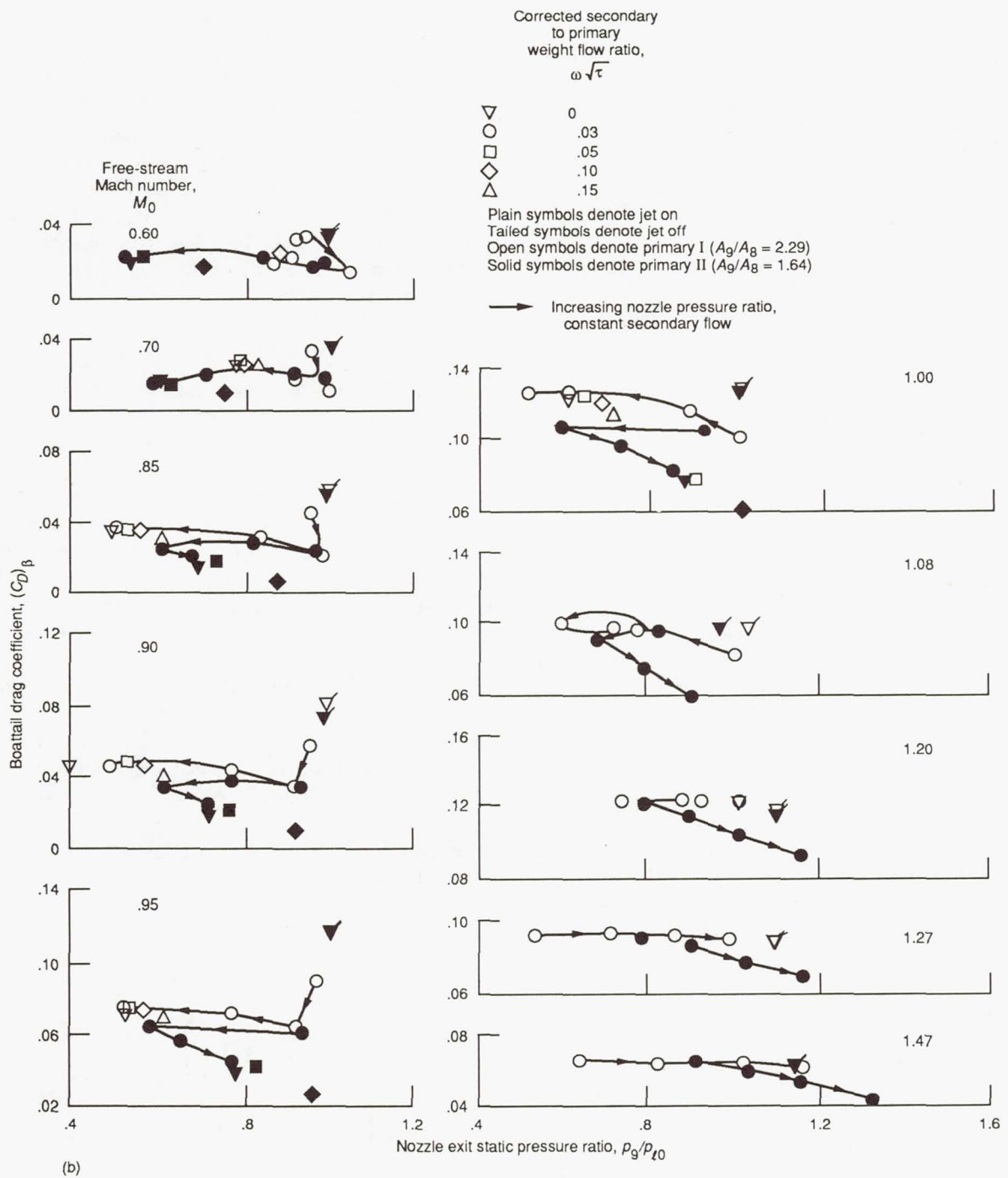
(b) Boattail angle, $\beta$, 10°; radius ratio, $r/d$, 0.5.

Figure 8–12.—Concluded.

pressure to free-stream static pressure. An example of this type of correlation at a subsonic cruise Mach number of 0.9 is shown in figure 8–13. This is a useful correlation in that the reference point can be shifted along the zero drag axis to accommodate variations in nozzle geometry (i.e., variation in $A_j/A_{max}$). Correlations like this one have been generated by various engine and airframe companies to cover a Mach number range from 0 to 2.0. Specific values of the ordinate and abscissa have been left off to protect the proprietary aspects of these industry-generated correlations.

79
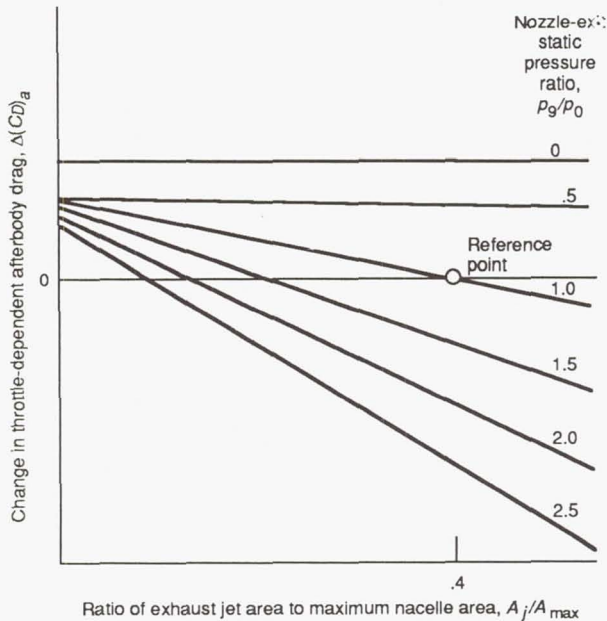
Figure 8–13.—Throttle-dependent afterbody drag. Free-stream Mach number, $M_0$, 0.9.

## 8.3 Installed Boattail Drag

A flight and wind tunnel investigation was conducted at NASA Lewis to determine the installed boattail drag of an underwing nacelle installation typical of a supersonic cruise aircraft. A coordinated flight and wind tunnel model program that used the best features of each test technique is illustrated in figure 5–18. A modified F–106 aircraft was used as the basic testbed aircraft. A new engine nacelle was added under each wing so that the nozzle stuck out behind the wing. This kind of engine installation has an important advantage, since the wing can be used to shield the inlet from angle-of-attack effects. An afterburning J–85 turbojet engine was used in each pod. These pods were 25 in. in diameter and were designed to accept any of the nozzles that gave good performance in the isolated tests.

In parallel to the flight tests a wind tunnel model program was conducted for all flight configurations. Two subscale models were tested in the Lewis 8- by 6-Foot Supersonic Wind Tunnel, as shown in figure 5–18. The 0.22-scale model was a half-span F–106 model mounted on a reflection plate. This model was tested with a turbojet engine simulator. The design characteristics of this simulator permitted independent operation over a wide range of both inlet mass flow ratios and nozzle pressure ratios that equalled those in flight. The maximum nacelle diameter for this model was 5.5 in. The 0.05-scale model was a sting-mounted, full-span model. For these tests the nacelles were closed with conical forebodies, and solid jet boundary simulators were used. The maximum nacelle diameter was only 1.25 in. Isolated nozzle models were also tested on the 8.5-in.-diameter jet-exit model, as shown in figure 5–18. These models were used to ascertain the

isolated nozzle performance, which was then compared with the installed performance to determine installation effects.

### 8.3.1 Installation Effect

The installation effect on boattail drag is shown in figure 8–14 for a sharp-junctured (conical), variable-flap ejector nozzle. Installation greatly reduced boattail drag at the higher subsonic speeds. Drag was about zero at Mach 0.8 to 0.9, where a compression shock was ahead of the nozzle. At Mach 0.95, where the shock was near the nozzle, the boattail drag went negative (thrust). The drag rose sharply when the compression shock moved off the end of the nozzle at the transonic Mach numbers.

### 8.3.2 Reynolds Number Effect

Flight and model tests made at Lewis on boattailed nozzles suitable for use on supersonic cruise and dash aircraft showed that the Reynolds number had a significant effect on boattail drag, as discussed in reference 8–7. This effect is shown in figure 8–15 for three different high-angle boattail geometries, whose nozzles were designated by four-digit numbers. The first two numbers correspond to the radius ratio $r/r_C$ multiplied by 100, and the second two numbers correspond to the terminal boattail angle. Thus, nozzle 2524 had a radius ratio $r/r_C$ of 0.25 and a terminal boattail angle of 24°. The radius ratio $r/r_C$ is defined as the ratio of the radius of the boattail shoulder to the radius of a complete circular-arc nozzle, with the same boattail angle and ratio of nozzle exit area to nacelle area. Two of the nozzles had 24° terminal angles and one had a 16° terminal angle. The projected area of the boattails equalled 75 percent of the projected area of the nacelle.

Figure 8–15 shows the Reynolds number effect on the boattail drag coefficient at Mach 0.9. The wind tunnel data
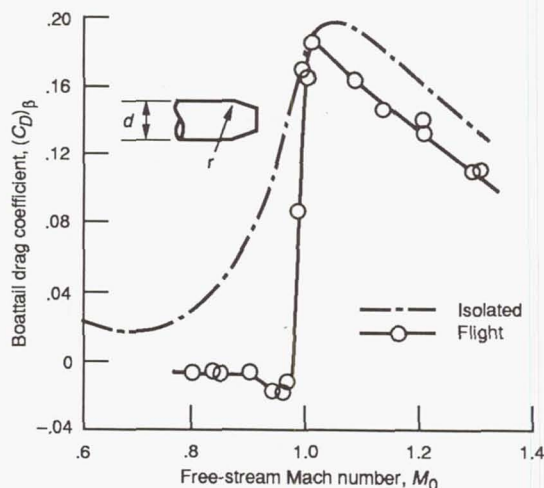


Figure 8–14.—Installation effect on boattail drag. Variable-flap ejector; radius ratio, $r/d$, 0.

80
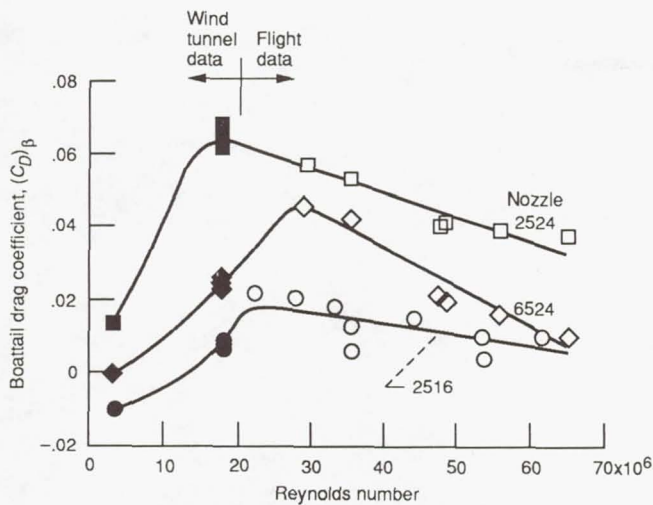
Figure 8–15.—Reynolds number effects on boattail drag. Free-stream Mach number, $M_0$, 0.9.

at a Reynolds number of $4 \times 10^6$ were obtained with the 0.05-scale model; the data at a Reynolds number of $18 \times 10^6$ were obtained with the 0.22-scale model. The open symbols represent the flight data, and the Reynolds number was varied by changing altitude. As can be seen in this figure, the drag coefficient reached a maximum near the low end of the flight Reynolds number range ($20 \times 10^6$ to $30 \times 10^6$) and then dropped off as the Reynolds number was either raised or lowered.

In considering this figure, observe those portions of the curves that begin at the peak and drop off as the Reynolds number is increased. The reduction in drag was primarily caused by a reduction in the amount of flow separation on the boattail. Nozzle 2516, which had a 16° boattail angle, had little separation at any condition and showed little change in drag over this Reynolds number range. The other two nozzles, however, were 24° boattails and incurred significant areas of separated flow. As the Reynolds number was increased in this range, the boundary layer became thinner. With a thinner

turbulent boundary layer, the flow will generally penetrate an adverse pressure gradient farther without separating. A minute change in the axial location of the separation results in a significant change in pressure level because of the sharp pressure rise downstream of the boattail shoulder. Therefore, increasing the Reynolds number in this range delayed the separation to a point farther downstream on the boattail. As the separation was reduced, more recompression was gained, resulting in lower drag.

Now consider those portions of the curves that begin at the peak and drop off as the Reynolds number is decreased. The reduction in drag in this range was primarily associated with a reduction of the overexpansion at the boattail shoulder. As the boundary layer became thicker at the lower Reynolds numbers, it softened the turn the flow made at the shoulder. This reduced the amount of overexpansion, raised the pressure level over the boattail, and reduced the drag. This effect had been observed previously during isolated nozzle tests, as discussed in reference 8–3.

## 8.4 References

8–1. Silhan, F.V.; and Cubbage, J.M., Jr.: Drag of Conical and Circular-Arc Boattail Afterbodies at Mach Numbers from 0.6 to 1.3. NACA RM–L56K22, 1957.

8–2. Shrewsbury, G.D.: Effect of Boattail Juncture Shape on Pressure Drag Coefficients of Isolated Afterbodies. NASA TM X–1517, 1968.

8–3. Blaha, B.J.; and Bresnahan, D.L.: Wind Tunnel Installation Effects on Isolated Afterbodies at Mach Numbers from 0.56 to 1.5. NASA TM X–52581, 1969.

8–4. Bergman, D.: Effects of Engine Exhaust Flow on Boattail Drag. AIAA Paper 70–132. Jan. 1970.

8–5. Cubbage, J.M., Jr.: Jet Effects on the Drag of Conical Afterbodies for Mach Numbers of 0.6 to 1.28. NACA RM–L57B21, 1957.

8–6. Harrington, D.E.: Jet Effects on Boattail Pressure Drag of Isolated Ejector Nozzles at Mach Numbers From 0.60 to 1.47. NASA TM X–1785, 1969.

8–7. Chamberlin, R.; and Blaha, B.J.: Flight and Wind Tunnel Investigation of the Effects of Reynolds Number on Installed Boattail Drag at Subsonic Speeds. NASA TM X–68162, 1973.

# Chapter 9

# Supersonic Dash Nozzles

Supersonic dash aircraft fly long distances subsonically but are also able to go supersonic for relatively short distances. Most fighter planes and some bombers, such as the FB-111, F-4, F-5, F-14, F-15, F-16, and F-18, fit this category. As shown in figure 9-1, for supersonic flight the nozzle is open in the afterburning, or reheat, position and has little projected boattail area, but at subsonic speeds the nozzle is in the closed, or dry power, position and has a large, aft-facing projected area. As a result, nozzle boattail drag can amount to a sizable percentage of overall airplane drag (15 percent would not be uncommon). These levels vary widely, depending upon boattail geometry and the local flowfield created by the airplane surfaces and the engine exhaust.

Afterburning turbofan engines, rather than turbojets, are used on supersonic dash aircraft for better subsonic fuel consumption. Because subsonic performance is more important, it is acceptable to compromise supersonic performance if it helps to minimize the nozzle weight. Some examples of supersonic dash nozzles are shown in figure 9-2. On the left is a variable convergent-divergent (C-D) nozzle shown in the subsonic cruise position. The tufts sticking out the top of the nozzle were used in flight tests to detect flow separation. In concept, the variable C-D nozzle is similar to the variable-flap ejector, described in chapter 5, except that on a turbofan engine the secondary airflow can be eliminated, since the fan flow can be used for cooling the afterburner liner and nozzle. In addition, the throat area variation is larger. In fact, the throat area can vary by a factor of 2 from nonafterburning to full afterburning. Some internal expansion is also needed for supersonic operation, but the nozzle area ratio would be less than that for the variable-flap ejector. These variations could be provided by constructing the boattail with overlapping flaps and seals and using enough actuators. To minimize the mechanical problems, however, these flaps should be short. Thus, at subsonic cruise speeds, the boattail on the variable C-D nozzle would be even larger and have steeper angles than the variable-flap ejector for a supersonic cruise aircraft. For the nozzle shown, the projected area is about 75 percent of the nacelle area and the maximum boattail angle is 24°. Putting a plug in the nozzle, as shown on the right, would decrease both the boattail area and angle. If the plug had adequate cooling, it could also be used to suppress infrared radiation from the hot engine parts. However, its structural weight would probably be higher than that of the C-D nozzle.



(a) Subsonic flight.
(b) Supersonic flight.
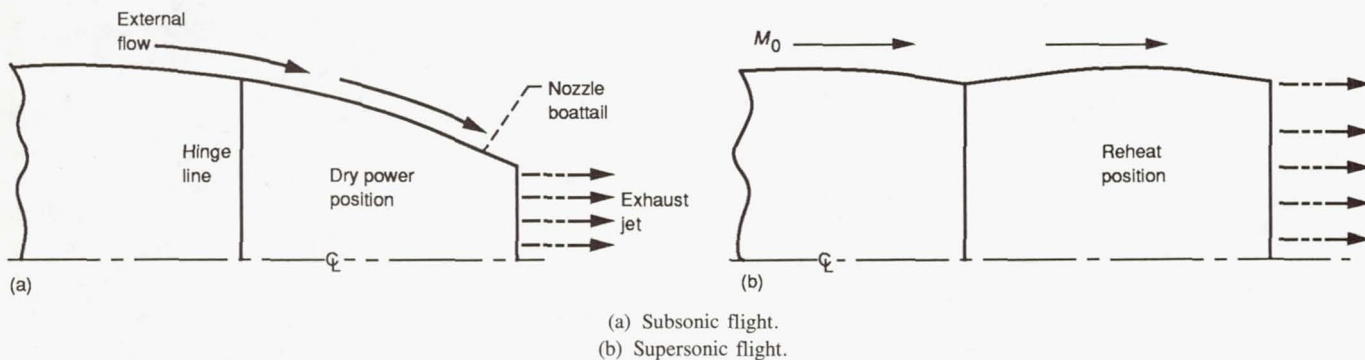
Figure 9-1.—Exhaust nozzle positions.

PAGE __82__ INTENTIONALLY BLANK
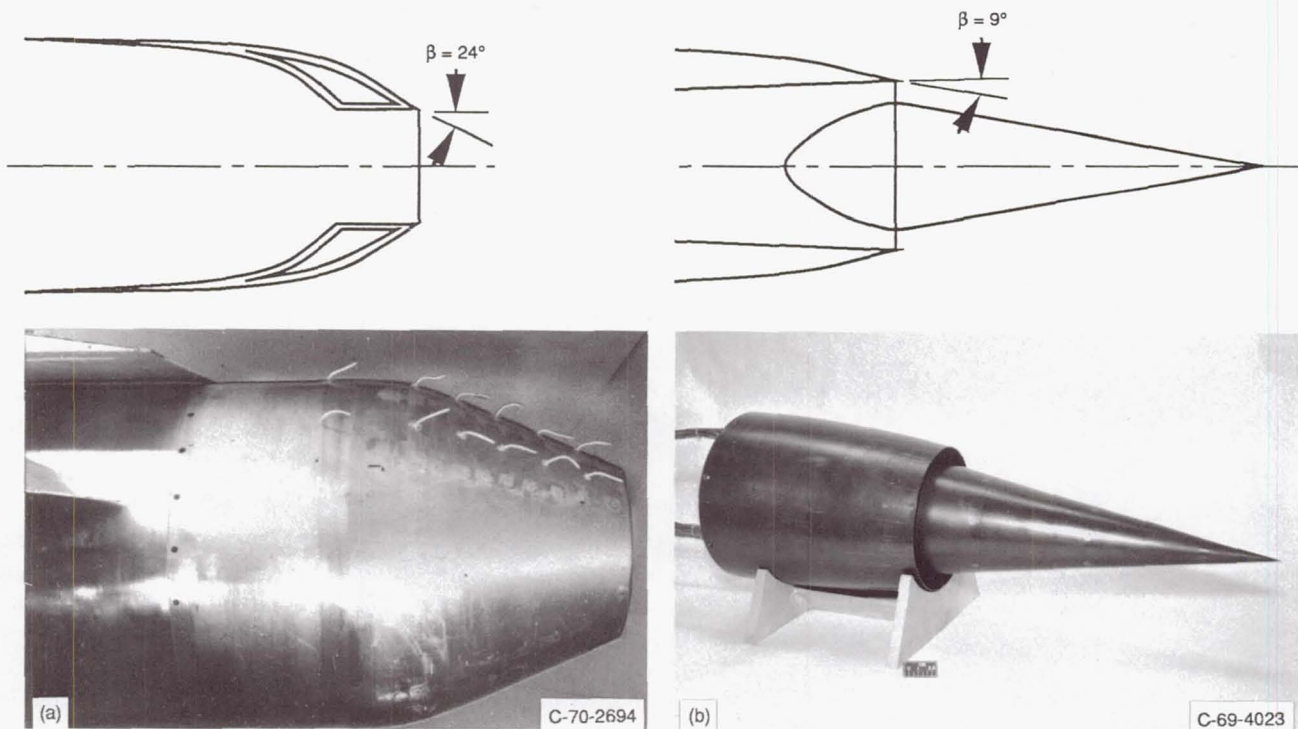
(a) Variable convergent-divergent.
(b) Plug.

Figure 9-2.—Exhaust nozzle concepts for supersonic dash aircraft.

## 9.1 Isolated Performance

The isolated performance of the two supersonic dash configurations discussed in the preceding section is shown in figure 9-3. For reference the internal performance of an ideal convergent nozzle without any external drag is also presented. The dropoff in performance of this nozzle with increasing pressure ratio ($>2.0$) was an indication of its underexpansion losses. Note that the plug nozzle had the same performance characteristics as the ideal convergent nozzle. The small decrease in performance with external flow resulted from the drag on the $9°$ circular-arc boattail. At a typical subsonic cruise pressure ratio of 2.8 for a turbofan engine, the plug nozzle provided a gross thrust coefficient of better than 97 percent. At the same nozzle pressure ratio the variable C–D nozzle had a slightly lower performance (about 96 percent), as shown by the single diamond point in figure 9-3. This difference in performance was due to the higher drag associated with the $24°$ boattail. Some additional discussion of the isolated performance of nozzles for supersonic dash aircraft is presented in reference 9-1.

The high-angle boattail shown for the variable C–D nozzle (fig. 9-2) operated near the limit for maintaining attached flow. Typical pressure distributions for this $24°$ boattail shape are shown in figure 9-4. If the flow remained attached, the distribution was as shown by the solid curve. If the flow separated locally, the distribution, as shown by the dashed curve, increased boattail drag. It was important then to define the separation characteristics of these high-angle boattails and to determine their sensitivity to Reynolds number and to installation effects. Flight tests of a series of these high-angle boattails conducted at the NASA Lewis Research Center showed some of these effects on boattail drag, as discussed in the following section.
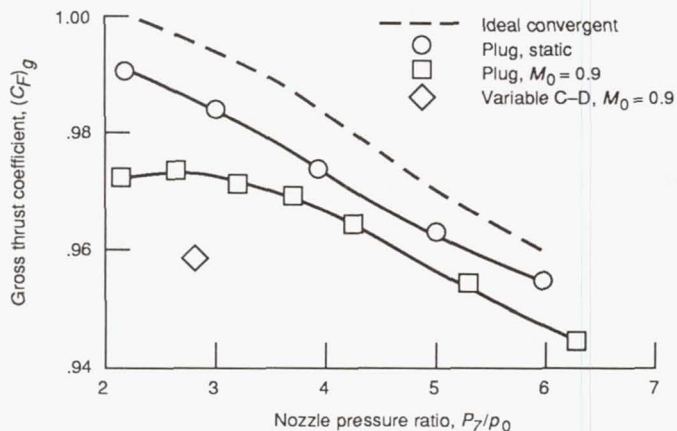


Figure 9-3.—Effect of external flow on supersonic dash nozzle performance.
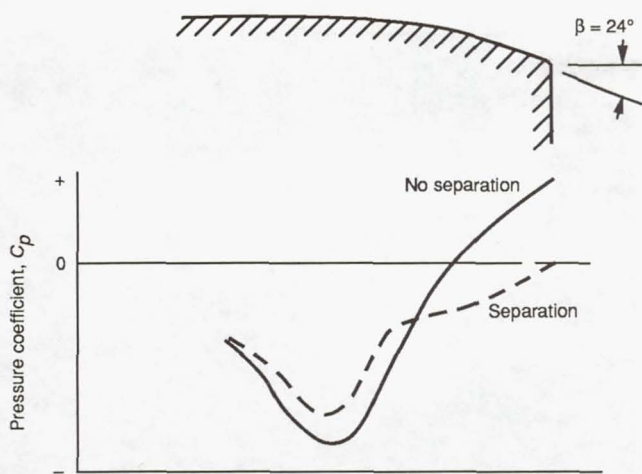
Figure 9-4.—Boattail pressure distribution. Variable convergent-divergent nozzle; free-stream Mach number, $M_0$, 0.90.

## 9.2 Nacelle Installation

The convergent-divergent nozzles that were test flown are shown in figure 9-5. These three nozzles all had the same projected boattail area and a 24° angle at the trailing edge. The top two were the same, except that the case 2 nozzle was moved upstream relative to the case 1 nozzle by about one-half nozzle diameter. The boattail juncture for these two was fairly sharp. The case 3 nozzle had a full circular-arc boattail.

Boattail drag divided by ideal primary thrust for these nozzles is shown in figure 9-6 as a function of Reynolds number, which was varied by flying the F-106 testbed aircraft at different altitudes. The Reynolds number was based on the length from the inlet cowl lip to the nozzle attachment point. The cases correspond to the nozzle designations of figure 9-5. With the case 1 nozzle at the lowest Reynolds number, the boattail drag was as much as 10 percent of the ideal primary gross thrust. Note that the drag was lowered considerably when this nozzle was moved forward (case 2). This decrease in drag was a result of the more favorable flowfield closer to the wing. However, the case 3 circular-arc contour provided the lowest drag of the three configurations.
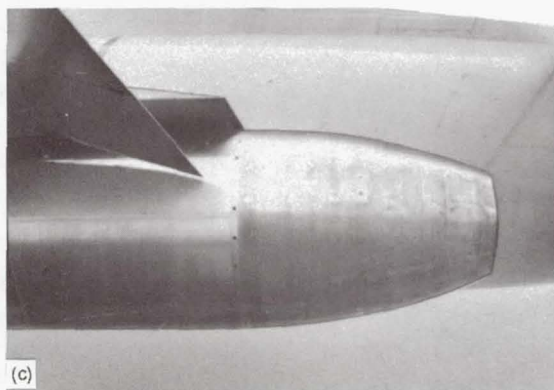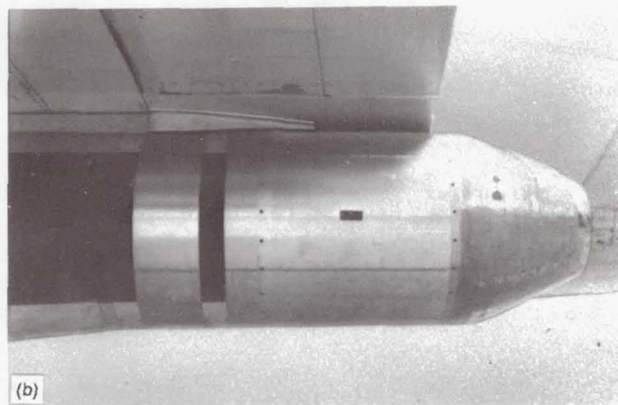


(a) Case 1: $r/d = 0.72$; extended one-half diameter.
(b) Case 2: $r/d = 0.72$.
(c) Case 3: circular arc.

Figure 9-5.—Variable convergent-divergent nozzles.
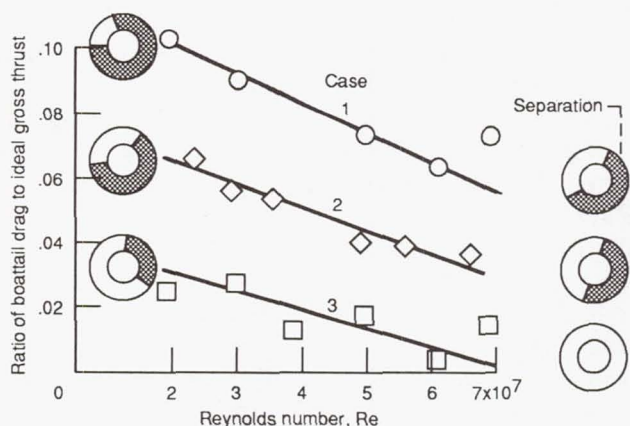
Figure 9-6.—Effect of Reynolds number on boattail drag. Boattail angle, $\beta$, 24°; free-stream Mach number, $M_0$, 0.9.

Separation was encountered with these three high-angle boattails and was detected by pressure measurements and tufts. Areas of separation are shown in figure 9-6 by the shaded regions. Note that separation was encountered with all the nozzles except the circular arc at the highest Reynolds number. Increasing the Reynolds number lessened the tendency of the external flow to separate and thus reduced drag for all the nozzles.

## 9.3 Fuselage Installation

In many fighter designs the engines are buried in the aft end of the fuselage as shown in figure 9-7. The NASA Langley Research Center studied the problems of aft-mounted nozzle configurations in the late 1960's and early 1970's, and in one series of tests made some parametric variations in the region of the nozzles shown by the solid lines. These investigations were conducted in Langley's 16-Foot Transonic Wind Tunnel.
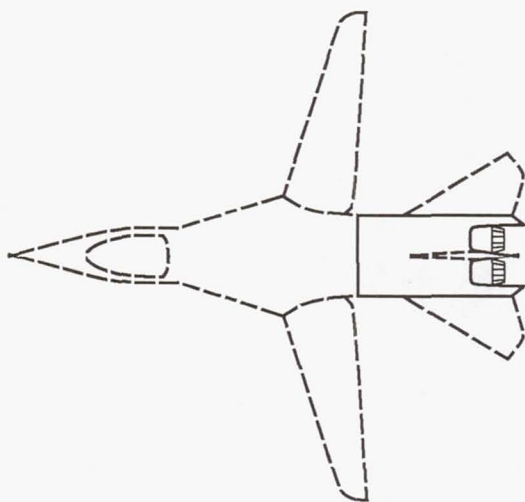


Figure 9-7.—Supersonic dash aircraft.
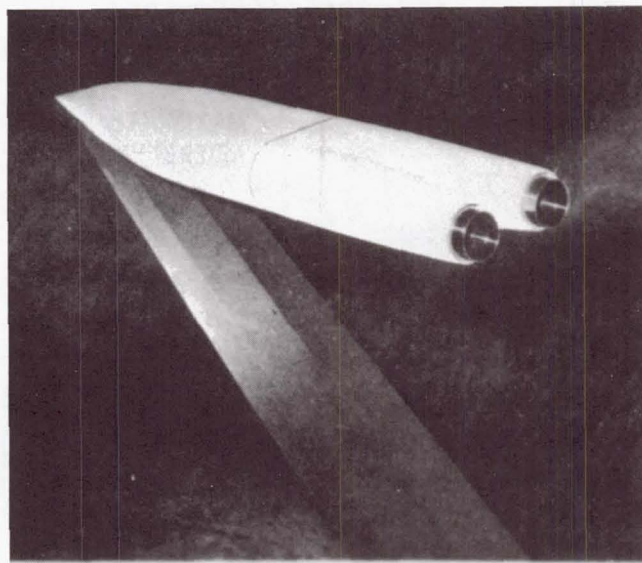


Figure 9-8.—Twin-engine afterbody nozzle model.

Some of the results are presented in references 9-2 to 9-9. A portion are summarized in this section.

The results presented herein were obtained with the twin-engine model shown in figure 9-8. The maximum diameter of the nozzles was 4.0 in., which represented about a 1/12-scale model. The engine exhaust jets were simulated with compressed air and were operated over a wide range of pressure ratios. The data presented herein were analyzed at pressure ratios representative of those for a turbofan engine. The circumferential line apparent at the midbody is a transverse cut closed with a flexible seal. The nonmetric forebody served as a support for the afterbody. All forces on the afterbody and nozzles were measured with two six-component balances arranged to yield a breakdown of the forces into (1) nozzle thrust minus drag and (2) afterbody drag. The presentation that follows deals with the effects of model configuration changes in the vicinity of the exhaust nozzles.

### 9.3.1 Jet Exit Axial Location

Results of a brief study on how jet exit axial location affects afterbody drag, extracted from reference 9-7, are presented in figure 9-9. The afterbody drag coefficient is based on nacelle maximum cross-sectional area, and drag variation with Mach number is shown.

All of the afterbodies were the same length and were shaped for minimum wave drag at Mach 1.001 by using the procedures of reference 9-8. The lower sketch in figure 9-9 indicates a configuration with the jet exits at the downstream end of the fuselage, for which the afterbody drag is shown by the circular points. From this downstream position the jet exits were moved forward on the fuselage by one-half body width as shown in the middle sketch and then by one full body width as shown in the top sketch. So that these latter two
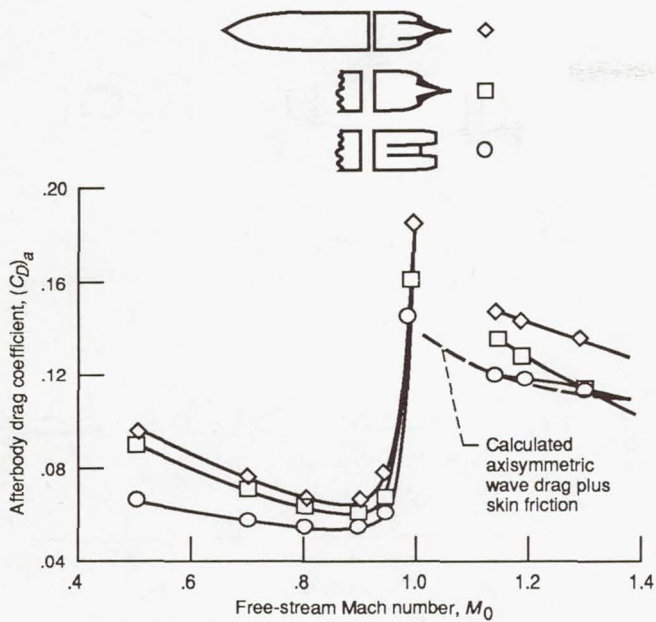
Figure 9-9.—Effect of jet exit axial location on afterbody drag.



(a) Military power.
(b) Maximum afterburning.

Figure 9-10.—Effect of interfairing shape on afterbody plus nozzle drag.

afterbodies would have the same area progression as that in the lower sketch, the cross-sectional area of the cylindrical jets was included. Although the direct thrust of the nozzles was excluded from these measurements, the results do include the effects of jet interference on afterbody drag.

The dashed curve shows calculated drag at low supersonic speeds for an axisymmetric afterbody having an area progression equal to that of the models, the values being the sum of wave drag and skin friction. The good agreement between the calculated drag and that measured on the afterbody with downstream exits improved confidence both in the theory and in the experimental techniques used.

At all speeds to Mach 1.3 the afterbody with jet exits at the extreme aft end showed the lowest drag. At subsonic speeds jet interference on the extended wedge interfairings increased the afterbody drag. At the higher speeds, however, the afterbodies with wedge-shaped extensions began to show increasing benefits from favorable jet interference.

### 9.3.2 Interfairing Shape

The effect of interfairing shape on the combined drag of the afterbody and the nozzles is shown in figure 9-10. The sketch on the upper right is a rear view of the nozzle installation; the shaded area shows the region in which the interfairing shapes were modified. The sketch on the upper left shows the basic afterbody, which had closely spaced nozzles located in the downstream position. The dashed line in the sketch indicates the elliptical interfairing contour in the plane of symmetry. Other shapes were circular arc, blunt, and blunt extended. The blunt interfairing had a flat base at the nozzle-fuselage juncture, and the blunt-extended interfairing terminated in a flat base approximately flush with the nozzle exits.
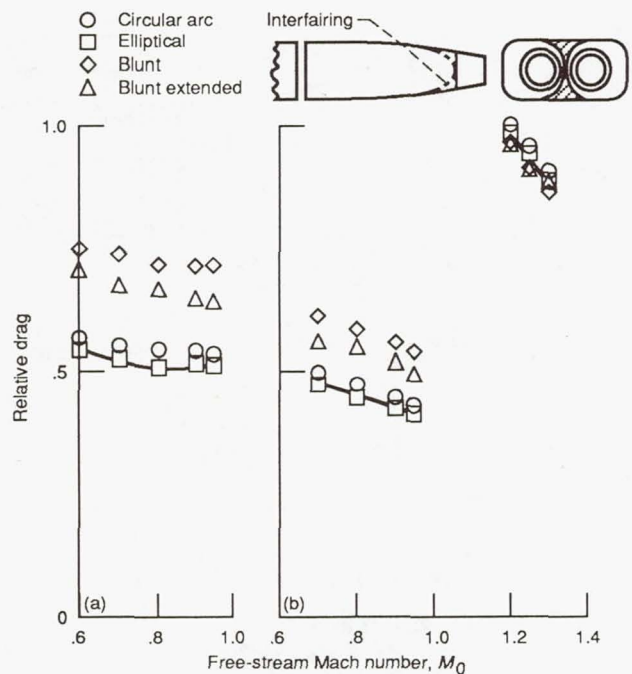
The results presented in the plots show relative drag as a function of Mach number, where the highest drag (at $M_0 = 1.2$) is given a value of unity. At subsonic speeds the afterbody with the elliptical interfairing showed the least drag for operation either at military power or with maximum afterburning. There is little choice between the elliptical and circular-arc shapes. Note that the use of a flat base was consistently detrimental at subsonic speeds. The data points at the upper right show all the interfairing shapes to have approximately the same drag at low supersonic speeds, although the flat-base interfairings did show slightly lower drag in this speed range.

### 9.3.3 Installation Effect on Nozzle Performance

To this point, interest has been centered on afterbody drag. Figure 9-11, prepared from material in references 9-3 and 9-9, is concerned with the installation effect on exhaust nozzle performance. The performance coefficient used for making comparisons is $\Delta[(F - D_n)/F_i]$, the sum of nozzle gross thrust minus nozzle boattail drag, taken as a ratio to ideal gross thrust. The drag term in this expression reflects only the drag on the nozzle boattails, indicated by the shaded regions in the sketches. This figure shows increments in the coefficient when the static performance of the nozzle was used as the reference. Results are presented for convergent and convergent-divergent nozzles.

The lower sketch in figure 9-11 represents a model in which the nozzles were installed in an aerodynamically smooth aft

(a) Military power ($M_0 = 0.8$).
(b) Maximum afterburning ($M_0 = 1.2$).
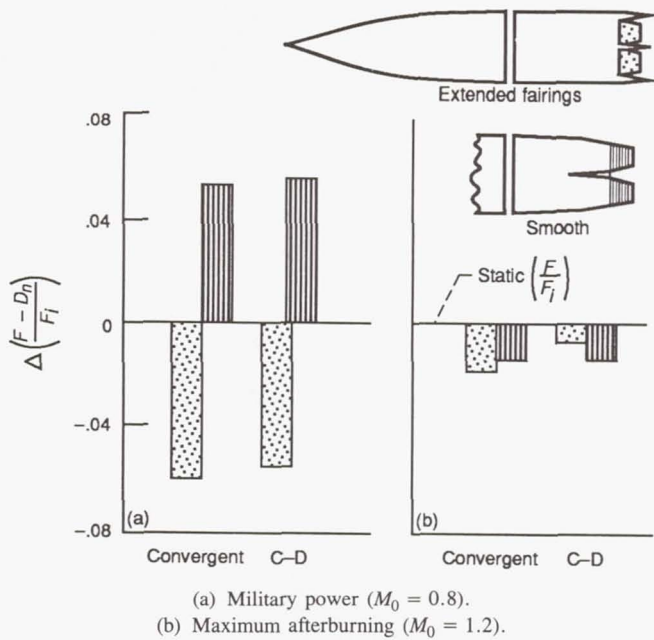
Figure 9-11.—Effect of installation on nozzle performance. Shaded areas represent measured drag surfaces.



(a) Military power ($M_0 = 0.8$).
(b) Maximum afterburning ($M_0 = 1.2$).

Figure 9-12.—Effect of afterbody boattail angle on nozzle performance. Shaded areas represent measured drag surfaces.

fuselage, for which the afterbody contours faired smoothly into those of the nozzle. With this installation at subsonic speeds, good pressure recovery in the external flow exerted a thrust on the nozzle boattail. The vertically hatched bars show that in the smooth installation, at Mach 0.8, the nozzle performance exceeded the static value by 5 or 6 percent of the ideal gross thrust for both types of exhaust nozzles.

Another type of installation is represented in the upper sketch, in which the afterbody incorporated extended fairings outboard of the nozzles and a fuselage extension between the nozzles. The presence of these extensions tended to disturb the streamline flow over the nozzle and to prevent good pressure recovery in the external flow. The result was a severe drag on the nozzle boattail. The shaded bars on the lower side of the plot at the left show that for Mach 0.8 the increased nozzle drag resulted in a large performance loss. The difference in performance between these two installations of 10 or 12 percent of ideal gross thrust at high subsonic speed represents about a 20 percent difference in net thrust, indicating that installation effects are important. These comparisons show that the nozzle operating environment had a critical influence on nozzle performance at high subsonic speeds but relatively less effect at supersonic speeds.

### 9.3.4 Afterbody Boattail Angle

Another factor to be considered in designing an exhaust nozzle installation, namely the boattail angle of the afterbody just upstream of the nozzle attachment, is shown in figure 9-12. Again, the basic configuration was the smooth twin-engine afterbody with closely spaced convergent nozzles. The
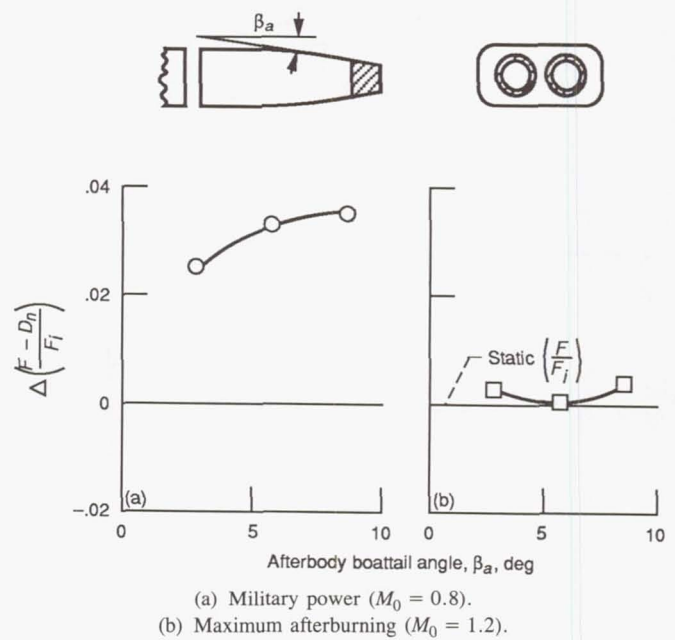
data present increments in the performance parameter as a function of afterbody boattail angle.

At Mach 0.8, with the nozzle in the military power setting, good pressure recovery in the external flow was realized. The nozzle installed performance exceeded the static performance in all cases and improved with increasing boattail angle.

The plot on the right shows that at low supersonic speed (e.g., Mach 1.2) pressure recovery in the external flow was relatively poor and that the nozzle performance was not significantly better here than for static operation. In this speed range afterbody boattail angle had little effect on the installed nozzle performance.

### 9.3.5 Nozzle Lateral Spacing

The effect of nozzle lateral spacing on nozzle performance and afterbody drag is shown in figure 9-13. The lower sketches represent the basic twin-engine afterbody with convergent nozzles. In the sketch on the upper left, which is a rear view of the nozzle installation, the spacing ratio is defined as the ratio of the distance $S$ between the nozzle centerlines to the nozzle diameter $d_n$ at the nozzle-fuselage juncture.

The left side of figure 9-13 shows how lateral spacing affected exhaust nozzle performance. The small rate of increase in performance with increased spacing at both subsonic and low supersonic speeds indicates that the mutual interference drag of the nozzles decreased with increasing distance between the nozzles. The effect of increasing spacing on nozzle performance then was beneficial but small.

The right side of this figure shows how lateral spacing affected the drag of the complete afterbody and nozzles.

Free-stream
Mach number,
$M_0$

○ 0.8 (military power)
△ 1.2 (maximum afterburning)
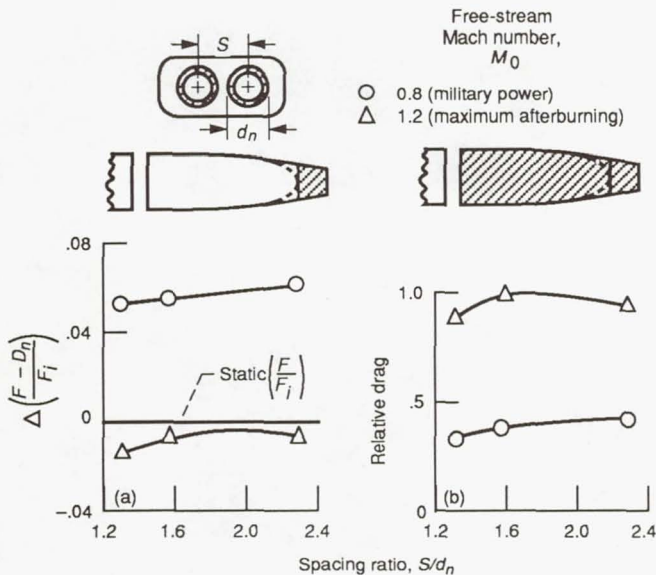
(a) Nozzle performance.
(b) Relative drag (afterbody plus nozzle).

Figure 9-13.—Effect of nozzle lateral spacing on nozzle performance and relative drag. Shades areas represent measured drag surfaces.



○ Military power ($\beta_n = 14°$)
□ Maximum afterburning ($\beta_n = 4°$)
Plan view

Figure 9-14.—Effect of tail interference on nozzle performance.

Relative drag is shown as a function of the spacing ratio. The drag tended to increase slightly as the space between the nozzles increased at both subsonic and low supersonic speeds. The net result was that lateral spacing of the exhaust nozzles was not a critical factor in the aerodynamic design of an afterbody-nozzle installation.

### 9.3.6 Tail Interference

The effect on exhaust nozzle performance of adding tail surfaces to the afterbody in the vicinity of the nozzle installation is shown in figure 9-14. The basic model was the aerodynamically smooth twin-engine afterbody with convergent-divergent nozzles. The plot presents the variation with Mach number of the change in nozzle performance that occurred when horizontal and vertical tail surfaces were added to the basic configuration. The direct drag of the tail surfaces did not enter into these measurements; the change in exhaust nozzle performance reflected only the change in nozzle drag caused by the proximity of the tail surfaces.

With the engines operating at military power, adding the tail surfaces caused a loss in nozzle performance at subsonic speeds. At Mach 0.95 this loss amounted to 4 percent of the ideal gross thrust (see the lower curve in fig. 9-14). The upper curve shows results obtained with the nozzle in the maximum afterburning setting. At this condition, adding the tail surfaces to the afterbody had a small, favorable effect on nozzle performance at all speeds below Mach 1.3.

## 9.4 Concluding Remarks

The installation problems associated with exhaust nozzles on supersonic dash aircraft can be summarized as follows. For underwing engine nacelles with high-angle boattails, increasing the Reynolds number tended to decrease the extent of flow separation and therefore tended to decrease drag. For the F-106 underwing nacelle installation a more forward location of the boattail tended to reduce drag. However, a pure circular-arc boattail had the least drag. For engines mounted in the fuselage a disturbance to the streamline flow near the nozzle boattail was detrimental. A shallow boattail angle was required for supersonic but not subsonic speed. The best performance was obtained with the nozzles downstream of the airframe terminus. Finally, the lateral spacing did not appear to be critical to the design of twin aft-body installations.

## 9.5 References

9-1. Harrington, D.E.: Performance of Convergent and Plug Nozzles at Mach Numbers From 0 to 1.97. NASA TM X-2112, 1970.

9-2. Runckel, J.F.: Aerodynamic Interference Between Exhaust System and Airframe. Aerodynamic Interference, AGARD CP-71-71, AGARD, Paris, France, 1970, pp. 15-1 to 15-10. (Also NASA TM X-66888.).

9-3. Corson, B.W., Jr.; and Runckel, J.F.: Exploratory Studies of Aircraft Afterbody and Exhaust-Nozzle Interaction. NASA TM X-1925, 1969.

9-4. Greathouse, W.K.: Blending Propulsion With Airframe. Space/Aeronautics, vol. 50, no. 5, Nov. 1968, pp. 59-68.

9-5. Migdal, D.; Miller, E.H.; and Schnell, W.C.: An Experimental Evaluation of Exhaust Nozzle/Airframe Interference. AIAA Paper 69-430, June 1969.

9-6. Throndson, L.W.: Close-Spaced Nozzles, Twin Jet Configuration. AIAA Paper 70-934, July 1970.

9-7. Berrier, B.L.; and Wood, F.H., Jr.: Effect of Jet Velocity and Axial Location of Nozzle Exit on the Performance of a Twin-Jet Afterbody Model at Mach Numbers up to 2.2. NASA TN D-5393, 1969.

9-8. Harris, R.V., Jr.: An Analysis and Correlation of Aircraft Wave Drag. NASA TM X-947, 1964.

9-9. Mercer, C.E.; and Berrier, B.L.: Effect of Afterbody Shape, Nozzle Type, and Engine Lateral Spacing on the Installed Performance of a Twin-Jet Afterbody Model. NASA TM X-1855, 1969.

# Chapter 10
# Nozzle Facilities and Test Techniques

The facilities used at the NASA Lewis Research Center to experimentally determine exhaust system performance are many and varied. Each serves a useful function in arriving at the overall performance of the installed exhaust nozzle. Table 10-I lists the facilities used to study supersonic cruise and supersonic dash aircraft. They include static test stands for measuring nozzle internal performance and noise; a wind tunnel for measuring external flow and installation effects; and a testbed aircraft for measuring full-scale installed performance and flyover noise.

Performance predictions for full-scale exhaust systems are normally determined by cold-flow, subscale model tests. The effect of hot flow on exhaust system thrust and pumping characteristics has been the subject of much speculation. Full-scale test data (refs. 10-1 and 10-2) indicate that predicting secondary pressure requirements (pumping characteristics) from cold-flow model tests can result in errors unless heat transfer to the secondary stream is accounted for. However, no errors in nozzle thrust coefficient were apparent from these tests, and no corrections to the measured thrust coefficient were applied to the cold-flow data.

The secondary to primary weight flow ratio can be corrected by multiplying it by the square root of the cold- to hot-flow total temperature ratio, in an attempt to correlate nozzle pumping characteristics. Although this has resulted in some success, full-scale data still indicate that a higher secondary pressure is required to pump a given corrected secondary weight flow ratio under hot conditions than under cold conditions, as pointed out in reference 10-3. The heat transfer process associated with the turbulent mixing zone within an ejector nozzle can affect pumping characteristics and therefore should be included in nozzle analyses, as recommended in reference 10-4.

Each of the nozzle testing techniques is discussed in this chapter as the NASA Lewis test facilities are described.

TABLE 10-I.—NASA LEWIS RESEARCH CENTER EXHAUST
SYSTEM TEST FACILITIES

| Facility | Type | Research area | Nozzle size, in. | Jet flow |
|---|---|---|---|---|
| SW-21 and CE-22 | Static stands | Internal performance | 8 to 12 | Ambient |
| Propulsion Systems Laboratory (PSL) | Static | Internal performance | Full size | Engine |
| 8- by 6-Foot Supersonic Wind Tunnel | Wind tunnel ($M_0 = 0$ to 2.0) | Isolated, with external flow | 6 to 8.5 | Ambient to 700 °F |
| | | Installation and Reynolds number effects | 1 to 5.5 | Ambient |
| F-106 | Aircraft ($M_0 = 0$ to 1.5) | Installation effects, Reynolds number effects, and noise | 25 | J-85 |
| Hot jet facilities | Static | Noise | 2 to 15 | 1000 to 2500 °F |

91

# 10.1 Static Test Stands

Static test stands provide the internal flow streams for nozzle testing but do not include any external or free-stream simulation; they can therefore be used only for measuring the internal performance of nozzles. However, good performance estimates can be obtained for both the takeoff and supersonic cruise configurations, since external flow effects are negligible at these flight conditions.

At NASA Lewis two sizes of static test stands have been used. The smaller stands (SW–21 and CE–22) test subscale models up to 12 in. in diameter and feature cold flow, as shown in table 10–I. The SW–21 stand was used for nozzle tests during the time period discussed in this report. It has since been dismantled and replaced by the CE–22 stand, which is similar but has been updated; for example, axial and side force can be measured in CE–22, whereas only axial force was measured in SW–21.

The larger static test stands in the Propulsion Systems Laboratory (PSL) at NASA Lewis can accommodate full-scale hardware, including the engine and its nozzle system. Thus, full-scale nozzle data can be obtained with realistic hot exhaust flow.

Static test stands are relatively cheap to operate and lend themselves to rapid model changes. Many configurations can be evaluated in a short time, and the more promising config-urations can then be further evaluated in wind tunnel and flight tests to obtain external flow and installation effects. A small and a large static stand are described in the following paragraphs.

## 10.1.1 SW–21

A schematic diagram of the SW–21 test stand and its nozzle support and air supply systems is shown in figure 10–1. As mentioned earlier, this facility was used to generate data for most of the nozzle configurations discussed in the preceding chapters of this report. A load cell was used to measure the axial force on the metric parts of the system; tare forces were then removed to obtain the nozzle gross thrust. Standard ASME calibration nozzles were used to verify the system thrust and airflow measurements.

The SW–21 stand provided two airflows for nozzle tests, a primary and a secondary flow. The static pressure in the plenum chamber could be reduced from ambient conditions to vary nozzle pressure ratio. The nozzle exhaust flow was ducted from the chamber through the altitude exhaust pipe.

A typical supersonic cruise configuration installed in the SW–21 facility is shown in figure 10–2. This particular configuration was an auxiliary-inlet ejector nozzle; the inlet doors were in the open position.
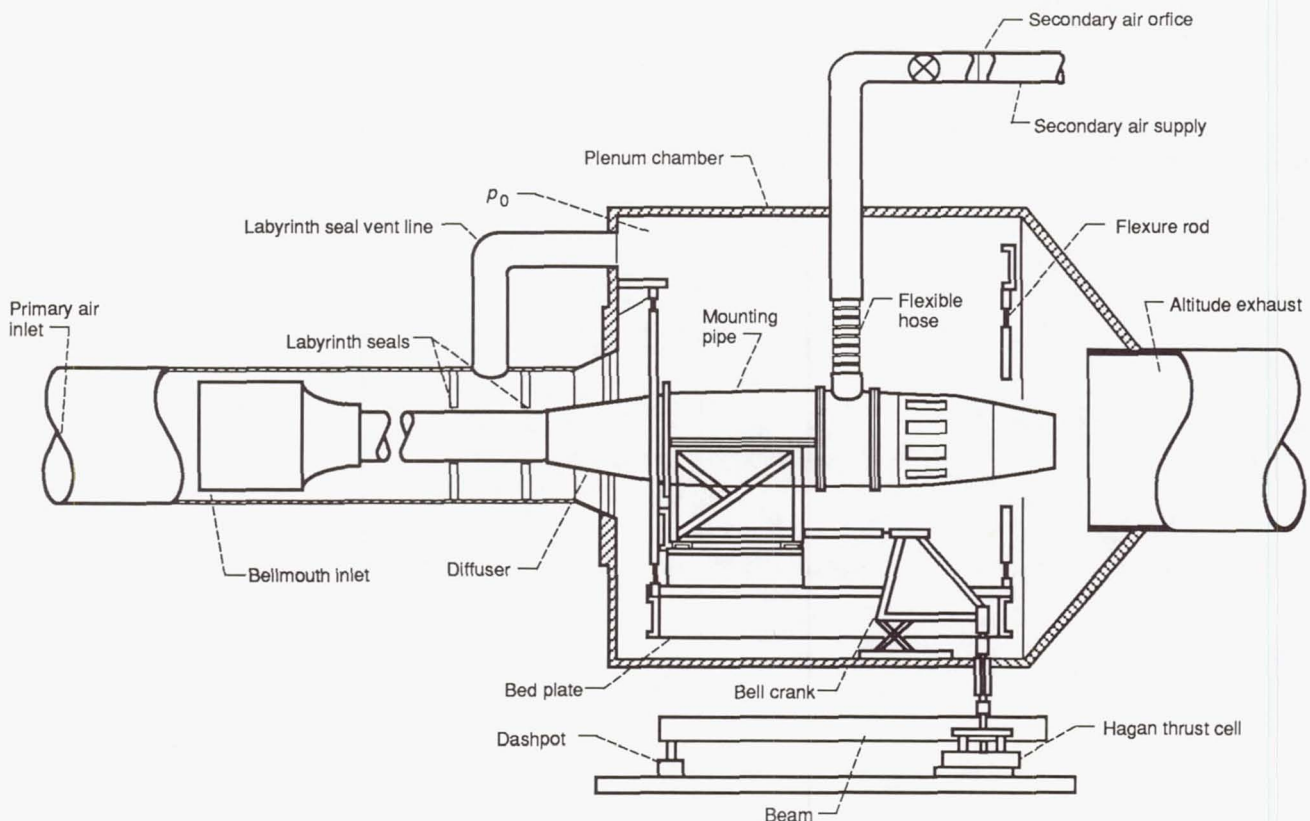


Figure 10–1.—Schematic of test stand showing nozzle support and air supply systems.
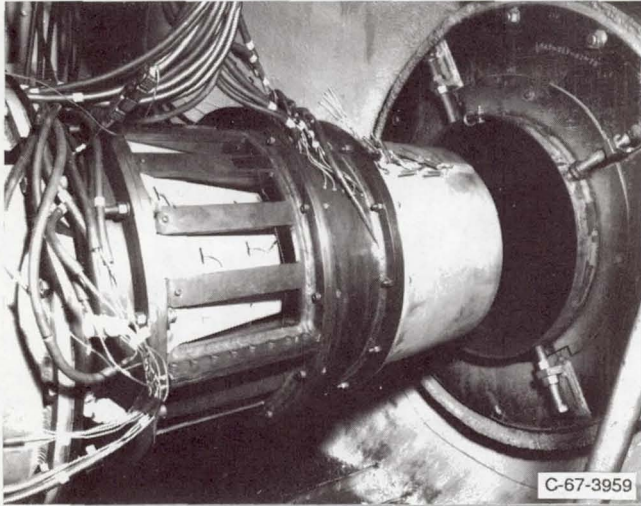
Figure 10-2.—Ejector nozzle installed in static test facility.

## 10.1.2 Propulsion Systems Laboratory Altitude Chamber

A typical engine and nozzle installation in the PSL altitude chamber is shown in figure 10-3. The figure shows the nacelle and one of the nozzle configurations that were later flown on the F-106 testbed aircraft to determine installation effects. All flight test hardware was checked out in the PSL facility prior to flight.

The nacelle shown in figure 10-3 contained a General Electric J-85 afterburning turbojet engine and a cylindrical ejector nozzle. The nacelle was a 25-in.-diameter cylinder with a bulged section located underneath the compressor area to accommodate the engine accessory package. The entire engine nacelle was mounted on a rigid platform suspended by four flexure rods. The forces on the nacelle were transmitted to a water-cooled load cell used to measure the nozzle thrust.

A forward bulkhead with a labyrinth seal around the inlet section of the nacelle separated the forward plenum cavity from the altitude chamber, providing a means of adjusting the exhaust pressure independent of the inlet pressure. Exhausters were used to control the test cell pressure and to eject the exhaust gases, which were directed into the duct immediately downstream of the nozzle exit plane. A minimal amount of air was discharged into the test cell through the bulkhead wall to keep the test cell purged of exhaust gases and cooled to an acceptable temperature level.

The primary airflow was supplied to the engine and metered through a bellmouth venturi. A separate supply was available for secondary airflow. Standard ASME sharp-edged orifices were used to meter the secondary airflow, which was supplied to a toroidal manifold surrounding the inlet section upstream of the compressor face. A range of predetermined cell ambient pressures were scheduled to vary the nozzle pressure ratio over an appropriate range for a given flight schedule.
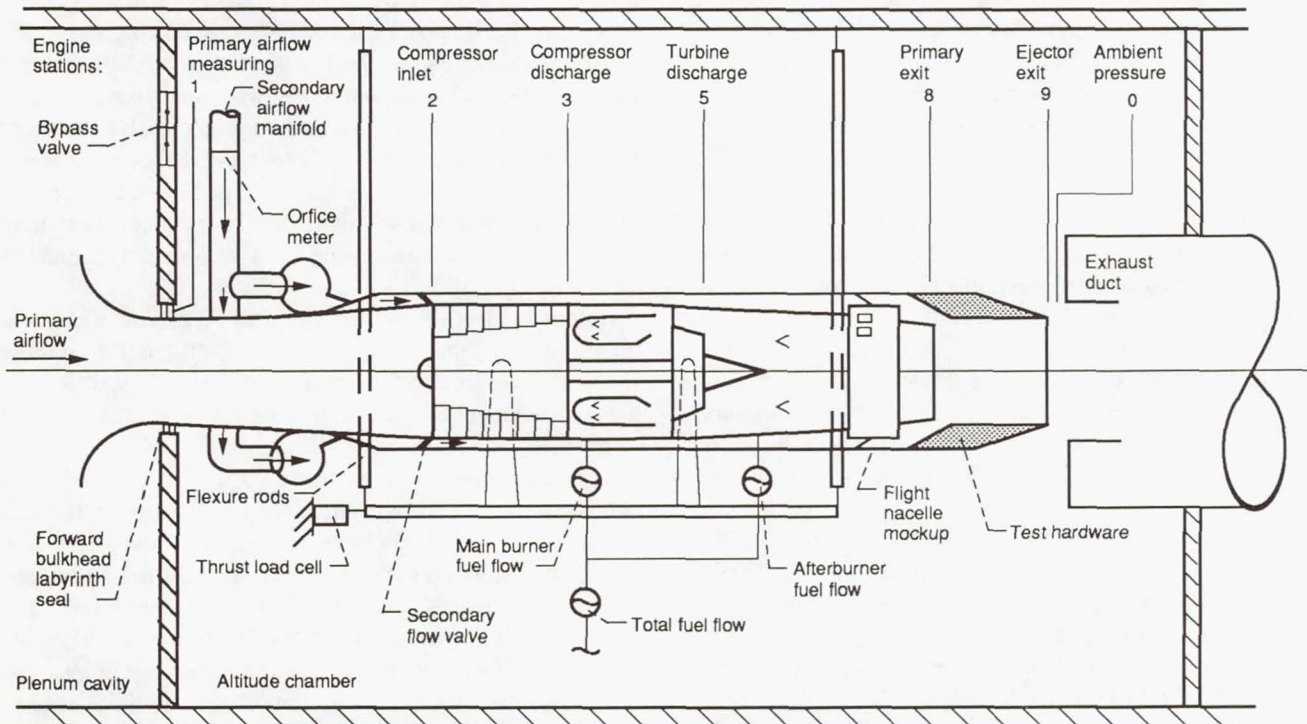


Figure 10-3.—Test installation in Propulsion Systems Laboratory altitude chamber.

93
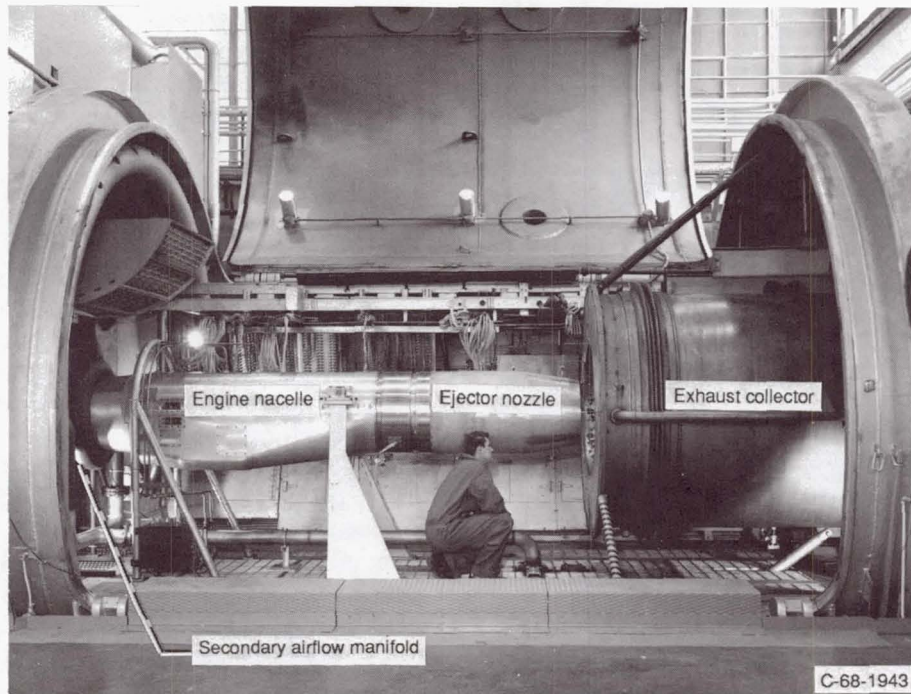
Figure 10–3.—Concluded.

## 10.2 Wind Tunnel

As mentioned previously, the external stream has a negligible effect at supersonic cruise speed, since the aft end of the nacelle is usually cylindrical and auxiliary inlets, if any, are closed. Most of the external stream effects occur at subsonic and transonic speeds, where the variable-geometry nacelle becomes boattailed and where free-stream air may be introduced through auxiliary inlets to prevent overexpansion of the primary exhaust flow in the secondary shroud.

The 8- by 6-Foot Supersonic Wind Tunnel at NASA Lewis has been modified to operate transonically, over a Mach number range from 0 to 2.0. Because of blockage effects and shock reflections from the tunnel walls, the jet exit model was limited to an 8.5-in. diameter. The model was supported in the test section by a long vertical strut. High-pressure primary and secondary air was ducted into the model through supply tubes passing through the strut. The primary air could be heated to about 700 °F.

A schematic view of the jet exit model in figure 10–4 shows the nozzle, the nozzle adapter, and the horizontal air supply passages suspended from the air supply tubes. A load cell in the model nose measured the axial forces on the metric parts of the system, which included only the adapter and nozzle sections. A choke plate and screens provided uniform flow at the nozzle inlet station. A standard ASME reference nozzle was used to verify load cell and airflow measurements.

Small models of complete aircraft can also be tested in the 8- by 6-Foot Supersonic Wind Tunnel, with corresponding reductions in the size of the nacelles used. One example is the 0.05-scale model of the F–106 testbed aircraft shown in figure 5–18(c). This aircraft model was small enough to avoid any transonic tunnel wall interference problems, but the nacelle diameter was only 1.25 in. The wing structure was thin and no pressurized air could be piped to the nacelle to simulate jet effects. For this reason, during nozzle tests the nacelle inlets were closed, and solid jet boundary simulators were used.

Larger models of aircraft can also be tested in the wind tunnel. An example is the 0.22-scale F–106 half-span model shown mounted on a reflection plate in figure 10–5. This model had a turbojet engine simulator in its 5.5-in.-diameter nacelle to provide the jet effects.

The engine simulator incorporated a six-stage, axial-flow compressor powered by a three-stage, axial-flow turbine, as shown in figure 10–6. High-pressure warm air was used to drive the turbine. It was possible to match the inlet mass flow ratio and the nozzle pressure ratio of the General Electric J–85 turbojet engine. The design characteristics of the simulator permitted independent operation over a wide range of inlet mass flow ratios and nozzle pressure ratios equal to those obtained in flight tests. The design and operating capabilities of this turbojet engine simulator are described in reference 10–5.
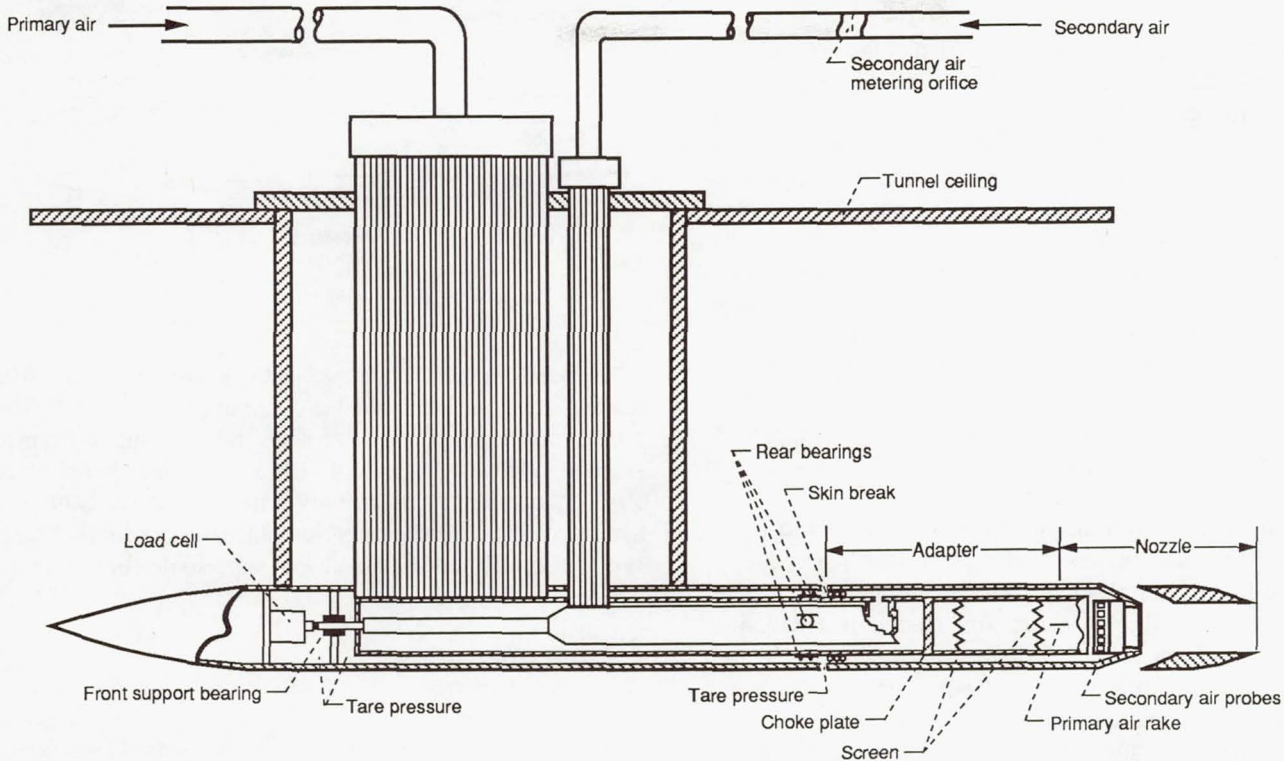
Figure 10-4.—8.5-in.-diameter jet exit model in 8- by 6-Foot Supersonic Wind Tunnel.
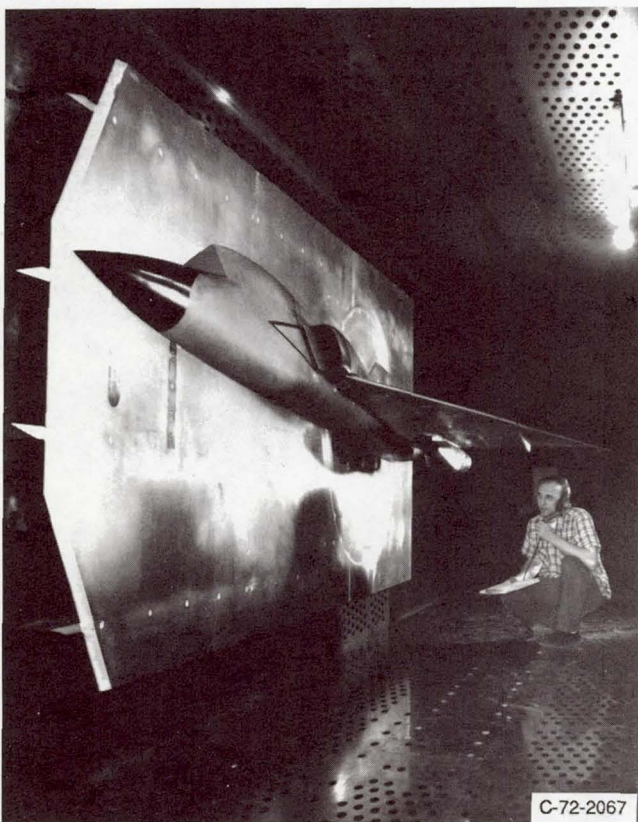


Figure 10-5.—0.22-Scale F-106 model in wind tunnel.
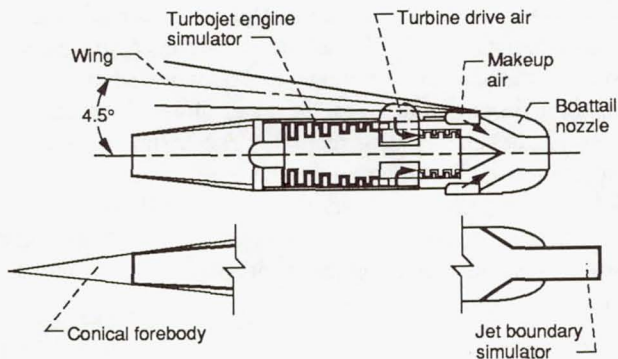


Figure 10-6.—0.22-Scale model turbojet simulator and nacelle installation.

This model was also tested with a conical forebody closing off the nacelle inlet and a solid jet boundary simulator mounted to the nozzle, as shown in figure 10-6. This permitted a direct comparison with the test data obtained from the smaller 0.05-scale aircraft model.

## 10.3 Testbed Aircraft

Installation effects refer to the distortion of the external flow by the airframe; this distortion varies with nacelle location. Although the most important airframe installation effects occur at subsonic and transonic speeds, the transonic performance of a nozzle is difficult to obtain in a wind tunnel because of tunnel wall interference effects. The transonic testing problem is made even more difficult because a large section of the airframe must be tested along with the exhaust nozzle. As a result the nozzle model must be smaller than desired when working within the size limits of existing wind tunnels.

One approach to this problem is to have a coordinated flight and wind tunnel test program that uses the best features of each testing technique. NASA Lewis has used this approach. A modified F–106 airplane was used as a transonic testbed for off-design testing of supersonic nozzles.

The modified F–106 aircraft in flight is shown in figure 5–18(b). Two new engine nacelles were installed under the wings so that the nozzles extended beyond the trailing edge. The placement of these nacelles simulated an installation on a typical supersonic cruise aircraft. Two nacelles were used to balance the thrust on the aircraft. One nacelle had a reference nozzle and the other a research nozzle. A simple normal-shock pitot inlet was adequate for the Mach number range of 0.55 to 1.45.

An afterburning J–85 turbojet engine was installed in each nacelle. The nacelles were 25 in. in diameter and were designed to accept any of the nozzles that had good performance in static and wind tunnel tests. The installation of a nacelle is shown in figure 10–7. The nacelles were tangent to the lower surface of the wing at its trailing edge and mounted to the wing through a forward and a rear link that allowed the nacelles to move in an axial direction. The axial movement, proportional to the thrust minus the drag, was taken out by a load cell to provide a direct measurement of nozzle thrust and drag. The nacelle and the test nozzle were also instrumented to obtain component performance and for diagnostic purposes.
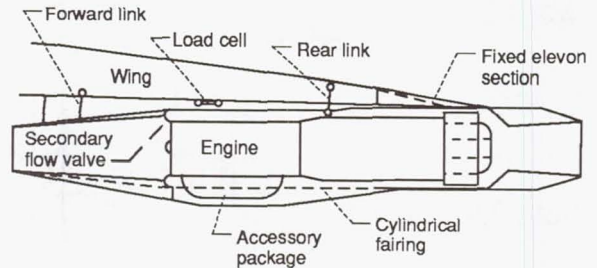


Figure 10–7.—Nacelle-engine installation on F–106.

Engineering aspects and first flight results of the NASA F–106 testbed aircraft are discussed in detail in reference 10–6. The nozzle performance measurements taken using calibrated engines and load cells on the F–106 are explained in reference 10–7. This testing technique proved to be an indispensable tool in determining the installed performance of supersonic exhaust systems at high subsonic and low supersonic flight speeds.

## 10.4 References

10-1. Wilsted, H.D; Huddleston, S.C.; and Ellis, C.W.: Effect of Temperature on Performance of Several Ejector Configurations. NACA RM E9E16, 1949.

10-2. Wallner, L.E.; and Jansen, E.T.; Full-Scale Investigation of Cooling Shroud and Ejector Nozzle for a Turbojet Engine–Afterburner Installation. NACA RM E51J04, 1951.

10-3. Samanich, N.E.; and Huntley, S.C.: Thrust and Pumping Characteristics of Cylindrical Ejectors Using Afterburning Turbojet Gas Generator. NASA TM X–52565, 1969.

10-4. Anderson, B.H.; Factors Which Influence the Analysis and Design of Ejector Nozzles. NASA TM X–67976, 1972.

10-5. Steffen, F.W.; et al.: A Turbojet Simulator for Mach Numbers up to 2.0. NASA TM X–67973, 1972.

10-6. Crabs, C.C.; Boyer, E.O.; and Mikkelson, D.C.: Engineering Aspects and First Flight Results of the NASA F–106 Transonic Propulsion Research Aircraft. NASA TM X–52559, 1969.

10-7. Groth, H.W.; Nozzle Performance Measurement on Underwing Nacelles of an F–106 Utilizing Calibrated Engines and Load Cells. NASA TM X–67816, 1971.

# Chapter 11
# Concluding Remarks

This report has summarized the in-house and contracted efforts of the NASA Lewis Research Center in supersonic exhaust nozzle research from 1963 to 1985. In sponsoring this effort the United States Supersonic Transport Program and the follow-on Supersonic Cruise Research Program produced two generations of supersonic cruise nozzles whose thrust performance was encouraging. All of the nozzle configurations had typically high thrust efficiency at the critical supersonic cruise flight condition. Two of the nozzles even exceeded the study goals and proved that nozzle efficiencies of over 98 percent are attainable at cruise when the design details of the exhaust system are carefully considered.

The off-design subsonic cruise performance, however, was more difficult to achieve because of interactions between internal and external flows. Operating at low nozzle pressure ratios required nozzles to produce a corresponding decrease in nozzle expansion ratio with a boattailed afterbody. Large aft-facing areas projected downstream when the nozzle was in this low-power position at subsonic cruise, making boattail drag a significant portion of the overall aircraft drag, especially at subsonic cruise, where the engine net thrust is low.

The study goal for the subsonic cruise flight condition proved to be the most difficult to attain; none of the configurations tested achieved it. The main losses were attributed to external drag and internal overexpansion. However, it appears that no fundamental problem exists with regard to these off-design conditions that cannot be solved by a concentrated research effort. Thus, attaining the study goals appears to be within reach.

For example, flight tests of an underwing nacelle installation, typical for a supersonic cruise aircraft, indicated that the installation effects at subsonic cruise were generally favorable for nozzles extending beyond the trailing edge of the wing. For this installation, a compression shock is located on the nacelle ahead of the boattail in a steeply rising pressure region that extends over the boattail surface and greatly reduces its drag.

In addition, several of the first- and second-generation nozzles were able to meet the study goals at both takeoff and transonic acceleration conditions. Features added to the nozzle for jet noise suppression have, however, resulted in lower nozzle thrust efficiencies at takeoff.

Mechanical design may well prove to be the most serious problem in obtaining an efficient variable-geometry exhaust nozzle for supersonic cruise aircraft. Why is this so? All of the nozzle parameters for obtaining good thrust and drag characteristics for supersonic cruise nozzles have been discussed herein and are well defined aerodynamically; the expansion ratios and area variations needed for efficient internal performance over a wide range of flight conditions are well known. The problem may be the inability to obtain optimum thrust minus drag with simple, lightweight designs that are easy to fabricate. This task remains extremely difficult because variable-geometry nozzles must operate for extended periods of time in a hostile internal flow environment of exhaust gases at high temperatures and pressures.

Some of the key items that must be considered in solving this problem are high-temperature materials for afterburning engines, cooling techniques, seals to minimize leakage of variable-geometry components, actuation systems, and the stability of components, both actuated and floating. Although not discussed in this report, reverse thrust capability and jet noise suppression impose additional design problems. Because they are required for high-speed civil transports, they further complicate a nozzle system in which cruise performance is highly critical.

The British-French Concorde, which recently celebrated its 20th year of flight, has proven that a commercial supersonic aircraft can be operated safely from existing airports. The Concorde's major drawbacks remain its small passenger capacity, its high fuel consumption, and its powerplants, which were designed before noise regulations were imposed. As aircraft noise rules become more stringent, low jet noise will be a driving factor in selecting nozzle concepts. Yet, the conflicting requirements, where takeoff is dominated by acoustics and supersonic cruise by aerodynamics, cannot be allowed to compromise the subsonic cruise or transonic acceleration performance.

In the years since the Concorde's maiden flight, NASA's Supersonic Cruise Research Program has generated knowledge that could lead to sizable gains over the Concorde technology. The most critical environmental issues still facing the construc-

tion of a future supersonic aircraft are its ability to meet increasing community sensitivity to noise, sonic booms, and atmospheric pollution. The propulsion system, which is the key to two of these environmental concerns, is being studied in continuing contracts with engine companies as well as within NASA itself.

Since the work reported herein was completed, NASA Lewis has been part of the initial phase of a third-generation study of supersonic nozzles. The new sponsoring program, the High-Speed Civil Transport (HSCT) Program, focuses on a 250- to 300-passenger aircraft with a range of 5500 to 6500 nautical miles, cruising at speeds between Mach 2 and 3. Early program efforts are under way at NASA's Lewis, Langley, and Ames Research Centers. Nozzle designs must address community noise, since an HSCT will have to meet the new Federal Aviation Administration Stage 3 noise rules. Examples of these third-generation nozzles include Boeing's aspirated coannular plug nozzle for their current baseline HSCT design, Pratt & Whitney's hypermix nozzle, and General Electric's two-dimensional coannular wedge nozzle. The difficulty in developing an acceptable nozzle is that noise is not the only driving factor: the nozzle must also be lightweight and perform well at all of the critical flight conditions for an HSCT.

The research effort in propulsion systems for supersonic cruise aircraft has been going on for over two decades. It appears that this effort is entering a new phase that will probably continue into the 21st century. Progress has been made, but a concerted effort is still required in the years ahead if a viable United States high-speed civil transport is to become a reality.

# Appendix A
# Symbols

| | |
|---|---|
| $A$ | area |
| $C_D$ | drag coefficient |
| $C_d$ | discharge coefficient |
| $C_F$ | thrust coefficient |
| $C_p$ | pressure coefficient |
| $C_V$ | velocity coefficient |
| $C_\theta$ | convergence factor |
| $D$ | drag |
| $d$ | diameter |
| $F$ | thrust |
| $L$ | length from primary exit to nozzle exit |
| $M$ | mach number |
| $\dot{m}$ | mass flow rate |
| $P$ | total pressure |
| $p$ | static pressure |
| $r$ | radius |
| $S$ | lateral spacing between adjacent nozzles |
| $s$ | distance from primary exit to minimum secondary shroud diameter |
| $T$ | total temperature |
| $t$ | static temperature |
| $V$ | velocity |
| $\dot{w}$ | weight flow rate |
| $x$ | axial distance |
| $\alpha$ | nozzle divergence half-angle |
| $\beta$ | boattail angle |
| $\gamma$ | ratio of specific heats |
| $\delta$ | boundary layer thickness |
| $\theta$ | nozzle convergence half-angle |
| $\lambda$ | divergence factor |
| $\tau$ | temperature ratio, $T_s/T_p$ |
| $\omega$ | weight flow ratio, $\dot{w}_s/\dot{w}_p$ |

Subscripts:

| | |
|---|---|
| $a$ | afterbody |
| $b$ | base |
| $C$ | circle |
| $c$ | coolant |
| $e$ | effective |
| $f$ | fan |
| $g$ | gross |
| $i$ | ideal |
| $j$ | jet |
| $l$ | local |
| max | maximum |
| min | minimum |
| $n$ | nozzle |
| $p$ | primary |
| $s$ | secondary |
| $w$ | wall |
| $x$ | axial distance |
| $\beta$ | boattail |
| $\eta$ | efficiency |

Stations:

| | |
|---|---|
| 0 | free stream |
| 7 | nozzle inlet |
| 8 | nozzle throat |
| 9 | nozzle exit |

# Appendix B
# Bibliography

Aircraft Propulsion. NASA SP–259, 1970.

Alford, J.S.; and Taylor, R.P.: Aerodynamic Stability Considerations of High-Pressure Ratio, Variable-Geometry Jet Nozzles. J. Aircraft, vol. 2, no. 4, July-Aug. 1965, pp. 308–311.

Anderson, B.H.: Factors Which Influence the Analysis and Design of Ejector Nozzles. NASA TM X–67976, 1972.

Beale, W.T.; and Povolny, J.H.: Internal Performance of Two-Dimensional Wedge Exhaust Nozzles. NACA RM E56K29b, Feb. 1957.

Beheim, M.A.; and Boksenbom, A.S.: Variable Geometry Requirements in Inlets and Exhaust Nozzles for High Mach Number Applications. NASA TM X–52447, 1968.

Bergman, D.: Effects of Engine Exhaust Flow on Boattail Drag. AIAA Paper 70–132, Jan. 1970.

Bergman, D.: Exhaust Nozzle Drag: Engine Versus Airplane Force Model. AIAA Paper 70–668, June 1970.

Bergman, D.: An Aerodynamic Drag Study of Jet Engine Nozzles. Inlets and Nozzles for Aerospace Engines, AGARD CP–91–71, AGARD, Paris, France, 1971, pp. 22–1 to 22–12.

Berrier, B.L.; and Wood, F.H., Jr.: Effect of Jet Velocity and Axial Location of Nozzle Exit on the Performance of a Twin-Jet Afterbody Model at Mach Numbers up to 2.2. NASA TN D–5393, 1969.

Blaha, B.J.: Effect of Nozzle Total Pressure and Base Bleed on the Stability Characteristics of a Sting-Supported Truncated Plug Nozzle. NASA TM X–1775, 1969.

Blaha, B.J.: Wind Tunnel Investigation of the Flow Field Under a 60° Swept Wing at Mach Numbers From 0.6 to 2.0. NASA TM X–52585, 1969.

Blaha, B.J.: Effect of Underwing Engine Nacelle Shape and Location on Boattail Drag and Wing Pressures at Mach Numbers From 0.56 to 1.46. NASA TM X–1979, 1970.

Blaha, B.J.; and Bresnahan, D.L.: Wind Tunnel Installation Effects on Isolated Afterbodies at Mach Numbers From 0.56 to 1.5. NASA TM X–52581, 1969.

Blaha, B.J.; and Johns, A.L.: Effect of Exit Area Variation on the Performance of an Auxiliary Inlet Ejector Nozzle at Mach Numbers From 0 to 1.27. NASA TM X–2182, 1971.

Blaha, B.J.; and Mikkelson, D.C.: Wind Tunnel Investigation of Airframe Installation Effects on Underwing Engine Nacelles at Mach Numbers From 0.56 to 1.46. NASA TM X–1683, 1968.

Blaha, B.J.; Mikkelson, D.C.; and Harrington, D.E.: Wind Tunnel Investigation of Installation Effects on Underwing Supersonic Cruise Exhaust Nozzles at Transonic Speeds. NASA TM X–52604, 1969.

Bowditch, D.N.: Inlet-Engine-Nozzle Wind Tunnel Test Techniques. NASA TM X–67870, 1971.

Bresnahan, D.L.: Experimental Investigation of a 10° Conical Turbojet Plug Nozzle With Iris Primary and Translating Shroud at Mach Numbers From 0 to 2.0. NASA TM X–1709, 1968.

Bresnahan, D.L.: Experimental Investigation of a 10° Conical Turbojet Plug Nozzle With Translating Primary and Secondary Shrouds at Mach Numbers From 0 to 2.0. NASA TM X–1777, 1969.

Bresnahan, D.L.: Performance of an Aerodynamically Positioned Auxiliary Inlet Ejector Nozzle at Mach Numbers From 0 to 2.0. NASA TM X–2023, 1970.

Bresnahan, D.L.: Internal Performance of a 10° Conical Plug Nozzle With a Multispoke Primary and Translating External Shroud. NASA TM X–2573, 1972.

Bresnahan, D.L.; and Johns, A.L.: Cold Flow Investigation of a Low Angle Turbojet Plug Nozzle With Fixed Throat and Translating Shroud at Mach Numbers From 0 to 2.0. NASA TM X–1619, 1968.

Brooke, D.; and Anderson, B.: Specialized Software Package for Ejector Nozzle Performance, Vols. 1 and 2. General Electric Company, Cincinnati, OH, 1983.

Burley, R.R.: Flight Investigation of Airframe Installation Effects on an Auxiliary Inlet Ejector Nozzle on an Underwing Engine Nacelle. NASA TM X–2396, 1971.

Burley, R.R.; and Mansour, A.H.: Static Performance of an Auxiliary Inlet Ejector Nozzle Using an Afterburning Turbojet Gas Generator. NASA TM X–1999, 1970.

Chamberlin, R.; and Blaha. B.J.: Flight and Wind Tunnel Investigation of the Effects of Reynolds Number on Installed Boattail Drag at Subsonic Speeds. NASA TM X–68162, 1973.

Chenoweth, F.C.; and Steffen, F.W.: Comparison of Experimental and Predicted Heat Transfer Characteristics for a Cylindrical Ejector. NASA TM X–1641, 1968.

Chenoweth, F.C.; and Lieberman, A.: Prediction of Heat-Transfer Characteristics for Ejector Exhaust Nozzles. Analytical Methods in Aircraft Aerodynamics, NASA SP–228, 1969, pp. 623–638.

Chenoweth, F.C.; and Lieberman, A.: Experimental Investigation of Heat Transfer Characteristics of a Film-Cooled Plug Nozzle With Translating Shroud. NASA TN D–6160, 1971.

Clark, J.S.; Graber, E.J.; and Straight, D.M.: Experimental Heat Transfer and Flow Results From an Air-Cooled Plug Nozzle System. NASA TM X–52897, 1970.

Clark, J.S.; and Lieberman, A.: Thermal Design Study of an Air-Cooled Plug Nozzle System for a Supersonic Cruise Aircraft. NASA TM X–2475, 1972.

Corson, B.W., Jr.; and Runckel, J.F.: Exploratory Studies of Aircraft Afterbody and Exhaust-Nozzle Interaction. NASA TM X–1925, 1969.

Crabs, C.C.; Boyer, E.O.; and Mikkelson, D.C.: Engineering Aspects and First Flight Results of the NASA F–106 Transonic Propulsion Research Aircraft. NASA TM X–52559, 1969.

Crabs, C.C.; Mikkelson, D.C.; and Boyer, E.O.: An Inflight Investigation of Airframe Effects on Propulsion System Performance at Transonic Speeds. NASA TM X–52677, 1969.

Cubbage, J.M., Jr.: Jet Effects on the Drag of Conical Afterbodies for Mach Numbers of 0.6 to 1.28. NACA RM L57B21, Apr. 1957.

Dusa, D.J.: Commercial Supersonic Transport Exhaust Nozzle Design Philosophy. Paper presented at the ASME 14th Annual International Gas Turbine Conference. Cleveland, OH, Mar. 9–13, 1969.

Dusa, D.J.; and McCardle. A.: Simplified Multi-Mission Exhaust Nozzle System. AIAA Paper 77–960, July 1977.

Fishbach, L.H., et al.: NASA Research in Supersonic Propulsion—A Decade of Progress. AIAA Paper 82–1048, June 1982 (also NASA TM–82862).

Graber, E.J., Jr.; and Clark, J.S.: Comparison of Predicted and Experimental Heat-Transfer and Pressure-Drop Results for an Air-Cooled Plug Nozzle and Supporting Struts. NASA TN D–6764, 1972.

Greathouse, W.K.: Blending Propulsion With Airframe. Space/Aeronautics, vol. 50, no. 6, Nov. 1968, pp. 59–68.

Groth, H.W.: Nozzle Performance Measurement on Underwing Nacelles of an F–106 Utilizing Calibrated Engines and Load Cells. NASA TM X–67816, 1971.

Groth, H.W.; Samanich, N.E.; and Blumenthal, P.Z.: Inflight Thrust Measuring System for Underwing Nacelles Installed on a Modified F–106 Aircraft. NASA TM X–2356, 1971.

Handbook of Supersonic Aerodynamics—Section 17. Ducts, Nozzles, and Diffusers. NAVWEPS Report 1488, Vol. 6, Jan. 1964.

Harrington, D.E.: Effect of a Rectangular Simulated Wing on the Pressure Drag Coefficient of Various Boattails at Mach Numbers From 0.60 to 1.47. NASA TM X-52609, 1969.

Harrington, D.E.: Jet Effects on Boattail Pressure Drag of Isolated Ejector Nozzles at Mach Numbers From 0.60 to 1.47. NASA TM X-1785, 1969.

Harrington, D.E.: Performance of Convergent and Plug Nozzles at Mach Numbers From 0 to 1.97. NASA TM X-2112, 1970.

Harrington, D.E.: Performance of a 10° Conical Plug Nozzle With Various Primary Flap and Nacelle Configurations at Mach Numbers From 0 to 1.97. NASA TM X-2086. 1970.

Harrington, D.E.; Nosek, S.M.; and Straight, D.M.: Cold-Flow Performance of Several Variations of a Ram-Air-Cooled Plug Nozzle for Supersonic Cruise Aircraft. NASA TM X-3110, 1974.

Harris, R.V., Jr.: An Analysis and Correlation of Aircraft Wave Drag. NASA TM X-947, 1964.

Head, V.L.: Flight Investigation of an Underwing Nacelle Installation of Three Variable-Flap Ejector Nozzles. NASA TM X-2478, 1972.

Herbert, M.V.: Centre-Body Nozzles for Supersonic Transport Aircraft. J. Roy. Aeronaut. Soc., vol. 71, no. 1, Jan. 1967. pp. 14-22.

Hesse, W.J.; and Mumford, N.V.S., Jr.: Jet Propulsion for Aerospace Applications. Second Edition, Pitman Publishing Corp., New York, 1964.

Howard, W.E.: Impact of Advanced Air Transport Technology, Part 1: Advanced High-Speed Aircraft. OTA-T-112-PT-1, Apr. 1980.

Huff, R.G.; and Anderson, A.R.: Internal Performance of Several Auxiliary Air Inlets Immersed in a Turbulent Boundary Layer at Mach Numbers of 1.3, 1.5, and 2.0. NACA RM E56J18, Jan. 1957.

Huntley, S.C.; and Samanich, N.E.: Performance of a 10° Conical Plug Nozzle Using a Turbojet Gas Generator. NASA TM X-52570, 1969.

Jeracki, R.J.; and Chenoweth, F.C.: Coolant Flow Effects on the Performance of a Conical Plug Nozzle at Mach Numbers From 0 to 2.0. NASA TM X-2076, 1970.

Johns, A.L.: Quiescent-Air Performance of a Truncated Plug Nozzle With Shroud and Plug Base Flows From a Common Source. NASA TM X-1807, 1969.

Johns, A.L.: Performance of an Auxiliary Inlet Ejector Nozzle With Floating Inlet Doors and Floating Single-Hinge Trailing-Edge Flaps. NASA TM X-2173, 1971.

Johns, A.L.; and Jeracki, R.J.: Preliminary Investigation of Performance of a Wedge Nozzle Applicable to a Supersonic Cruise Aircraft. NASA TM X-2169, 1971.

Johns, A.L.; and Steffen, F.W.: Performance of an Auxiliary Inlet Ejector Nozzle With Fixed Doors and Single-Hinge Trailing-Edge Flaps. NASA TM X-2027, 1970.

Johns, A.L.; and Steffen, F.W.: Performance of an Auxiliary Inlet Ejector Nozzle With Fixed Inlet Doors and Triple-Hinge Trailing-Edge Flaps. NASA TM X-2034, 1970.

Kochendorfer, F.D.; and Rousso, M.D.: Performance Characteristics of Aircraft Cooling Ejectors Having Short Cylindrical Shrouds. NACA RM E51E01, May 1951.

Kozlowski, H.; and Packman, A.B.: Aerodynamic and Acoustic Tests of Duct-Burning Turbofan Exhaust Nozzles. NASA CR-2628, 1976.

Kozlowski, H.; and Packman, A.B.: Flight Effects on the Aerodynamic and Acoustic Characteristics of Inverted Velocity Profile Coannular Nozzles. NASA CR-3018, 1978.

Lieberman, A.: Comparison of Predicted and Experimental Wall Temperatures for a Cylindrical Ejector Exhaust Nozzle Operated With a Turbojet Gas Generator. NASA TN D-6465, 1971.

Low Speed Test of a Naturally Aspirated Co-Annular Nozzle, Vol. I. NASA CR-168043, 1983.

Mansour, A.H.; and Burley, R.R.: Internal Thrust and Pumping Performance of an Auxiliary Inlet Ejector Nozzle With Clamshell Thrust Reverser. NASA TM X-52621, 1969.

Mercer, C.E.; and Berrier, B.L.: Effect of Afterbody Shape, Nozzle Type, and Engine Lateral Spacing on the Installed Performance of a Twin-Jet Afterbody Model. NASA TM X-1855, 1969.

Migdal, D.; Miller, E.H.; and Schnell, W.C.: An Experimental Evaluation of Exhaust Nozzle/Airframe Interference. AIAA Paper 69-430, June 1969.

Mikkelson, D.C.; and Blaha, B.J.: Flight and Wind Tunnel Investigation of Installation Effects on Underwing Supersonic Cruise Exhaust Nozzles at Transonic Speeds. NASA TM X-52827, 1970.

Mikkelson, D.C.; and Head, V.L.: Flight Investigation of Airframe Installation Effects on a Variable Flap Ejector Nozzle of an Underwing Engine Nacelle at Mach Numbers From 0.5 to 1.3. NASA TM X-2010, 1970.

Miller, E.H.; and Migdal, D.: Separation and Stability Studies of a Convergent-Divergent Nozzle. J. Aircraft, vol. 7, no. 2, Mar.-Apr. 1970, pp. 159-163.

Nelson, D.P.: Model Aerodynamic Test Results for Two Variable Cycle Engine Coannular Exhaust Systems at Simulated Takeoff and Cruise Conditions. (PWA-5550-37, Pratt & Whitney Aircraft; NASA Contract NAS3-20061) NASA CR-159818, 1980.

Nelson, D.P.: Model Aerodynamic Test Results for a Refined Actuated Inlet Ejector Nozzle at Simulated Takeoff and Cruise Conditions. (PWA-5768-29, Pratt & Whitney Aircraft; NASA Contract NAS3-22738) NASA CR-168051, 1983.

Rao, G.V.R.: Contoured Rocket Nozzles. Ninth International Astronautical Congress, F. Hecht, ed., Vol. 2, Springer-Verlag, 1958, pp. 752-763.

Rao, G.V.R.: Approximation of Optimum Thrust Nozzle Contour. ARS J., vol. 30, no. 6, June 1960, pp. 561-563.

Runckel, J.F.: Aerodynamic Interference Between Exhaust System and Airframe. Aerodynamic Interference, AGARD CP-71-71, AGARD, Paris, France, 1970, pp. 15-1 to 15-10 (also NASA TM X-66888).

Samanich, N.E.; and Burley, R.R.: Flight Performance of Auxiliary Inlet Ejector and Plug Nozzle at Transonic Speeds. AIAA Paper 70-701, June 1970. (also NASA TM X-52784, 1970.)

Samanich, N.E.; and Huntley, S.C.: Thrust and Pumping Characteristics of Cylindrical Ejectors Using Afterburning Turbojet Gas Generator. NASA TM X-52565, 1969.

Samanich, N.E.; and Chamberlin, R.: Flight Investigation of Installation Effects on a Plug Nozzle Installed on an Underwing Nacelle. NASA TM X-2295, 1971.

Shrewsbury, G.D.: Effect of Boattail Juncture Shape on Pressure Drag Coefficients of Isolated Afterbodies. NASA TM X-1517, 1968.

Shrewsbury, G.D.: Effect of a Simulated Wing on the Pressure Drag Coefficients of Various 15° Boattails at Mach Numbers From 0.56 to 1.00. NASA TM X-1662, 1968.

Shrewsbury, G.D.; and Jones, J.R.: Static Performance of an Auxiliary Inlet Ejector Nozzle for Supersonic Cruise Aircraft. NASA TM X-1653, 1968.

Silhan, F.V.; and Cubbage, J.M., Jr.: Drag of Conical and Circular-Arc Boattail Afterbodies at Mach Numbers From 0.6 to 1.3. NACA RM L56K22, Jan. 1957.

Sivo, J.N.; Meyer, C.L.; and Peters, F.J.: Experimental Evaluation of Rocket Exhaust Diffusers for Altitude Simulation. NASA TN D-298, 1960.

Steffen, F.W.: Performance of a 10° Conical Plug Nozzle With a Stowed Thrust Reverser at Mach Numbers From 0 to 2.0. NASA TM X-2116, 1970.

Steffen, F.W.; and Bresnahan, D.L.: Static Test Results From Exhaust Nozzles With Novel Features for Supersonic Aircraft Applications. Conference on Aircraft Aerodynamics, NASA SP-124, 1966, pp. 245-257.

Steffen, F.W.; and Johns, A.L.: Performance of a Fixed Geometry Wind Tunnel Model of an Auxiliary Inlet Ejector With a Clamshell Flow Diverter From Mach Number 0 to 1.2. NASA TM X-2037, 1970.

Steffen, F.W.; and Jones, J.R.: Performance of a Wind Tunnel Model of an Aerodynamically Positioned Variable Flap Ejector at Mach Numbers From 0 to 2.0. NASA TM X-1639, 1968.

Steffen, F.W., et al.: A Turbojet Simulator for Mach Numbers up to 2.0. NASA TM X-67973, 1972.

Straight, D.M.; Harrington, D.E.; and Nosek, S.M.: Experimental Cold-Flow Evaluation of a Ram-Air-Cooled Plug Nozzle Concept for Afterburning Turbojet Engines. NASA TM X-2811, 1973.

Swan, W.C.: A Discussion of Selected Aerodynamic Problems on Integration of Propulsion Systems With the Airframe on Transport Aircraft. Aerodynamics of Power Plant Installation, Part 1, Agardograph-103–PT–1, AGARD, Neuilly-Sur-Seine, France, 1965, pp. 23–68.

Tables of Compressible Flow Functions. Pratt & Whitney Aircraft, 1963.

Throndson, L.W.: Close-Spaced Nozzles, Twin Jet Configuration. AIAA Paper 70–934, July 1970.

Wagenknecht, C.D.; and Bediako, E.D.: Aerodynamic Performance Investigation of Advanced Mechanical Suppressor and Ejector Nozzle Concepts for Jet Noise Reduction. (R83AEB122–3, General Electric Co.; NASA Contract NAS3–23038) NASA CR–174860, 1985.

Wallner, L.E.; and Jansen, E.T.: Full-Scale Investigation of Cooling Shroud and Ejector Nozzle for a Turbojet Engine–Afterburner Installation. NACA RM E51J04, Dec. 1951.

Wasko, R.A.: Stability Characteristics of a Sting-Supported Collapsible Plug Nozzle at Mach Numbers From 0 to 2.0. NASA TM X–1704, 1968.

Wasko, R.A.; and Harrington, D.E.: Performance of a Collapsible Plug Nozzle Having Either Two-Position Cylindrical or Variable Angle Floating Shrouds at Mach Numbers From 0 to 2.0. NASA TM X–1657, 1968.

Wilcox, F.A.; Samanich, N.E.; and Blaha, B.J.: Flight and Wind Tunnel Investigation of Installation Effects on Supersonic Cruise Exhaust Nozzles at Transonic Speeds. NASA TM X–52586, 1969.

Wilsted, H.D.; Huddleston, S.C.; and Ellis, C.W.: Effect of Temperature on Performance of Several Ejector Configurations, NACA RM E9E16, June 1949.

# NASA
National Aeronautics and
Space Administration

# Report Documentation Page

| 1. Report No. NASA RP–1235 | 2. Government Accession No. | 3. Recipient's Catalog No. |
|---|---|---|

| 4. Title and Subtitle | 5. Report Date |
|---|---|
| Exhaust Nozzles for Propulsion Systems With Emphasis on Supersonic Cruise Aircraft | May 1990 |
| | 6. Performing Organization Code |

| 7. Author(s) | 8. Performing Organization Report No. |
|---|---|
| Leonard E. Stitt | E–4789 |
| | 10. Work Unit No. 505–69–61 |

| 9. Performing Organization Name and Address | 11. Contract or Grant No. |
|---|---|
| Sverdrup Technology, Inc. NASA Lewis Research Center Group Cleveland, Ohio 44135–3191 | NAS3–25266 |
| | 13. Type of Report and Period Covered Reference Publication |

| 12. Sponsoring Agency Name and Address | 14. Sponsoring Agency Code |
|---|---|
| National Aeronautics and Space Administration Lewis Research Center Cleveland, Ohio 44135–3191 | |

15. Supplementary Notes

16. Abstract

This compendium summarizes the contributions of the NASA Lewis Research Center and its contractors to supersonic exhaust nozzle research over two decades, from 1963 to 1985. Two major research and technology efforts sponsored this nozzle research work—the United States Supersonic Transport (SST) Program and the follow-on Supersonic Cruise Research (SCR) Program. They account for two generations of nozzle technology: the first from 1963 to 1971, and the second from 1971 to 1985. The publication is organized as follows: First, the equations used to calculate nozzle thrust are introduced. Then the general types of nozzles are presented, followed by a discussion of those types proposed for supersonic aircraft. Next, the first-generation nozzles designed specifically for the Boeing SST and the second-generation nozzles designed under the SCR program are separately reviewed and then compared. A chapter on throttle-dependent afterbody drag is included, since drag has a major effect on the off-design performance of supersonic nozzles. A chapter on the performance of supersonic dash nozzles follows, since these nozzles have similar design problems. Finally, the nozzle test facilities used at NASA Lewis during this nozzle research effort are identified and discussed. These facilities include static test stands, a transonic wind tunnel, and a flying testbed aircraft. A concluding section points to the future: a third generation of nozzles designed for a new era of high-speed civil transports to produce even greater advances in performance, to meet new noise rules, and to ensure the continuity of over two decades of NASA research.

| 17. Key Words (Suggested by Author(s)) | 18. Distribution Statement |
|---|---|
| Propulsion systems; Exhaust nozzles; Supersonic cruise; Supersonic dash; Installation effects; Boattail drag; Nozzle cooling; Nozzle facilities; Flight tests | Unclassified – Unlimited Subject Category 07 |

| 19. Security Classif. (of this report) | 20. Security Classif. (of this page) | 21. No of pages | 22. Price* |
|---|---|---|---|
| Unclassified | Unclassified | 107 | A06 |

NASA FORM 1626 OCT 86     *For sale by the National Technical Information Service, Springfield, Virginia 22161     NASA-Langley, 1990